Sensorless control of electric motors by signal injection

Dilshad Surroop

PSL UNIVERSITÉ PARIS

THÈSE DE DOCTORAT

DE L'UNIVERSITÉ PSL

Préparée à MINES Paris

Sensorless control of electric motors by signal injection

Commande sans capteur de moteurs électriques par injection de signal

Soutenue par

Dilshad Surroop

Le 10 février 2022

École doctorale n°621

Ingénierie des Systèmes, Matériaux, Mécanique, Energétique

Spécialité

Mathématiques et Automatique

Composition du jury :

Jean-Michel Coron Professeur, Sorbonne Université	*Président*
Vincent Andrieu Directeur de recherche, CNRS	*Rapporteur*
Malek Ghanes Professeur, Centrale Nantes	*Rapporteur*
Xuefang Lin-Shi Professeure, INSA Lyon	*Examinatrice*
Pascal Combes Docteur, Schneider Electric	*Examinateur*
Philippe Martin Maître de Recherche, MINES Paris	*Codirecteur de thèse*
Pierre Rouchon Professeur, MINES Paris	*Directeur de thèse*

MINES PARIS | PSL

Sensorless control of electric motors by signal injection

Dilshad Surroop

Centre Automatique et Systèmes
Mines Paris

Contents

List of Figures

Nomenclature

Roman symbols

Symbol	Description	Unit
$\mathcal{C}$	Concordia's matrix	–
c	Symmetric carrier	V
e_s	Back electromotive force	V
$\imath_s$	Stator currents	A
$\mathcal{J}$	Rotation matrix with angle $\pi/2$	–
K^k	Convolution powers of the characteristic function	–
$\widetilde{K}^k$	Reconstruction kernels	–
L_1	Stator self-inductance per phase	H
L_2	Stator inductance fluctuation	H
L_{ii}	Stator windings self-inductances	H
L_d, L_q	d and q-axis inductances	H
M_{ij}	Mutual inductances	H
n	Number of pole pairs	–
o, $\mathcal{O}$	Uniform "small o" and "big O" of analysis	–
$\mathcal{P}(\theta)$	Park's matrix	–
P_k	k^{th}-order demodulation estimator	–
$\mathcal{R}(\theta)$	Rotation matrix with angle θ	–
R_s	Stator resistance	Ω
$\mathcal{S}(\theta)$	Saliency matrix	H^{-1}
$\mathcal{S}_2(\theta)$	Second-order saliency matrix	$\Omega\,\mathrm{H}^{-2}$
s_i^*	Inverter gate pulses	–
s_0	Injected signal/Natural injection/First carrier	V, –
s_1	Primitive of s_0/Second carrier	V s, –
T_l	Load torque	N m
T_{pwm}	PWM period	s
T_s	Sigma-Delta sampling time	s
u_{pwm}	Impressed PWM voltage	V
u_s	Stator voltage	V
u_m	PWM amplitude	V
w	Sawtooth carrier	V
y_v	Virtual measurement	–

Greek symbols

Symbol	Description	Unit
α^k	Coefficients of the k^{th}-order reconstruction kernel $\widetilde{K}^k$	–
Δ	Finite backward difference operator	–
ε	Small parameter/Injection period/PWM period	–,s
θ	Rotor (electrical) angle	rad
$\Sigma\Delta$	Sigma-Delta modulator/Analog-to-Digital converter	–
τ	Delay operator	–
ϕ_s	Stator flux linkage	Wb
ϕ_m	Permanent magnet flux linkage	Wb
ω	Rotor (electrical) speed	$\mathrm{rad\,s^{-1}}$

Superscripts, subscripts

Symbol	Description
x^{abc}	x components in the three-phased stationary frame abc: $(x^a\ x^b\ x^c)^T$
$x^{\alpha\beta}$	x components in the two-phased stationary frame: $\alpha\beta$: $(x^\alpha\ x^\beta)^T$
x^{dq}	x components in the two-phased synchronous frame dq: $(x^d\ x^q)^T$
x^{ref}, x_{ref}	Reference for x
$\overline{x}$	Average of x/Truncated averaged or non-perturbed state
$\breve{x}$	Full averaged state
$\tilde{x}$	Auxiliary state in the averaging theory
$\hat{x}$	Estimate of x
$x_{\Sigma\Delta}$	Sigma-Delta encoding of x

Abbreviations

ADC	Analog-to-Digital Converter
AWGN	Additive White Gaussian Noise
CT/DT-$\Sigma\Delta$	Continuous-Time/Discrete-Time $\Sigma\Delta$
EMF	Electromotive Force
IGBT	Insulated Gate Bipolar Transistor
INFORM	Indirect Flux detection by Online Reactance Measurement
I/SM-PMSM	Interior/Surface-Mounted PMSM
LPF	Low-Pass Filter
PLL	Phase-Locked Loop
PMSM	Permanent Magnet Synchronous Motor
PSC-PWM	Phase-Shifted Carrier Pulse-Width Modulation
PSD	Power Spectral Density
PWM	Pulse-Width Modulation
VFD	Variable-Frequency Drive

Introduction – version française

1 Contexte

Depuis son invention au XIX^{e} siècle, le moteur électrique s'est progressivement intégré dans tous les pans de l'industrie, allant du contrôle de pompes pour des applications en chauffage, ventilation, climatisation (HVAC) à la plus récente motorisation des véhicules électriques. Les enjeux énergétiques du siècle présent alliés à une électrification croissante des sociétés modernes conféreront au moteur électrique un rôle croissant dans les décennies à venir, prolongeant ainsi sa constante évolution au fil du temps.

À partir du XX^{e} siècle, le développement conjoint de l'automatique, de l'électronique de puissance, des microprocesseurs et de la commande des moteurs électriques a marqué le début de ces évolutions, contribuant notamment à l'essor de nouvelles technologies de contrôle. À l'origine, les premiers moteurs nécessitaient d'être directement connectés au réseau électrique, opérant alors sur le point de fonctionnement fixé par les propriétés de l'alimentation du réseau. Si cela peut s'avérer suffisant pour des opérations élémentaires, un tel procédé s'avère limité dès lors que l'on souhaite maîtriser les transitoires de courant au démarrage ou changer de point de fonctionnement en cours d'opération. Une manière d'y remédier consiste à équiper les moteurs électriques d'un variateur de vitesse, qui permet de contrôler précisément la vitesse du moteur à l'aide de différentes lois de commande tout en maîtrisant l'afflux de courant au démarrage. Ces lois ont elles aussi connu des évolutions conséquentes au fil des années . La commande scalaire V/f en boucle ouverte, qui consiste à faire varier l'amplitude et la fréquence d'entrée afin de commander la vitesse de rotation en gardant un ratio constant entre ces deux quantités (d'où son nom), a progressivement été supplantée par la commande vectorielle en boucle fermée, plus efficace et qui prend en compte la dynamique propre du moteur pour établir la commande, contrairement à la loi V/f. Plus récemment encore, la technique dite de la commande directe du couple, plus coûteuse en ressources de calcul, procède à un asservissement du couple produit au lieu de la vitesse. Ces deux dernières méthodes — commande vectorielle et commande directe du couple —, nécessitent néanmoins d'avoir accès à la position du rotor pour être implémentées.

De cette nécessité est né, dans les années 90, un nouveau standard dans la conception d'algorithme de commande des moteurs électriques : le contrôle « sans capteurs ». Cette dénomination désigne la volonté de s'affranchir du capteur de position pour estimer cette dernière, en exploitant uniquement les quantités électriques mesurées que sont les courants et tensions statoriques. La présence d'un encodeur pour récupérer la position est en effet nuisible à plusieurs égards : la fiabilité du capteur, son encombrement, son coût ou encore son

utilisation en milieux délétères sont autant de raisons qui poussent en faveur d'une estimation de la position sans avoir recours à un encodeur mécanique.

Deux grandes catégories de méthodes d'estimation sans capteurs se distinguent dès lors. L'*estimation passive* s'appuie sur le modèle d'excitation fondamentale du système, à savoir le modèle d'état lorsque les harmoniques à haute fréquence sont exclues de la modélisation. En faisant appel notamment à un observateur d'état, il est alors possible, sous réserve d'observabilité du système, de reconstruire asymptotiquement la position du rotor. L'*estimation active*, quant à elle, regroupe les stratégies basées sur la saillance de la machine, et exploite donc les anisotropies magnétiques du rotor à travers la réponse du moteur à des signaux à haute fréquence. Cette réponse, qui se lit comme une perturbation de courant, porte l'information de position qui est alors rendue disponible par une procédure de démodulation adéquate. Ces signaux à haute fréquence peuvent être exogènes, c'est la technique de l'*injection de signal*, ou endogènes, en utilisant les harmoniques crées par la Modulation de Largeur d'Impulsions (MLI) utilisée pour commander l'étage de puissance du variateur de vitesse, et donc indirectement le système. Des deux classes de méthodes susmentionnées — active et passive —, seule la seconde permet de surmonter les problèmes d'observabilité à basse vitesse lorsque la position du rotor n'est pas mesurée.

Cette thèse s'inscrit dans la lignée des méthodes d'estimation active endogène, et a pour ambition de développer une méthode d'estimation « sans capteur » de la position du rotor sans perturbation extérieure du système, en s'appuyant uniquement sur l'excitation induite par l'onduleur. Ce type de stratégie a été esquissée vers la fin des années 90, mais chacune des implémentations proposées jusqu'à présent nécessitent une modification du schéma de calcul de la MLI ou l'usage de capteurs supplémentaires. C'est la terminologie même de « sans capteurs » qui se retrouve dénaturée par de tels procédés, puisque l'encodeur est finalement remplacé par une sonde annexe, amenant avec elle un coût et une complexité supplémentaires qui sont difficilement soutenables en vue d'une application industrielle. L'estimation de la position sans la mesurer directement, tout en conservant une MLI standard ainsi que les capteurs déjà à disposition, laisse donc entrevoir une réduction des coûts engendrés et des progrès en termes de fiabilité et de performances de la machine.

La méthode développée se concentre essentiellement sur les Moteurs Synchrones à Aimants Permanents (PMSM). Présentant un meilleur rendement, une densité massique et volumique de puissance plus importante que les moteurs à induction, ces moteurs synchrones sont particulièrement employés en robotique, dans la conception de machines-outils de haute précision et prennent une place de plus en plus importante dans la motorisation des systèmes de transport pour leur efficacité supérieure.

Les travaux réalisés durant cette thèse s'articulent autour de trois axes majeurs. D'une part, le développement d'outils mathématiques, notamment basée sur la théorie de la moyennisation, est mis en œuvre afin de mieux saisir les effets de l'injection de signal ou de l'onduleur sur l'état du système et ses sorties. Une telle étude met en évidence la possibilité de récupérer des *mesures virtuelles* lorsque le signal est excité par des signaux à haute fréquence. D'autre part, après avoir déterminé l'expression analytique de la perturbation induite par l'injection ou l'onduleur, l'extraction de l'information contenue dans cette perturbation est présentée. Cette

récupération s'appuie sur une théorie générale de la démodulation de signaux analogiques multiplexés. Celle-ci s'attache à prendre en compte les spécificités propres à la sortie physique, à savoir la présence d'une double échelle de temps lent/rapide au sein des porteuses du signal multiplexé. Enfin, les deux orientations théoriques se rejoignent pour traiter particulièrement de l'estimation de position sans capteur des PMSM à partir uniquement des harmoniques induites par l'onduleur, et ce sans capteur supplémentaire. L'analyse théorique permet d'exhiber la forme de la perturbation sur les courants, là où la théorie de la démodulation développée est employée pour extraire l'information de position contenue dans cette perturbation. Le traitement spécifique du moteur synchrone souligne les difficultés propres à ce type de système, notamment le rôle de la saturation magnétique dans la qualité de l'estimation produite.

2 Plan

Le manuscrit est structuré autour des articles listés ci-après afin de rendre chaque chapitre autonome. En particulier, certaines parties se recouvrent — comme la démodulation esquissée aux chapitres 2 et 3 et qui est synthétisée au chapitre 4. Ce manuscrit s'organise comme suit

Le chapitre 1 couvre la modélisation des PMSM, de leur principe de fonctionnement à leur représentation d'état en passant par la définition usuelle des repères stationnaires et synchrones qui permettent de simplifier les équations du modèle. Ce chapitre englobe de surcroît un survol de la littérature portant sur les techniques d'estimation « sans capteurs » passives et actives de la position, reposant soit sur le modèle d'excitation fondamentale, soit sur la réponse à des signaux hautes fréquences. Cette dernière méthode inclut, entre autres, l'injection de signal et la stratégie développée dans ce manuscrit.

Le chapitre 2 pose les fondations de la théorie de la moyennisation pour les systèmes contrôlés en utilisant l'injection de signal. La moyennisation à l'ordre deux pour l'étude des effets induits par l'injection de signal est désormais standard, et permet d'exhiber la mesure virtuelle rendue disponible par la perturbation du système. En poussant les calculs à l'ordre supérieur, il est possible de raffiner ces effets perturbatifs sur l'état du système. Une telle étude met en évident la possibilité de récupérer jusqu'à deux mesures virtuelles supplémentaires. Deux cas sont traités numériquement : celui d'une dynamique linéaire ad hoc équipée d'une mesure non linéaire, et celui d'un PMSM sans mesure de position contrôlé par une entrée analogique.

Le chapitre 3 étend la théorie de la moyennisation aux systèmes contrôlés par des signaux MLI. La modulation de l'entrée peut se décomposer en deux signaux ayant chacun leur fréquence propre : une fréquence fondamentale correspondant à l'entrée analogique, et un terme « quasi-périodique » évoluant à la fréquence de la MLI. Il est alors montré que ce terme à haute fréquence agit naturellement comme une injection de signal traditionnelle sur le système, et qu'elle permet donc de récupérer des informations supplémentaires sur celui-ci. De manière analogue au chapitre 2, le même type de mesure virtuelle et d'estimation est obtenue pour ces systèmes contrôlés par des signaux en

tout ou rien. Ce chapitre forme le fondement théorique de la méthode développée dans ce mémoire.

Le chapitre 4 traite de l'extraction des mesures virtuelles des sorties mesurées. Un cadre générique est posé, celui de la démodulation de signaux analogiques multiplexés, où l'information est modulée par des porteuses présentant une double échelle de temps lent/rapide. Cette particularité portant sur les porteuses s'explique par la forme que prend la mesure virtuelle lorsque le système est commandé par une MLI. Ce chapitre détaille la conception de filtre passe-bas ainsi que la procédure de filtrage mises en place afin d'extraire chacune des composantes du signal multiplexé.

Le chapitre 5 couvre la problématique de la détection synchrone appliquée à la sortie d'un modulateur Sigma-Delta (ΣΔ). Les variateurs de vitesse étudiés dans cette thèse sont équipés d'un convertisseur Sigma-Delta pour encoder digitalement les courants mesurés. Tandis que la procédure de démodulation décrite au chapitre 4 s'applique directement aux signaux analogiques, la transposition de cette méthode au flux binaire issu du ΣΔ n'est pas immédiate. Ce chapitre confirme théoriquement et numériquement cette idée, à savoir la commutation entre la procédure de démodulation et la conversion opérée par le modulateur ΣΔ, qu'il soit continu ou discret.

Le chapitre 6, enfin, rassemble les différentes pièces du puzzle pour les appliquer à l'estimation de position sans capteur d'un PMSM en utilisant les harmoniques naturelles induites par l'onduleur. Sont détaillés dans ce chapitre la forme de la mesure virtuelle pour ce système, ainsi que l'application spécifique de la procédure de démodulation sur les courants statoriques mesurés. Une méthode alternative, consistant à déphaser les porteuses pour chacune des tensions d'entrée, est également proposée afin d'améliorer la qualité de l'estimation de position. La simulation et les résultats expérimentaux parachèvent cette analyse, et mettent en évidence le rôle de la saturation magnétique dans l'estimation produite.

3 Contributions

Certains résultats de cette thèse ont été publiés dans

[Sur+19a] D. Surroop, P. Combes, P. Martin et P. Rouchon. « A New Demodulation Procedure for a Class of Multiplexed Signals ». In : *Annual Conference of the IEEE Industrial Electronics Society (IECON)*. 2019, p. 48-53

[Sur+19b] D. Surroop, P. Combes, P. Martin et P. Rouchon. « Third-order Virtual Measurements with Signal Injection ». In : *2019 IEEE 58th Conference on Decision and Control (CDC)*. 2019, p. 642-647

[Sur+20b]D. Surroop, P. Combes, P. Martin et P. Rouchon. « Sensorless Rotor Position Estimation by PWM-induced Signal Injection ». In : *IECON 2020 The 46th Annual Conference of the IEEE Industrial Electronics Society*. 2020, p. 367-372

[Sur+20a] D. Surroop, P. Combes, P. Martin et P. Rouchon. « Adding Virtual Measurements by PWM-induced Signal Injection ». In : *American Control Conference*. 2020, p. 2692-2698

[SCM21a] D. Surroop, P. Combes et P. Martin. « Error Analysis of a Demodulation Procedure for Multicarrier Signals with Slowly-varying Carriers ». In : *2021 29th European Signal Processing Conference (EUSIPCO)*. 2021, p. 1636-1640

[SCM21b] D. Surroop, P. Combes et P. Martin. « Error Estimates in Second-order Continuous-time Sigma-Delta Modulators ». In : *ICASSP 2021 - 2021 IEEE International Conference on Acoustics, Speech and Signal Processing (ICASSP)*. 2021, p. 5445-5448

[SCM21c] D. Surroop, P. Combes et P. Martin. « Towards an Industrially Implementable PWM-injection Scheme ». In : *2021 IEEE International Electric Machines Drives Conference (IEMDC)*. 2021, p. 1-6

En outre, les brevets suivants ont été déposés

[Com+20] P. Combes, D. Surroop, P. Martin et P. Rouchon. « Estimation of the amplitude of a periodic component in a measured signal through a Delta-Sigma modulator ». Brev. EP3709500 (A1), US11264935 (B2), CN111697893 (A). 2020

[Com+21a] P. Combes, D. Surroop, P. Martin et P. Rouchon. « A Variable Speed Drive for the Sensorless PWM Control of an AC Motor by Exploiting PWM-Induced Artefacts ». Brev. EP3799293 (A1), US11264935 (B2), CN112564583 (A). 2021

[Com+21b] P. Combes, D. Surroop, P. Martin et P. Rouchon. « A Variable Speed Drive for the Sensorless PWM Control of an AC Motor with Current Noise Rejection ». Brev. EP4020793 (A1), US2022200507 (A1), CN114744947 (A). 2021

Introduction

1 Context

Since its invention in the 19th century, electric motors have been progressively integrated into all areas of industry, from pump control for heating, ventilation and air conditioning (HVAC) applications to the more recent motorisation of electric vehicles. The energetic challenges of the present century combined with the increasing electrification of modern societies will give the electric motor a growing role in the decades to come, continuing its constant evolution over time.

From the 20th century onwards, the joint development of automation, power electronics, microprocessors and motor control marked the beginning of these developments, contributing in particular to the development of new control technologies. Originally, the first motors required direct connection to the electrical grid and worked at the operating point set by the properties of the grid. While this may be sufficient for basic operations, such a process is limited when it is desired to control current transients at start-up or to change the operating point during operation. One way of overcoming this is to equip electric motors with a Variable Frequency Drive (VFD), which allows the motor speed to be precisely configured by means of different algorithms while controlling the starting current flow. These laws have also undergone significant development over the years. The scalar V/f open-loop control, which consists of varying the input amplitude and frequency in order to control the rotation speed while maintaining a constant ratio between these two quantities (hence its name), has gradually been supplanted by the more efficient vector Field-Oriented Control (FOC), which takes into account the motor's own dynamics to design the control law, unlike the V/f law. Even more recently, the technique known as Direct Torque Control (DTC), which is more costly in terms of computing resources, uses the torque produced instead of the speed. The latter two methods —vector control and direct torque control— nevertheless require access to the rotor position to be implemented.

From this need was born, in the 1990s, a new standard in the design of electric motor control algorithms: sensorless control. This name refers to the desire of getting rid of the position sensor to estimate it, using only the measured electrical quantities, i.e. the stator currents and voltages. The presence of an encoder to recover the position is in fact harmful in several regards: the reliability of the sensor, its size, its cost or its use in adverse environments are different reasons that push in favour of estimating the position without resorting to a mechanical encoder.

Two main categories of sensorless estimation methods can therefore be distinguished. *Pas-*

sive estimation is based on the fundamental excitation model of the system, i.e. the state-space model when high-frequency harmonics are excluded from the modeling. By using a state observer, it is then possible, subject to the observability of the system, to asymptotically reconstruct the rotor position. *Active estimation*, on the other hand, groups together strategies based on the machine saliency, and thus exploits the magnetic anisotropies of the rotor through the motor response to high-frequency signals. This response, read as a current disturbance, carries the position information which is then made available by an appropriate demodulation procedure. These high-frequency signals can be exogenous, this is the signal injection technique, or endogenous, using the harmonics created by the Pulse-Width Modulation (PWM) used to control the power stage of the Variable Frequency Drive, and thus indirectly the system. Of the two classes of methods mentioned above —active and passive— only the latter overcomes the observability problems at low speed when the rotor position is not measured.

This thesis is in the line of endogenous active estimation methods, and aims at developing a "sensorless" estimation method of the rotor position without any external disturbance of the system, relying only on the inverter-induced excitation. This type of strategy was sketched out in the late 1990s, but each of the implementations proposed so far required a modification of the PWM calculation scheme or the use of additional sensors. The "sensorless" terminology is thereby distorted by such processes, since the encoder is ultimately replaced by another sensor, bringing with it additional cost and complexity that are hardly sustainable for industrial applications. Estimating the position without measuring it directly, while keeping a standard PWM scheme and the sensors already available, therefore may lead to cost reductions as well as improvements in terms of machine reliability and performance.

The developed method primarily focuses on Permanent Magnet Synchronous Motors (PMSM). With higher efficiency and higher power density than their induction counterpart, these synchronous motors are particularly used in robotics, in the design of high precision machine tools and are becoming increasingly important in the motorisation of transport systems due to their higher efficiency.

This thesis revolves around three major axes. On the one hand, the development of mathematical tools, based on the averaging theory, is developed to better grasp the signal injection or inverter effects on the system states and outputs. Such a study highlights the possibility of recovering virtual measurements when the system is excited by high-frequency signals. On the other hand, after having determined the analytical expression of the disturbance induced by the injection or the inverter, the extraction of the information contained in this disturbance is presented. This recovery is based on a general theory of demodulation of multiplexed analog signals, which takes into account the specificities of the physical output, i.e. the presence of a double slow/fast time scale within the carriers of the multiplexed signal. The two theoretical orientations eventually come together to deal with the sensorless position estimation of a PMSM based solely on the harmonics induced by the inverter, without any additional sensor. The theoretical analysis exhibits the current ripple expression, where the demodulation theory is used to extract the position information contained in this ripple. The specific treatment of the synchronous motor highlights the difficulties specific to this type of system, in particular the role of magnetic saturation in the quality of the estimate produced.

2 Outline

The thesis is structured around the papers listed below so that each chapter is self-contained. Especially, some parts overlap —such as the demodulation theory started in chapters 2 and 3 and synthesized in chapter 4. The manuscript is organized as follows

Chapter 1 covers the modeling of PMSM, from their operating principle to their state representation, including the usual definition of stationary and synchronous frames that allow to simplify the model equations. In addition, this chapter includes a literature review of passive and active "sensorless" position estimation techniques, based either on the fundamental excitation model or on the response to high frequency signals. The latter method includes, among others, signal injection and the strategy developed in this manuscript.

Chapter 2 lays out the foundations of averaging theory for systems controlled using signal injection. Second-order averaging for the study of signal injection effects is now standard, and allows the virtual measurement made available by the system disturbance to be exhibited. By pushing the calculations to higher orders, it is possible to refine these perturbative effects on the system state. Such a study highlights the possibility of recovering up to two additional virtual measurements. Two cases are treated numerically: that of an ad hoc linear dynamics equipped with a non-linear measurement, and that of a PMSM without position measurement controlled by an analog input.

Chapter 3 extends the averaging theory to systems controlled by PWM signals. The input modulation can be decomposed into two signals, each with its own frequency: a fundamental frequency corresponding to the analog input, and a "quasi-periodic" term evolving at the PWM frequency. It is then shown that this high-frequency term acts as a natural signal injection on the system, and that it therefore allows additional information to be recovered from it. In a similar way to chapter 2, the same type of virtual measurement and estimation is obtained for those systems controlled by on-off signals. This chapter forms the theoretical basis of the method developed in this thesis.

Chapter 4 deals with the extraction of virtual measurements from measured outputs. A generic framework is set up, that of the demodulation of multiplexed analog signals, where the information is modulated by carriers with a double slow/fast time scale. The reason for this carrier feature is the form that the virtual measurement takes when the system is driven by a PWM. This chapter details the low-pass filter design and filtering procedure used to extract each component of the multiplexed signal.

Chapter 5 covers the problem of synchronous detection applied to the output of a Sigma-Delta ($\Sigma\Delta$) modulator. The variable speed drives studied in this thesis are equipped with a Sigma-Delta converter to digitally encode the measured currents. While the demodulation procedure described in chapter 4 is directly applicable to analog signals, the transposition of this method to the bitstream from the $\Sigma\Delta$ is not immediate. This

chapter confirms theoretically and numerically this idea, namely the commutation between the demodulation procedure and the conversion operated by the ΣΔ, and this for discrete and continuous modulators.

Chapter 6, finally, gathers the different pieces of the puzzle to apply them to the sensorless position estimation of a PMSM using the natural harmonics induced by the inverter. The form of the virtual measurement for this system is detailed in this chapter, as well as the specific application of the demodulation procedure on the measured stator currents. An alternative method, consisting in phase-shifting the carriers for each of the input voltage, is also proposed to improve the quality of the position estimation. Simulation and experimental results complete this analysis, and highlight the impact of magnetic saturation on the obtained estimation.

3 Contributions

Some results of this thesis have been published in

[Sur+19a] D. Surroop, P. Combes, P. Martin, and P. Rouchon. "A New Demodulation Procedure for a Class of Multiplexed Signals." In: *Annual Conference of the IEEE Industrial Electronics Society (IECON)*. 2019, pp. 48–53

[Sur+19b] D. Surroop, P. Combes, P. Martin, and P. Rouchon. "Third-order Virtual Measurements with Signal Injection." In: *2019 IEEE 58th Conference on Decision and Control (CDC)*. 2019, pp. 642–647

[Sur+20a] D. Surroop, P. Combes, P. Martin, and P. Rouchon. "Adding Virtual Measurements by PWM-induced Signal Injection." In: *American Control Conference*. 2020, pp. 2692–2698

[Sur+20b]D. Surroop, P. Combes, P. Martin, and P. Rouchon. "Sensorless Rotor Position Estimation by PWM-induced Signal Injection." In: *IECON 2020 The 46th Annual Conference of the IEEE Industrial Electronics Society*. 2020, pp. 367–372

[SCM21a] D. Surroop, P. Combes, and P. Martin. "Error Analysis of a Demodulation Procedure for Multicarrier Signals with Slowly-varying Carriers." In: *2021 29th European Signal Processing Conference (EUSIPCO)*. 2021, pp. 1636–1640

[SCM21b] D. Surroop, P. Combes, and P. Martin. "Error Estimates in Second-order Continuous-time Sigma-Delta Modulators." In: *ICASSP 2021 - 2021 IEEE International Conference on Acoustics, Speech and Signal Processing (ICASSP)*. 2021, pp. 5445–5448

[SCM21c] D. Surroop, P. Combes, and P. Martin. "Towards an Industrially Implementable PWM-injection Scheme." In: *2021 IEEE International Electric Machines Drives Conference (IEMDC)*. 2021, pp. 1–6

The following patents were also filed

[Com+20] P. Combes, D. Surroop, P. Martin, and P. Rouchon. "Estimation of the amplitude of a periodic component in a measured signal through a Delta-Sigma modulator." Pat. EP3709500 (A1), US11264935 (B2), CN111697893 (A). 2020

[Com+21a] P. Combes, D. Surroop, P. Martin, and P. Rouchon. "A Variable Speed Drive for the Sensorless PWM Control of an AC Motor by Exploiting PWM-Induced Artefacts." Pat. EP3799293 (A1), US11264935 (B2), CN112564583 (A). 2021

[Com+21b] P. Combes, D. Surroop, P. Martin, and P. Rouchon. "A Variable Speed Drive for the Sensorless PWM Control of an AC Motor with Current Noise Rejection." Pat. EP4020793 (A1), US2022200507 (A1), CN114744947 (A). 2021

Chapter 1

Sensorless position estimation for PMSM

Résumé Ce chapitre présente succintement la modélisation des Moteurs Synchrones à Aimants Permanents, de leur représentation d'état aux diverses transformations couramment employées pour simplifier le modèle d'état. Après avoir rappelé les enjeux de l'observabilité à basse vitesse, les principales stratégies d'estimation de la position du rotor — basées sur le modèle d'état ou sur la saillance — sont exposées.

Abstract This chapter briefly covers the standard modeling of Permanent Magnet Synchronous Motors, from their state-space model to the multiple transformations commonly used to simplify the equations. After stating the observability issues at low speed, the main strategies for estimating the rotor position —fundamental excitation and saliency-based strategies— are presented.

1.1 PMSM modeling

1.1.1 Structure and operating principles

The Permanent Magnet Synchronous Motor (PMSM) emerged in the early 70s as an attractive substitute to the widespread induction motor. Its high efficiency, reduced torque ripple and high volumetric and massic power densities relative to alternative machine architectures has fostered its deployment especially when high performance control is demanded. They naturally found their way in the powering of various industrial devices, from machine tools to electric vehicles, passing by standard residential applications, and is the most likely to represent the workhorse of the industry in the future.

Among the numerous assets of these motors lies a rather simple construction principle. Its general geometric structure consists of three-phase windings housed in the stator surrounding a rotor exhibiting permanent magnets. When the stator windings are connected to a three-phase AC source, they produce a rotating magnetic field that drags the rotor, thus producing a torque and the rotation of the machine, so that at steady-state, the rotor evolves at the same *synchronous* speed as the rotating field.

Several designs for PMSM rotors are available [VZ18, Chapter 1], mainly depending on the permanent magnets location on or in the rotor core. When the $d-$ and $q-$ axis inductances differ, the motor exhibits *magnetic saliency*. This saliency is found in Interior (I-) and Inset PMSM, where the permanent magnets are buried inside the rotor laminations. The absence

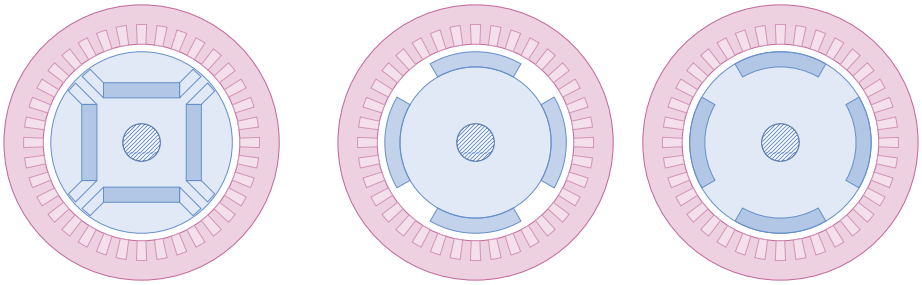

(a) Interior (b) Surface-Mounted (c) Inset

Figure 1.1: Different PMSM rotor structures along with distributed stator windings

of magnetic saliency (i.e. when the $d-$ and $q-$ axis inductances are equal) is found for instance in Surface-Mounted (SM-) PMSM, with permanent magnets embedded on the rotor outer surface. These different designs are depicted in Fig. 1.1.

1.1.2 State-space model of a PMSM

The standard state-space model of a sinusoidal PMSM in the dq-frame is given by [Kra+13],

$$\frac{d\phi_s^{dq}}{dt} = u_s^{dq} - R_s i_s^{dq} - \omega \mathcal{J} \phi_s^{dq} \tag{1.1a}$$

$$\frac{J}{n}\frac{d\omega}{dt} = n i_s^{dq^T} \mathcal{J} \phi_s^{dq} - T_l \tag{1.1b}$$

$$\frac{d\theta}{dt} = \omega, \tag{1.1c}$$

where $(\phi_s^{dq}, \omega, \theta)$ is the system state: ϕ_s^{dq} is the stator flux linkage, ω the rotor (electric) angular velocity, θ the rotor (electric) angular position. In addition, i_s^{dq} denotes the stator current, u_s^{dq} the stator voltage, $T_e := n i_s^{dq^T} \mathcal{J} \phi_s^{dq}$ the electromagnetic torque. The perturbation T_l denotes the load torque and the constant parameter R_s is the stator resistance. Finally, J is the moment of inertia, n the number of pole pairs and $\mathcal{J}$ the rotation matrix with angle $\pi/2$. Such a modeling discards practical imperfections such as slot harmonics as well as various physical effects like iron losses due to Foucault's currents and hysteresis, and skin effects.

This model describes the electric and mechanical dynamics in the dq-frame, namely the synchronous frame, rotating at the rotor speed. A rotation matrix —with angle θ— transforms this two-axis synchronous frame into the two-axis stationary one, the so-called $\alpha\beta$-frame, which in turn can be transformed into the three-axis stationary abc-frame thanks to the inverse Concordia transformation $\mathcal{C}^{-1} = \mathcal{C}^T$, with

$$\mathcal{C} := \sqrt{\frac{2}{3}} \begin{pmatrix} \cos(0) & \cos(2\pi/3) & \cos(4\pi/3) \\ \sin(0) & \sin(2\pi/3) & \sin(4\pi/3) \\ 1/\sqrt{2} & 1/\sqrt{2} & 1/\sqrt{2} \end{pmatrix} = \sqrt{\frac{2}{3}} \begin{pmatrix} 1 & -1/2 & -1/2 \\ 0 & \sqrt{3/2} & -\sqrt{3/2} \\ 1/\sqrt{2} & 1/\sqrt{2} & 1/\sqrt{2} \end{pmatrix}.$$

This abc-frame corresponds to the physical and stationary system where the actual inputs, the three-phase input voltages u_s^{abc} are imposed to the system. These voltages define the voltages

in the dq-frame through the relation $u_s^{dq} = \mathcal{R}(-\theta)\mathcal{C}u_s^{abc} =: \mathcal{P}(-\theta)u_s^{abc}$, where $\mathcal{R}(\theta)$ is the rotation matrix with angle θ, and $\mathcal{P}$ denotes Park's transformation [Par29; Par33], pushing directly the abc-frame to the dq-frame. For sensorless control, the only measurement is the current $\imath_s^{abc} = \mathcal{C}^T\mathcal{R}(\theta)\imath_s^{dq}$, or equivalently $\imath_s^{\alpha\beta} = \mathcal{R}(\theta)\imath_s^{dq}$ since $\imath_s^a + \imath_s^b + \imath_s^c = 0$ (we assume the motor is star connected, see Fig. 1.2).

To complete the model, a current-flux relation should be provided. Assuming there is no magnetic saturation, this relation is linear and reads

$$L_d\imath_s^d = \phi_s^d - \phi_m, \qquad L_q\imath_s^q = \phi_s^q, \tag{1.2a}$$

with ϕ_m the permanent magnet flux and L_d, L_q the d and q-axis inductances. This model however falls short at seizing magnetic saturation that actually occurs in working condition. An alternative approach consists in considering a polynomial expression of the current with respect to the flux linkages which comes from an energy-based modeling of the PMSM, see chapter 6 for further details.

For some sensorless strategies detailed below, it is useful to consider the voltage equations in the stationary $\alpha\beta$-frame. Applying a rotation to (1.1a) then yields

$$\frac{d\phi_s^{\alpha\beta}}{dt} = u_s^{\alpha\beta} - R_s\imath_s^{\alpha\beta}; \tag{1.3}$$

likewise, the unsaturated current-flux relation in the $\alpha\beta$-frame reads

$$\phi_s^{\alpha\beta} = \begin{pmatrix} L_1 + L_2\cos 2\theta & L_2\sin 2\theta \\ L_2\sin 2\theta & L_1 - L_2\cos 2\theta \end{pmatrix}\imath_s^{\alpha\beta} + \phi_m\begin{pmatrix}\cos\theta \\ \sin\theta\end{pmatrix}, \tag{1.4}$$

with $L_1 := (L_q + L_d)/2$ the (average) stator self-inductance per phase and $L_2 := (L_d - L_q)/2$ the stator inductance fluctuation.

1.2 Variable-frequency drive technology and data acquisition

This section touches on the industrial realization of PMSM control. Complete experimental setups are fleshed out in Combes' and Jebai's theses [Com15; Jeb13].

1.2.1 Voltage generation and power stage

Variable-Frequency Drives essentially consist of two sections: on the one hand the power stage, realizing the power conversion from the grid; on the other, a set of devices and processors embedding the motor control algorithms. The power stage comprises three stages: an AC/DC rectifier converting the AC grid voltage into a DC voltage; a DC/DC link that supplies the inverter with a more stable DC voltage than the rectifier output; and finally, a DC/AC inverter which, from the DC voltage, supplies the motor with a three-phase voltage with variable frequency and amplitude.

This last conversion step avoids the use of a linear amplifier, which is impossible to implement as it would generate consequent power losses when high power is involved. Instead, the

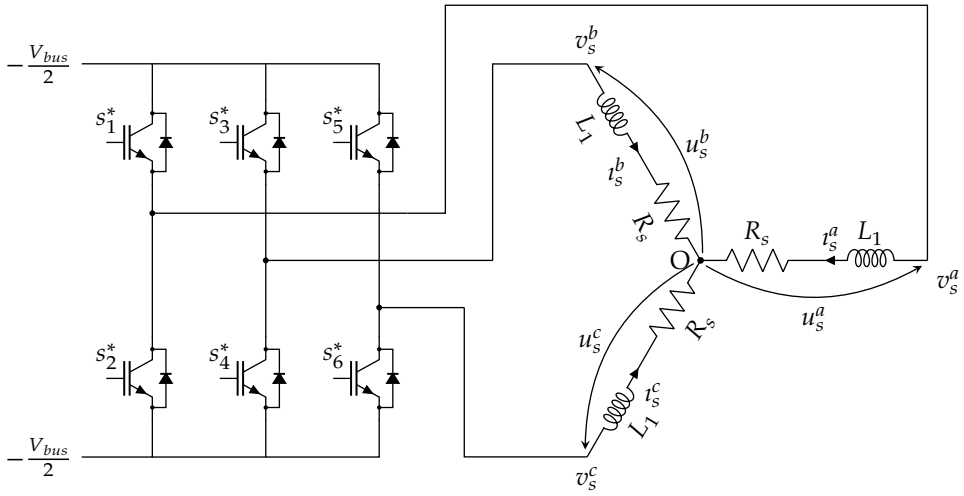

Figure 1.2: Two-level, three-phased inverter linked to a star-connected stator

inverter modulates the input signal by Pulse-Width Modulation (PWM), and produces square-wave signals whose duty cycles are modulated so that the specified voltages are obtained in average. For sinusoidal PWM, each input is compared to a fast-varying carrier typically evolving at 4 kHz (see chapter 3 for a detailed analysis), and sends to the inverter bridge pulses s_i^* that control the Insulated Gate Bipolar Transistors (IGBT), see Fig. 1.2. Three PWM signals are thereby produced, and, on average, generates the control (analog) signals. The PWM voltages then feed the stator windings of the PMSM, and create the rotating magnetic field that drags the rotor. Imperfections related to the DC/AC conversion by the inverter such as voltage drops and dead times must nevertheless be taken into account when implementing such a system (see [Com15, Section 2.3] and [Jeb13, Section 3.2] for further details).

1.2.2 Data acquisition and Sigma-Delta ADC

Different strategies can be deployed to measure the stator currents. Hall-effect sensors or a resistive shunt coupled with an amplifier are for instance two valid techniques to accurately achieve the measurements. These analog data are then converted into a digital stream using an Analog-to-Digital Converter (ADC) to feed the controlling processors. This conversion is often realized using a standard Nyquist-rate ADC that samples the current output at the PWM frequency. While these converters suffice at estimating the average current, they fail at capturing high-frequency harmonics (see Fig. 1.3), namely the inverter-induced harmonics, which are of utmost importance for the sensorless strategy developed in this thesis. Modern drives now embed Sigma-Delta modulator to ensure galvanic insulation as well as robustness with respect to electromagnetic interferences. They achieve high resolution through oversampling of the analog currents and noise shaping (meaning the Signal-to-Noise ratio in enhanced in the signal bandwidth, rejecting the noise amplification out of it). Typically, their sampling rate is in the order of 10 MHz, corresponding to 1000 to 10 000 times the typical PWM frequency.

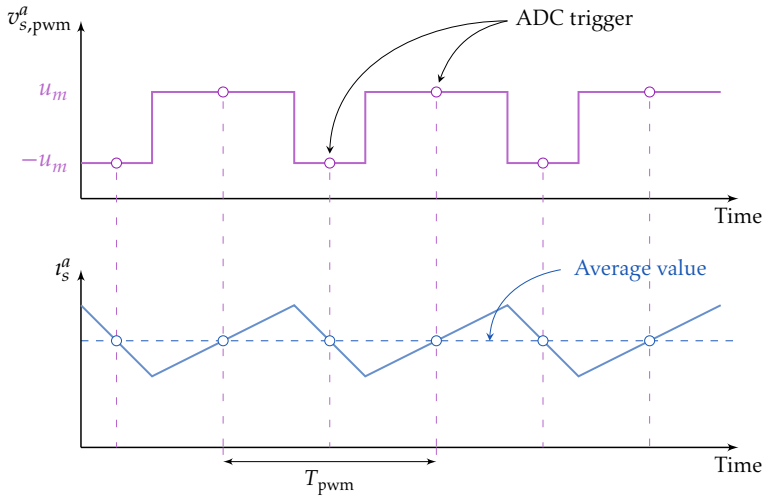

Figure 1.3: Nyquist-rate ADC data acquisition: data retrievals are triggered at the middle of a PWM pulse so as to avoid the oscillatory effects, but fail at seizing the current ripples

The cost of this high-rate sampling is the output quantization, which is generally limited to one bit. The output bitstream then needs to be processed by a Field Programmable Array Gate (FPGA): through the digital filtering (using a sinc^k filter) and the decimation, the average current is digitalized with a greater resolution than with most standard Nyquist-rate ADC. Besides the traditional sinc^k filter, a wide variety of filtering procedures can be applied to the $\Sigma\Delta$ bitstream (see chapter 5). Among others, the estimation of the PWM-induced ripple that carries the rotor position knowledge when suitably decoded. Figure 1.4 summarizes the $\Sigma\Delta$ ADC operating principle, and illustrates the possibility of demodulating high-frequency components encompassed in the analog input, on the contrary to standard ADC.

1.3 Low-speed observability issues

1.3.1 Low-speed observability properties of PMSM

The implementation of sophisticated PMSM control laws such as Field-Oriented Control (FOC) or Direct Torque Control (DTC) require the position knowledge to close their feedback loop. This is problem-free when the drive is equipped with a mechanical encoder to retrieve the rotor position, but several reasons push toward the sensor removal. Indeed, the presence of an encoder increases the system complexity by the induced bulkiness, reduces the ability to work in adverse environments, reduces the drive reliability, increases the global cost and brings a potential source of failure. Estimating the position without measuring it turns out to be of major importance for high-performance industrial applications. The so-called *sensorless control* is now a standard in the control of PMSM, and addresses this estimation issue with the sole knowledge of the electrical quantities —stator currents and voltages.

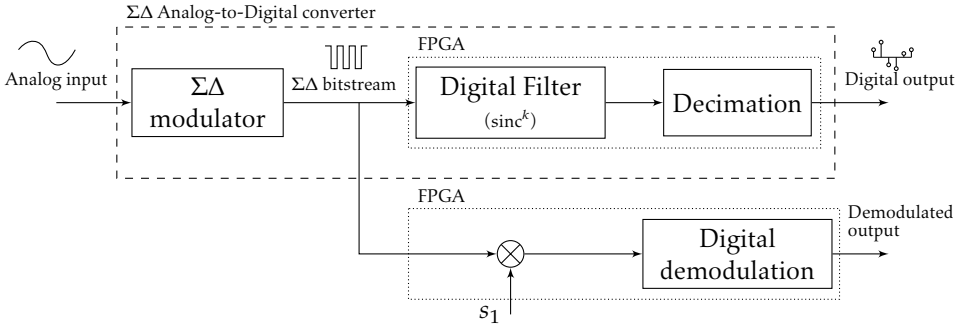

Figure 1.4: Operating principle of a ΣΔ ADC: when the ΣΔ output bitstream is available, a suitable demodulation procedure extracts the current ripple

Its feasibility inherently depends on the observability properties of the system. The PMSM observability at low speed has been studied, for example, by Glumineau and de León-Morales [GDLM05, Chapter 2], Koteich [Kot16, Chapters 10-11], and Jebai [Jeb13, Chapter 4] who took into account a magnetic saturation model. These studies state the first-order non-observability of PMSM on permanent trajectories where $\omega = 0$. However, with an additional persistent excitation (e.g. a signal injection), nonlinear observability conditions at zero speed are satisfied. This observability degeneracy at low-speed emphasizes the difficulties in deriving a sensorless method that covers the entire speed range, and the need for alternative strategies to estimate the rotor position.

1.3.2 Overview of the main sensorless strategies

Sensorless techniques can broadly be classified into two categories: *fundamental excitation* and *high-frequency excitation* strategies. While the former describes methods based on the dynamic model of the PMSM, the latter is based on the motor saliency (either inherently present for salient motors with $L_d \neq L_q$ or induced by the magnetic saturation for non-salient motors), and relies on the high-frequency harmonics, either from an external probing signal or by the PWM itself. A comprehensive treatment of sensorless strategies is covered by Glumineau and de León Morales [GDLM05], Wang et al. [WZX20].

These two strategies are not mutually exclusive, and overlap between these two are common. Hybrid control for instance, using the back EMF integration at high speed and signal injection at low speed, is more or less standard. The derivation of the position through a Luenberger observer using the additional knowledge that comes with the excitation could also be implemented for the design of an efficient sensorless observer-controller.

Notice also that sensorless estimation can also be thought the other way around, by modifying the mechanical design of the machine for the sole purpose of sensorless control [Bia+17; Fag+11]. Bianchi et al. for instance [Bia+08] have shown the benefits of particular inset PM motors (Fig. 1.1c), as the range of currents in the dq-plane where the motor stays salient (considering both saturation and cross-coupling) is larger than any traditional motor design.

1.4 Fundamental excitation strategies

1.4.1 Back EMF methods

Back Electromotive Force (EMF) methods are one of the first strategies developed for the control of electrical motors, and are still widespread in the industry for both salient and non-salient PMSM. Particularly effective beyond 10% to 20% of the nominal speed [FSO92], these strategies rely on the variations of the back EMF amplitude with respect to the rotor position due to the interaction between the stator currents and the rotor poles. An instance of implementation is proposed for example by Genduso et al. [Gen+10].

To sketch the main lines of the method, consider a non-salient PMSM, i.e. where $L_2 = 0$ (equivalently $L_d = L_q$). The voltage equation (1.1a) in the $\alpha\beta$-frame then reads

$$u_s^{\alpha\beta} = R_s i_s^{\alpha\beta} + L_1 \frac{di_s^{\alpha\beta}}{dt} + e_s^{\alpha\beta}, \qquad e_s^{\alpha\beta} := \omega\phi_m \begin{pmatrix} -\sin\theta \\ \cos\theta \end{pmatrix},$$

where $e_s^{\alpha\beta}$ is the back EMF expressed in the $\alpha\beta$-frame. With the sole knowledge of both the stator voltages and currents, one can derive the rotor position and speed by

$$\theta = \arctan\left(-\frac{e_s^\alpha}{e_s^\beta}\right), \qquad \omega = \frac{1}{\phi_m}\sqrt{e_s^{\alpha 2} + e_s^{\beta 2}}.$$

Nonetheless, at standstill or low speed, the integration of the back EMF becomes ineffective since the back-EMF amplitude and frequency weaken as the speed decreases. The method is also sensitive to the variation of the resistance during operation.

Concerning salient-poles machines, Chen et al. [Che+00b; Che+03] developed the concept of extended back EMF, transforming the salient PMSM model into an equivalent cylindrical (non-salient) pole model by a exhibiting a modified expression for the back EMF. The same derivation of the position eventually applies to the extended back EMF.

1.4.2 Observer-based techniques

A wide range of observer-based strategies have been developed to asymptotically estimate the motor state variables, and especially the position [AW06]. These so-called soft-sensors reconstruct the motor states from its measured outputs, and are particularly suited to fault-tolerant control —through the comparison of the measured quantities and their estimates— and parameters identification —with an evaluation of model parameters together with the motor states.

A non-exhaustive scan of the different approaches highlights in the first instance the nonlinear gradient observer designed by Lee et al. [Lee+10]. Later, the so-called *Bernard-Praly* observer [BP18] extended Lee's observer to estimate both the rotor position and the magnet's flux, as its variation during operation cannot be neglected. Bernard and Praly prolonged their technique to the case where the position as well as the stator resistance are unknown [BP20]. Alternatively, Henwood et al. implemented a nonlinear Luenberger observer [HMP12] to estimate the position and the magnet flux as well, along with proofs of its robustness.

Alternative strategies include sliding mode observers [GZ09; KSL11; Che+00a], Extended Kalman Filters, notably by Bolognani et al. [BOZ99; BTZ03] or Model-Reference Adaptive Systems (MRAS) [KKK03; KG06]. These model-based strategies —including back-EMF integration— nonetheless, do not get round the zero-speed observability degeneracy. This limitation often comes down to a persistent excitation condition, where the speed is assumed to be lower-bounded.

1.5 Saliency-based methods

Considered as the main category of position estimation schemes, saliency-based methods rest on the position dependency of stator phase inductances. The stator inductance fluctuation term L_2 arising in (1.4) conveys this dependency, and underpins the possibility to extract the position from this magnetic anisotropy. On the contrary to observer-based techniques, saliency-based methods cover the full speed range, including standstill, and can be applied under both steady-state and transient operations. This anisotropy is probed using the motor response to high-frequency signals that are either exogenous to the system —it is the periodic excitation, or *signal injection* technique— or endogenous, and correspond to the excitation provided by the inverter (see Fig. 1.2).

These two techniques –periodic and PWM excitation— usually come under two flavors: they are either continuous or discontinuous, whether the high-frequency signal or the PWM modifications are always present in the control law or not. Discontinuous excitation methods are often employed to reduce the eventual shortcomings of the superimposition of an HF signal. Also, they focus on the low speed range, as fundamental excitation techniques can take over at medium to high speeds. These discontinuous techniques often go hand in hand with observers to complete the information sparsity. A concise review of excitation techniques is given by Briz and Degner [Bri+04; BD11].

1.5.1 Periodic excitation – Signal injection

Signal injection consists in superimposing a high-frequency signal to the control law —by high-frequency is meant significantly higher than the fundamental excitation frequency. This injection creates ripple on the current measurements which carries information on the rotor position if properly decoded. Several types of injections can be found in the literature, depending on the shape and the injection axis.

In the following, ε denotes the injection period; on top of the fundamental excitation $u_s^{\alpha\beta}$ (resp. u_s^{dq}) is superimposed the injected signal $u_{s,\mathrm{inj}}^{\alpha\beta}$ (resp. $u_{s,\mathrm{inj}}^{dq}$)

Rotating signal injection Proposed by Jansen and Lorenz [JL95], cosine and sine waves are injected on the α and β-axis voltage. The injected voltage then reads, in the $\alpha\beta$-frame,

$$u_{s,\mathrm{inj}}^{\alpha} = u_{\mathrm{inj}} \cos \tfrac{t}{\varepsilon}, \qquad u_{s,\mathrm{inj}}^{\beta} = u_{\mathrm{inj}} \sin \tfrac{t}{\varepsilon}.$$

The derivation of the position is subsequently described, the core of the method being transposable to the other schemes. For a PMSM operated at low speed under the application of a high-frequency signal injection, both the resistive voltage drop and the back EMF can be neglected, so that the PMSM can be considered as a purely inductive load. Under these assumptions, equation (1.4) can be rewritten so that the motor response to this HF signal is

$$\frac{d\phi_{s,\text{inj}}^{\alpha\beta}}{dt} = u_{s,\text{inj}}^{\alpha\beta},$$

where the subscript x_{inj} denotes the response of x to the injection. Integrating the previous equation, and plugging it into the inverse of equation (1.3) gives the following expression for the current response

$$i_{s,\text{inj}}^{\alpha\beta} = \varepsilon \frac{u_{\text{inj}}}{L_1^2 - L_2^2} \begin{pmatrix} L_1 - L_2\cos 2\theta & -L_2 \sin 2\theta \\ -L_2 \sin 2\theta & L_1 + L_2 \cos 2\theta \end{pmatrix} \begin{pmatrix} \sin \frac{t}{\varepsilon} \\ -\cos \frac{t}{\varepsilon} \end{pmatrix}.$$

It appears that the induced current ripple introduced by the injection carries information on the rotor position if $L_2 \neq 0$. With a suitable demodulation procedure —generally a synchronous detection— the position information can be extracted from the measured current ripple.

The principal force of this technique is its stability properties, since the injection is operated on the fixed frame $\alpha\beta$. However, significant torque ripple is introduced by this type of injection.

Pulsating sinusoidal signal injection Implemented, for instance, by Ha et al. [Ha+03], Liu and Zhu [LZ14], this injection scheme consists in superimposing a sine wave to the estimated d-axis voltage. The injection in the estimated dq-frame then reads

$$u_{s,\text{inj}}^{\hat{d}} = u_{\text{inj}} \cos \frac{t}{\varepsilon}, \qquad u_{s,\text{inj}}^{\hat{q}} = 0.$$

Compared to the rotating injection, the pulsating sine wave alternative reduces the induced torque ripple. But to preserve the sinusoidal shapes of the two previous injection schemes, the injection frequency is limited by the PWM frequency. The inverter acting as a low-pass filter on its input, the sinusoid will be irremediably deformed, should its frequency be close to the PWM one.

Pulsating square signal injection In order to overcome the frequency limitation and to achieve better dynamic performances, the previous sine wave can be replaced by a square. Similar to the pulsating sinusoidal injection, this method consists in injecting a square wave on the estimated d-axis voltage. The injected signal can be written as

$$u_{s,\text{inj}}^{\hat{d}} = u_{\text{inj}}(-1)^k, \qquad u_{s,\text{inj}}^{\hat{q}} = 0$$

with k the index of the injected voltage. This injection has been studied, for example, by Yoon et al. [Yoo+09], Messali et al. [Mes+18] and Jebai [Jeb13].

One potential shortcoming of the signal injection technique —shared by the three above mentioned procedures— is the excitation of unmodeled dynamics. As noticed by Åström in the context of adaptive control [Åst83; Åst84], bringing highly-oscillating signals to the

command may give birth to instability mechanisms if the gains of the unmodeled dynamics at high frequencies are sizeable. This problem however has not prevented yet electrical engineers from exploiting this strategy for the control of electric motors, as the abundant literature may testify. Also, superimposing a fast-varying signal to the fundamental excitation is known to bring additional acoustic noise into the device. Some methods were designed to mitigate these adverse effects, including Jung's low-frequency injection [Jun+11] and Jiang's injection at pseudo-random frequencies [JS11] to spread the acoustic spectra, leading to a reduction of its perception [JS11].

1.5.2 PWM excitation

PWM excitation methods rely on the current ripples induced by the inverter commutations. These methods are based on substantial hardware requirements, such as the modification of the PWM scheme [Sch96], the use of current-derivative sensors [Gao+07], or/and of oversampling Analog-to-Digital converters [WX04]. This raises the question of the relevance of these methods for sensorless control, since it ultimately requires another probe or Analog-to-Digital converter —often expensive and coming with its own drawbacks— to replace the mechanical encoder. It amounts to replacing a mechanical sensor by another, thus increasing the circuitry complexity, only available in laboratories inherently limits the benefits of sensorless control.

INFORM method Schröedl's INFORM [Sch96] —Indirect Flux detection by Online Reactance Measurements— is among the first PWM excitation methods. The INFORM method relies on the injection of voltage pulses —or test sequences— in addition to the fundamental PWM signal to induce specific current ripple patterns. The extraction of the position is then achieved using a current derivative sensor. The method has known some recent improvements, for example by Robeischl and Schröedl [RS04], that minimizes the current deviations induced by the test sequences, but still need a specific hardware to be fully exploited. As mentioned earlier, the INFORM can naturally be combined with a medium to high speed estimation technique, such as the back EMF strategy, to cover the full range of speed. Such an hybrid implementation is for instance proposed by Schröedl et al. [SHS06].

Modifications of the PWM scheme share some of the shortcomings of signal injection: additional acoustic noise and current/torque ripple are introduced, even though recent works focused on limiting these drawbacks [DSM10]. This being said, some modifications prove to be helpful in reducing the acoustic noise. Prior to Jiang's method of pseudo-random injection frequencies, Habetler and Divan [HD91] developed the "PWM"-counterpart of this technique, as the carrier frequency of the inverter is modulated —instead of the injection itself— to reduce the noise perception of the inverter. The coupling of these two strategies —PWM modifications to guarantee the position extraction from the induced ripple on top of a randomized PWM frequency to mitigate the acoustic noise—, provided its feasibility, might be saving regarding this noise issue.

Natural switching harmonics scheme The inverter naturally creates current ripples, and the induced switching harmonics can be exploited to recover the rotor position. This idea stems from Ogasawara and Akagi [OA98], and has been extended for instance by Wang and Xu [WX04] to include new hardware equipments. This method, which is compatible with both Sinusoidal PWM and Space-Vector PWM, gets round the issues related to the modification of the PWM scheme, especially the introduction of additional acoustic noise and the output distortions. However, the two aforementioned implementations both require a high-rate, high-accuracy Analog-to-Digital converter to estimate the current derivative di/dt. The estimation based on the switching harmonics can also be achieved using Rogowski coils to measure the current derivative, as done by Gao et al. [Gao+07], though this sensor is non-standard either.

Endogenous signal injection The present thesis is in line with this natural switching harmonics PWM excitation strategy. More precisely, the PWM harmonics are exploited to recover the rotor position without neither modifying the PWM scheme, nor supplying the drive with an additional probe or ADC. Admittedly, an oversampling ADC is used to digitally encode the three-phase currents in the method developed in this manuscript. The one actually employed is nevertheless a standard Sigma-Delta modulator, which is nowadays widespread in Variable-Frequency Drives [Sor15]. It is shown in chapter 3 that the high-frequency components of the PWM input act like an *endogenous* square injection —as in the signal injection scheme. Hence, knowing an analytical expression of the induced perturbation on the measured output opens the way to the design of a suitable demodulation procedure that extracts this additional knowledge. This procedure turns out to work on the analog output (chapter 4) but also on its $\Sigma\Delta$ encoding (chapter 5) without additional hardware. This strategy is validated on numerical and experimental data; the results are eventually compiled in chapter 6.

Chapter 2

Higher-order averaging theory for exogenous signal injection

Part of this chapter —section 2.3— was published in the Proceedings of CDC 2019, under the title *Third-order virtual measurements with signal injection* [Sur+19b].

Résumé Dans ce chapitre, on s'intéresse à l'analyse par averaging des systèmes contrôlés par injection de signal exogène. La théorie générale de l'averaging à un ordre quelconque est, dans un premier temps, développée : elle met en évidence l'existence d'une transformation quasi-identité reliant l'état perturbé du système à son état moyenné. L'averaging fournit alors un théorème de comparaison permettant de confirmer la validité de cette transformation sur un temps fini, qui peut ensuite être étendue à l'infini sous certaines hypothèses de stabilité sur le système moyenné. Cette stratégie est d'abord validée à l'ordre trois sur un système SISO et contrôlé par injection de signal. Il est mis en évidence la possibilité de récupérer, au deuxième ordre, des mesures virtuelles en plus de celles du premier ordre. De plus, l'averaging à l'ordre trois analyse plus finement les effets de l'injection exogène sur l'état du système. Cette même théorie est appliquée sur un système MIMO général, en prenant en compte les spécificités du modèle d'un PMSM. Les mesures virtuelles supplémentaires obtenues à l'ordre deux s'expriment dans ce cas à l'aide d'une seconde matrice de saillance, cette dernière dépendant de la résistance stator. L'averaging à l'ordre trois est enfin validée numériquement sur le modèle linéaire d'un PMSM saillant, et illustre la possibilité d'extraire une information supplémentaire à l'aide de la mesure virtuelle d'ordre deux.

Abstract In this chapter, we focus on the averaging analysis of systems controlled thanks to exogenous signal injection. The general theory of averaging at any order is first developed: this theory highlights the existence of a near-identity transformation linking the perturbed state of the system to the averaged one. The averaging comparison theorem confirms the validity of this transformation over a finite time, which can be continued to infinity under stability assumptions on the averaged system. This strategy is first validated at the third order on a SISO system and controlled by signal injection. On top of the first-order virtual measurement, additional second-order virtual outputs are made available. The effects of the exogenous injection on the system state are also more finely described by this third-order averaging theory. Likewise, this theory is applied to a general MIMO system by taking into account the specificities of the PMSM model. In this case, the additional second-order

virtual measurements are expressed using a second saliency matrix that depends on the stator resistance. Third-order averaging is finally validated numerically on the linear model of a salient PMSM, and illustrates the possibility of extracting additional information using the second-order virtual measurement.

2.1 Introduction

Introduced by the seminal work of Krylov, Bogoliubov and Mitropolski [KB47; BM61], the averaging process found its way both in the analysis of multiscale systems and the design of control laws for nonlinear systems. Gurvits and Li for instance [GL93] apply the averaging theory to compute the behavior of nonholonomic systems when the input is a fast-varying signal in view of designing time-varying feedback control for motion planning. In the same vein, signal injection is also reminiscent of Sussman's first control solution of nonholonomic systems. In [SL93], Sussmann and Liu generate a "Lie-Bracket extension" of driftless control systems thanks to highly oscillatory sinusoids with large magnitudes. This Lie-Bracket extension being easily controllable, a control law is designed on the extended system beforehand, and a sequence of control inputs for the original system converging to the trajectory of the Lie-Bracket-extended system is computed. Likewise, Fliess et al. [Fli+92] used high-frequency control inputs on flat systems to generate a virtual control on average.

In the same vein, adding a fast-varying signal on top of the fundamental input may solve inherent observability degeneracies. This *signal injection* technique produces additional outputs, the so-called *virtual measurements*, and are read as high-frequency responses to the injection. For nonlinear systems, these induced responses may carry additional information on the system that can be exploited to overcome losses of observability. A conceptualization of the signal injection technique based on the second-order averaging theory has been developed by Jebai et al. [Jeb+16] and Combes et al. [Com+16b]. These ideas are extended in the present chapter; namely, it is proved that pushing the computations to the next order results in the acquisition of yet additional virtual measurements.

In this chapter, the applications and adaptations of the averaging theorem are based on the proof revisited by Ellison, Sáenz and Dumas [ESD90], relying on Besjes' lemma [Bes69]. They completed the original work by Bogoliubov-Mitropolski to higher order (higher than two) and refined the analysis in the periodic case, which is the natural framework for signal injection techniques. The comparison theorem as well as the extension of the different virtual measurements estimates are thoroughly detailed in this chapter, as they will require substantial modifications to suit the study of PWM-controlled systems. Indeed, in the next chapter, the obtained results will be subject to adaptation for PWM-controlled systems.

In full generality, we consider nonlinear affine systems of the form

$$\begin{aligned}\dot{\bar{x}} &= f(\bar{x}) + g(\bar{x})u,\\ y &= h(\bar{x}),\end{aligned}$$

where $\bar{x} \in \mathbb{R}^n, f : \mathbb{R}^n \to \mathbb{R}^n, g : \mathbb{R}^n \to \mathbb{R}^n \times \mathbb{R}^m, u \in \mathbb{R}^m, h : \mathbb{R}^n \to \mathbb{R}^p, m, n, p \in \mathbb{N}$. When a system is controlled using the signal injection technique, a fast-varying signal $s_0(\tau/\varepsilon)$, $\varepsilon \ll 1$,

is superimposed to the control u, so that the system reads, in the fast timescale $t = \tau/\varepsilon$,

$$\dot{x} = \varepsilon(f(x) + g(x)(u + s_0(t))).$$

The purpose of this chapter is to study the effects of such an injection on the perturbed state x and the measured output y. The averaging theory will provide a relation between the perturbed state x and the original one $\overline{x}$.

The outline of this chapter is the following: we start by recalling the fundamental results pertaining to the averaging theory —from the derivation of the estimate to its continuation to infinity—, regardless of signal injection, in section 2.2. Although no new results are given in this section, they form the theoretical backbone of the chapter, and will be subject to adaptations, especially when taking into account state discontinuities as in chapter 3. In section 2.3, this theory is applied to Single-Input Single-Output linear systems with a linear dynamics and a nonlinear output controlled thanks to signal injection. This result is subsequently generalized to nonlinear Multiple-Input Multiple-Output systems in section 2.4, with eventually numerical experiments on a PMSM.

2.2 Generic higher-order averaging theory

The ensuing results and proofs follow the description given in the reference book on the averaging by Sanders et al. [SVM05, Chapter 2]. In this section, we recall both the comparison result encapsulated in theorem 2.2 with its proof, as well as the continuation to infinity of this estimate, provided that additional stability hypothesis on the system are made. While the first subsection 2.2.1 is standard, the second subsection 2.2.2 lays out an original proof of the continuation result at the third order. Overall, this section forms the theoretical backbone of the analysis of signal injection.

2.2.1 Comparison result

In the following, we consider x solution of

$$\dot{x} = \varepsilon f^1(x,t) + \ldots + \varepsilon^k f^k(x,t) + \varepsilon^{k+1} f^{[k+1]}(x,t,\varepsilon), \qquad x(0) = a; \tag{2.1}$$

where $f^1, \ldots, f^k : (x,t) \in \mathbb{R}^n \times \mathbb{R}^+ \to \mathbb{R}^n$ and $f^{[k+1]} : (x,t,\varepsilon) \in \mathbb{R}^n \times \mathbb{R}^+ \times \mathbb{R}^+ \to \mathbb{R}^n$ are Lipschitz in x and T-periodic in t. We consider $D \subset \mathbb{R}^n$ a bounded open set D containing the initial condition a. The solution x is assumed to stay in the subset D for $0 \leq \varepsilon \leq \varepsilon_0$ and $0 \leq t \leq L/\varepsilon$, with $L, \varepsilon_0 > 0$ two constants. Throughout this chapter, the notation $\mathcal{O}$ denotes the uniform "big O" symbol of analysis, namely $f(x,t,\varepsilon) = \mathcal{O}(\varepsilon^p)$ if there exists $K > 0$ independent of x, t and ε such that $\| f(x,t,\varepsilon) \| \leq K\varepsilon^p$. This "big O" is restricted to a timescale $1/\varepsilon$ when results using this notation (e.g. theorem 2.2) are only available on this limited time interval. Likewise, the notation o denotes the uniform "small o" symbol of analysis, namely $f(x,t,\varepsilon) = o(\varepsilon^p)$ if $\lim \| f(x,t,\varepsilon) \|/\varepsilon^p = 0$ when $\varepsilon \to 0$, uniformly in x and t.

The modern approach of the averaging theory relies on the next lemma 2.1 by Besjes [Bes69]; the given proof follows the one developed in Sanders et al. [SVM05].

Lemma 2.1 (Besjes). *Assume $\varphi : (x,s) \in \mathbb{R}^n \times \mathbb{R}^+ \to \mathbb{R}^n$ is Lipschitz in x, T-periodic with zero mean in t, and bounded for all s and $x \in D$. Assume the solution x of (2.1) is defined for $0 \leq t \leq L/\varepsilon$. Then there exists $c_1 > 0$ such that*

$$\left\| \int_0^t \varphi(x(s),s)\, ds \right\| \leq c_1.$$

Proof. We start by dividing the interval $[0,t]$ into subintervals of length T, i.e. $[0,T], \ldots, [(m-1)T, mT]$ and a remainder $[mT,t]$, with $m = \lfloor t/T \rfloor$. Minkowski's inequality yields

$$\left\| \int_0^t \varphi(x(s),s)\, ds \right\| \leq \sum_{i=1}^{m} \left\| \int_{(i-1)T}^{iT} \varphi(x(s),s)\, ds \right\| + \left\| \int_{mT}^{t} \varphi(x(s),s)\, ds \right\|.$$

Each integral term for $i = 1, \ldots, m$ is estimated as follows

$$\begin{aligned} \left\| \int_{(i-1)T}^{iT} \varphi(x(s),s)\, ds \right\| &= \left\| \int_{(i-1)T}^{iT} [\varphi(x(s),s) - \varphi(x((i-1)T,s))]\, ds \right\| \\ &\leq \lambda_\varphi \int_{(i-1)T}^{iT} \| x(s) - x((i-1)T) \|\, ds \\ &\leq \lambda_\varphi \int_{(i-1)T}^{iT} c_2 \varepsilon\, ds, \end{aligned}$$

where the first equality holds since φ is T-periodic in the second argument with zero mean; the second stems from the Lipschitz inequality applied on φ, with λ_φ its Lipschitz constant, and the third holds because $\dot{x} = \mathcal{O}(\varepsilon)$. As for the estimate on the final subinterval $[mT,t]$, as φ is bounded, the integral of $\varphi(x(s),s)$ on this leftover is bounded by $T \times \| \varphi \|_\infty$. Gathering the two estimates,

$$\left\| \int_0^t \varphi(x(s),s)\, ds \right\| \leq m\lambda_\varphi c_2 T\varepsilon + T \| \varphi \|_\infty.$$

By definition of m, $mT \leq t \leq L/\varepsilon$, therefore $m\lambda_\varphi c_2 T\varepsilon + T\| \varphi \|_\infty \leq L\lambda_\varphi c_2 + T\| \varphi \|_\infty =: c_1$. □

Before stating the comparison theorem, we describe the technique to average the time-varying equation for x in order to obtain a stationary system. This derivation of the averaged equations is achieved thanks to the following so-called *near-identity transformation*,

$$\check{x} = x + \varepsilon\varphi^1(x,t) + \ldots + \varepsilon^k \varphi^k(x,t).$$

where $\varphi^1, \ldots, \varphi^k$ can be selected so that the state $\check{x}$ verifies the *full averaged* equation

$$\dot{\check{x}} = \varepsilon g^1(\check{x}) + \ldots + \varepsilon^k g^k(\check{x}) + \varepsilon^{k+1} g^{[k+1]}(\check{x}, t, \varepsilon), \tag{2.2}$$

where the function g^1 is the average $g^1(x) := \int_0^T f^1(x,s)\, ds$ of f^1 with respect to its second argument, and $g^2, \ldots, g^k, g^{[k+1]}$ depend on choice made for $\varphi^1, \ldots, \varphi^k$. The "averaged" denomination stems from the fact that $g^1, \ldots, g^k$ do not depend on the time, with only the $k+1^{th}$ power of epsilon being time-varying. The explicit computation of these g^i and φ^i is conducted in subsection 2.4.1 specifically for systems controlled using the signal injection technique. To get rid of the last instationary term $g^{[k+1]}$, consider $\bar{x}$ solution of the *truncated averaged equation*

$$\dot{\bar{x}} = \varepsilon g^1(\bar{x}) + \ldots + \varepsilon^k g^k(\bar{x}).$$

On the contrary, the full averaged equation (2.3), the truncated averaged equation is entirely stationary. The application of the shorter near-identity transformation to $\overline{x}$ defines the following auxiliary state $\tilde{x}$

$$\tilde{x} = \overline{x} + \varepsilon\varphi^1(\overline{x}, t) + \ldots + \varepsilon^{k-1}\varphi^{k-1}(\overline{x}, t). \tag{2.3}$$

With this definition, one can prove that $\tilde{x}$ satisfies an equation of the form

$$\dot{\tilde{x}} = \varepsilon f^1(\tilde{x}, t) + \ldots + \varepsilon^k(f^k(\tilde{x}, t) + h^k(\tilde{x}, t)) + \varepsilon^{k+1}\tilde{f}^{[k+1]}(\tilde{x}, t, \varepsilon),$$

where $h^k(x, t)$ is Lipschitz in x, T-periodic with zero mean in t. The practical use of the subsequent comparison theorem 2.2 is to provide a relation between the states x and $\tilde{x}$: simply put, x and $\tilde{x}$ differs by a term in ε^k on a timescale $1/\varepsilon$. In practice, x denotes the system with the injection, $\overline{x}$, the solution of the truncated averaged equation, is the original system while $\tilde{x}$ and $\tilde{x}$ are auxiliary states, mainly used to connect x and $\overline{x}$.

Theorem 2.2 (Averaging theorem)**.** *Given the systems*

$$\dot{x} = \varepsilon f^1(x, t) + \ldots + \varepsilon^k f^k(x, t) + \varepsilon^{k+1} f^{[k+1]}(x, t, \varepsilon)$$
$$\dot{\tilde{x}} = \varepsilon f^1(\tilde{x}, t) + \ldots + \varepsilon^k(f^k(\tilde{x}, t) + h^k(\tilde{x}, t)) + \varepsilon^{k+1}\tilde{f}^{[k+1]}(\tilde{x}, t, \varepsilon)$$

with f^1,...,f^k Lipschitz in x, T-periodic in t, $f^{[k+1]}$ and $\tilde{f}^{[k+1]}$ continuous, and h^k Lipschitz in x, T-periodic with zero mean in t. The two solutions x and $\tilde{x}$, starting from the same initial condition, are related, for $0 \leq \varepsilon \leq \varepsilon_0$ and $0 \leq t \leq L/\varepsilon$, by

$$x(t) = \tilde{x}(t) + \mathcal{O}(\varepsilon^k),$$

and the shorter near-identity transformation (2.3) reads

$$x(t) = \overline{x}(t) + \varepsilon\varphi^1(\overline{x}, t) + \ldots + \varepsilon^{k-1}\varphi^{k-1}(\overline{x}, t) + \mathcal{O}(\varepsilon^k).$$

Proof. Setting $J^k f(x, t) := \varepsilon f^1(x, t) + \ldots + \varepsilon^k f^k(x, t)$ and $E(t) = x(t) - \tilde{x}(t)$, we have

$$\| E(t) \| \leq \varepsilon \int_0^t \| J^k f(x, s) - J^k f(\tilde{x}, s) \| ds + \varepsilon^k \left\| \int_0^t h^k(\tilde{x}, s)\, ds \right\|$$
$$+\varepsilon^{k+1} \int_0^t \| f^{[k+1]}(x, s, \varepsilon) - \tilde{f}^{[k+1]}(\tilde{x}, s, \varepsilon) \| ds.$$

Using the Lipschitz constant λ_J of $J^k f$ for first integral term, Besjes' inequality for the second, and bounding the last term by $c_2 t$ with c_2 being the max of the last integrand on $\overline{D} \times [0, T]$, the following estimate holds

$$\| E(t) \| \leq \varepsilon\lambda_J \int_0^t \| E(s) \| ds + c_1\varepsilon^k + \varepsilon^{k+1} c_2 t.$$

The application of Gronwall's lemma [SVM05, Lemma 1.3.3] eventually yields

$$\| E(t) \| \leq \varepsilon^k \Big(\frac{c_2}{\lambda_J} + c_1 \Big) e^{\lambda_J \varepsilon t}.$$

For $0 \leq t \leq L/\varepsilon$, we thus have $\| E(t) \| \leq c_3\varepsilon^k$ with $c_3 := (c_2/\lambda_J + c_1)e^{\lambda_J L}$, i.e. $x(t) = \tilde{x}(t) + \mathcal{O}(\varepsilon^k)$. Replacing this estimate in the near-identity transformation (2.3) finally provides the comparison between the original state and the averaged one. □

2.2.2 Continuation to infinity of the averaging theorem

The averaging theorem 2.2 provides an estimate that is only available on a timescale $1/\varepsilon$, regardless of whether the solution remain bounded or not. Indeed, drift phenomena in phase or amplitude might occur as time increases, leading to a progressive deterioration of the estimate. This approximation, thereby, is very limited for the asymptotic control of dynamical systems, as it requires the approximation validity for every time t. Stability properties, however, may be saving in continuing the estimate to infinity. Namely, if the averaged system's origin is assumed to be locally exponentially stable, the result provided by theorem 2.2 can be prolonged to infinity instead of being time-restricted. This result was derived by both Eckhaus and Sanchez-Palencia for first-order averaging. Combes et al. [Com+16a] gave a version of this lemma at the second-order. Here, we adapt the proof of the lemma at the third order. By and large, this means the near-identity transformation holds without restriction on the time interval; the result is encapsulated in theorem 2.5, the skeleton of proof being easily transposable to the averaging of any order.

We start by recalling two fundamentals lemma

Lemma 2.3 (Poincaré-Lyapunov)**.** *Consider the system*

$$\dot{x} = (A + B(t))x + g(x,t), \qquad x(t_0) = x_0, \qquad t \geq t_0,$$

where x, $x_0 \in \mathbb{R}^n$; $A \in \mathbb{R}^{n\times n}$ is a constant Hurwitz matrix, i.e. with all eigenvalues having strictly negative real part, and $B : \mathbb{R}^+ \to \mathbb{R}^{n\times n}$ is a continuous matrix such that

$$\lim_{t\to+\infty} \| B(t) \| = 0.$$

The vector field is assumed to be continuous with respect to both t and x and continuously differentiable with respect to x in a neighborhood of $x = 0$; moreover, we assume

$$g(x,t) = o(\|x\|) \qquad as \ \|x\| \to 0,$$

uniformly in t. Then there exist constants C, δ, $\mu > 0$ such that if $\|x_0\| \leq \delta/C$

$$\|x(t)\| \leq C\|x_0\| e^{-\mu(t-t_0)}, \qquad t \geq t_0.$$

The basin of attraction $\{x \in \mathbb{R}; \|x\| \leq \delta/C\}$ is called the Poincaré-Lyapunov domain.

Lemma 2.4. *Consider two solutions x_1 and x_2 of the system*

$$\dot{x} = (A + B(t))x + g(x,t)$$

for which the conditions of the Poincaré-Lyapunov theorem 2.3 are satisfied. If both x_1 and x_2 start in the Poincaré-Lyapunov domain at t_0, the following estimate holds

$$\|x_1(t) - x_2(t)\| \leq C\|x_1(t_0) - x_2(t_0)\| e^{-\mu(t-t_0)}.$$

Lemmas 2.3 and 2.4 are a precise way of stating that the origin is a locally exponentially stable equilibrium point (on the Poincaré-Lyapunov domain). Under this assumption for the averaged equation, the following theorem 2.5 extends the result of theorem 2.2 —namely the comparison given by the near-identity transformation— to infinity.

Theorem 2.5 (Continuation to infinity)**.** *Consider the two systems*

$$\dot{\overline{x}} = \varepsilon g^1(\overline{x}) + \ldots + \varepsilon^k g^k(\overline{x}), \tag{2.4a}$$

$$\dot{x} = \varepsilon f^1(x,t) + \ldots + \varepsilon^k f^k(x,t) + \varepsilon^{k+1} f^{[k+1]}(x,t,\varepsilon), \tag{2.4b}$$

Assume the origin is locally exponentially stable for the averaged system (2.4a)*. Then there exists a compact neighborhood $\mathcal{V}$ of the origin and $\varepsilon_0 > 0$ such that for all $\varepsilon \in [0, \varepsilon_0)$ and $\overline{x}_0 \in \mathcal{V}$, the solution $\overline{x}(t)$ of equation* (2.4a) *starting from $\overline{x}_0$ at 0 and the solution $x(t)$ of equation* (2.4b) *starting from $x_0 = \overline{x}_0 + \varepsilon\varphi(\overline{x}_0, 0) + \varepsilon^2\varphi(\overline{x}_0, 0)$ are defined on $[0, +\infty)$ and*

$$\sup_{t\geq 0} \| x(t) - \overline{x}(t) - \varepsilon\varphi^1(\overline{x}, t) - \varepsilon^2\varphi^2(\overline{x}, t) \| \leq C\varepsilon^3,$$

where $C > 0$ is a constant independent ε, and φ^1, φ^2 are defined by the near-identity transformation between x and $\overline{x}$.

Proof. Start by choosing $\mathcal{V}$ a compact included in the Poincaré-Lyapunov set. The application of the averaging theorem 2.2 produces the desired estimate only on a timescale $1/\varepsilon$, i.e. there exist $\tilde{\varepsilon}_0 > 0$, two constants $C_1, L > 0$ independent of ε such that for $0 \leq \varepsilon \leq \tilde{\varepsilon}_0$,

$$\| x(t) - \overline{x}(t) - \varepsilon\varphi^1(\overline{x}, t) - \varepsilon^2\varphi^2(\overline{x}, t) \| \leq C_1\varepsilon^3, \qquad 0 \leq \varepsilon t \leq L. \tag{2.5}$$

Define the partition of time $I_m := \left[\frac{mL}{\varepsilon}, \frac{(m+1)L}{\varepsilon}\right]$ for $m \geq 0$, so that

$$[0, +\infty) = \bigcup_{m\in\mathbb{N}} I_m = \bigcup_{m\in\mathbb{N}} \Big[\frac{mL}{\varepsilon}, \frac{(m+1)L}{\varepsilon}\Big].$$

Define as well $\overline{x}_{(m)}$ as the solution of

$$\dot{\overline{x}} = \varepsilon g^1(\overline{x}) + \ldots + \varepsilon^k g^k(\overline{x}), \qquad \overline{x}_{(m)}(\tfrac{mL}{\varepsilon}) = x(\tfrac{mL}{\varepsilon}). \tag{2.6}$$

As the initial condition $x(mL/\varepsilon)$ for $\overline{x}_{(m)}$ is not necessarily in $\mathcal{V}$, there is no prior guarantee that each $\overline{x}_{(m)}$ stays in $\mathcal{V}$. Thus we start by proving that $x(mL/\varepsilon) \in \mathcal{V}$ for $m \in \mathbb{N}$. The two functions φ^1 and φ^2 are continuous and T-periodic in the second-argument, they are consequently bounded on $\mathcal{V} \times \mathbb{R}^+$, say by β_1 and β_2 respectively. Then estimate (2.5) reads

$$\| x(t) - \overline{x}(t) \| \leq \beta_1\varepsilon + \beta_2\varepsilon^2 + C_1\varepsilon^3, \qquad 0 \leq \varepsilon t \leq L.$$

Besides, as the origin is a locally exponentially stable equilibrium for $\overline{x}$, and $\overline{x}_0$ is in the Poincaré-Lyapunov domain, lemma 2.3 reads

$$\| \overline{x}(\tfrac{L}{\varepsilon}) \| \leq C \| \overline{x}_0 \| e^{-\mu L/\varepsilon};$$

Introducing $\delta_{\mathcal{V}} := d(0, \mathcal{V}^c) > 0$ the distance between the origin and the complementary $\mathcal{V}^c$ of $\mathcal{V}$ (which is positive since $\mathcal{V}$ is a neighborhood of the origin), one can select $\varepsilon_0 < \tilde{\varepsilon}_0$ such that

$$C \| \overline{x}_0 \| e^{-\mu L/\varepsilon_0} + \beta_1\varepsilon_0^2 + \beta_2\varepsilon_0^2 + C_1\varepsilon_0^3 < \delta_{\mathcal{V}}.$$

i.e. $\| x(L/\varepsilon) \| < \delta_{\mathcal{V}}$, which means $x(L/\varepsilon) \in \mathcal{V}$. This argument can easily be reproduced for any $m \in \mathbb{N}$ so that $x(mL/\varepsilon) \in \mathcal{V}$; the same choice of ε_0 being valid for any m. Therefore, $\overline{x}_{(m)}$ also stays in $\mathcal{V}$.

Now define ψ as follows

$$\psi(x,t) := x + \varepsilon\varphi^1(x,t) + \varepsilon^2\varphi^2(x,t).$$

If f and g are smooth enough, as φ^1 and φ^2 inherits the regularity from these two vector fields, they are at least continuously differentiable. In particular, they are Lipschitz on the compact subset $\mathcal{V}$, and we respectively write $\lambda_{1,\mathcal{V}}$, $\lambda_{2,\mathcal{V}}$ their Lipschitz constant on $\mathcal{V}$. By Poincaré-Lyapunov lemma 2.3, $\bar{x}$ stays in $\mathcal{V}$, so since ψ is Lipschitz in x, the following inequality holds

$$\| \psi(\bar{x}, t) - \psi(\bar{x}_{(m)}, t) \| \leq (1 + \varepsilon\lambda_{1,\mathcal{V}} + \varepsilon^2\lambda_{2,\mathcal{V}}) \| \bar{x} - \bar{x}_{(m)} \|, \qquad t \in I_m.$$

Taking the sup on t of the former equation then yields

$$\| \psi(\bar{x}, \cdot) - \psi(\bar{x}_{(m)}, \cdot) \|_{I_m} \leq (1 + \lambda_{1,\mathcal{V}} + \varepsilon^2\lambda_{2,\mathcal{V}}) \| \bar{x} - \bar{x}_{(m)} \|_{I_m}, \tag{2.7}$$

where $\| \cdot \|_{I_m} := \sup_{t \in I_m} \| \cdot \|$. Owing to the averaging theorem, the estimate (2.5) holds on every interval I_m, namely

$$\| x(t) - \bar{x}_{(m)} - \varepsilon\varphi^2(\bar{x}_{(m)}, t) - \varepsilon^2\varphi^2(\bar{x}_{(m)}, t) \| \leq C_1\varepsilon^3, \qquad t \in I_m.$$

Using the expression for ψ and taking the sup yields

$$\| x - \psi(\bar{x}_{(m)}, \cdot) \|_{I_m} \leq C_1\varepsilon^3. \tag{2.8}$$

By lemma 2.4, there exist two constants $C_2, \mu > 0$ such that for $t \in I_m$

$$\begin{aligned} \| \bar{x}(t) - \bar{x}_{(m)}(t) \| &\leq C_2 \left\| \bar{x}\left(\tfrac{mL}{\varepsilon}\right) - \bar{x}_{(m)}\left(\tfrac{mL}{\varepsilon}\right) \right\| e^{-\mu(t - mL/\varepsilon)} \\ &\leq C_2 \| \bar{x} - \bar{x}_{(m)} \|_{I_{m-1}} e^{-\mu L/\varepsilon}. \end{aligned}$$

Again, taking the sup on $t \in I_m$ yields

$$\| \bar{x} - \bar{x}_{(m)} \|_{I_m} \leq C_2 \| x_1 - \bar{x}_{(m)} \|_{I_{m-1}} e^{-\mu L/\varepsilon}. \tag{2.9}$$

The error between $x(t)$ and its second-order averaged approximation $\psi(\bar{x}, t)$ can be estimated as follows

$$\begin{aligned} \| x - \psi(\bar{x}, \cdot) \|_{I_m} &\leq \| x - \psi(\bar{x}_{(m)}, \cdot) \|_{I_m} + \| \psi(\bar{x}_{(m)}, \cdot) - \psi(\bar{x}, \cdot) \|_{I_m} \\ &\leq C_1\varepsilon^3 + (1 + \varepsilon\lambda_{1,\mathcal{V}} + \varepsilon^2\lambda_{2,\mathcal{V}}) \| \bar{x}_{(m)} - \bar{x} \|_{I_m} \\ &\leq C_1\varepsilon^3 + C_2(1 + \varepsilon\lambda_{1,\mathcal{V}} + \varepsilon^2\lambda_{2,\mathcal{V}}) \| \bar{x}_{(m)} - \bar{x} \|_{I_{m-1}} e^{-\mu L/\varepsilon}. \end{aligned}$$

The first inequality is obtained by Minkowski's inequality; the second bound comes from both (2.8) and (2.7) and the third bound follows from the exponential decay rate (2.9)

$$\lim_{\varepsilon \to 0} C_2(1 + \varepsilon\lambda_{1,\mathcal{V}} + \varepsilon^2\lambda_{2,\mathcal{V}}) e^{-\mu L/\varepsilon} = 0,$$

therefore for any $\kappa < 1$, there exists $\varepsilon_0 > 0$ such that $1 + \varepsilon\lambda_{1,\mathcal{V}} + \varepsilon^2\lambda_{2,\mathcal{V}} \leq \kappa$ for $\varepsilon \leq \varepsilon_0$.

$$\begin{aligned} \| x - \psi(\bar{x}, \cdot) \|_{I_m} &\leq C_1\varepsilon^3 + \kappa \| \bar{x}_{(m)} - \bar{x} \|_{I_{m-1}} \leq C_1\varepsilon^3 \sum_{j=0}^{m-1} \kappa + \kappa^m \| \bar{x}_{(m)} - \bar{x} \|_{I_0} \\ &\leq \frac{C_1}{1 - \kappa}\varepsilon^3. \end{aligned}$$

since by lemma 2.4, $\| \bar{x}_{(m)} - \bar{x} \|_{I_0} \leq \| \bar{x}_{(m)}(0) - \bar{x}(0) \| = 0$, the two states x and $\bar{x}$ sharing the same initial condition on 0. Setting $C := C_1/(1 - \kappa)$ eventually concludes the proof. □

This proof can easily be transposed to the averaging at any order. Indeed, it suffices to change the expression for ψ by the k^{th}-order near-identity transformation.

2.3 Second-order virtual measurements for linear dynamics

In this section, the application of the averaging theory to derive two additional virtual-meausrements is detailed. In order to be self-contained, this section also presents an ad hoc recovery procedure of these virtual measurements, based on Gram-Schmidt's orthogonalization process. The demodulation will be generalized to any multiplexed analog signals, and is thoroughly detailed in chapter 4.

2.3.1 Context

Signal injection is a control technique that has become widely used for the "sensorless" control of electric motors at low velocity since its introduction by [JL95; CL98] ("sensorless" meaning only the currents are measured, but neither the rotor position nor its velocity). Its consists in superimposing a fast-varying signal on the control, which creates some small ripple in the measured currents; this ripple contains information about the rotor position that can be used to suitably control the motor. At first sight, the method might seem peculiar to electric motors, with a usually somewhat heuristic analysis. The essence of the method was then conceptualized in [Com+16a] as the creation of new "virtual measurements" which can be extracted from the actual measured output, hence providing means to overcome observability degeneracies; the main ingredient of the analysis is second-order averaging, following the ideas introduced in [Jeb+16]. Developments following these ideas, with an application to magnetic levitation systems, can be found in [YOZ18; Yi+19].

The purpose of this section is to extend [Com+16a] by showing that more virtual measurements can be produced with a finer analysis of the ripple thanks to third-order averaging. To keep the computations as simple as possible and focus on the important ideas, we restrict to Single-Input Single-Output systems with a linear dynamics; nonlinear Multiple-Input Multiple-Output systems could nevertheless be addressed along the same lines (see section 2.4). More precisely, consider the system

$$\dot{x} = Ax + Bu \tag{2.10a}$$
$$y = h(x), \tag{2.10b}$$

where (x, y, u) belongs to a compact subset of $\mathbb{R}^n \times \mathbb{R} \times \mathbb{R}$, and A, B are constant matrices; the measured output $y = h(x)$ is assumed smooth enough (i.e. at least $\mathcal{C}^3$). We show that by superimposing on the control u a periodic signal with small period ε, we can make available the so-called virtual measurements

$$Y_1 = H_1(x) := \varepsilon h'(x)B \tag{2.11a}$$
$$Y_2 = H_2(x) := \frac{\varepsilon^2}{2} h''(x)(B,B) = \frac{\varepsilon^2}{2} B^T h''(x)B \tag{2.11b}$$
$$Y_3 = H_3(x) := \varepsilon^2 h'(x)AB, \tag{2.11c}$$

which can be used in addition to $Y_0 = H_0(x) := h(x)$ to control (2.10a). The contribution with respect to [Com+16a] is threefold:

— an analysis of the output ripple by third-order averaging, with a simpler derivation (subection 2.3.2)

— a much more elaborated procedure to extract the virtual measurements from the output ripple (subsection 2.3.3)

— a numerical simulation demonstrating the method is indeed effective, even though the output ripple may be very small and buried into noise (subsection 2.3.4).

2.3.2 Averaging theory

Assume we have designed a suitable control law

$$u = \alpha(\eta, Y, t)$$
$$\dot{\eta} = a(\eta, Y, t),$$

where $\eta \in \mathbb{R}^q$ and Y is the vector (Y_0, Y_1, Y_2, Y_3). In other words, the closed-loop system

$$\dot{\overline{x}} = A\overline{x} + B\alpha(\overline{\eta}, H(\overline{x}), t) \tag{2.12a}$$
$$\dot{\overline{\eta}} = a(\overline{\eta}, H(\overline{x}), t) \tag{2.12b}$$

has the desired exponentially stable behaviour, where $H := (H_0, H_1, H_2, H_3)$. We have changed the notation of the state to $(\overline{x}, \overline{\eta})$, so as to distinguish between the solutions of (2.12) and of (2.14) below. Now consider the modified control law

$$u = \alpha(\eta, \overline{H}(x), t) + s_0\left(\tfrac{t}{\varepsilon}\right) \tag{2.13a}$$
$$\dot{\eta} = a(\eta, \overline{H}(x), t) \tag{2.13b}$$
$$\overline{H}(x) = H(x - \varepsilon B s_1\left(\tfrac{t}{\varepsilon}\right) - \varepsilon^2 AB s_2\left(\tfrac{t}{\varepsilon}\right)) + \mathcal{O}(\varepsilon^3), \tag{2.13c}$$

where s_0 is a 1-periodic function with zero mean, s_1 is the primitive of s_0 with zero mean, and s_2 the primitive of s_1 with zero mean (notice s_1 and s_2 are also 1-periodic). The closed-loop system then reads

$$\dot{x} = Ax + B\alpha(\eta, \overline{H}(x), t) + Bs_0\left(\tfrac{t}{\varepsilon}\right) \tag{2.14a}$$
$$\dot{\eta} = a(\eta, \overline{H}(x), t) \tag{2.14b}$$
$$\overline{H}(x) = H(x - \varepsilon B s_1\left(\tfrac{t}{\varepsilon}\right) - \varepsilon^2 AB s_2\left(\tfrac{t}{\varepsilon}\right)) + \mathcal{O}(\varepsilon^3). \tag{2.14c}$$

Theorem 2.6. *Let $(x(t), \eta(t))$ and $(\overline{x}(t), \overline{\eta}(t))$ be respectively the solutions of (2.14) and (2.12), with initial condition $(x(0), \eta(0))$ and $(\overline{x}(0), \overline{\eta}(0)) = (x(0) - \varepsilon B s_1(0) - \varepsilon^2 AB s_2(0), \eta(0))$. Then for all $t \geq 0$,*

$$x(t) = \overline{x}(t) + \varepsilon B s_1\left(\tfrac{t}{\varepsilon}\right) + \varepsilon^2 AB s_2\left(\tfrac{t}{\varepsilon}\right) + \mathcal{O}(\varepsilon^3) \tag{2.15a}$$
$$\eta(t) = \overline{\eta}(t) + \mathcal{O}(\varepsilon^3) \tag{2.15b}$$
$$y(t) = H_0(\overline{x}(t)) + H_1(\overline{x}(t)) s_1\left(\tfrac{t}{\varepsilon}\right) + H_2(\overline{x}(t)) s_1^2\left(\tfrac{t}{\varepsilon}\right) + H_3(\overline{x}(t)) s_2\left(\tfrac{t}{\varepsilon}\right) + \mathcal{O}(\varepsilon^3). \tag{2.15c}$$

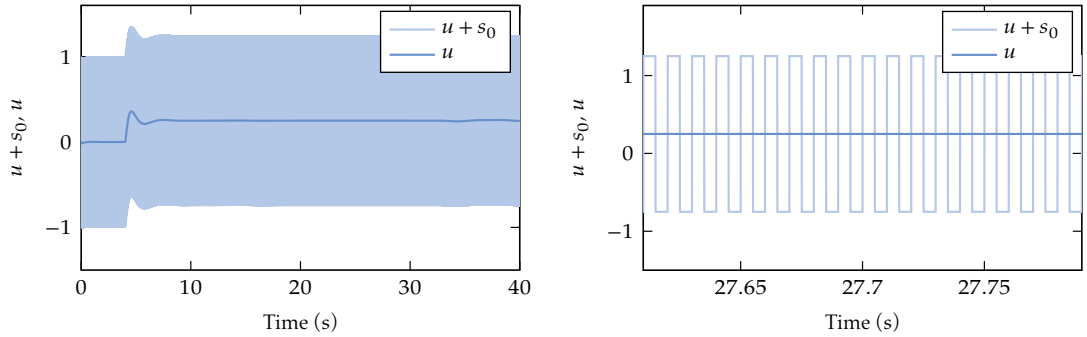

(a) Full view (b) Zoom

Figure 2.1: Control inputs u and $u + s_0$. Full view (left), zoom (right).

Proof. The proof is an application of higher-order averaging for differential equations (theorem 2.2), with slow time dependance [SVM05, section 3.3]: consider the two equations

$$\begin{aligned}\frac{d\overline{X}}{d\sigma}(\sigma) &= \varepsilon f^1(\overline{X}, \varepsilon\sigma, \sigma) + \mathcal{O}(\varepsilon^4)\\ \frac{d\widetilde{X}}{d\sigma}(\sigma) &= \varepsilon f^1(\widetilde{X}, \varepsilon\sigma, \sigma) + \varepsilon^3 k^3(\widetilde{X}, \varepsilon\sigma, \sigma) + \mathcal{O}(\varepsilon^4),\end{aligned}$$

where f^1, k^3 are T-periodic with respect to their third variable and k^3 has zero-mean with respect to its third variable; according to theorem 2.2, the solutions of these two equations starting from the same initial condition are related by

$$\widetilde{X}(\sigma) = \overline{X}(\sigma) + \mathcal{O}(\varepsilon^3) \tag{2.16}$$

on the timescale $1/\varepsilon$. It is possible to extend this relation to an infinite timescale by the continuation theorem 2.5, provided that the averaged system has an exponentially stable equilibrium, and that the initial condition is in a compact subset of the region of attraction of this equilibrium. In our case, we first rewrite (2.14) in the fast timescale $\sigma := t/\varepsilon$

$$\frac{dx}{d\sigma} = \varepsilon\left[Ax + B\alpha(\eta, \overline{H}(x), \varepsilon\sigma) + Bs_0(\sigma)\right] \tag{2.17a}$$

$$\frac{d\eta}{d\sigma} = \varepsilon a(\eta, \overline{H}(x), \varepsilon\sigma). \tag{2.17b}$$

We introduce the new coordinates $(\tilde{x}, \tilde{\eta})$ such that

$$\begin{bmatrix}\tilde{x}\\ \tilde{\eta}\end{bmatrix} = \begin{bmatrix}x\\ \eta\end{bmatrix} - \varepsilon\begin{bmatrix}Bs_1(\sigma)\\ 0\end{bmatrix} - \varepsilon^2\begin{bmatrix}ABs_2(\sigma)\\ 0\end{bmatrix}. \tag{2.18}$$

Notice (2.14c) simply reads

$$\overline{H}(x) = H(\tilde{x}) + \mathcal{O}(\varepsilon^3).$$

Differentiating with respect to σ and expanding to third order yields the system in the new

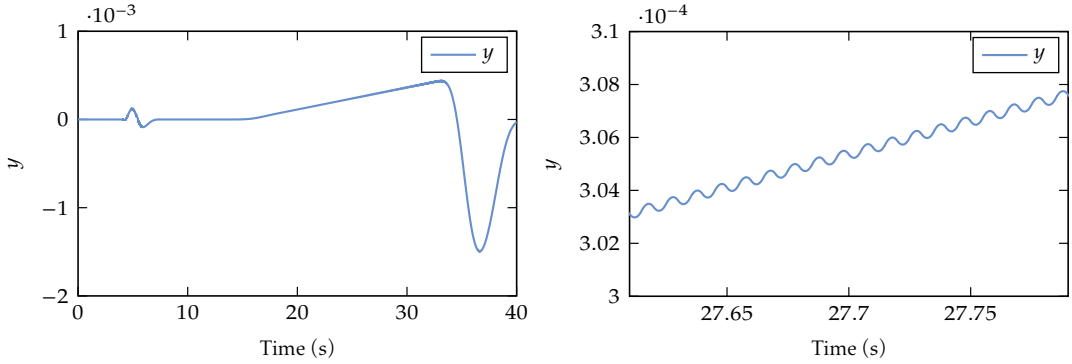

(a) Full view (b) Zoom

Figure 2.2: Measured output y. Full view (left), zoom (right).

coordinates

$$\frac{d\tilde{x}}{d\sigma} = \varepsilon\left[A\tilde{x} + B\alpha(\tilde{\eta}, H(\tilde{x}), \varepsilon\sigma)\right] + \varepsilon^3 A^2 B s_2(\sigma) + \mathcal{O}(\varepsilon^4) \tag{2.19a}$$

$$\frac{d\tilde{\eta}}{d\sigma} = \varepsilon a(\tilde{\eta}, H(\tilde{x}), \varepsilon\sigma) + \mathcal{O}(\varepsilon^4). \tag{2.19b}$$

By (2.16), we then get

$$\tilde{x} = \overline{x} + \mathcal{O}(\varepsilon^3)$$
$$\tilde{\eta} = \overline{\eta} + \mathcal{O}(\varepsilon^3).$$

Replacing $(\tilde{x}, \tilde{\eta})$ by (x, η) using transformation (2.18) in the two previous equations, we have the desired result

$$x = \overline{x} + \varepsilon B s_1(\sigma) + \varepsilon^2 A B s_2(\sigma) + \mathcal{O}(\varepsilon^3)$$
$$\eta = \overline{\eta} + \mathcal{O}(\varepsilon^3).$$

Plugging this expression for x in $y = h(x)$ and Taylor expanding to second order yields (2.15c), thus concluding the proof. □

The practical use of the theorem is the following. Assume we can compute a third-order estimate $\widehat{Y}$ of Y from the knowledge of only the actual measurement y. Using the relation between x and $\overline{x}$, we have

$$\widehat{Y} = H(\overline{x}) + \mathcal{O}(\varepsilon^3) = \overline{H}(x) + \mathcal{O}(\varepsilon^3).$$

The control law with signal injection

$$u = \alpha(\eta, \widehat{Y}, t) + s_0\left(\tfrac{t}{\varepsilon}\right) \tag{2.20a}$$

$$\dot{\eta} = a(\eta, \widehat{Y}, t) \tag{2.20b}$$

is then practically implementable and will control (2.10) as desired in average.

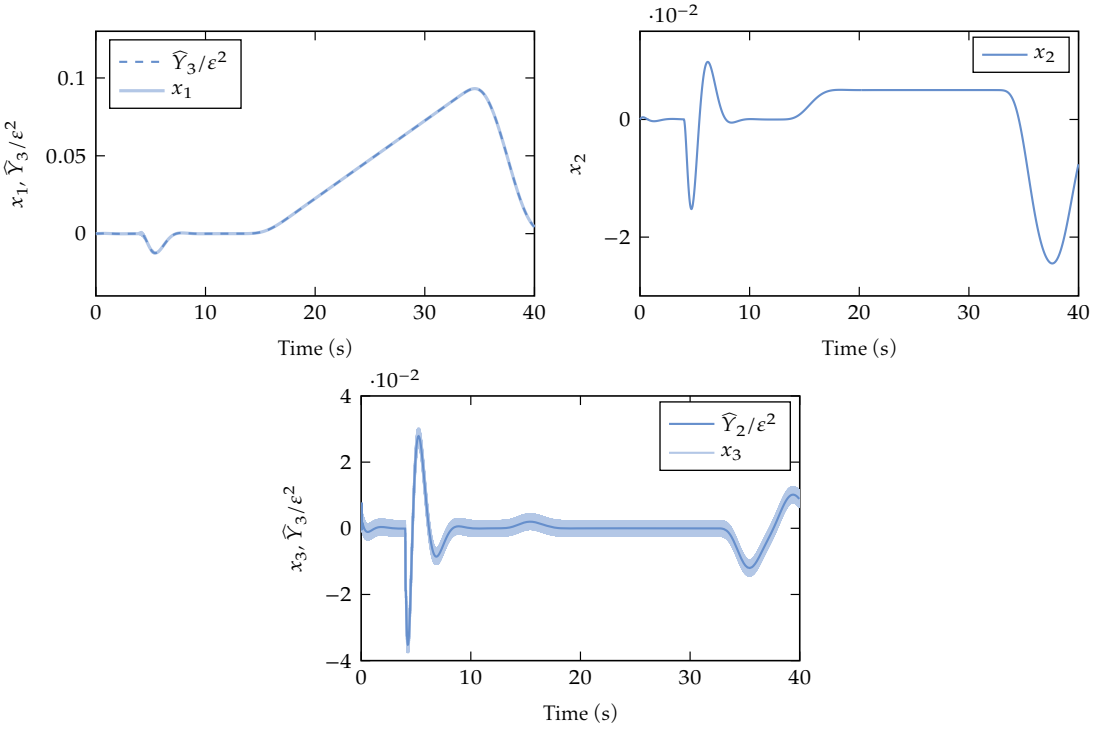

Figure 2.3: State x_1 and estimate $\widehat{Y}_3$ (top left); x_2 (top right); x_3 and estimate $\widehat{Y}_2$ (middle).

2.3.3 Demodulation of the virtual measurements

In this subsection, we show how to estimate the virtual measurements from the ripple in the actual measurement. Consider the composite signal

$$y(t) = Y_0(t) + Y_1(t)s_1\left(\tfrac{t}{\varepsilon}\right) + Y_2(t)s_1^2\left(\tfrac{t}{\varepsilon}\right) + Y_3(t)s_2\left(\tfrac{t}{\varepsilon}\right) + \mathcal{O}(\varepsilon^3),$$

where $Y_0, \dots, Y_3$ are in $\mathcal{C}^3$ and $Y_0^{(3)}, \dots, Y_3^{(3)}$ are bounded. Theorem 2.10 below states that $Y_0, \dots, Y_3$ can be estimated at third order thanks to periodic low-pass filters.

Decomposition on an orthogonal basis

We first rewrite y as a decomposition on the periodic orthogonal signals $(1, s_1, s_2, S_1)$,

$$y(t) = \widetilde{Y}_0(t) + \widetilde{Y}_1(t)s_1\left(\tfrac{t}{\varepsilon}\right) + \widetilde{Y}_2(t)S_1\left(\tfrac{t}{\varepsilon}\right) + \widetilde{Y}_3(t)s_2\left(\tfrac{t}{\varepsilon}\right) + \mathcal{O}(\varepsilon^3). \tag{2.21}$$

The signals $1, s_1, s_2$ are orthogonal (for the scalar product $\langle f, g\rangle = \int_0^1 f(\tau)g(\tau)d\tau$); indeed, $\langle 1, s_1\rangle = \langle 1, s_2\rangle = 0$ since s_1, s_2 have zero mean, and $\langle s_1, s_2\rangle = \frac{1}{2}\int_0^1 (s_1^2)'(\sigma)d\sigma = 0$. S_1 is then obtained from s_1^2 by Gram-Schmidt orthogonalization,

$$S_1(t) := s_1^2(t) - \overline{s_1^2} - \frac{\langle s_1^2, s_1\rangle}{\overline{s_1^2}}s_1(t) - \frac{\langle s_1^2, s_2\rangle}{\overline{s_2^2}}s_2(t).$$

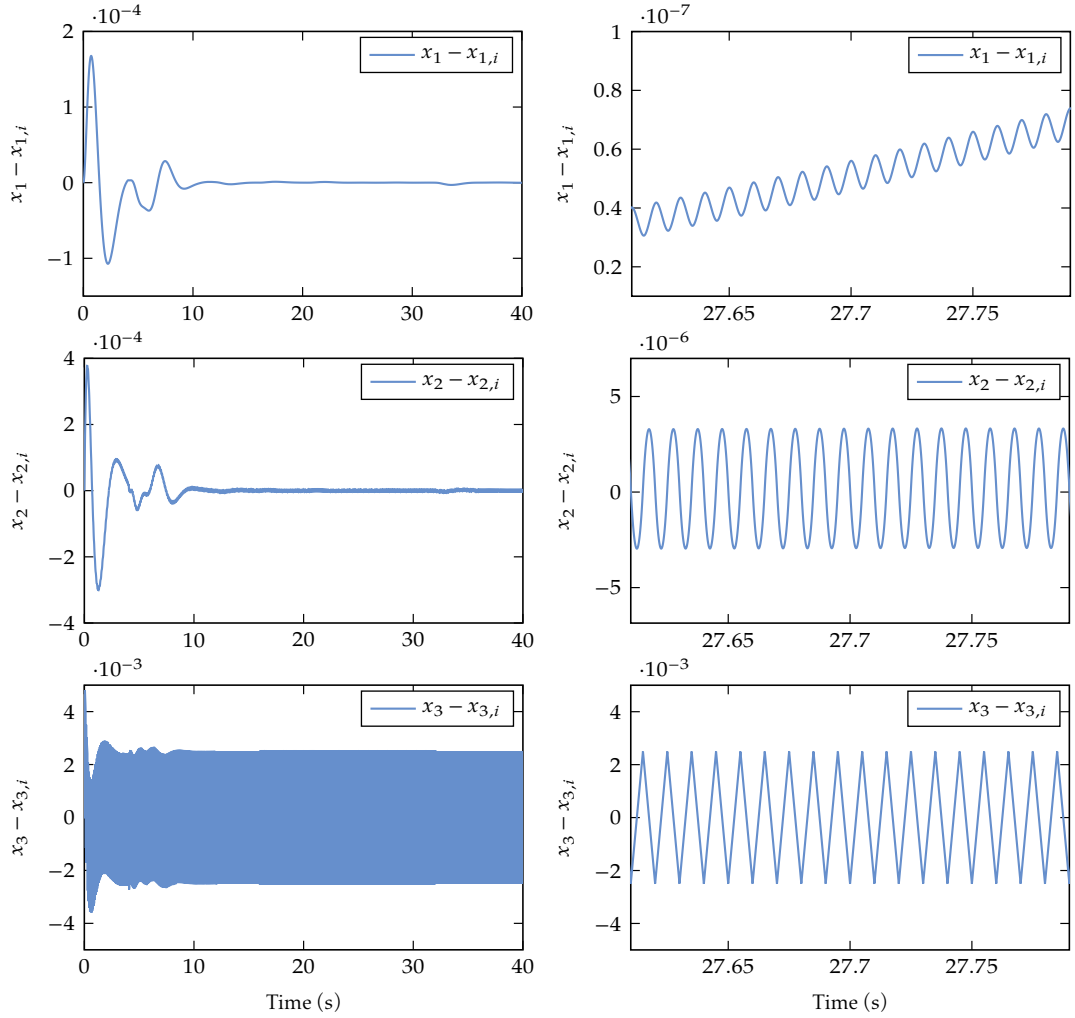

Figure 2.4: Difference $x - x_i$ between x (controlled using the virtual measurements) and x_i (controlled using the actual state x). Full view (left), zoom (right).

As a consequence, the "coordinates" $\widetilde{Y}_i$ are

$$\widetilde{Y}_0(t) = Y_0(t) + \overline{s_1^2} Y_2(t), \qquad \widetilde{Y}_1(t) = Y_1(t) + \frac{\langle s_1^2, s_1 \rangle}{\overline{s_1^2}} Y_2(t),$$
$$\widetilde{Y}_2(t) = Y_2(t), \qquad \widetilde{Y}_3(t) = Y_3(t) + \frac{\langle s_1^2, s_2 \rangle}{\overline{s_2^2}} Y_2(t).$$

Extraction of the Y_i using iterated moving averages

We now turn to the design of the demodulating filters, which are based on iterated moving averages of the form

$$M^1(\varphi)(t) := \frac{1}{\varepsilon} \int_{t-\varepsilon}^{t} \varphi(\sigma) d\sigma, \qquad M^k(\varphi)(t) := \frac{1}{\varepsilon} \int_{t-\varepsilon}^{t} M_\varphi^{k-1}(\sigma) d\sigma, \qquad k \geq 2.$$

We first recall a basic result on finite differences.

Lemma 2.7. *Let φ be C^3 with $\varphi^{(3)}$ bounded. Then the p^{th}-order backward difference*

$$\Delta^p \varphi(t) := \sum_{i=0}^{p} \binom{p}{i} (-1)^i \varphi(t - i\varepsilon)$$

satisfies

$$\| \Delta^p \varphi^{(3-p)} \|_\infty \lesssim \varepsilon^p \| \varphi^{(3)} \|_\infty, \qquad p = 0, \dots, 3;$$

$\varphi \lesssim \psi$ means there exists $K > 0$ such that $\varphi \leq K\psi$.

Proof. For simplicity, we just prove as an example the case $p = 2$. By the Taylor-Lagrange formula, there exists $t_1 \in [t - \varepsilon, t]$ and $t_2 \in [t - 2\varepsilon, t]$ such that,

$$\begin{aligned} \varphi'(t - \varepsilon) &= \varphi'(t) - \varepsilon \varphi''(t) + \frac{\varepsilon^2}{2} \varphi^{(3)}(t_1) \\ \varphi'(t - 2\varepsilon) &= \varphi'(t) - 2\varepsilon \varphi''(t) + 2\varepsilon^2 \varphi^{(3)}(t_2). \end{aligned}$$

Therefore,

$$\Delta^p \varphi'(t) = -\varepsilon^2 \varphi^{(3)}(t_1) + 2\varepsilon^2 \varphi^{(3)}(t_2);$$

hence the desired inequality

$$\| \Delta^p \varphi' \|_\infty \leq 3\varepsilon^2 \| \varphi^{(3)} \|_\infty. \qquad \square$$

This lemma is used to prove the following result, which has an important role on the filter design.

Lemma 2.8. *Let φ be C^3 with $\varphi^{(3)}$ bounded, and ζ be a 1-periodic function with zero mean. Then, the following estimate holds*

$$\| M^3(\varphi \check{\zeta}) \|_\infty \lesssim \varepsilon^3 \| \varphi^{(3)} \|_\infty \| \zeta^{(-3)} \|_\infty,$$

with $\zeta^{-(j+1)}$ the zero-mean primitive of $\zeta^{(-j)}$ (where $\zeta^{(0)} = \zeta$), and $\check{\zeta}(t) := \zeta(\frac{t}{\varepsilon})$.

Proof. Integrating by parts three times and using the periodicity of ζ_j gives

$$\begin{aligned} M(\varphi \check{\zeta})(t) = \Delta^1 \varphi(t) \zeta^{(-1)}\left(\tfrac{t}{\varepsilon}\right) - \varepsilon \Delta^1 \varphi'(t) \zeta^{(-2)}\left(\tfrac{t}{\varepsilon}\right) + \varepsilon^2 \Delta^1 \varphi''(t) \zeta^{(-3)}\left(\tfrac{t}{\varepsilon}\right) \\ -\varepsilon^2 \int_{t-\varepsilon}^{t} \varphi^{(3)}(\sigma) \zeta^{(-3)}\left(\tfrac{\sigma}{\varepsilon}\right) d\sigma. \end{aligned} \tag{2.22}$$

We now dominate the last two terms: clearly,

$$\left| \varepsilon^2 \int_{t-\varepsilon}^{t} \varphi^{(3)}(\sigma) \zeta^{(-3)}\left(\tfrac{\sigma}{\varepsilon}\right) \right| \leq \varepsilon^3 \| \varphi^{(3)} \|_\infty \| \zeta^{(-3)} \|_\infty;$$

lemma 2.7 applied to the third term yields

$$\left| \varepsilon^2 \Delta^1 \varphi''(t) \zeta^{(-3)}\left(\tfrac{t}{\varepsilon}\right) \right| \lesssim \varepsilon^3 \| \varphi^{(3)} \|_\infty \| \zeta^{(-3)} \|_\infty.$$

Notice that if $\|f\|_\infty \leq K$ then $\| M^p(f) \|_\infty \leq K$; therefore applying M^1 and M^2 to these two terms yields the same bounds. Consider next the second term of (2.22); its moving average is

$$-\varepsilon M\Big((\Delta^1 \varphi') \check{\zeta}^{(-2)} \Big)(t) = -\varepsilon \Delta^2 \varphi'(t) \zeta^{(-3)}\left(\tfrac{t}{\varepsilon}\right) + \varepsilon \int_{t-\varepsilon}^{t} \Delta^1 \varphi''(\sigma) \zeta^{(-3)}\left(\tfrac{\sigma}{\varepsilon}\right) d\sigma.$$

Using again lemma 2.7, the two terms of the right-hand side are similarly dominated by $\varepsilon^3 \| \varphi^{(3)} \|_\infty \| \zeta^{(-3)} \|_\infty$, and so are their moving averages.

Finally, consider the first term of (2.22). Its moving average is

$$M\Big((\Delta^1\varphi)\check{\zeta}^{(-1)}\Big)(t) = \Delta^2\varphi(t)\zeta^{(-2)}\left(\tfrac{t}{\varepsilon}\right) - \varepsilon\Delta^2\varphi'(t)\zeta^{(-3)}\left(\tfrac{t}{\varepsilon}\right) + \varepsilon\int_{t-\varepsilon}^{t}\Delta^1\varphi''(\sigma)\zeta^{(-3)}\left(\tfrac{\sigma}{\varepsilon}\right)d\sigma.$$

Likewise, by lemma 2.7, the last two terms of the right-hand side are also dominated by $\varepsilon^3 \| \varphi^{(3)} \|_\infty \| \zeta^{(-3)} \|_\infty$, and so are their moving average; as for the first term, integrating by parts its moving average yields

$$M\Big((\Delta^2\varphi)\check{\zeta}^{(-2)}\Big)(t) = \Delta^3\varphi(t)\zeta^{(-3)}\left(\tfrac{t}{\varepsilon}\right) - \int_{t-\varepsilon}^{t}\Delta^2\varphi'(\sigma)\zeta^{(-3)}\left(\tfrac{\sigma}{\varepsilon}\right)d\sigma.$$

Using lemma 2.7 to the right-hand side ends the proof. □

We then recover the $\widetilde{Y}_i$ from a suitable linear combination of shifted thrice-iterated moving averages $M^3(y)$ thanks to the following lemma.

Lemma 2.9. *Let φ be $\mathcal{C}^3$ with $\varphi^{(3)}$ bounded. Define*

$$P[\varphi](t) := \frac{17}{4}M^3(\varphi)(t) - 5M^3(\varphi)(t-\varepsilon) + \frac{7}{4}M^3(\varphi)(t-2\varepsilon).$$

Then the operator P is the identity up to third order,

$$P[\varphi](t) = \varphi(t) + \mathcal{O}(\varepsilon^3).$$

Proof. Again, consider first a single moving average of φ. Doing a change of variable in the integral and computing the Taylor expansion of φ gives

$$\begin{aligned}\frac{1}{\varepsilon}\int_{t-\varepsilon}^{t}\varphi(\sigma)d\sigma = \frac{1}{\varepsilon}\int_0^{\varepsilon}\varphi(t-\sigma)d\sigma &= \frac{1}{\varepsilon}\int_0^{\varepsilon}\Big[\varphi(t) - \sigma\varphi'(t) + \frac{\sigma^2}{2}\varphi''(t)\Big]d\sigma + \mathcal{O}(\varepsilon^3)\\ &= \varphi(t) - \frac{\varepsilon}{2}\varphi'(t) + \frac{\varepsilon^2}{6}\varphi''(t) + \mathcal{O}(\varepsilon^3).\end{aligned}$$

We iterate the previous calculations to get the expressions of $M^2(\varphi)$ and $M^3(\varphi)$,

$$\begin{aligned}M^2(\varphi)(t) &= M(\varphi)(t) - \frac{\varepsilon}{2}M(\varphi')(t) + \frac{\varepsilon^2}{6}M(\varphi'')(t) = \varphi(t) - \varepsilon\varphi'(t) + \frac{7}{12}\varphi''(t) + \mathcal{O}(\varepsilon^3),\\ M^3(\varphi)(t) &= \varphi(t) - \frac{3}{2}\varepsilon\varphi'(t) + \frac{15}{12}\varepsilon^2\varphi''(t) + \mathcal{O}(\varepsilon^3).\end{aligned}$$

Finally, we compute the shifted triple moving average for $k = 0, 1, 2$. This yields

$$\begin{pmatrix} M^3(\varphi)(t) \\ M^3(\varphi)(t-\varepsilon) \\ M^3(\varphi)(t-2\varepsilon)\end{pmatrix} = \underbrace{\begin{pmatrix} 1 & -\frac{3}{2} & \frac{15}{12} \\ 1 & -\frac{5}{2} & \frac{39}{12} \\ 1 & -\frac{7}{2} & \frac{75}{12}\end{pmatrix}}_{:=\mathfrak{A}}\begin{pmatrix} \varphi(t) \\ \varepsilon\varphi'(t) \\ \varepsilon^2\varphi''(t)\end{pmatrix} + \mathcal{O}(\varepsilon^3).$$

Let $\alpha = \begin{pmatrix}1 & 0 & 0\end{pmatrix}\mathfrak{A}^{-1} = \begin{pmatrix}17/4 & -5 & 7/4\end{pmatrix}$. This yields the desired conclusion

$$P[\varphi](t) = \alpha\begin{pmatrix}M^3(\varphi)(t) & M^3(\varphi)(t-\varepsilon) & M^3(\varphi)(t-2\varepsilon)\end{pmatrix}^T = \varphi(t) + \mathcal{O}(\varepsilon^3).$$ □

Combining the three previous lemmas, thereom 2.10 estimates the Y_i.

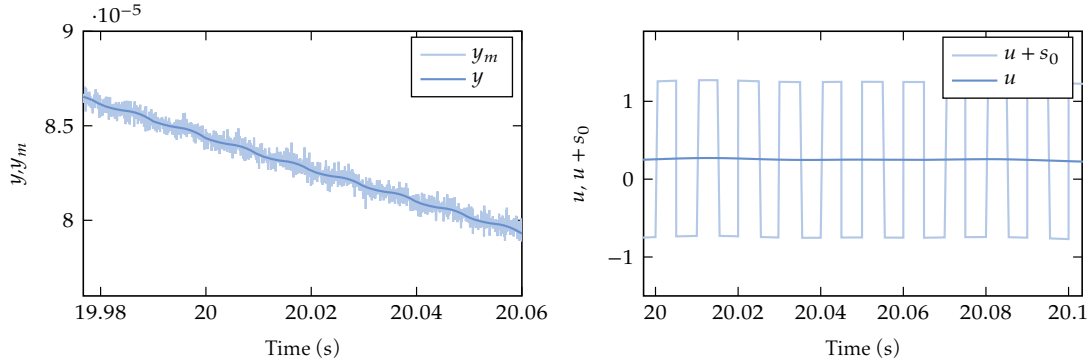

Figure 2.5: Zoom on the measured output (left) with noise. On the control (right).

Theorem 2.10. *Considering the operator P defined in lemma 2.9, we have an estimate for each of the Y_i with an accuracy of $\mathcal{O}(\varepsilon^3)$, namely*

$$\widehat{Y}_2(t) := \frac{1}{\overline{S_1^2}} P[y\check{S}_1](t) = Y_2(t) + \mathcal{O}(\varepsilon^3) \tag{2.23a}$$

$$\widehat{Y}_3(t) := \frac{1}{\overline{s_2^2}} P[y\check{s}_2](t) - \frac{\langle s_1^2, s_2\rangle}{\overline{s_2^2}} \widehat{Y}_2(t) = Y_3(t) + \mathcal{O}(\varepsilon^3) \tag{2.23b}$$

$$\widehat{Y}_1(t) := \frac{1}{\overline{s_1^2}} P[y\check{s}_1](t) - \frac{\langle s_1^2, s_1\rangle}{\overline{s_1^2}} \widehat{Y}_2(t) = Y_1(t) + \mathcal{O}(\varepsilon^3) \tag{2.23c}$$

$$\widehat{Y}_0(t) := P[y](t) - \overline{s_1^2} \widehat{Y}_2(t) = Y_0(t) + \mathcal{O}(\varepsilon^3). \tag{2.23d}$$

Proof. Let first determine the estimate for Y_2. Computing $P[y\check{S}_1]$, we get

$$\begin{aligned} P[y\check{S}_1](t) = {} & P[\widetilde{Y}_0\check{S}_1](t) + P[\widetilde{Y}_1\check{s}_1\check{S}_1](t) + P\big[\widetilde{Y}_2(\check{S}_1^2 - \overline{S_1^2})\big](t) + P[\widetilde{Y}_2\overline{S_1^2}](t) \\ & + P[\widetilde{Y}_3\check{s}_2\check{S}_1](t) + \mathcal{O}(\varepsilon^3). \end{aligned}$$

Since P is a linear combination of shifted M^3 and S_1, s_1S_1, s_2S_1 and $S_1^2 - \overline{S_1^2}$ have zero mean, we have by lemma 2.8

$$P[y\check{S}_1](t) = P[\widetilde{Y}_2\overline{S_1^2}](t) + \mathcal{O}(\varepsilon^3).$$

Consequently, using lemma 2.9, we have the following estimate for $\widetilde{Y}_2$ (which is equal to Y_2)

$$\widehat{Y}_2(t) = \frac{1}{\overline{S_1^2}} P[y\check{S}_1](t) = Y_2(t) + \mathcal{O}(\varepsilon^3).$$

Let compute $\widehat{Y}_3$. The same calculations for $P[y\check{s}_2]$ provide

$$P[y\check{s}_2](t) = \overline{s_2^2}\,\widetilde{Y}_3(t) = \overline{s_2^2}\Big(Y_3(t) + \frac{\langle s_1^2, s_2\rangle}{\overline{s_2^2}} Y_2(t)\Big),$$

that is, by definition of $\widehat{Y}_3$ (2.23b)

$$\widehat{Y}_3(t) = Y_3(t) + \mathcal{O}(\varepsilon^3).$$

Following the previous lines, we get the estimates $\widehat{Y}_0$, $\widehat{Y}_1$. □

2.3.4 A worked example

We illustrate the interest of the method on the system

$$\dot{x}_1 = x_2 \tag{2.24a}$$
$$\dot{x}_2 = x_3 \tag{2.24b}$$
$$\dot{x}_3 = u + d \tag{2.24c}$$
$$y = x_1 x_2 + \frac{x_3^3}{3} \tag{2.24d}$$

where d is an unknown disturbance. We would like x_1 to track the reference x_1^{ref} while rejecting the disturbance, with a time response of about a few time units. We want to operate around steady state, i.e. near states of the form $(x_1^{ss}, 0, 0)$ and inputs such that $u^{ss} + d^{ss} = 0$. Notice the system is not first-order observable around steady state because of the very degenerate output y, which makes the control problem far from obvious. Nonetheless, the virtual measurements for this system are

$$Y_1 = \varepsilon \begin{pmatrix} x_2 & x_1 & x_3^2 \end{pmatrix} \begin{pmatrix} 0 \\ 0 \\ 1 \end{pmatrix} = \varepsilon x_3^2$$
$$Y_2 = \frac{\varepsilon^2}{2} \begin{pmatrix} 0 & 0 & 1 \end{pmatrix} \begin{pmatrix} 0 & 1 & 0 \\ 1 & 0 & 0 \\ 0 & 0 & 2x_3 \end{pmatrix} \begin{pmatrix} 0 \\ 0 \\ 1 \end{pmatrix} = \varepsilon^2 x_3$$
$$Y_3 = \varepsilon^2 \begin{pmatrix} x_2 & x_1 & x_3^2 \end{pmatrix} \begin{pmatrix} 0 \\ 1 \\ 0 \end{pmatrix} = \varepsilon^2 x_1,$$

hence first-order observability is restored thanks to Y_2 and Y_3, without even considering y and Y_1. Notice third-order averaging is paramount, since the virtual measurement Y_1 stemming from second-order averaging is still degenerate. With $Y_3 = \varepsilon^2 x_1$ and $Y_2 = \varepsilon^2 x_3$, the system is completely linear and can therefore be easily controlled. We design a classical controller-observer, with observer

$$\begin{pmatrix} \dot{\hat{x}}_1 \\ \dot{\hat{x}}_2 \\ \dot{\hat{x}}_3 \end{pmatrix} = \begin{pmatrix} \hat{x}_2 \\ \hat{x}_3 \\ u \end{pmatrix} + L \begin{pmatrix} Y_3/\varepsilon^2 - \hat{x}_1 \\ Y_2/\varepsilon^2 - \hat{x}_3 \end{pmatrix}$$

and integral controller

$$u = -k_1 \hat{x}_1 - k_2 \hat{x}_2 - k_3 \hat{x}_3 - k_I \eta_I$$
$$\dot{\eta}_I = \frac{Y_3}{\varepsilon^2} - x_1^{\text{ref}}.$$

The 3×2 matrix L and $K = \begin{pmatrix} k_1 & k_2 & k_3 & k_I \end{pmatrix}$ are chosen such that the eigenvalues of the observer are $\left(-13.98,\ -1.57 \pm 1.59i\right)$ and those of the controller are $\left(-1.20 \pm 1.77i,\ -2.00 \pm 0.58i\right)$, which ensures a time response of a few time units and a reasonable robustness; the observer is faster than the controller, in accordance with Loop Transfer Recovery (at the plant

input). Setting $\eta := \begin{pmatrix}\hat{x}_1 & \hat{x}_2 & \hat{x}_3 & \eta_I\end{pmatrix}^T$, this controller-observer reads

$$\begin{aligned} u &= -K\eta \\ \dot{\eta} &= M\eta + Nx_1^{\mathrm{ref}}(t) + \tilde{L}\begin{pmatrix} Y_3/\varepsilon^2 \\ Y_2/\varepsilon^2 \end{pmatrix}, \end{aligned}$$

where the matrices $\tilde{L}$, M and N are

$$\tilde{L} := \begin{pmatrix} & L & \\ 1 & & 0 \end{pmatrix}, \quad M = \begin{pmatrix} -l_{11} & 1 & -l_{12} & 0 \\ -l_{21} & 0 & 1-l_{22} & 0 \\ -k_1 - l_{31} & -k_2 & -k_3 - l_{32} & -k_I \\ 0 & 0 & 0 & 0 \end{pmatrix}, \quad N := \begin{pmatrix}0 & 0 & 0 & -1\end{pmatrix}^T.$$

Following section 2.3.2, this yields the implementable control law for (2.24a)–(2.24c), which is a particular case of (2.20),

$$\begin{aligned} u &= -K\eta + s_0(\tfrac{t}{\varepsilon}) \\ \dot{\eta} &= M\eta + Nx_1^{\mathrm{ref}}(t) + \tilde{L}\begin{pmatrix} \widehat{Y}_3/\varepsilon^2 \\ \widehat{Y}_2/\varepsilon^2 \end{pmatrix}, \end{aligned}$$

where $\widehat{Y}_2$ and $\widehat{Y}_3$ are obtained from the actual measurement (2.24d) by the demodulation procedure of subsection 2.3.3. The injected signal s_0 is a square wave of amplitude 1 and frequency 100, which ensures the oscillation is fast with respect to the time constants of the closed-loop system; $n := 2$ is used in the demodulating filter.

The test scenario is the following: at $t = 0\,\mathrm{s}$ the system starts at rest at the origin, with the reference x_1^{ref} set to 0; at $t = 4\,\mathrm{s}$, a step disturbance d of magnitude -0.25 is applied; for $12 \le t \le 32\,\mathrm{s}$, x_1^{ref} is a slow (filtered) ramp with slope 5×10^{-2}, meaning the system must slowly move while nearly first-order unobservable; finally, at $t = 32\,\mathrm{s}$, x_1^{ref} is a filtered step so as to quickly return to 0.

Without noise on the actual output y, the performance is excellent: the reference is tracked and the disturbance is rejected (Fig. 2.3). In fact the system behaves nearly as in the ideal situation where it is controlled directly from x_1, x_3 without signal injection (Fig. 2.4); the ripple is visible on x_3 because it is directly affected by the input, but is much smaller on x_1, x_2, as anticipated by the averaging analysis. A zoomed view for $27.6 \le t \le 27.8\,\mathrm{s}$ gives a better insight of the signals: Fig. 2.4 (right) illustrates (2.15a); Fig. 2.1 shows the square wave in the control signal; Fig. 2.2 shows the ripple in the actual output is really tiny near steady state, with a strange form caused by the nonlinearity of this output.

With a measured output y_m corrupted by noise, one thus might fear the ripple is much too small to be useful; this is not the case since the demodulation process is essentially a low-pass filter. Indeed, the system performs as desired (Fig. 2.6a and 2.6b), even though the output ripple is buried into noise (Fig. 2.5). The measurement noise used in the simulation is a band-limited white noise with noise power 1×10^{-18} and sample time $1 \times 10^{-5}\,\mathrm{s}$.

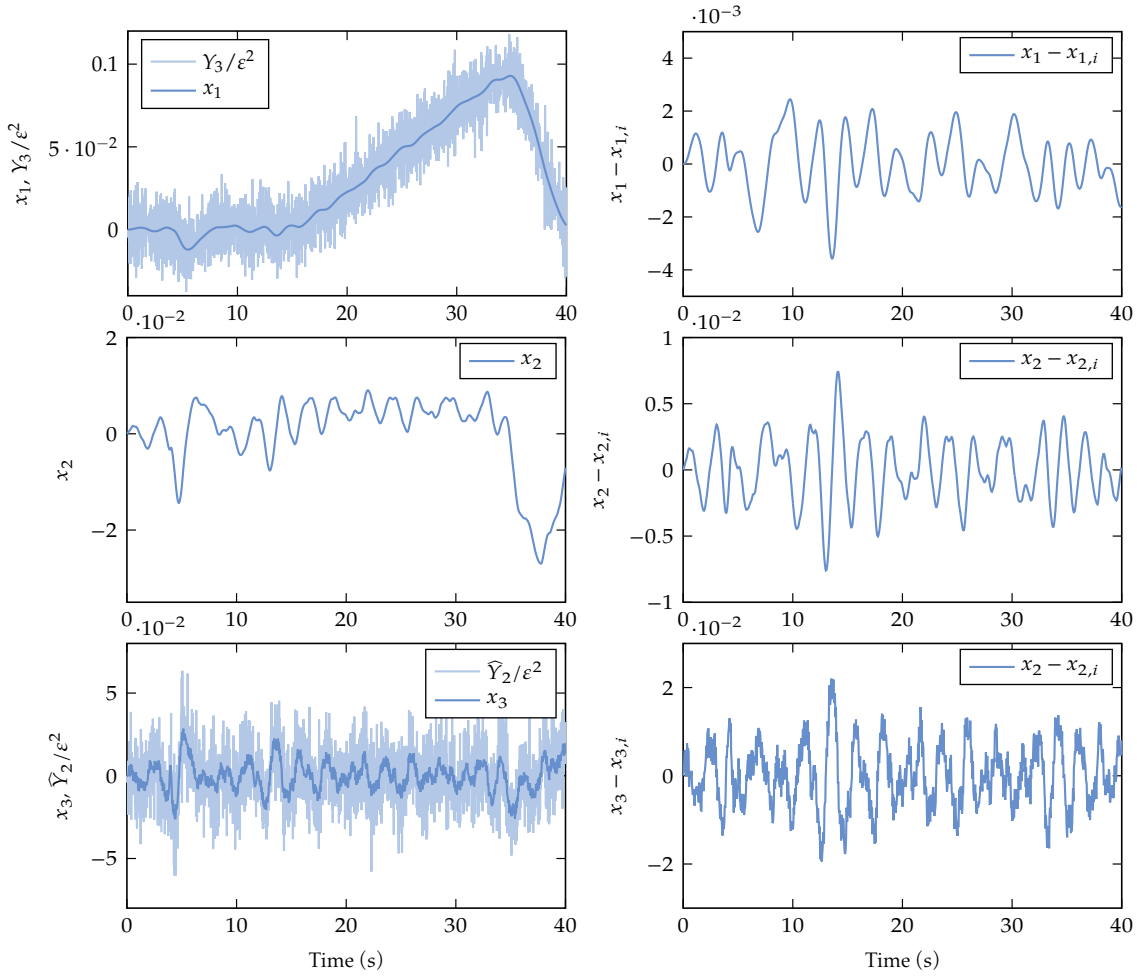

(a) x_1, x_2, x_3, estimates $\hat{Y}_3/\varepsilon^2$ and $\hat{Y}_2/\varepsilon^2$ (b) $x - x_i$, $i = 1, 2, 3$

Figure 2.6: Left: state and estimates x_1 and $\hat{Y}_3/\varepsilon^2$ (top); x_2 (middle); x_3 and $\hat{Y}_2/\varepsilon^2$ (bottom). Right: difference between x (signal injection) and x_i (ideal control).

2.4 Third-order averaging theorem and signal injection

Before generalizing this study to MIMO systems with a nonlinear dynamics, it should be pointed out that the averaging theory might not be employed in the same way at orders higher than three to recover the virtual measurements. Indeed, the application of theorem 2.2 at order k requires that the two equations for x and $\tilde{x}$ only differ at the $k+1^{\text{th}}$ order and at the k^{th} order by a term h^k with zero mean. In the linear case for $k = 3$, this third-order term is $\varepsilon^3 A^2 B s_2$, as conveyed by equation (2.19a). As this third-order term will stay at higher orders in the expression for $\tilde{x}$, it will eventually hinder the application of the averaging theorem to compare the original system and the one with signal injection. The presence of the zero-mean periodic term at the k^{th} order only is nevertheless guaranteed by the quasi-identity transformation,

but at the cost of a modification of the averaged system, which then differs from the original system (meaning there exists a g^i with $i \geq 2$ in theorem 2.2 that is different from zero). The comparison remains valid, but with a system different from the original, and will require corrections to the control terms when the latter uses the virtual measurements. In this section, (more particularly in subsection 2.4.2), under the assumption that the model describes a PMSM, we show that the comparison theorem remains applicable with an averaged system that corresponds exactly to the unperturbed system, thus making a posteriori corrections unnecessary.

Furthermore, while the first-order virtual measurement (Y_1 in equation (2.11)) can be derived by a standard timescale separation —which is the technique historically used for electric motors [JL95] by neglecting the voltage drop response to the high-frequency signal, see subsection 1.4.1—, it reveals insufficient to extract the two other virtual measurements Y_2 and Y_3. As a matter of fact, a standard low-frequency/high-frequency separation is not helpful in distinguishing the second and third-order in ε HF components. The two second-order virtual measurements that are derived thanks to the third-order averaging theory are modulated on high-frequency signals sharing the same frequency —the injection frequency—, namely s_1, s_2 and s_1^2. In this regard, the averaging theory to study the injection effects is paramount.

We now generalize in this section the application of the averaging theory to MIMO systems controlled thanks to signal injection. For the sake of clarity, we restrict the study to open-loop systems, and keep at bay the slow-time variation of the input. In the following, f, g and h denote smooth enough mappings, i.e. at least C^4 and Lipschitz on D. In order to simplify the ensuing computations, we will eventually take into account the specificities of the state-space model of a PMSM.

2.4.1 Solving the homological equations

In section 2.2, we stated the existence the near-identity transformation that brings an instationary system into an averaged one, with only the last power in ε being time-dependent. Even if the existence of such a transformation can be theoretically proved without loss of generality, we will specifically focus on the derivation of the near-identity transformation for systems controlled thanks to signal injection, i.e. of the form

$$\dot{x} = \varepsilon(f(x) + g(x)s_0(t)). \tag{2.25}$$

With a slight abuse of notation, the vector field f also encompasses the term $g(x)u$. This trick will turn out to be harmless, as discussed in subsection 2.4.2. We consider the generic third-order near-identity transformation

$$x = \check{x} + \varepsilon\varphi^1(\check{x}, t) + \varepsilon^2\varphi^2(\check{x}, t) + \varepsilon^3\varphi^3(\check{x}, t), \tag{2.26}$$

where φ^1, φ^2 and φ^3 are yet to be defined. According to subsection 2.2.1, they can be selected so that $\check{x}$ satisfies the full averaged equation, which is of the form

$$\dot{\check{x}} = \varepsilon g^1(\check{x}) + \varepsilon^2 g^2(\check{x}) + \varepsilon^3 g^3(\check{x}) + \varepsilon^4 g^{[4]}(\check{x}, t, \varepsilon),$$

where $g^1(\check{x}) := \int_0^1 (f(\check{x}) + g(\check{x})s_0(t))\,dt = f(\check{x})$, g^2 and g^3 being stationary. The process consists in computing successively φ^1, g^2, φ^2, g^3 etc. Following this procedure, to compute φ^1, start by derivating (2.26) with respect to t; this yields

$$\dot{x} = \dot{\check{x}} + \varepsilon \partial_t \varphi^1(\check{x}, t) + \text{terms in } \varepsilon^2.$$

Replacing in the previous equation $\dot{x}$ and $\dot{\check{x}}$ by their expression (2.25) and (2.26) respectively yields

$$\varepsilon(f(x) + g(x)s_0(t)) = \varepsilon(f(\check{x}) + \partial_t \varphi^1(\check{x}, t)) + \text{terms in } \varepsilon^2.$$

Since $f(x) = f(\check{x}) + \text{terms in } \varepsilon^2$, and $g(x) = g(\check{x}) + \text{terms in } \varepsilon^2$, the identification of the first-order in ε terms gives $\partial_t \varphi^1(\check{x}, t) = g(\check{x})s_0(t)$. A wide range of φ^1 matches this constraint —namely $g(\check{x})$ applied to any primitive of s_0—, and each choice leads to a different set of equations for the averaged equation. We select $\varphi^1(\check{x}, t) = g(\check{x})s_1(t)$ where s_1 is the zero-mean primitive of s_0. The remaining of the proof consists in computing successively g^2, φ^2 and g^3, along the lines above. To obtain g^2, we compute $\dot{x}$ by differentiating (2.26) with respect to t on the one hand, and by plugging the transformation (2.26) into the system (2.25) and Taylor expanding on the other hand. The full derivative of (2.26) with respect to the time reads

$$\begin{aligned} \dot{x} &= \dot{\check{x}} + \varepsilon dg_{\check{x}}(\dot{\check{x}})s_1(t) + \varepsilon g(\check{x})s_0(t) + \varepsilon^2 \partial_t \varphi^2(\check{x}, t) + \text{terms in } \varepsilon^3 \\ &= \dot{\check{x}} + \varepsilon g(\check{x})s_0(t) + \varepsilon^2 dg_{\check{x}}(f(\check{x}))s_1(t) + \varepsilon^2 \partial_t \varphi^2(\check{x}, t) + \text{terms in } \varepsilon^3, \end{aligned} \tag{2.27}$$

where $dg_x(h)$ denotes the differential of g in x evaluated in h. As for the Taylor expansion,

$$\begin{aligned} \dot{x} &= \varepsilon f(x) + \varepsilon g(x)s_0(t) \\ &= \varepsilon f(\check{x}) + \varepsilon^2 df_{\check{x}}(g(\check{x})s_1(t)) + \varepsilon g(\check{x})s_0(t) + \varepsilon^2 dg_{\check{x}}(g(\check{x})s_1(t))s_0(t) + \text{terms in } \varepsilon^3. \end{aligned} \tag{2.28}$$

Identifying the terms in ε^2 in the two previous equations (2.27) and (2.28) yields

$$g^2(\check{x}) + \partial_t \varphi^2(\check{x}, t) + dg_{\check{x}}(f(\check{x}))s_1(t) = df_{\check{x}}(g(\check{x})s_1(t)) + dg_{\check{x}}(g(\check{x})s_1(t))s_0(t).$$

Since $\partial_t \varphi^2$ and s_1 have zero mean in t, taking the average of the previous equation then yields

$$g^2(\check{x}) = \int_0^1 dg_{\check{x}}(g(\check{x})s_1(\sigma))s_0(\sigma)\,d\sigma.$$

Notice that in the SISO case, $s_0 s_1$ has zero mean, since it is the derivative of $s_1^2/2$. This property however does not hold in the MIMO case, as coupling terms between the components of s_0 and s_1 arise. Selecting φ^2 such that its mean is zero, we have

$$\begin{aligned} \varphi^2(\check{x}, t) = {} & df_{\check{x}}(g(\check{x})s_2(t)) - dg_{\check{x}}(f(\check{x}))s_2(t) \\ & + \int_0^t dg_{\check{x}}(g(\check{x})s_1(\sigma))s_0(\sigma)\,d\sigma - \int_0^1 \int_0^\sigma dg_{\check{x}}(g(\check{x})s_1(\tau))s_0(\tau)\,d\tau\,d\sigma. \end{aligned} \tag{2.29}$$

We now turn to the computation of g^3. The process is repeated once again: on the one hand, we compute the derivative of the near-identity transform (2.26), focusing this time on the third-order terms in ε

$$\begin{aligned} \dot{x} &= \dot{\check{x}} + \text{terms in } \varepsilon + \varepsilon d_x \varphi^1_{(\check{x},t)}(\dot{\check{x}}) + \varepsilon^2 d_x \varphi^2_{(\check{x},t)}(\dot{\check{x}}) + \varepsilon^3 \partial_t \varphi^3(\check{x}, t) + \text{terms in } \varepsilon^4 \\ &= \text{terms in } \varepsilon^1 \text{ and } \varepsilon^2 + \varepsilon^3 g^3(\check{x}) + \varepsilon^3 d_x \varphi^1_{(\check{x},t)}(g^2(\check{x})) + \varepsilon^3 d_x \varphi^2_{(\check{x},t)}(f(\check{x})) + \varepsilon^3 \partial_t \varphi^3(\check{x}, t) \\ &\quad + \text{terms in } \varepsilon^4. \end{aligned} \tag{2.30}$$

On the other hand, inserting (2.26) into (2.25) and Taylor expanding gives

$$\begin{aligned}\dot{x} &= \varepsilon f(x) + \varepsilon g(x)s_0(t)\\ &= \varepsilon f(\check{x}) + \varepsilon^2 df_{\check{x}}(\varphi^1(\check{x},t)) + \varepsilon^3 df_{\check{x}}(\varphi^2(\check{x},t)) + \frac{\varepsilon^3}{2}d^2f_{\check{x}}(\varphi^1(\check{x},t),\varphi^1(\check{x},t))\\ &\quad +\varepsilon g(\check{x})s_0(t) + \varepsilon^2 dg_{\check{x}}(\varphi^1(\check{x},t))s_0(t) + \varepsilon^3 dg_{\check{x}}(\varphi^2(\check{x},t))s_0(t) + \frac{\varepsilon^3}{2}d^2g_{\check{x}}(\varphi^1(\check{x},t),\varphi^1(\check{x},t))s_0(t)\\ &\quad +\text{terms in } \varepsilon^4. \end{aligned} \tag{2.31}$$

As (2.30) and (2.31) describe the same state, the identification of the third-order terms in ε in both equations gives

$$\begin{aligned}g^3(\check{x}) + d_x\varphi^2_{(\check{x},t)}(f(\check{x})) + d_x\varphi^1_{(\check{x},t)}(g^2(\check{x})) + \partial_t\varphi^3(\check{x},t) &= df_{\check{x}}(\varphi^2(\check{x},t))\\ &\quad + \frac{1}{2}d^2f_{\check{x}}(\varphi^1(\check{x},t),\varphi^1(\check{x},t)) + dg_{\check{x}}(\varphi^2(\check{x},t))s_0(t) + \frac{1}{2}d^2g_{\check{x}}(\varphi^1(\check{x},t),\varphi^1(\check{x},t))s_0(t).\end{aligned}$$

Therefore, taking the mean of the previous equation —with $\partial_t\varphi^3(\check{x},t)$ and $df_{\check{x}}(\varphi^2(\check{x},t))$ having zero mean—, g^3 satisfies

$$\begin{aligned}g^3(\check{x}) = \frac{1}{2}\int_0^1 \Big[d^2f_{\check{x}}(\varphi^1(\check{x},\sigma),\varphi^1(\check{x},\sigma)) + d^2g_{\check{x}}(\varphi^1(\check{x},\sigma),\varphi^1(\check{x},\sigma))s_0(\sigma)\Big]d\sigma\\ + \int_0^1 \Big[dg_{\check{x}}(\varphi^2(\check{x},\sigma))s_0(\sigma) - d_x\varphi^1_{(\check{x},\sigma)}(g^2(\check{x})) - d_x\varphi^2_{(\check{x},\sigma)}(f(\check{x}))\Big]d\sigma.\end{aligned}$$

The computation of φ^3 and $g^{[4]}$ can ultimately be dropped, as only the truncated transformation (2.3) is used to derive $\overline{x}$ and then $\tilde{x}$.

2.4.2 Application to MIMO systems with nonlinear dynamics

The application of the previous process to solve the homological equations lead to a truncated averaged equation of the form

$$\dot{\overline{x}} = \varepsilon g^1(\overline{x}) + \varepsilon^2 g^2(\overline{x}) + \varepsilon^3 g^3(\overline{x}).$$

Nonetheless, to eventually obtain a meaningful comparison without modifying the control law, the desired comparison is carried out with the system without injection, i.e. $\overline{x}$ verifying

$$\dot{\overline{x}} = \varepsilon f(\overline{x}). \tag{2.32}$$

Henceforth, $\overline{x}$ will denote the solution of (2.32). We will show that, under the simplifying hypotheses gathered in equation (2.41) , we can consider $\overline{x}$ as the solution of original system (2.32) instead of the truncated averaged equation.

Consider the change of coordinates

$$\tilde{x} := \overline{x} + \varepsilon\varphi^1(\overline{x},t) + \varepsilon^2\varphi^2(\overline{x},t). \tag{2.33}$$

This change of coordinates is obtained by applying the near-identity transformation derived in the previous subsection to the original state $\overline{x}$ without injection. Therefore, the two functions φ^1 and φ^2 are defined by

$$\varphi^1(\overline{x},t) := g(\overline{x})s_1(t), \tag{2.34a}$$

$$\varphi^2(\overline{x},t) := df_{\overline{x}}(g(\overline{x})s_2(t)) - dg_{\overline{x}}(f(\overline{x}))s_2(t). \tag{2.34b}$$

Notice the difference between (2.34b) and the expression (2.29) obtained when solving the homological equations. Under the assumption (2.41) that the system describes a PMSM, the two integral terms in (2.29) are zero.

The first step consists in looking for the dynamics of $\tilde{x}$. Computing the total derivative of the transformation (2.33) with respect to t gives

$$\dot{\tilde{x}} = \dot{\overline{x}} + \varepsilon d_x \varphi^1_{(\overline{x},t)}(\dot{\overline{x}}) + \varepsilon \partial_t \varphi^1(\overline{x},t) + \varepsilon^2 d_x \varphi^2_{(\overline{x},t)}(\dot{\overline{x}}) + \varepsilon^2 \partial_t \varphi^2(\overline{x},t). \tag{2.35}$$

The next step consists in expressing the previous right-hand side as a function of $\tilde{x}$ and t only. The first right-hand side term in (2.35) is simply given by the dynamics of $\overline{x}$

$$\dot{\overline{x}} = \varepsilon f(\overline{x}).$$

The two following terms in (2.35) can be expressed thanks to the expression (2.34a) for φ^1

$$\varepsilon d_x \varphi^1_{(\overline{x},t)}(\dot{\overline{x}}) = \varepsilon^2 d g_{\overline{x}}(f(\overline{x}))s_1(t), \tag{2.36a}$$
$$\varepsilon \partial_t \varphi^1(\overline{x},t) = \varepsilon g(\overline{x})s_0(t). \tag{2.36b}$$

As for the two last terms, using expression (2.34b) for φ^2, they read

$$\begin{aligned}\varepsilon^2 d_x \varphi^2_{(\overline{x},t)}(\dot{\overline{x}}) &= \varepsilon^3 d^2 f_{\overline{x}}(g(\overline{x})s_2(t), f(\overline{x})) - \varepsilon^3 d^2 g_{\overline{x}}(f(\overline{x}), f(\overline{x}))s_2(t) \\ &\quad + \varepsilon^3 d f_{\overline{x}}\big(d g_{\overline{x}}(f(\overline{x}))s_2(t)\big) - \varepsilon^3 d g_{\overline{x}}\big(d f_{\overline{x}}(f(\overline{x}))\big)s_2(t), \qquad (2.36c)\\ \varepsilon^2 \partial_t \varphi^2(\overline{x},t) &= \varepsilon^2 \left[d f_{\overline{x}}(g(\overline{x})s_1(t)) - d g_{\overline{x}}(f(\overline{x}))s_1(t)\right]. \qquad (2.36d)\end{aligned}$$

Collecting the five equations (2.32), (2.36a) to (2.36d) (and dropping the last two (zero) terms in (2.36c) thanks to (2.41)) allows us to rewrite (2.35) as follows

$$\begin{aligned}\dot{\tilde{x}} &= \varepsilon(f(\overline{x}) + g(\overline{x})s_0(t)) + \varepsilon^2 d f_{\overline{x}}(g(\overline{x})s_1(t)) \\ &\quad + \varepsilon^3 [d^2 f_{\overline{x}}(g(\overline{x})s_2(t), f(\overline{x})) - d^2 g_{\overline{x}}(f(\overline{x}), f(\overline{x}))s_2(t)]. \qquad (2.37)\end{aligned}$$

Equation (2.37) only exhibits terms depending on $\overline{x}$ and t in its right-hand side. The third-order term in ε in (2.37) reads (replacing by $\tilde{x}$ by its expression (2.35) as a function of $\overline{x}$ and Taylor expanding at the first order)

$$\begin{aligned}&\varepsilon^3\Big[d^2 f_{\overline{x}}(g(\overline{x})s_2(t), f(\overline{x})) - d^2 g_{\overline{x}}(f(\overline{x}), f(\overline{x}))s_2(t)\Big] = \\ &\qquad \varepsilon^3\Big[d^2 f_{\tilde{x}}(g(\tilde{x})s_2(t), f(\tilde{x})) - d^2 g_{\tilde{x}}(f(\tilde{x}), f(\tilde{x}))s_2(t)\Big] + \text{terms in } \varepsilon^4. \qquad (2.38)\end{aligned}$$

Likewise, replacing $\tilde{x}$ by its expression (2.35) and Taylor expanding yields for the term of order ε^2 in (2.37)

$$\begin{aligned}\varepsilon^2 d f_{\overline{x}}(g(\overline{x})s_1(t)) &= \varepsilon^2 d f_{\tilde{x}}(g(\overline{x})s_1(t)) - \varepsilon^3 d^2 f_{\tilde{x}}(\varphi^1(\overline{x},t), \varphi^1(\overline{x},t)) + \text{ terms in } \varepsilon^4 \\ &= \varepsilon^2 d f_{\tilde{x}}(g(\overline{x})s_1(t)) - \varepsilon^3 d^2 f_{\tilde{x}}(\varphi^1(\tilde{x},t), \varphi^1(\tilde{x},t)) + \text{ terms in } \varepsilon^4. \qquad (2.39)\end{aligned}$$

Notice already that the third-order terms in the two previous equations compensate each other. Finally, replacing $\tilde{x}$ by its expression (2.35) and Taylor expanding yields for the term of

order ε in (2.37)

$$\begin{aligned}\varepsilon(f(\overline{x})+g(\overline{x})s_0(t)) &= \varepsilon(f(\tilde{x})+g(\tilde{x})s_0(t)) - \varepsilon^2 df_{\tilde{x}}(\varphi^1(\overline{x},t)) - \varepsilon^2 dg_{\tilde{x}}(\varphi^1(\overline{x},t))s_0(t)\\ &\quad -\varepsilon^3 df_{\tilde{x}}(\varphi^2(\overline{x},t)) - \varepsilon^3 dg_{\tilde{x}}(\varphi^2(\overline{x},t))s_0 + \frac{\varepsilon^3}{2}d^2f_{\tilde{x}}(\varphi^1(\overline{x},t),\varphi^1(\overline{x},t))\\ &\quad +\frac{\varepsilon^3}{2}d^2g_{\tilde{x}}(\varphi^1(\overline{x},t),\varphi^1(\overline{x},t))s_0(t) + \text{ terms in } \varepsilon^4\\ &= \varepsilon(f(\tilde{x})+g(\tilde{x})s_0(t)) - \varepsilon^2 df_{\tilde{x}}(g(\overline{x})s_1(t)) - \varepsilon^3 df_{\tilde{x}}(\varphi^2(\tilde{x},t))\\ &\quad +\frac{\varepsilon^3}{2}d^2f_{\tilde{x}}(\varphi^1(\tilde{x},t),\varphi^1(\tilde{x},t)) + \text{ terms in } \varepsilon^4, \end{aligned} \tag{2.40}$$

where we used that the following quantities are zero (these results are proved in subsection 2.5.3 for a PMSM)

$$dg_{\tilde{x}}(\varphi^1(\overline{x},t)) = dg_{\tilde{x}}(\varphi^2(\overline{x},t)) = d^2g_{\tilde{x}}(\varphi^1(\overline{x},t),\varphi^1(\overline{x},t)) = 0. \tag{2.41}$$

Gathering the three Taylor expansions (2.38) to (2.40), equation (2.35) can now be written entirely as a function of $\tilde{x}$

$$\begin{aligned}\dot{\tilde{x}} &= \varepsilon(f(\tilde{x})+g(\tilde{x})s_0(t)) + \varepsilon^3[d^2f_{\tilde{x}}(g(\tilde{x})s_2(t),f(\tilde{x})) - d^2g_{\tilde{x}}(f(\tilde{x}),f(\tilde{x}))s_2(t) - df_{\tilde{x}}(\varphi^2(\tilde{x},t))]\\ &\quad +\frac{\varepsilon^3}{2}d^2f_{\tilde{x}}(g(\tilde{x})s_1(t),g(\tilde{x})s_1(t)) + \text{terms in } \varepsilon^4, \end{aligned} \tag{2.42}$$

which we write under the form

$$\dot{\tilde{x}} = \varepsilon(f(\tilde{x})+g(\tilde{x})s_0(t)) + \varepsilon^3 f_1^3(\tilde{x},t) + \varepsilon^3 f_2^3(\tilde{x},t) + \text{ terms in } \varepsilon^4,$$

with f_1^3 and f_2^3 defined as follows

$$f_1^3(\tilde{x},t) := d^2f_{\tilde{x}}(g(\tilde{x})s_2(t),f(\tilde{x})) - d^2g_{\tilde{x}}(f(\tilde{x}),f(\tilde{x}))s_2(t) - df_{\tilde{x}}(\varphi^2(\tilde{x},t)), \tag{2.43a}$$

$$f_2^3(\tilde{x},t) := \frac{1}{2}d^2f_{\tilde{x}}(g(\tilde{x})s_1(t),g(\tilde{x})s_1(t)). \tag{2.43b}$$

The second-order differential $d^2f_{\tilde{x}}$ being bilinear, the expression for f_1^3 is linear in the excitation signal s_2. This signal s_2 is by definition the zero-mean primitive of s_1, which means f_1^3 also has zero mean, i.e.

$$\int_0^1 \left[d^2f_{\tilde{x}}(g(\tilde{x})s_2(\sigma),f(\tilde{x})) - d^2g_{\tilde{x}}(f(\tilde{x}),f(\tilde{x}))s_2(\sigma) - df_{\tilde{x}}(\varphi^2(\tilde{x},\sigma))\right]d\sigma = 0.$$

However, without additional assumptions on the dynamics, f_2^3 is quadratic in s_1; its mean is consequently not necessarily zero. The averaging process might be hindered by such a term as it may introduce a slow drift. Estimates on a time length of magnitude ε, or decreased accuracy on a longer time interval can nonetheless be obtained in the presence of non-zero in mean terms. For the time being, assume f_2^3 has zero mean; we will see that for a PMSM, for *rotating sine wave* and *pulsating sine and square wave* injections, f_2^3 also has zero mean. Under this assumption on f_2^3, the averaging theorem 2.2 can be rewritten as follows

Theorem 2.11 (Third-order comparison theorem)**.** *Consider x and $\tilde{x}$ satisfying*

$$\begin{aligned}\dot{x} &= \varepsilon[f(x)+g(x)s_0(t)]\\ \dot{\tilde{x}} &= \varepsilon[f(\tilde{x})+g(\tilde{x})s_0(t)] + \varepsilon^3 k^3(\tilde{x},t) + \mathcal{O}(\varepsilon^4),\end{aligned}$$

with f and g Lipschitz, $k^3(x,t)$ Lipschitz in x, periodic with zero mean in t. Then the following estimate for the solutions holds, on a timescale $1/\varepsilon$

$$x(t) = \tilde{x}(t) + \mathcal{O}(\varepsilon^3).$$

The application of the theorem then provides a relation between the original state and the one with signal injection:

$$\begin{aligned} x(t) &= \overline{x}(t) + \varepsilon\varphi^1(\overline{x},t) + \varepsilon^2\varphi^2(\overline{x},t) + \mathcal{O}(\varepsilon^3) \\ &= \overline{x}(t) + \varepsilon g(\overline{x})s_1(t) + \varepsilon^2\Big[df_{\overline{x}}(g(\overline{x})s_2(t)) - dg_{\overline{x}}(f(\overline{x}))s_2(t)\Big] + \mathcal{O}(\varepsilon^3). \end{aligned}$$

Knowing the perturbed state as a function of the non-perturbed one is an end in itself, since the injection effects are finely described by the previous equation: a first-order ripple carried by the fast-varying signal s_1 as well as a second-order ripple carried by s_2 are superimposed to $\overline{x}$ to form the state x with an accuracy in $\mathcal{O}(\varepsilon^3)$. Inserting this expression for x into the measurement $y = h(x)$ finally provides the measured output y as a function of $\overline{x}$, still with an accuracy in $\mathcal{O}(\varepsilon^3)$

$$\begin{aligned} y = h(\overline{x}) &+ \varepsilon dh_{\overline{x}}(g(\overline{x})s_1(t)) + \frac{\varepsilon^2}{2}d^2h_{\overline{x}}(g(\overline{x})s_1(t), g(\overline{x})s_1(t)) \\ &+\varepsilon^2 dh_{\overline{x}}\Big(df_{\overline{x}}(g(\overline{x})s_2(t)) - dg_{\overline{x}}(f(\overline{x}))s_2(t)\Big) + \mathcal{O}(\varepsilon^3). \end{aligned} \tag{2.44}$$

Additional virtual measurements are available, provided that they are different from zero and independent of the first-order virtual measurement. One of these is modulated by the components of the matrix $s_1 s_1^T$, the other by s_2. Moreover, replacing $f(x)$ by $f(x) + g(x)u$ interestingly does not change the expression of the measurement (2.44), since it only intervenes in the second-order in ε Lie-Bracket term, and is ultimately compensated, without changing the shape of the equation. Also, throughout this section, the operated simplifications only rested on the hypotheses (2.41) on the differentials of g, which means encompassing the open-loop control into f had no impact on the previous derivations.

2.5 Application of third-order averaging to the PMSM

The results of section 2.4 are now applied on the state-space model of PMSM. The objective is twofold: on the one hand, to check the aforementioned assumptions, namely that equation (2.41) holds and f_2^3 (see equation (2.43b)) has zero mean for the different types of injections considered in subsection 1.5.1; on the other hand, to obtain an explicit formulation for the two additional virtual measurements, and see if they can be harnessed to gain knowledge on the system.

2.5.1 State-space model

We re-write the state-space model of a PMSM in the dq-frame under the form

$$\begin{aligned} \dot{x} &= f(x) + g(x)u + g_d(x)T_l \\ y &= h(x), \end{aligned}$$

with $x = \begin{pmatrix}\phi_s^d & \phi_s^q & \omega & \theta\end{pmatrix}^T$, $u = \begin{pmatrix}u_s^a & u_s^b & u_s^c\end{pmatrix}^T$, $f(x) = \begin{pmatrix}f_d & f_q & f_\omega & f_\theta\end{pmatrix}$, $g_d(x) = \begin{pmatrix}0 & 0 & -1 & 0\end{pmatrix}$ and

$$
\begin{aligned}
f_d(x) &= -R_s i_s^d + \omega\phi_s^q, & f_q(x) &= -R_s i_s^q - \omega\phi_s^d,\\
f_\omega(x) &= \frac{n^2}{J}\left(-i_s^d\phi_s^q + i_s^q\phi_s^d\right), & f_\theta(x) &= \omega,\\
g(x) &= \begin{pmatrix}\mathcal{R}(-\theta)\mathcal{C}\\ \mathbb{0}_{1\times 3}\\ \mathbb{0}_{1\times 3}\end{pmatrix} = \sqrt{\frac{2}{3}}\begin{pmatrix}\cos\theta & \cos(\theta-\frac{2\pi}{3}) & \cos(\theta+\frac{2\pi}{3})\\ -\sin\theta & -\sin(\theta-\frac{2\pi}{3}) & -\sin(\theta+\frac{2\pi}{3})\\ 0 & 0 & 0\\ 0 & 0 & 0\end{pmatrix},\\
h(x) &= i_s^{\alpha\beta} = \mathcal{R}(\theta)\begin{pmatrix}i_s^d & i_s^q\end{pmatrix}^T, & i_s^d(x) &= \frac{\phi_s^d - \phi_m}{L_d}, \qquad i_s^q(x) = \frac{\phi_s^q}{L_q}.
\end{aligned}
$$

The injected voltage in the *abc*-frame is denoted by $s_0 = s_0^{abc}$ (the absence of superscript implicitly denotes the signal in the *abc*-frame). Like any other quantities in this three-axis frame, the injection is subject to Concordia and Park's transformation. Once the model is given, the remaining task merely boils down to the computation of the different terms in equations (2.41), (2.43b) and (2.44).

2.5.2 First-order virtual measurement

The first-order virtual measurement is given by the first-order term in (2.44)

$$y_{v,1} := dh_{\overline{x}}(g(\overline{x})s_1(t)).$$

The differential of h on x applied to z, by definition of the Jacobian, is $dh_x(z) := J_h(x)z$. The mapping h gives the current in the $\alpha\beta$-frame, namely

$$h(x) = i^{\alpha\beta} = \mathcal{R}(\theta)\begin{pmatrix}\frac{\phi^d-\phi_m}{L_d} & \frac{\phi_q}{L_q}\end{pmatrix}^T = \begin{pmatrix}\cos\theta\times\frac{\phi^d-\phi^m}{L_d} - \sin\theta\times\frac{\phi^q}{L_q}\\ \sin\theta\times\frac{\phi^d-\phi^m}{L_d} + \cos\theta\times\frac{\phi^q}{L_q}\end{pmatrix},$$

which means the Jacobian of h is

$$J_h(x) = \begin{pmatrix}\frac{1}{L_d}\cos\theta & -\frac{1}{L_q}\sin\theta & 0 & \mathcal{R}(\theta+\pi/2)\left(\frac{\phi^d-\phi^m}{L_d} \quad \frac{\phi^q}{L_q}\right)^T\\ \frac{1}{L_d}\sin\theta & +\frac{1}{L_q}\cos\theta & 0 & \end{pmatrix} \in \mathbb{R}^{2\times 4}.$$

Defining $\tilde{J}_h(x) := (J_h(x))_{1\le i,j\le 2}$, the first-order virtual measurement is thus given by

$$
\begin{aligned}
dh_{\overline{x}}(g(\overline{x})s_1(t)) &= \tilde{J}_h(\overline{x})\mathcal{R}(-\bar{\theta})\mathcal{C}s_1^{abc}(t)\\
&= \mathcal{S}(\bar{\theta})s_1^{\alpha\beta}(t) = \frac{L_q+L_d}{2L_dL_q}\begin{pmatrix}1+\frac{L_q-L_d}{L_q+L_d}\cos 2\bar{\theta} & \frac{L_q-L_d}{L_q+L_d}\sin 2\bar{\theta}\\ \frac{L_q-L_d}{L_q+L_d}\sin 2\bar{\theta} & 1-\frac{L_q-L_d}{L_q+L_d}\cos 2\bar{\theta}\end{pmatrix}s_1^{\alpha\beta}(t),
\end{aligned}
$$

with $\mathcal{S}(\theta)$ the so-called saliency matrix, and $s_1^{\alpha\beta} := \mathcal{C}s_1^{abc}$. This is a well-known result [Jeb+16], which could have been obtained without resorting to the third-order averaging theory. This statement however does not hold for the derivation of the two potential second-order virtual measurements, where this theory is paramount.

2.5.3 Proof of the averaging assumptions

Along with the derivation of the new virtual measurements, we prove that the different quantities that have been assumed to be either zero —equation (2.41)— or with zero mean effectively holds when considering the state-space model of a PMSM. We start by proving the first and third equalities in (2.41): the first-order differential of g on x applied to $z = \begin{pmatrix} z_1 & z_2 & z_3 & z_4 \end{pmatrix}^T \in \mathbb{R}^4$ is

$$dg_x(z) = \begin{pmatrix} & -\mathcal{R}(\frac{\pi}{2} - \theta)\mathcal{C} & \\ 0 & 0 & 0 \\ 0 & 0 & 0 \end{pmatrix} z_4. \tag{2.45}$$

By (2.34a), the expression of $\varphi^1(x,t) = g(x)s_1^{abc} = \begin{pmatrix} s_1^{dq} & 0 & 0 \end{pmatrix}^T \in \mathbb{R}^4$, with

$$s_1^{dq} := \begin{pmatrix} \mathcal{R}(-\theta)s_1^{\alpha\beta} \\ 0 \\ 0 \end{pmatrix}, \qquad s_1^{\alpha\beta} := \mathcal{C}s_1^{abc} \in \mathbb{R}^2.$$

This means the fourth component of φ^1 is zero, therefore $dg_x(\varphi^1(x,t)) = 0$. Moreover, based on (2.45), without computing its expression, the second-order differential of g on x applied to z twice only depends on z_4 (as dg_x only depends on the fourth variable θ). Since $\varphi^1(x,t)$ has no fourth component either, the third equality in (2.41) holds, namely

$$d^2g_x(g(x)s_1, g(x)s_1) = 0.$$

As for the second equality $dg_x(\varphi^2(x,t)) = 0$, likewise, we show that the fourth coefficients of φ^2 is also zero. On the one hand,

$$dg_x(f(x))s_2 = \begin{pmatrix} & -\mathcal{R}(\frac{\pi}{2} - \theta)\mathcal{C} & \\ 0 & 0 & 0 \\ 0 & 0 & 0 \end{pmatrix} f_\theta(x)s_2,$$

means $[dg_x(f(x))s_2)]_4 = 0$. On the other, the Jacobian of f reads

$$J_f(x) = \begin{pmatrix} -\frac{R_s}{L_d} & \omega & \phi^q & 0 \\ -\omega & -\frac{R_s}{L_q} & -\phi^d & 0 \\ \frac{n^2}{J}\phi^q(\frac{1}{L_d} - \frac{1}{L_q}) & \frac{n^2}{J}\phi^d(\frac{1}{L_d} - \frac{1}{L_q}) + \frac{\phi_m}{L_d} & 0 & 0 \\ 0 & 0 & 1 & 0 \end{pmatrix}.$$

With $g(x)s_2 = \begin{pmatrix} s_2^d & s_2^q & 0 & 0 \end{pmatrix}^T$, we obtain $[df_x(g(x)s_2)]_4 = 0$. Which means $[\varphi^2(x,t)]_4 = 0$, hence $dg_x(\varphi^2) = 0$. This concludes the proof of (2.41) when the state-space model of a PMSM is considered. We now turn to the mean of f_2^3. The second-order differential of f in x reads for $z \in \mathbb{R}^4$

$$d^2f_x(z,z) = 2\begin{pmatrix} z_2z_3 & -z_1z_3 & \frac{n^2}{J}(\frac{1}{L_d} - \frac{1}{L_q})z_1z_2 & 0 \end{pmatrix}^T.$$

Replacing z by $\varphi^1 = \begin{pmatrix} s_1^d & s_1^q & 0 & 0 \end{pmatrix}^T$, the evaluation of the second-order differential reads

$$d^2 f_x(\varphi^1(x,t), \varphi^1(x,t)) = \begin{pmatrix} 0 & 0 & \frac{n^2}{J}(\frac{1}{L_d} - \frac{1}{L_q}) s_1^d s_1^q & 0 \end{pmatrix}^T.$$

For the three type of injections described in subsection 1.5.1, the two signals s_1^d and s_1^q are orthogonal. Indeed, in the pulsating case, the $q-$ axis injection being zero, $s_1^q = 0$, and for the rotating injection, s_1^α and s_1^β are sine waves in quadrature, so are s_1^d and s_1^q. Consequently,

$$\int_0^1 d^2 f_x(\varphi^1(x,\sigma), \varphi^1(x,\sigma))\, d\sigma = 0.$$

In other words, f_2^3 has zero mean.

2.5.4 Second-order virtual measurements

After tedious but straightforward computations, the additional second-order virtual measurements for the state-space model of a PMSM are

$$\begin{aligned} d^2 h_{\overline{x}}(g(\overline{x})s_1(t), g(\overline{x})s_1(t)) &= 0, \\ dh_{\overline{x}}\Big(df_{\overline{x}}(g(\overline{x})s_2(t)) - dg_{\overline{x}}(f(\overline{x}))s_2(t)\Big) &= \mathcal{S}_2(\bar{\theta}) s_2^{\alpha\beta}(t), \end{aligned}$$

where $\mathcal{S}_2(\theta)$ is the so-called second-order saliency matrix defined by

$$\mathcal{S}_2(\bar{\theta}) := -\frac{R_s(L_q^2 + L_d^2)}{2L_d^2 L_q^2} \begin{pmatrix} 1 + \frac{L_q^2 - L_d^2}{L_q^2 + L_d^2}\cos 2\bar{\theta} & \frac{L_q^2 - L_d^2}{L_q^2 + L_d^2}\sin 2\bar{\theta} \\ \frac{L_q^2 - L_d^2}{L_q^2 + L_d^2}\sin 2\bar{\theta} & 1 - \frac{L_q^2 - L_d^2}{L_q^2 + L_d^2}\cos 2\bar{\theta} \end{pmatrix}. \tag{2.46}$$

Eventually, the measured currents (2.44) in the $\alpha\beta$-frame read

$$\imath^{\alpha\beta} = \overline{\imath^{\alpha\beta}} + \varepsilon \mathcal{S}(\bar{\theta}) s_1^{\alpha\beta} + \varepsilon^2 \mathcal{S}_2(\bar{\theta}) s_2^{\alpha\beta} + \mathcal{O}(\varepsilon^3).$$

This second-order saliency matrix shares the same shape as its first-order counterpart. One noticeable difference between $\mathcal{S}$ and $\mathcal{S}_2$ though is the presence of the stator resistance in the latter. While the first virtual measurement can be harnessed to estimate the position, the second one may provide the evolution of the resistance, as its value can vary with the temperature and the operating conditions. Also, knowing the shape of the second-order term in the expression for the measurement can help in designing more accurate estimators for the first-order term.

2.5.5 Demodulation of the second-order virtual measurements

The demodulation procedure to recover the second-order virtual measurements is once again sketched to suit the specificities of the measured currents of a PMSM. A generic extraction process is fully detailed in chapter 4, and applied to experimental data in chapter 6 for the first-order virtual measurement recovery.

Assume first the second-order component in the measured currents is available with an accuracy in $\mathcal{O}(\varepsilon^3)$ (following for instance the process described in subsection 2.3.3), i.e.

$$y_{v,2}(t) = \varepsilon^2 \mathcal{S}_2(\bar{\theta}) s_2^{\alpha\beta}(t) + \mathcal{O}(\varepsilon^3).$$

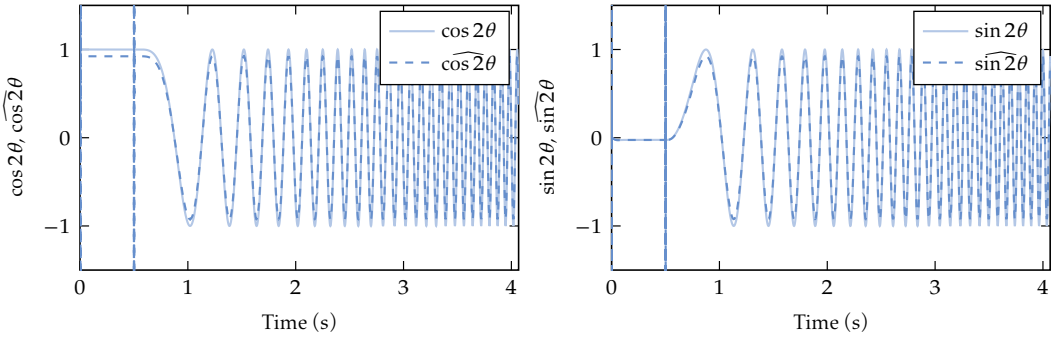

(a) $\cos 2\theta$, $\widehat{\cos 2\theta}$ (b) $\sin 2\theta$, $\widehat{\sin 2\theta}$

Figure 2.7: $\cos 2\theta$, its estimate (left), $\sin 2\theta$, its estimate (right) during the first four seconds.

A standard least-square method is used to estimate $\cos 2\bar{\theta}$ and $\sin 2\bar{\theta}$ from this virtual measurement $y_{v,2}$ thanks to the particular structure of the second-order saliency matrix $\mathcal{S}_2(\bar{\theta})$, see (2.46). Start by defining the two following quantities

$$\begin{pmatrix} \lambda & \mu \\ \mu & \nu \end{pmatrix} := \overline{s_2^{\alpha\beta} s_2^{\alpha\beta^T}} = \int_0^1 s_2^{\alpha\beta}(\sigma) s_2^{\alpha\beta^T}(\sigma)\, d\sigma, \qquad \begin{pmatrix} y_{11} & y_{12} \\ y_{21} & y_{22} \end{pmatrix} := \frac{-2L_d^2 L_q^2}{R_s(L_d^2+L_q^2)} \frac{y_{v,2}}{\varepsilon^2}.$$

and $L := \frac{L_d^2+L_q^2}{L_q^2-L_d^2}$. With these notations, the second-order virtual measurement $y_{v,2} = \varepsilon^2 \mathcal{S}_2(\theta) s_2^{\alpha\beta}$ can be rewritten as follows

$$\underbrace{\begin{pmatrix} \lambda & \mu \\ \mu & \nu \\ -\mu & \lambda \\ -\nu & \mu \end{pmatrix}}_{:=P} \begin{pmatrix} \cos 2\bar{\theta} \\ \sin 2\bar{\theta} \end{pmatrix} = L \underbrace{\begin{pmatrix} y_{11}-\lambda \\ y_{12}-\mu \\ y_{21}-\mu \\ y_{22}-\nu \end{pmatrix}}_{:=d}.$$

The least-square solution of this (consistent) overdetermined linear system in $\cos 2\bar{\theta}$ and $\sin 2\bar{\theta}$ is therefore given by

$$\begin{aligned} \begin{pmatrix} \cos 2\bar{\theta} \\ \sin 2\bar{\theta} \end{pmatrix} &= L[P^T P]^{-1} P^T d = \frac{L}{\lambda^2+2\mu^2+\nu^2} P^T d \\ &= \frac{L}{\lambda^2+2\mu^2+\nu^2} \begin{pmatrix} \lambda y_{11} + \mu(y_{12}-y_{21}) - \nu y_{22} - \lambda^2 + \nu^2 \\ \mu(y_{11}+y_{22}) + \nu y_{12} + \lambda y_{21} - 2\mu(\lambda+\nu) \end{pmatrix}. \end{aligned}$$

Estimates $\widehat{\cos 2\bar{\theta}}$, $\widehat{\sin 2\bar{\theta}}$ for $\cos 2\bar{\theta}$, $\sin 2\bar{\theta}$ are obtained with the same formulas, using instead of the actual y_{ij} their estimated values

$$\begin{pmatrix} \hat{y}_{11} & \hat{y}_{12} \\ \hat{y}_{21} & \hat{y}_{22} \end{pmatrix} := \frac{-2L_d^2 L_q^2}{R_s(L_d^2+L_q^2)} \frac{\hat{y}_{v,2}}{\varepsilon^2} = \frac{-2L_d^2 L_q^2}{R_s(L_d^2+L_q^2)} \frac{y_{v,2}}{\varepsilon^2} + \mathcal{O}(\varepsilon).$$

Table 2.1: Rated parameters

Rated power	400 W	Number of pole pairs n	2
Rated voltage (RMS)	400 V	Stator resistance R_s	4.25 Ω
Rated current (RMS)	1.66 A	d-axis inductance L_d	43.25 mH
Rated speed	1800 RPM	q-axis inductance L_q	69.05 mH
Rated torque	2.12 N m	Permanent magnet flux linkage ϕ_m	0.277 Wb

We thus have

$$\begin{aligned}\widehat{\cos 2\bar{\theta}} &:= L\frac{\lambda\hat{y}_{11} + \mu(\hat{y}_{12} - \hat{y}_{21}) - \nu\hat{y}_{22} - \lambda^2 + \nu^2}{\lambda^2 + 2\mu^2 + \nu^2} \\ &= \cos 2\bar{\theta} + \mathcal{O}(\varepsilon), \\ \widehat{\sin 2\bar{\theta}} &:= L\frac{\mu(\hat{y}_{11} + \hat{y}_{22}) + \nu\hat{y}_{12} + \lambda\hat{y}_{21} - 2\mu(\lambda + \nu)}{\lambda^2 + 2\mu^2 + \nu^2} \\ &= \sin 2\bar{\theta} + \mathcal{O}(\varepsilon).\end{aligned}$$

Finally, an estimate $\hat{\bar{\theta}}$ of $\bar{\theta}$ is given by

$$\hat{\bar{\theta}} := \frac{1}{2}\operatorname{atan2}(\widehat{\sin 2\bar{\theta}}, \widehat{\cos 2\bar{\theta}}) + k\pi = \bar{\theta} + \mathcal{O}(\varepsilon). \tag{2.47}$$

2.5.6 Numerical results

The recovery of the additional virtual measurement, described by the second-order saliency matrix, is now validated on a numerical experiment. To recover the position, a standard rotating square wave injection is used, with $s_0^\alpha = \cos\frac{t}{\varepsilon}$ and $s_0^\beta = \sin\frac{t}{\varepsilon}$; the injection frequency is set to $\varepsilon^{-1} = 4$ kHz. The method is tested on a salient-poles machine model, whose rated parameters are gathered in table 2.1. The scenario is the following: the motor, as well as the reference, starts and stays at rest between 0 and 0.5 s. The speed reference then describes a ramp, going from 0 to 4 Hz (electrical) in 5 s. From 5.5 to 10 s, the motor stays at constant speed. During the whole scenario, the motor carries a load torque of around 50 % of its nominal value. The extraction of $\cos 2\theta$ and $\sin 2\theta$ is depicted in Fig. 2.7, and shows the good agreement between the actual values and their respective estimates. The position is reconstructed using equation (2.47), see Fig. 2.8, where the error estimate $\theta - \hat{\theta}$ shares the same order of magnitude as the injection period ε^{-1}.

The numerical results confirm the possibility of recovering the rotor position from the second-order virtual measurement $y_{v,2}$. While this position estimation can be achieved using the first-order virtual measurement, the second-order one may serve alternative purposes. Indeed, $y_{v,2}$ carries information on the stator resistance that can be extracted using the prior position estimate (thanks to the first-order virtual measurement). Such a result turns out to be particularly relevant when the stator resistance is not well-known and is subject to significant variations.

Knowing the expression of the perturbed measurement with an increased accuracy can also be used to enhance the estimators quality. For a PMSM model indeed, the first second-order

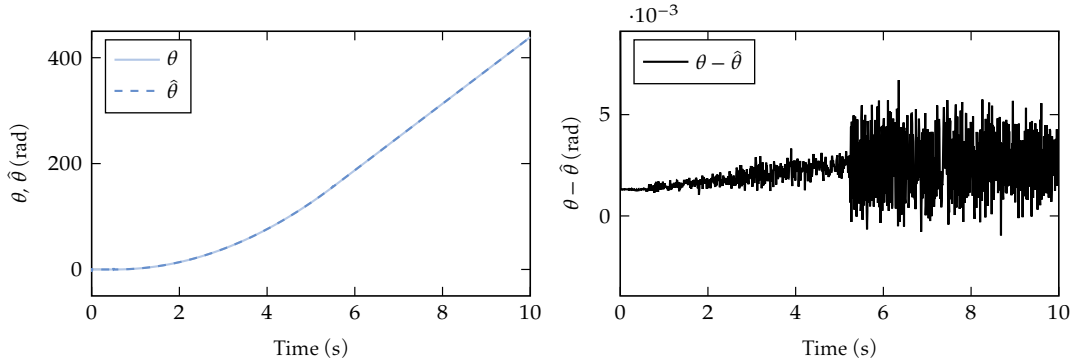

(a) Position θ and estimate $\hat{\theta}$ (rad)

(b) Error $\theta - \hat{\theta}$ (rad)

Figure 2.8: Position θ, its estimate $\hat{\theta}$ (left), position error $\theta - \hat{\theta}$ (right).

virtual measurement, modulated by s_1^2, is zero. This means that, up to the second-order, the perturbed measurement is only modulated by periodic signals with zero mean, namely s_1 and s_2. The application to the perturbed output of lemma 2.8 together with the estimator given in lemma 2.9 improves the recovery accuracy. Put simply, $P[i_s^{\alpha\beta}] = \overline{i_s^{\alpha\beta}} + \mathcal{O}(\varepsilon^3)$ whereas a first-order development of $i_s^{\alpha\beta}$ may only yield an estimate in $\mathcal{O}(\varepsilon^2)$, should the higher-order term be modulated by a signal with non-zero mean.

A few caveats coming along this method are noticeable though. While this method is properly defined when the PMSM model assumes a linear current-flux relation, it might fail at capturing magnetic saturation effects on the additional virtual measurements, thus producing inaccurate position estimates. As illustrated by the experimental results in chapter 6 (Fig. 6.5), saturation effects induce an error estimate drift (when the position is recovered from the first-order virtual measurement) under the same speed reference tracking scenario with different load torque values. In this regard, an energy-based modeling approach [Jeb13] to derive a saturated current-flux relation could be useful in understanding this discrepancy, but at the cost of a greater complexity in the virtual measurement expressions.

Another theoretical limitation of the third-order averaging theory to derive additional virtual outputs arises when substituting the analog voltage input by its modulated output (using PWM, multilevel converters, or any scheme), thereby introducing state discontinuities (as well as potential non-idealities such as voltage drops in the IGBT) into the controlled system. In chapter 3, the computations are conducted up to the second-order in ε to derive the same type of estimates for hybrid systems controlled via an inverter. Third-order results in this context are yet to be proven.

Finally, under reserve of overcoming these limitations, the virtual measurement $y_{v,2}$ amplitude is dominated by ε^2, and is consequently subject to potential distortions other than a complete corruption by the measurement noise. Nevertheless, this may turn out to be exploitable when the injection frequency is relatively low [Jun+11], making the term in ε^2 sizable.

2.6 Conclusion

This chapter has laid out the foundations of the averaging theory at any order, detailing in particular the set of transformations pushing a perturbed system to a stationary one, all by connecting the two by a comparison theorem. This comparison being valid only on a finite timescale in all generality, additional assumptions of the stability of the system allow to extend this estimate to infinity. When the perturbed system corresponds to the system controlled by signal injection, it is shown that virtual measurements are made available by an adequate demodulation procedure. The classical averaging has been slightly modified to take into account the specificities of the non-linear model of a PMSM, so as to obtain a comparison between the unperturbed system and the system with injection, without the need for a posteriori compensation. From this study, the expression of the virtual measurements for PMSM equipped with a linear current-flux relation was derived. The first-order virtual measure allows the recovery of position information through the so-called saliency matrix. As for the second-order virtual measurement, a higher-order saliency matrix is highlighted, which has the same structure as its first-order counterpart, but depends on the stator resistance, which can be estimated by exploiting this new virtual measurement.

Chapter 3

Second-order averaging theory for endogenous signal injection

This chapter is adapted from *Adding virtual measurements by PWM-induced signal injection* [Sur+20a], published in the Proceedings of ACC 2020.

Résumé L'injection de signal exogène présente plusieurs limites, notamment lorsque le système contrôlé l'est par un onduleur. Pour ces systèmes électromécaniques, le signal MLI d'entrée, qui est un signal carré modulé, génère une perturbation en sortie de manière *endogène*, c'est-à-dire sans ajout de signal. Cet effet sur la sortie laisse donc entrevoir la possibilité d'extraire de cette perturbation une information supplémentaire sur le système. Là où l'analyse par averaging développée au chapitre 2 s'appliquait aux systèmes étant Lipschitz par rapport à l'état, pour les systèmes contrôlés par MLI, une discontinuité par rapport à l'état est introduite dans le terme de perturbation endogène. Une adaptation de cette théorie au cas précis des systèmes contrôlés par MLI est développée dans ce chapitre. Cette théorie permet d'obtenir une expression analytique de la perturbation induite par la MLI, permettant alors de bénéficier des mêmes effets que l'injection de signal traditionnelle (exogène). De manière analogue à l'injection de signal exogène conceptualisée au chapitre précédent, il est possible de récupérer la même mesure virtuelle qui peut alors être employée dans le bouclage de sortie du système, et ce sans les inconvénients engendrés par l'ajout d'un signal extérieur.

Abstract Exogenous signal injection technique has several limitations, especially when the system is controlled by an inverter. For these electromechanical systems, the PWM input signal, which is a modulated square-wave signal, generates an output perturbation in an *endogenous* way, i.e. without adding an signal. This effect on the output therefore suggests the possibility of extracting additional information on the system from this ripple. While the averaging analysis developed in chapter 2 applies to state-Lipschitz systems, for PWM-controlled systems, state-discontinuities are introduced in the endogenous perturbation term. An adaptation of this theory to the very specific case of PWM-controlled systems is developed in this chapter. This theory derives an analytical expression of the PWM-induced output perturbation, thus leading to the same effects as the traditional signal injection. Consequently, similar to the exogenous case conceptualized in the previous chapter, it is possible to recover the exact same virtual measured output allowing the output looping of the system, without the inconvenience of adding an external signal.

3.1 Introduction

Signal injection is a control technique which consists in adding a fast-varying probing signal to the control input. This excitation creates a small ripple in the measurements, which contains useful information if properly decoded. The idea was introduced in [JL95; CL98] for controlling electric motors at low velocity using only measurements of currents. It was later conceptualized in [Com+16a] as a way of producing "virtual measurements" that can be used to control the system, in particular to overcome observability degeneracies. Signal injection is a very effective method, see e.g. applications to electromechanical devices along these lines in [Jeb+16; YOZ18], but it comes at a price: the ripple it creates may in practice yield unpleasant acoustic noise and excite unmodeled dynamics. Also, in the very common situation where the device is fed by a Pulse Width Modulation (PWM) inverter, the frequency of the probing signal may not be as high as desired so as not to interfere with the PWM (typically, it cannot exceed 500 Hz in an industrial drive with a 4 kHz-PWM frequency).

The goal of this chapter is to demonstrate that, for PWM-operated devices, it is possible to benefit from signal injection *without an external probing signal*, by suitably using the excitation provided by the PWM itself, as e.g. in [WX04]. More precisely, consider the Single-Input Single-Output system

$$\dot{x} = f(x) + g(x)u, \tag{3.1a}$$
$$y = h(x), \tag{3.1b}$$

where u is the control input and y the measured output. We first show in section 3.2 that when the control is impressed through PWM, the dynamics may be written as

$$\dot{x} = f(x) + g(x)(u + s_0(u, \tfrac{t}{\varepsilon})), \tag{3.2}$$

with s_0 1-periodic and zero-mean in the second argument, i.e. $s_0(u, \sigma + 1) = s_0(u, \sigma)$ and $\int_0^1 s_0(u, \sigma)\, d\sigma = 0$ for all u; ε is the PWM period, assumed small. The difference with usual signal injection is that the probing signal s_0 generated by the modulation process now depends not only on time, but also on the control input u. This makes the situation more complicated, in particular because s_0 can be discontinuous in both its arguments. Nevertheless, we show in section 3.3 that the second-order averaging analysis of chapter 2 can be extended to this case. In the same way, we show in section 3.4 that the demodulation procedure of [Com+16a] can be adapted to make available the so-called virtual measurement

$$y_v := H_1(x) := \varepsilon h'(x) g(x),$$

in addition to the actual measurement $y_a := H_0(x) := h(x)$. This extra signal is likely to simplify the design of a control law, as illustrated on a numerical example in section 3.5.

Finally, we list some definitions used throughout the chapter; S denotes a function of two variables, which is T-periodic in the second argument, i.e. $S(v, \sigma + T) = S(v, \sigma)$ for all v.

— The mean of S in the second argument is the function (of one variable)

$$\overline{S}(v) := \frac{1}{T} \int_0^T S(v, \sigma)\, d\sigma;$$

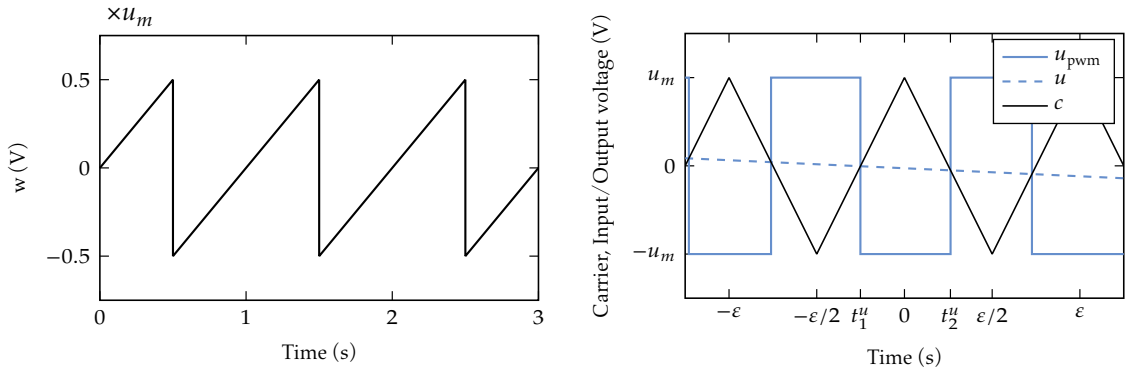

(a) Sawtooth carrier w

(b) PWM: u is compared to c to produce u_{pwm}

Figure 3.1: Sawtooth carrier (left) and PWM signal (right).

S has zero mean in the second argument if $\overline{S}$ is identically zero.

— If S has zero mean in the second argument, its zero-mean primitive in the second argument is defined by

$$S_1(v,\tau) := \int_0^\tau S(v,\sigma)\,d\sigma - \frac{1}{T}\int_0^T\int_0^\tau S(v,\sigma)\,d\sigma d\tau;$$

notice S_1 is T-periodic in the second argument since S has zero mean in the second argument as well.

— The moving average $M(k)$ of a signal k is defined by

$$M(k)(t) := \frac{1}{\varepsilon}\int_{t-\varepsilon}^t k(\tau)\,d\tau.$$

— $\mathcal{O}$ denotes the uniform "big O" symbol of analysis, namely $f(z,t,\varepsilon) = \mathcal{O}(\varepsilon^p)$ if $|f(z,t,\varepsilon)| \leq K\varepsilon^p$ for ε small enough, with $K > 0$ independent of z, t and ε.

3.2 PWM-induced signal injection

When the control input u in (3.1a) is impressed through a PWM process with period ε, the resulting dynamics reads

$$\dot{x} = f(x) + g(x)\mathcal{M}(u, \tfrac{t}{\varepsilon}), \tag{3.3}$$

with $\mathcal{M}$ 1-periodic and mean u in the second argument; the detailed expression for $\mathcal{M}$ is given below. Setting $s_0(u,\sigma) := \mathcal{M}(u,\sigma) - u$, (3.3) obviously takes the form (3.2), with s_0 1-periodic and zero-mean in the second argument.

Classical PWM with period ε and range $[-u_m, u_m]$ is obtained by comparing the input signal u to the ε-periodic triangular carrier defined by

$$c(t) := \begin{cases} u_m + 4\,\mathrm{w}(\frac{t}{\varepsilon}) & \text{if } -\frac{u_m}{2} \leq \mathrm{w}(\frac{t}{\varepsilon}) \leq 0 \\ u_m - 4\,\mathrm{w}(\frac{t}{\varepsilon}) & \text{if } 0 \leq \mathrm{w}(\frac{t}{\varepsilon}) \leq \frac{u_m}{2}; \end{cases}$$

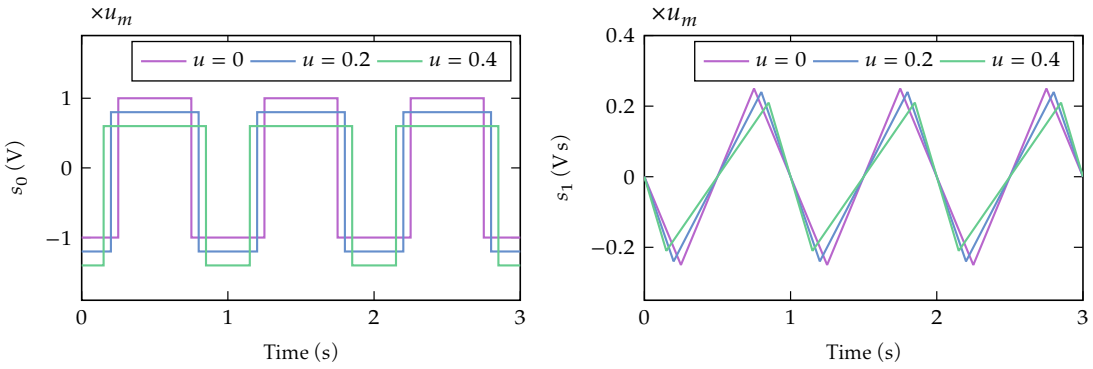

Figure 3.2: $s_0(u,\cdot)$ (left) and $s_1(u,\cdot)$ (right) for $u = 0, 0.2, 0.4$.

the 1-periodic function $\mathrm{w}(\sigma) := u_m \bmod(\sigma + \frac{1}{2}, 1) - \frac{u_m}{2}$ wraps the normalized time $\sigma = \frac{t}{\varepsilon}$ to $[-\frac{u_m}{2}, \frac{u_m}{2}]$. If u varies slowly enough, it crosses the carrier c exactly once on each rising and falling ramp, at times $t_1^u < t_2^u$ such that

$$u(t_1^u) = u_m + 4\,\mathrm{w}\Big(\frac{t_1^u}{\varepsilon}\Big), \qquad u(t_2^u) = u_m - 4\,\mathrm{w}\Big(\frac{t_2^u}{\varepsilon}\Big).$$

The PWM-encoded signal is therefore given by

$$u_{\mathrm{pwm}}(t) = \begin{cases} u_m & \text{if } -\frac{u_m}{2} < \mathrm{w}(\frac{t}{\varepsilon}) \le \mathrm{w}(\frac{t_1^u}{\varepsilon}) \\ -u_m & \text{if } \mathrm{w}(\frac{t_1^u}{\varepsilon}) < \mathrm{w}(\frac{t}{\varepsilon}) \le \mathrm{w}(\frac{t_2^u}{\varepsilon}) \\ u_m & \text{if } \mathrm{w}(\frac{t_2^u}{\varepsilon}) < \mathrm{w}(\frac{t}{\varepsilon}) \le \frac{u_m}{2}. \end{cases}$$

Fig. 3.1b illustrates the signals u, c and u_{pwm}. The function

$$\begin{aligned} \mathcal{M}(u,\sigma) &:= \begin{cases} u_m & \text{if } -2u_m < 4\,\mathrm{w}(\sigma) \le u - u_m \\ -u_m & \text{if } u - u_m < 4\,\mathrm{w}(\sigma) \le u_m - u \\ u_m & \text{if } u_m - u < 4\,\mathrm{w}(\sigma) \le 2u_m \end{cases} \\ &= u_m + \operatorname{sign}(u - u_m - 4\,\mathrm{w}(\sigma)) + \operatorname{sign}(u - u_m + 4\,\mathrm{w}(\sigma)), \end{aligned}$$

which is obviously 1-periodic and with mean u with respect to its second argument, therefore completely describes the PWM process since $u_{\mathrm{pwm}}(t) = \mathcal{M}(u(t), \frac{t}{\varepsilon})$.

Finally, the induced zero-mean probing signal is

$$\begin{aligned} s_0(u,\sigma) &:= \mathcal{M}(u,\sigma) - u \\ &= u_m - u + u_m \operatorname{sign}\Big(\tfrac{u-u_m}{4} - \mathrm{w}(\sigma)\Big) + u_m \operatorname{sign}\Big(\tfrac{u-u_m}{4} + \mathrm{w}(\sigma)\Big), \end{aligned}$$

and its zero-mean primitive in the second argument is

$$s_1(u,\sigma) := (1 - \tfrac{u}{u_m})\,\mathrm{w}(\sigma) - \Big|\tfrac{u-u_m}{4} - \mathrm{w}(\sigma)\Big| + \Big|\tfrac{u-u_m}{4} + \mathrm{w}(\sigma)\Big|.$$

Remark 3.1. As s_0 is only piecewise continuous, one might expect problems to define the "solutions" of (3.2). But as noted above, if the input $u(t)$ of the PWM encoder varies slowly

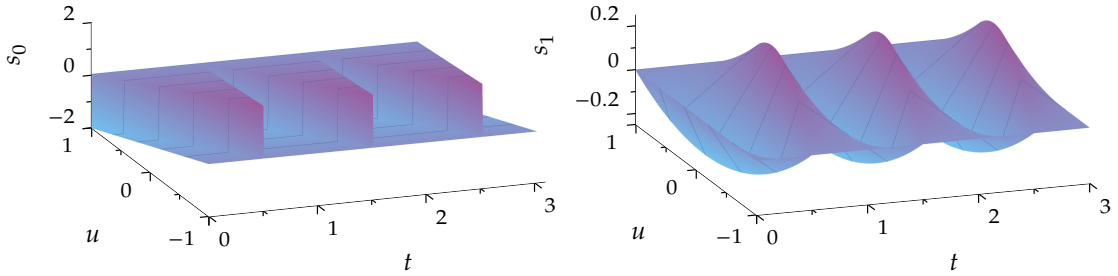

Figure 3.3: 3D view of s_0 (left) and s_1 (right)

enough, its output $u_{\text{pwm}}(t) = \mathcal{M}(u(t), \frac{t}{\varepsilon})$ will have exactly two discontinuities per PWM period. Chattering is therefore excluded, which is enough to ensure the existence and uniqueness of the solutions of (3.2), see [LB96], without the need for the more general Filippov theory [Fil88]. Of course, we assume (without loss of generality in practice) that f, g and h in (3.1) are smooth enough.

Notice also s_1 is continuous and piecewise C^1 in both its arguments (see Fig. 3.3 where a 3D view of each function is depicted). The regularity in the second argument was to be expected as $s_1(u, \cdot)$ is a primitive of $s_0(u, \cdot)$; on the other hand, the regularity in the first argument stems from the specific form of s_0.

3.3 Averaging and PWM-induced injection

Section 3.3.1 outlines the overall approach and states the main theorem 3.1, which is proven in the somewhat technical section 3.3.2. As a matter of fact, the proof can be skipped without losing the main thread; suffice to say that if s_0 were Lipschitz in the first argument, the proof would essentially be an extension of the analysis by "standard" second-order averaging of [Com+16a], with more involved calculations.

3.3.1 Main result

Assume we have designed a suitable control law

$$\begin{aligned} \overline{u} &= \alpha(\overline{\eta}, \overline{Y}, t) \\ \dot{\overline{\eta}} &= a(\overline{\eta}, \overline{Y}, t), \end{aligned}$$

where $\overline{\eta} \in \mathbb{R}^q$, for the system

$$\dot{\overline{x}} = f(\overline{x}) + g(\overline{x})\overline{u}, \qquad \overline{Y} = H(\overline{x}) := \begin{pmatrix} h(\overline{x}) \\ \varepsilon h'(\overline{x}) g(\overline{x}) \end{pmatrix}.$$

By "suitable", we mean the resulting closed-loop system

$$\dot{\overline{x}} = f(\overline{x}) + g(\overline{x})\alpha(\overline{\eta}, H(\overline{x}), t) \tag{3.4a}$$

$$\dot{\overline{\eta}} = a(\overline{\eta}, H(\overline{x}), t) \tag{3.4b}$$

has the desired exponentially stable behavior. We have changed the notations of the variables with $\bar{\cdot}$ to easily distinguish between the solutions of (3.4) and of (3.7) below. Of course, this describes an unrealistic situation:

— PWM is not taken into account

— the control law is not implementable, as it uses not only the actual output $\overline{y}_a = h(\overline{x})$, but also the a priori not available virtual output $\overline{y}_v = \varepsilon h'(\overline{x})g(\overline{x})$.

Define now (up to $\mathcal{O}(\varepsilon^2)$) the function

$$\overline{H}(x,\eta,\sigma,t) := H\Big(x - \varepsilon g(x) s_1\big(\alpha(\eta,H(x),t),\sigma\big)\Big) + \mathcal{O}(\varepsilon^2), \tag{3.5}$$

where s_1 is the zero-mean primitive of s_0 in the second argument, and consider the control law

$$u = \alpha(\eta,\overline{H}(x,\eta,\tfrac{t}{\varepsilon},t),t) \tag{3.6a}$$
$$\dot{\eta} = a(\eta,\overline{H}(x,\eta,\tfrac{t}{\varepsilon},t),t). \tag{3.6b}$$

The resulting closed-loop system, including PWM, reads

$$\dot{x} = f(x) + g(x)m\big(\alpha(\eta,\overline{H}(x,\eta,\tfrac{t}{\varepsilon},t),t),\tfrac{t}{\varepsilon}\big) \tag{3.7a}$$
$$\dot{\eta} = a(\eta,\overline{H}(x,\eta,\tfrac{t}{\varepsilon},t),t). \tag{3.7b}$$

Though PWM is now taken into account, the control law (3.6) still seems to contain unknown terms. Nevertheless, it will turn out from the following result that it can be implemented.

Theorem 3.1. *Let $(x(t),\eta(t))$ be the solution of (3.7) starting from (x_0,η_0), and define $u(t) := \alpha(\eta(t),\bar{H}(x(t)),t)$ and $y(t) := H(x(t))$; let $(\overline{x}(t),\overline{\eta}(t))$ be the solution of (3.4) starting from $(x_0 - \varepsilon g(x_0)s_1(u(0),0),\eta_0)$, and define $\overline{u}(t) := \alpha(\overline{\eta}(t),H(\overline{x}(t)),t)$. Then, for all $t \geq 0$,*

$$x(t) = \overline{x}(t) + \varepsilon g(\overline{x}(t))s_1(\overline{u}(t),\tfrac{t}{\varepsilon}) + \mathcal{O}(\varepsilon^2) \tag{3.8a}$$
$$\eta(t) = \overline{\eta}(t) + \mathcal{O}(\varepsilon^2) \tag{3.8b}$$
$$y(t) = H_0(\overline{x}(t)) + H_1(\overline{x}(t))s_1(\overline{u}(t),\tfrac{t}{\varepsilon}) + \mathcal{O}(\varepsilon^2). \tag{3.8c}$$

The practical meaning of the theorem is the following. As the solution $(x(t),\eta(t)))$ is piecewise C^1, we have by Taylor expansion using (3.8a)-(3.8b) that $u(t) = \overline{u}(t) + \mathcal{O}(\varepsilon^2)$. In the same way, as s_1 is also piecewise C^1, we have

$$s_1(u(t),\tfrac{t}{\varepsilon}) = s_1(\overline{u}(t),\tfrac{t}{\varepsilon}) + \mathcal{O}(\varepsilon^2).$$

As a consequence, we can invert (3.8a)-(3.8b), which yields

$$\overline{x}(t) = x(t) - \varepsilon g(x(t))s_1(u(t),\tfrac{t}{\varepsilon}) + \mathcal{O}(\varepsilon^2) \tag{3.9a}$$
$$\overline{\eta}(t) = \eta(t) + \mathcal{O}(\varepsilon^2). \tag{3.9b}$$

Using this into (3.5), we then get

$$\begin{aligned}\overline{H}(x(t),\eta(t),\tfrac{t}{\varepsilon},t) &= H\Big(x(t) - \varepsilon g(x(t))s_1(u(t),\tfrac{t}{\varepsilon})\Big) + \mathcal{O}(\varepsilon^2),\\ &= H(\overline{x}(t)) + \mathcal{O}(\varepsilon^2).\end{aligned} \tag{3.10}$$

On the other hand, we will see in section 3.4 that, thanks to (3.8c), we can produce an estimate $\widehat{Y} = H(\overline{x}) + \mathcal{O}(\varepsilon^2)$. This means the PWM-fed dynamics (3.3) acted upon by the implementable feedback

$$u = \alpha(\eta, \widehat{Y}, t), \qquad \dot{\eta} = a(\eta, \widehat{Y}, t).$$

behaves exactly as the "ideal" closed-loop system (3.4), except for the presence of a small ripple (described by (3.8a)-(3.8b)).

Remark 3.2. Notice that, according to Remark 3.1, $H_0(\overline{x}(t))$ and $H_1(\overline{x}(t))$ in (3.8c) may be as smooth as desired (the regularity is inherited from only f, g, h, α, a); on the other hand, $s_1(u(t), \frac{t}{\varepsilon})$ is only continuous and piecewise C^1. Nevertheless, this is enough to justify all the Taylor expansions performed in the chapter.

3.3.2 Proof of Theorem 3.1

Because of the lack of regularity of s_0, we must go back to the fundamentals of the second-order averaging theory presented in [SVM05, chapter 2] (with slow time dependence [SVM05, section 3.3]). We first introduce two ad hoc definitions.

Definition 3.1. A function $\varphi(X, \sigma)$ is *slowly-varying in average* if there exists $\lambda > 0$ such that for $k \in \mathbb{N}^*$ and ε small enough,

$$\int_a^{a+T} \| \varphi(p(\varepsilon\sigma) + \varepsilon^k q(\sigma), \sigma) - \varphi(p(\varepsilon\sigma), \sigma) \| \, d\sigma \leq \lambda T \varepsilon^k,$$

where p, q are continuous with q bounded; a and $T > 0$ are arbitrary constants. Notice that if φ is Lipschitz in the first variable then it is slowly-varying in average. The interest of this definition is that it is satisfied by s_0.

Definition 3.2. A function ϕ is $\mathcal{O}(\varepsilon^3)$ *in average* if there exists $K > 0$ such that

$$\left\| \int_0^{\sigma} \phi(q(s), s) \, ds \right\| \leq K \, \varepsilon^3 \sigma,$$

for all $\sigma \geq 0$. Clearly, if ϕ is $\mathcal{O}(\varepsilon^3)$ then it is $\mathcal{O}(\varepsilon^3)$ in average.

The proof of Theorem 3.1 follows the same steps as [SVM05, chapter 2], but with weaker assumptions. We first rewrite (3.7) in the fast timescale $\sigma := t/\varepsilon$ as

$$\frac{dX}{d\sigma} = \varepsilon F(X, \sigma, \varepsilon\sigma), \tag{3.11}$$

where $X := (x, \eta)$ and

$$F(X, \sigma, \tau) := \begin{pmatrix} f(x) + g(x) m\big(\alpha(\eta, \overline{H}(x, \eta, \sigma, \tau), \tau)\big) \\ a(\eta, \overline{H}(x, \eta, \sigma, \tau), \tau) \end{pmatrix}.$$

Notice F is 1-periodic in the second argument. Consider also the so-called averaged system

$$\frac{d\overline{X}}{d\sigma} = \varepsilon \overline{F}(\overline{X}, \varepsilon\sigma), \tag{3.12}$$

where $\overline{F}$ is the mean of F in the second argument.

Define the near-identity transformation

$$X = \widetilde{X} + \varepsilon W(\widetilde{X}, \sigma, \varepsilon\sigma), \tag{3.13}$$

where $\widetilde{X} := (\tilde{x}, \tilde{\eta})$ and

$$W(\widetilde{X}, \sigma, \tau) := \begin{pmatrix} g(\tilde{x}) \\ 0 \end{pmatrix} s_1\Big(\alpha(\tilde{\eta}, H(\tilde{x}, \tilde{\eta}, \sigma, \tau), \tau), \sigma\Big).$$

Inverting (3.13) yields

$$\widetilde{X} = X - \varepsilon W(X, \sigma, \varepsilon\sigma) + \mathcal{O}(\varepsilon^2). \tag{3.14}$$

By lemma 3.2, this transformation puts (3.11) into

$$\frac{d\widetilde{X}}{d\sigma} = \varepsilon\overline{F}(\widetilde{X}, \varepsilon\sigma) + \varepsilon^2\Phi(\widetilde{X}, \sigma, \varepsilon\sigma) + \phi(\widetilde{X}, \sigma, \varepsilon\sigma); \tag{3.15}$$

Φ is periodic and zero-mean in the second argument, and slowly-varying in average, and ϕ is $\mathcal{O}(\varepsilon^3)$ in average.

By lemma 3.3, the solutions $\overline{X}(\sigma)$ and $\widetilde{X}(\sigma)$ of (3.12) and (3.15), starting from the same initial conditions, satisfy $\widetilde{X}(\sigma) = \overline{X}(\sigma) + \mathcal{O}(\varepsilon^2)$. As a consequence, the solution $X(\sigma)$ of (3.11) starting from X_0 and the solution $\overline{X}(\sigma)$ of (3.12) starting from $X_0 - \varepsilon W(X_0, 0, 0)$ are related by $X(\sigma) = \overline{X}(\sigma) + \varepsilon W(\overline{X}(\sigma), \sigma, \varepsilon\sigma) + \mathcal{O}(\varepsilon^2)$, which is exactly (3.8a)-(3.8b). Inserting (3.8a) in $y = h(x)$ and Taylor expanding yields (3.8c).

Remark 3.3. If s_0 were differentiable in the first variable, Φ would be Lipschitz and ϕ would be $\mathcal{O}(\varepsilon^3)$ in (3.15), hence the averaging theory of chapter 2 would directly apply.

Remark 3.4. Here, we prove for simplicity only the estimation $\widetilde{X}(\sigma) = \overline{X}(\sigma) + \mathcal{O}(\varepsilon^2)$ on a timescale $1/\varepsilon$. The continuation to infinity follows from the exponential stability of (3.4), exactly as in theorem 2.5. Notice that in the proof of theorem 2.5, the stability hypothesis concerns the averaged state, so that the proof ensues in the same way as in chapter 2. Likewise, lemma 3.3 is proved without slow-time dependence, the generalization being obvious as in [SVM05, section 3.3].

Lemma 3.2. *The transformation (3.13) puts (3.11) into (3.15), where Φ is periodic and zero-mean in the second argument, and slowly-varying in average, and ϕ is $\mathcal{O}(\varepsilon^3)$ in average.*

Proof. To determine the expression for $d\widetilde{X}/d\sigma$, the objective is to compute $dX/d\sigma$ as a function of $\widetilde{X}$ with two different methods. On the one hand we replace X with its transformation (3.13) in the closed-loop system (3.11), and on the other hand we differentiate (3.13) with respect to σ.

We first compute $s_0(\alpha(\eta, \overline{H}(x, \eta, \sigma, \varepsilon\sigma), \varepsilon\sigma), \sigma)$ as a function of $\widetilde{X} = (\tilde{x}, \tilde{\eta})$. Exactly as in (3.10), with $(\tilde{x}, \tilde{\eta})$ replacing $(\overline{x}, \overline{\eta})$, and (3.14) replacing (3.9), we have

$$\overline{H}(x, \eta, \sigma, \varepsilon\sigma) = H(\tilde{x}) + \mathcal{O}(\varepsilon^2).$$

Therefore, by Taylor expansion

$$\alpha(\eta, \overline{H}(x, \eta, \sigma, \varepsilon\sigma), \varepsilon\sigma) = \alpha(\tilde{\eta}, H(\tilde{x}), \varepsilon\sigma) + \varepsilon^2 K_\alpha(\widetilde{X}, \sigma),$$

with K_α bounded. The lack of regularity of s_0 prevents further Taylor expansion; nonetheless, we still can write

$$s_0(\alpha(\eta,\overline{H}(x,\eta,\sigma,\varepsilon\sigma),\varepsilon\sigma),\sigma) = s_0(\alpha(\tilde{\eta},H(\tilde{x}),\varepsilon\sigma) + \varepsilon^2 K_\alpha(\widetilde{X},\sigma),\sigma).$$

Finally, inserting (3.13) into (3.11) and Taylor expanding, yields after tedious but straightforward computations,

$$\begin{aligned}\frac{dX}{d\sigma} &= \varepsilon\overline{F}(\widetilde{X},\varepsilon\sigma) + \varepsilon G(\widetilde{X})s_0^{\alpha,+}(\tilde{\cdot}) + \varepsilon^2\overline{F}'(\widetilde{X},\varepsilon\sigma)G(\widetilde{X})s_1^\alpha(\tilde{\cdot})\\ &\quad + \varepsilon^2 G'(\widetilde{X})G(\widetilde{X})s_1^\alpha(\tilde{\cdot})s_0^{\alpha,+}(\tilde{\cdot}) + \mathcal{O}(\varepsilon^3);\end{aligned} \tag{3.16}$$

where we have introduced the following notations

$$\begin{aligned}(\tilde{\cdot}) &:= (\widetilde{X},\sigma,\varepsilon\sigma), & s_i^\alpha(\tilde{\cdot}) &:= s_i(\alpha(\tilde{\eta},H(\tilde{x}),\varepsilon\sigma),\sigma),\\ s_0^{\alpha,+}(\tilde{\cdot}) &:= s_0(\alpha(\tilde{\eta},H(\tilde{x}),\varepsilon\sigma) + \varepsilon^2 K_\alpha(\widetilde{X},\sigma),\sigma), & \Delta s_0^\alpha(\tilde{\cdot}) &:= s_0^{\alpha,+}(\tilde{\cdot}) - s_0(\tilde{\cdot}),\\ \overline{F}(X,\varepsilon\sigma) &:= \begin{pmatrix} f(x) + g(x)\alpha(\eta,H(x),\varepsilon\sigma)\\ a(\eta,H(x),\varepsilon\sigma)\end{pmatrix}, & G(X) &:= \begin{pmatrix} g(x)\\ 0\end{pmatrix}.\end{aligned}$$

We now time-differentiate (3.13), which reads with the previous notations $X = \widetilde{X} + \varepsilon G(\widetilde{X})s_1^\alpha(\tilde{\cdot})$. This yields

$$\frac{dX}{d\sigma} = \frac{d\widetilde{X}}{d\sigma} + \varepsilon G'(\widetilde{X})\frac{d\widetilde{X}}{d\sigma}s_1^\alpha(\tilde{\cdot}) + \varepsilon G(\widetilde{X})\partial_1 s_1^\alpha(\tilde{\cdot})\frac{d\widetilde{X}}{d\sigma} + \varepsilon G(\widetilde{X})s_0^\alpha(\tilde{\cdot}) + \varepsilon^2 G(\widetilde{X})\partial_3 s_1^\alpha(\tilde{\cdot}), \tag{3.17}$$

since $\partial_2 s_1^\alpha = s_0^\alpha$. Now assume $\widetilde{X}$ satisfies

$$\frac{d\widetilde{X}}{d\sigma} = \varepsilon\overline{F}(\widetilde{X},\varepsilon\sigma) + \varepsilon G(\widetilde{X})\Delta s_0^\alpha(\tilde{\cdot}) + \varepsilon^2\Psi(\tilde{\cdot}), \tag{3.18}$$

where $\Psi(\tilde{\cdot})$ is yet to be computed. Inserting (3.18) into (3.17),

$$\begin{aligned}\frac{dX}{d\sigma} &= \varepsilon\overline{F}(\widetilde{X},\varepsilon\sigma) + \varepsilon G(\widetilde{X})\Delta s_0^\alpha(\tilde{\cdot}) + \varepsilon^2\Psi(\tilde{\cdot})\\ &\quad + \varepsilon^2 G'(\widetilde{X})\overline{F}(\widetilde{X},\varepsilon\sigma)s_1^\alpha(\tilde{\cdot}) + \varepsilon^2 G'(\widetilde{X})G(\widetilde{X})\Delta s_0^\alpha(\tilde{\cdot})s_1^\alpha(\tilde{\cdot})\\ &\quad + \varepsilon^2 G(\widetilde{X})\partial_1 s_1^\alpha(\tilde{\cdot})\overline{F}(\widetilde{X},\varepsilon\sigma) + \varepsilon^2 G(\widetilde{X})\partial_1 s_1^\alpha(\tilde{\cdot})G(\widetilde{X})\Delta s_0^\alpha(\tilde{\cdot})\\ &\quad + \varepsilon G(\widetilde{X})s_0^\alpha(\tilde{\cdot}) + \varepsilon^2 G(\widetilde{X})\partial_3 s_1^\alpha(\tilde{\cdot}) + \mathcal{O}(\varepsilon^3).\end{aligned}$$

Next, equating (3.19) and (3.16), Ψ satisfies

$$\begin{aligned}\Psi(\tilde{\cdot}) &= [\overline{F},G](\widetilde{X},\varepsilon\sigma)s_1^\alpha(\tilde{\cdot}) + G'(\widetilde{X})G(\widetilde{X})s_0^\alpha(\tilde{\cdot})s_1^\alpha(\tilde{\cdot}) - G(\widetilde{X})\partial_1 s_1^\alpha(\tilde{\cdot})\overline{F}(\widetilde{X},\varepsilon\sigma) - G(\widetilde{X})\partial_3 s_1^\alpha(\tilde{\cdot})\\ &\quad - G(\widetilde{X})\partial_1 s_1^\alpha(\tilde{\cdot})G(\widetilde{X})\Delta s_0^\alpha(\tilde{\cdot}).\end{aligned} \tag{3.19}$$

This gives the expressions of Φ and ϕ in (3.15),

$$\begin{aligned}\Phi(\tilde{\cdot}) &:= [\overline{F},G](\widetilde{X},\varepsilon\sigma)s_1^\alpha(\tilde{\cdot}) + G'(\widetilde{X})G(\widetilde{X})s_0^\alpha(\tilde{\cdot})s_1^\alpha(\tilde{\cdot}) - G(\widetilde{X})\partial_1 s_1^\alpha(\tilde{\cdot})\overline{F}(\widetilde{X},\varepsilon\sigma) - G(\widetilde{X})\partial_3 s_1^\alpha(\tilde{\cdot}),\\ \phi(\tilde{\cdot}) &:= \varepsilon^2\Psi_1(\tilde{\cdot}) + \varepsilon G(\widetilde{X})\Delta s_0^\alpha,\end{aligned}$$

with

$$\Psi_1(\tilde{\cdot}) := -G(\widetilde{X})\partial_1 s_1^\alpha(\tilde{\cdot})G(\widetilde{X})\Delta s_0^\alpha(\tilde{\cdot}).$$

The last step is to check that Φ and ϕ satisfy the assumptions of the lemma. Since s_0^α, s_1^α, $s_0^\alpha s_1^\alpha$, $\partial_1 s_1^\alpha$ and $\partial_3 s_1^\alpha$ are periodic and zero-mean in the second argument, and slowly-varying in

average, so is Φ. There remains to prove that $\phi = \mathcal{O}(\varepsilon^3)$ in average. Since Δs_0^α is slowly-varying in average,

$$\int_0^\sigma \| \Delta s_0^\alpha(\tau(s)) \| ds \leq \lambda_0 \sigma \varepsilon^2.$$

with $\lambda_0 > 0$. G being bounded by a constant c_g, this implies

$$\Big\| \int_0^\sigma \varepsilon G(\widetilde{X}(s)) \Delta s_0^\alpha(\tau(s))\, ds \Big\| \leq c_g \lambda_0 \sigma \varepsilon^3.$$

Similarly, $\partial_1 s_1$ being bounded by c_{11}, Ψ_1 satisfies

$$\Big\| \int_0^\sigma \varepsilon^2 \Psi_1(\tau(s))\, ds \Big\| \leq c_g^2 c_{11} \lambda_0 \sigma \varepsilon_0 \varepsilon^3.$$

Summing the two previous inequalities yields

$$\Big\| \int_0^\sigma \phi(\tau(s))\, ds \Big\| \leq \lambda_0 c_g (1 + c_{11} c_g \varepsilon_0) \sigma \varepsilon^3,$$

which concludes the proof. □

Lemma 3.3. *Let $\overline{X}(\sigma)$ and $\widetilde{X}(\sigma)$ be respectively the solutions of (3.12) and (3.15) starting at 0 from the same initial conditions. Then, for all $\sigma \geq 0$, $\widetilde{X}(\sigma) = \overline{X}(\sigma) + \mathcal{O}(\varepsilon^2)$.*

Proof. Let $E(\sigma) := \widetilde{X}(\sigma) - \overline{X}(\sigma)$. Then,

$$\begin{aligned} E(\sigma) &= \int_0^\sigma \Big[\frac{d\widetilde{X}}{d\sigma}(s) - \frac{d\overline{X}}{d\sigma}(s) \Big] ds \\ &= \varepsilon \int_0^\sigma [F(\widetilde{X}(s)) - F(\overline{X}(s))]\, ds + \varepsilon^2 \int_0^\sigma \Phi(\tau(s))\, ds + \int_0^\sigma \phi(\tau(s))\, ds. \end{aligned}$$

As F is Lipschitz with constant λ_F,

$$\varepsilon \int_0^\sigma \| F(\widetilde{X}(s)) - F(\overline{X}(s)) \| ds \leq \varepsilon \lambda_F \int_0^\sigma \| E(s) \| ds.$$

On the other hand, there exists by lemma 3.4 c_1 such that

$$\varepsilon^2 \Big\| \int_0^\sigma \Phi(\tau(s))\, ds \Big\| \leq c_1 \varepsilon^2.$$

Finally, as ϕ is $\mathcal{O}(\varepsilon^3)$ in average, there exists c_2 such that

$$\Big\| \int_0^\sigma \phi(\tau(s))\, ds \Big\| \leq c_2 \varepsilon^3 \sigma.$$

The summation of these estimations yields

$$\| E(\sigma) \| \leq \varepsilon \lambda_F \int_0^\sigma \| E(s) \| ds + c_1 \varepsilon^2 + c_2 \varepsilon^3 \sigma.$$

Then by Gronwall's lemma [SVM05, Lemma 1.3.3]

$$\| E(\sigma) \| \leq \left(\frac{c_2}{\lambda_F} + c_1 \right) e^{\lambda_F \sigma} \varepsilon^2,$$

which means $\widetilde{X} = \overline{X} + \mathcal{O}(\varepsilon^2)$. □

The following lemma is an extension of Besjes' lemma 2.1 when φ is no longer Lipschitz, but only slowly-varying in average.

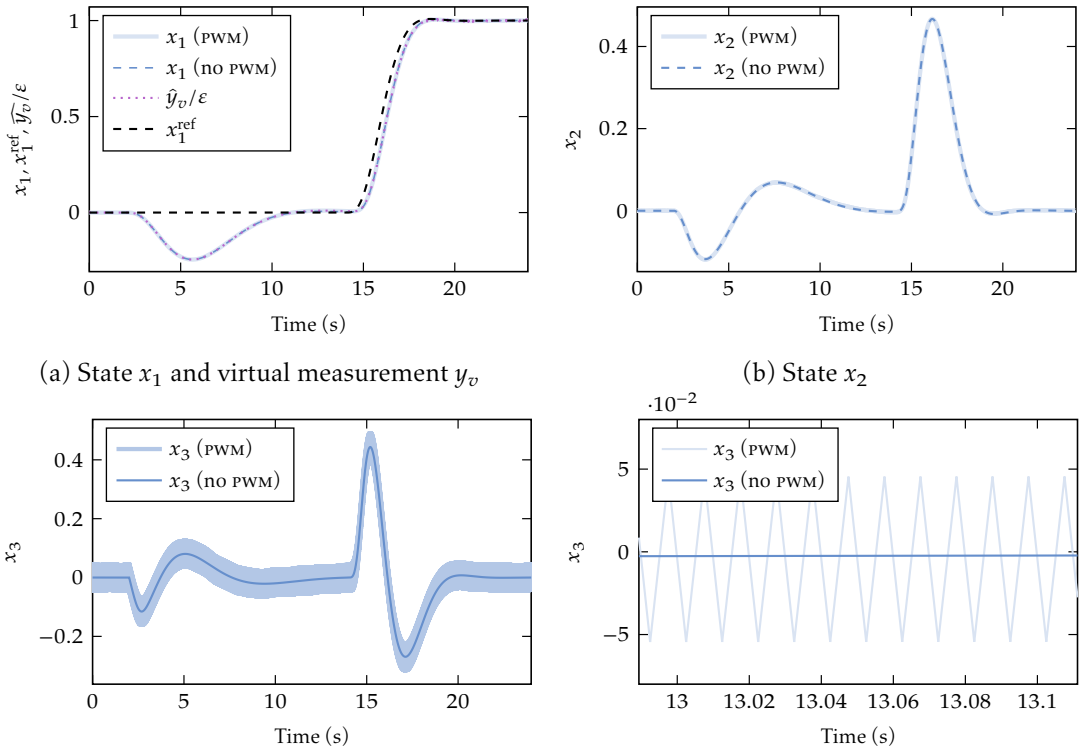

(a) State x_1 and virtual measurement y_v

(b) State x_2

(c) State x_3

(d) State x_3, zoom on (c)

Figure 3.4: States x_1, x_2, x_3 with ideal and actual control laws.

Lemma 3.4. *Assume $\varphi(\chi, \sigma)$ is bounded, slowly-varying in average, T-periodic and zero-mean in the second argument. Assume the solution $X(\sigma)$ of $\dot{X} = \mathcal{O}(\varepsilon)$ is defined for $0 \leq \sigma \leq L/\varepsilon$. Then, there exists $c_1 > 0$ such that*

$$\left\| \int_0^\sigma \varphi(X(s), s)\, ds \right\| \leq c_1.$$

Proof. Along the lines of the Besjes' lemma proof 2.1, we divide the interval $[0, t]$ in m subintervals $[0, T]$, ..., $[(m-1)T, mT]$ and a remainder $[mT, t]$. By splitting the integral on those intervals, we write

$$\begin{aligned}\int_0^\sigma \varphi(x(s), s)\, ds = &\sum_{i=1}^{m} \int_{(i-1)T}^{iT} \varphi(x((i-1)T), s)\, ds + \sum_{i=1}^{m} \int_{(i-1)T}^{iT} \left[\varphi(x(s), s) - \varphi(x((i-1)T), s)\right] ds \\ &+ \int_{mT}^{\sigma} \varphi(x(s), s)\, ds,\end{aligned}$$

where each of the integral in the first sum are zero as φ is periodic with zero mean. Since φ is bounded, the remainder is also bounded by a constant $c_2 > 0$. Besides

$$x(s) = x((i-1)T) + \int_{(i-1)T}^{s} \dot{x}(\tau)\, d\tau = x((i-1)T) + \varepsilon q(s),$$

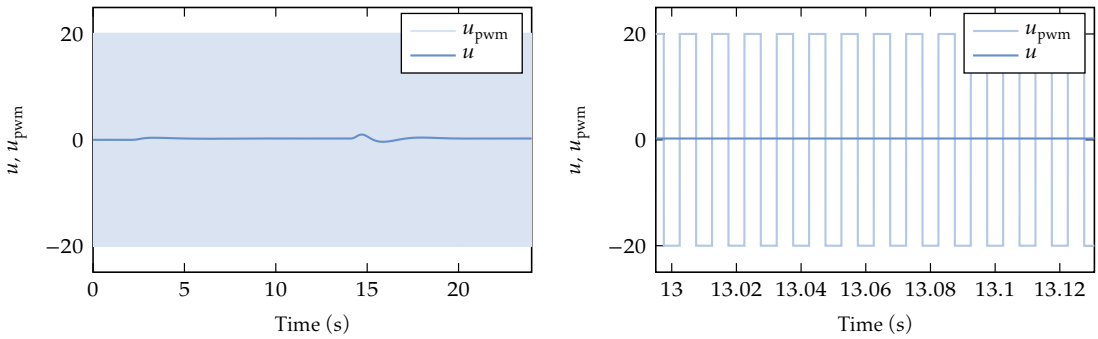

Figure 3.5: Control input u and its modulation u_{pwm}; full view (left), zoom (right).

with q continuous and bounded. By hypothesis, there exists $\lambda > 0$ such that for $0 \leq i \leq m$,

$$\int_{(i-1)T}^{iT} \| \varphi(x(s), s) - \varphi(x((i-1)T), s) \| \, ds \leq \lambda T \varepsilon.$$

Therefore by summing the previous estimations,

$$\left\| \int_0^{\sigma} \varphi(x(s), s) \, ds \right\| \leq m\lambda T \varepsilon + c_2,$$

with $mT \leq t \leq L/\varepsilon$, consequently $m\lambda T\varepsilon + c_2 \leq \lambda L + c_2$; which concludes the proof. □

3.4 Virtual measurement extraction

From (3.8c), we can write the measured signal y as

$$y(t) = y_a(t) + y_v(t) s_1(u(t), \tfrac{t}{\varepsilon}) + \mathcal{O}(\varepsilon^2),$$

where the signal u feeding the PWM encoder is known. The following result shows y_a and y_v can be estimated from y thanks to a suitable demodulation procedure, for use in a control law as described in section 3.3.1.

Theorem 3.5. *Consider the estimators $\hat{y}_a$ and $\hat{y}_v$ defined by*

$$\begin{aligned} \hat{y}_a(t) &:= \frac{3}{2} M(y)(t) - \frac{1}{2} M(y)(t - \varepsilon) \\ k_\Delta(t) &:= (y(t) - \hat{y}_a(t)) s_1(u(t), \tfrac{t}{\varepsilon}) \\ \hat{y}_v(t) &:= \frac{M(k_\Delta)(t)}{\overline{s_1^2}(u(t))}, \end{aligned}$$

where M is the moving average operator defined in section 3.1, and $\overline{s_1^2}$ the mean of s_1^2 in the second argument (c.f. end of section 3.1). Then,

$$\hat{y}_a(t) = y_a(t) + \mathcal{O}(\varepsilon^2) \tag{3.20a}$$

$$\hat{y}_v(t) = y_v(t) + \mathcal{O}(\varepsilon^2). \tag{3.20b}$$

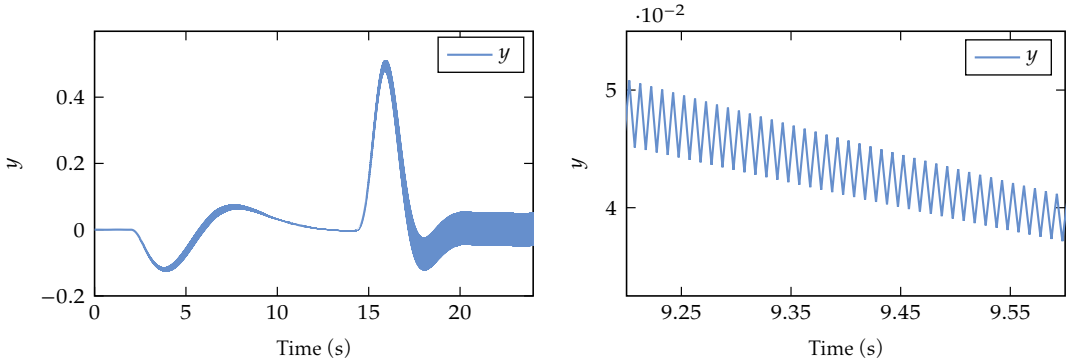

Figure 3.6: Measured output y; full view (left), zoom (right).

Recall that by construction $y_v(t) = \mathcal{O}(\varepsilon)$, hence (3.20b) is essentially a first-order estimation; notice also that $\overline{s_1^2}(u(t))$ is always non-zero when $u(t)$ does not exceed the range of the PWM encoder.

Proof. Taylor expanding y_a, y_v, u and s_1 yields

$$\begin{aligned} y_a(t-\tau) &= y_a(t) - \tau \dot{y}_a(t) + \mathcal{O}(\tau^2) \\ y_v(t-\tau) &= y_v(t) + \mathcal{O}(\varepsilon)\mathcal{O}(\tau) \\ s_1(u(t-\tau),\sigma) &= s_1(u(t) + \mathcal{O}(\tau),\sigma) = s_1(u(t),\sigma) + \mathcal{O}(\tau); \end{aligned}$$

in the second equation, we have used $\dot{y}_v(t) = \mathcal{O}(\varepsilon)$. The moving average of y_a then reads

$$\begin{aligned} M(y_a)(t) &= \frac{1}{\varepsilon}\int_0^\varepsilon y_a(t-\tau)d\tau = \frac{1}{\varepsilon}\int_0^\varepsilon (y_a(t) - \tau\dot{y}_a(t) + \mathcal{O}(\tau^2))d\tau \\ &= y_a(t) - \frac{\varepsilon}{2}\dot{y}_a(t) + \mathcal{O}(\varepsilon^2). \end{aligned} \tag{3.21}$$

A similar computation for $k_v(t) := y_v(t)s_1(u(t), \frac{t}{\varepsilon})$ yields

$$\begin{aligned} M(k_v)(t) &= \frac{1}{\varepsilon}\int_0^\varepsilon y_v(t-\tau)s_1(u(t-\tau), \tfrac{t-\tau}{\varepsilon})\,d\tau \\ &= y_v(t)\left(\overline{s_1}(u(t)) + \mathcal{O}(\varepsilon)\right) + \mathcal{O}(\varepsilon^2) \\ &= \mathcal{O}(\varepsilon^2), \end{aligned} \tag{3.22}$$

since s_1 is 1-periodic and zero mean in the second argument. Summing (3.21) and (3.22), we eventually find

$$M(y)(t) = y_a(t) - \frac{\varepsilon}{2}\dot{y}_a(t) + \mathcal{O}(\varepsilon^2).$$

As a consequence, we get after another Taylor expansion

$$\frac{3}{2}M(y)(t) - \frac{1}{2}M(y)(t-\varepsilon) = y_a(t) + \mathcal{O}(\varepsilon^2),$$

which is the desired estimation (3.20a). On the other hand, (3.20a) implies

$$k_\Delta(t) = y_v(t)s_1^2(u(t), \tfrac{t}{\varepsilon}) + \mathcal{O}(\varepsilon^2).$$

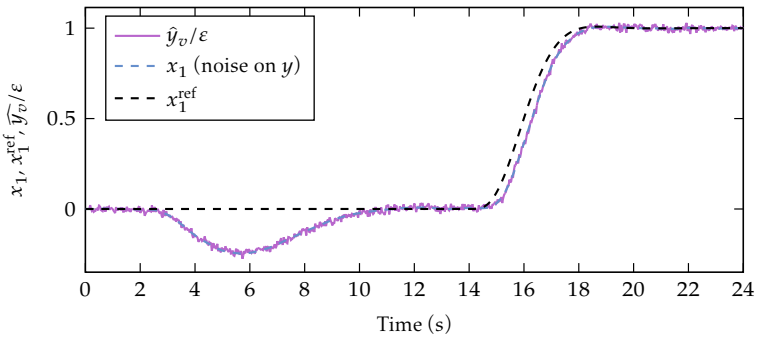

Figure 3.7: x_1^{ref}, x_1, and $\hat{y}_v$ in the presence of noise.

Proceeding as for $M(k_v)$, we find

$$\begin{aligned} M(k_\Delta)(t) &= \frac{1}{\varepsilon}\int_0^\varepsilon y_v(t-\tau)s_1^2(u(t-\tau), \tfrac{t-\tau}{\varepsilon})\,d\tau = y_v(t)\left(\overline{s_1^2}(u(t)) + \mathcal{O}(\varepsilon)\right) + \mathcal{O}(\varepsilon^2) \\ &= y_v(t)\overline{s_1^2}(u(t)) + \mathcal{O}(\varepsilon^2). \end{aligned}$$

Dividing by $\overline{s_1^2}(u(t))$ yields the desired estimation (3.20b). □

3.5 Numerical example

We illustrate the interest of the approach on the system

$$\begin{aligned} \dot{x}_1 &= x_2 \\ \dot{x}_2 &= x_3 \\ \dot{x}_3 &= u + d \\ y &= x_2 + x_1x_3, \end{aligned}$$

where d is an unknown disturbance; u will be impressed through PWM with frequency 1 kHz (i.e. $\varepsilon = 10^{-3}$) and range $[-20, 20]$. The objective is to control x_1, while rejecting the disturbance d, with a response time of a few seconds. We want to operate around equilibrium points, which are of the form $(x_1^{eq}, 0, 0; -d^{eq}, d^{eq})$, for x_1^{eq} and d^{eq} constant. Notice the observability degenerates at such points, which renders the design of a control law not trivial. Nevertheless the PWM-induced signal injection makes available the virtual measurement

$$y_v = \varepsilon \begin{pmatrix} x_3 & 1 & x_1 \end{pmatrix} \begin{pmatrix} 0 & 0 & 1 \end{pmatrix}^T = \varepsilon x_1,$$

from which it is easy to design a suitable control law, without even using the actual output $y_a = x_2 + x_1x_3$. The system being now fully linear, we can use a classical controller-observer,

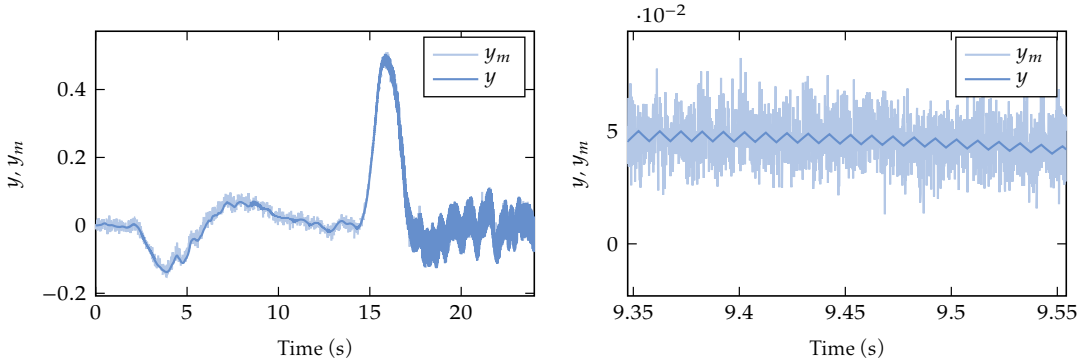

Figure 3.8: Measured output y with and without noise; full view (left), zoom (right).

with disturbance estimation to ensure an implicit integral effect. The observer is thus given by

$$\begin{aligned}
\dot{\hat{x}}_1 &= \hat{x}_2 + l_1\left(\tfrac{y_v}{\varepsilon} - \hat{x}_1\right)\\
\dot{\hat{x}}_2 &= \hat{x}_3 + l_2\left(\tfrac{y_v}{\varepsilon} - \hat{x}_1\right)\\
\dot{\hat{x}}_3 &= u + \hat{d} + l_3\left(\tfrac{y_v}{\varepsilon} - \hat{x}_1\right)\\
\dot{\hat{d}} &= l_d\left(\tfrac{y_v}{\varepsilon} - \hat{x}_1\right),
\end{aligned}$$

and the controller by

$$u = -k_1\hat{x}_1 - k_2\hat{x}_2 - k_3\hat{x}_3 - k_d\hat{d} + kx_1^{\text{ref}}.$$

The gains are chosen to place the observer eigenvalues at $(-1.19, -0.73, -0.49 \pm 0.57i)$ and the controller eigenvalues at $(-6.59, -3.30 \pm 5.71i)$. The observer is slower than the controller in accordance with dual Loop Transfer Recovery, thus ensuring a reasonable robustness. Setting $\eta := \begin{pmatrix}\hat{x}_1 & \hat{x}_2 & \hat{x}_3 & \hat{d}\end{pmatrix}^T$, this controller-observer obviously reads

$$u = -K\eta + kx_1^{\text{ref}} \tag{3.23a}$$
$$\dot{\eta} = M\eta + L\tfrac{y_v}{\varepsilon}, \tag{3.23b}$$

where the matrices K, L and M are

$$K := \begin{pmatrix}k_1 & k_2 & k_3 & k_d\end{pmatrix}, \quad L := \begin{pmatrix}l_1 & l_2 & l_3 & l_d\end{pmatrix}, \quad M = \begin{pmatrix}-l_1 & 1 & 0 & 0\\ -l_2 & 0 & 1 & 0\\ -l_3 - k_1 & -k_2 & -k_3 & 1 - k_d\\ -l_d & 0 & 0 & 0\end{pmatrix}.$$

Finally, this ideal control law is implemented as

$$u_{\text{pwm}}(t) = \mathcal{M}(-K\eta + kx_1^{\text{ref}}, \tfrac{t}{\varepsilon}) \tag{3.24a}$$
$$\dot{\eta} = M\eta + L\tfrac{\hat{y}_v}{\varepsilon}, \tag{3.24b}$$

where $\mathcal{M}$ is the PWM function described in section 3.2, and $\hat{y}_v$ is obtained by the demodulation process of section 3.4. The test scenario is the following: at $t = 0\,\text{s}$, the system starts at rest at the origin; from $t = 2\,\text{s}$, a disturbance $d = -0.25$ is applied to the system; at $t = 14\,\text{s}$, a filtered

unit step is applied to the reference x_1^{ref}. In Fig. 3.4 the ideal control law (3.23), i.e. without PWM and assuming y_v known, is compared to the true control law (3.24): the behavior of (3.24) is excellent, it is nearly impossible to distinguish the two situations on the responses of x_1 and x_2 as by (3.8a) the corresponding error is only $\mathcal{O}(\varepsilon^2)$; the ripple is visible on x_3, where it is $\mathcal{O}(\varepsilon)$. The corresponding control signals u and u_{pwm} are displayed in Fig. 3.5, and the corresponding measured outputs in Fig. 3.6.

To investigate the sensitivity to measurement noise, the same test was carried out with band-limited white noise (power density 1×10^{-9}, sample time 1×10^{-5}) added to y. Even though the ripple in the measured output is buried in noise, see Fig. 3.8, the virtual output is correctly demodulated and the control law (3.24) still behaves very well.

Chapter 4

Error analysis of a demodulation procedure for multicarrier signals with slowly-varying carriers

This chapter collects the results from two papers: one published in the proceedings of IECON19 under the title *A New Demodulation Procedure for a Class of Multiplexed Signals* [Sur+19a], the other in the proceedings of EUSIPCO21 under the title *Error Analysis of a Demodulation Procedure for Multicarrier Signals with Slowly-Varying Carriers* [SCM21a].

Résumé Que ce soit dans le cadre de l'injection endogène ou exogène, la conception d'une procédure d'extraction des mesures virtuelles est nécessaire afin de pouvoir exploiter l'information supplémentaire portée par la perturbation induite. Ce chapitre propose une synthèse des techniques de démodulation esquissées aux chapitres 2 et 3, et développe une procédure de démodulation générique des signaux analogiques multiplexés par des porteuses présentant une variation lente par rapport au temps. Cette dernière spécificité décrit la nature de la perturbation induite dans le cas endogène, où la dépendance du ripple de sortie par rapport à la commande introduit une échelle de temps lente dans l'évolution de la porteuse. À partir d'une combinaison linéaire adéquate de moyennes mobiles itérées, il est possible d'extraire chacune des composantes d'un tel signal multiplexé avec une précision asymptotique arbitrairement petite. Lorsque le signal d'entrée présente des perturbations périodiques — à chaque commutation pour un système piloté par MLI à cause des décharges des capacités parasites—, il est possible de changer la base de démodulation afin d'annihiler la corruption du signal engendrée tout en conservant l'ordre de l'estimation asymptotique.

Abstract Whether it is for endogenous or exogenous signal injection, the design of a virtual measurements extraction procedure is necessary to exploit the additional knowledge carried by the induced perturbation. This chapter synthesizes the demodulation techniques outlined in chapters 2 and 3, and presents a generic demodulation procedure for analog signals multiplexed by slowly-varying carriers. This slow-time dependency comes from the output ripple in the endogenous case that depends on the control input. Using a suitable linear combination of iterated moving averages, each component of such a multiplexed signal is extracted with an arbitrarily small asymptotic accuracy. When the input signal exhibits periodic disturbances —at every switching for a PWM-driven system due to parasitic capacitances discharges—, a new demodulation basis is designed so as to annihilate the signal corruption while preserving the order of the asymptotic estimation.

4.1 Introduction

We consider a composite signal y of the form

$$y(t) := \sum_{i=1}^{n} z_i(t) s_i(t, \tfrac{t}{\varepsilon}) + d(t, \tfrac{t}{\varepsilon}) + \mathcal{O}(\varepsilon^k), \tag{4.1}$$

where the s_i's are (known) 1-periodic functions in the second variable; ε being a (known) "small" parameter, the s_i's can be seen as rapidly-oscillating carriers with slowly-varying shapes modulating the (unknown) z_i's. The function d is a disturbance, also 1-periodic in the second variable, about which little is known except that for each t the support of $d(t, \cdot)$ is contained in a "well-behaved" known subset D_t of $[0, 1)$. In other words, on each period of the carriers, part of the signal y is garbled and considered useless. Finally, the $\mathcal{O}(\varepsilon^k)$ term corresponds to "small" disturbances, where $\mathcal{O}$ denotes the (uniform) "big O" symbol of analysis, i.e. $f(t, \varepsilon) = \mathcal{O}(\varepsilon^k)$ if $\|f(t, \varepsilon)\| \leq K\varepsilon^k$ for some K independent of t and ε.

The objective is to recover by an implementable causal process the unknown z_i's with an accuracy of up to $\mathcal{O}(\varepsilon^k)$ from the known y and s_i's, provided the s_i's and z_i's satisfy some suitable regularity assumptions.

The motivation for this problem is the following. When operating an AC electric motor through a PWM inverter with period ε, an analysis based on the theory of averaging reveals that the currents in the motor have the form

$$y(t) = y_a(t) + \varepsilon y_v(t) s(t, \tfrac{t}{\varepsilon}) + d(t, \tfrac{t}{\varepsilon}) + \mathcal{O}(\varepsilon^2),$$

which is a particular instance of (4.1) with $z_1 := y_a$, $z_2 := \varepsilon y_v$, $s_1 := 1$, and $s_2 := s$, where s is determined by the PWM process defined in chapter 3. The $\mathcal{O}(\varepsilon^2)$ term corresponds to a small higher-order term which can be ignored. The disturbance d consists of short spikes appearing at each PWM commutation, due to stray capacitances in the power electronics. A typical signal y is shown in Fig. 4.3, see also [Sur+20b, Fig. 9] for experimental data. In "sensorless" industrial drives, these currents are the only measurements, and controlling the motor at or near standstill with this sole information is a difficult problem for several theoretical and technological reasons. A way to achieve this it to extract y_a and εy_v from the modulated currents y; a suitable processing of y_v then gives access to the motor angular position (see chapter 6), which is instrumental in controlling the motor. It is therefore very important to ensure the demodulation error is at most $\mathcal{O}(\varepsilon^2)$.

The demodulation procedure proposed in this chapter, essentially consisting of multiplications by known signals followed by low-pass filters, is reminiscent of various schemes in communication theory and signal processing. Nevertheless, nothing really close seems to exist in the literature, let alone a quantitative analysis of the demodulation error:

— it is of course a generalization of coherent demodulation in quadrature carrier multiplexing, with more than two carriers not restricted to sine and cosine, see e.g. [LD10, section 4.4]; but even in this simple case, no analysis of the error is usually performed, the challenges being more on carrier reconstruction

— it somewhat looks like synchronous decorrelating detection in Code-Division Multiple

Access (CDMA) communication systems, where the s_i's would play the roles of the signature waveforms and the z_i's the role of the symbols, see e.g. [Ver98, section 5.1]; but the encoded signals being there digital, the issues and analysis are very different

— it is also akin to multicarrier reception, with or without multiple access, see e.g [Glo05, section 12.2] and [Yan09, section 2.2]; but once again that field is exclusively concerned with digital encoded signals

— finally, it bears some resemblance for its filtering part with the interpolation/compensation filters used in $\Delta\Sigma$ analog-to-digital converters, see e.g. [PST17, chapter 14].

The chapter synthesizes and extends the previous work (chapter 2, section 2.3.3 and chapter 3, section 3.4) in two ways that are paramount for the intended application: on the one hand, it considers carriers with slowly-varying shapes, which makes the error analysis much more difficult; on the other hand, the procedure is not restricted to "orthogonal" demodulation, hence can directly handle the disturbance d without ad-hoc prefiltering as in [Sur+20b].

The chapter runs as follows: in section 4.2, we collect notations and definitions, in particular the $\mathcal{A}_k$ regularity property; in section 4.3 we state and prove the main result; in section 4.4 we illustrate this result and confirm the error estimates with numerical experiments.

4.2 Notations and definitions

We collect here definitions used throughout the chapter. The most important notion is the $\mathcal{A}_k$ regularity property introduced in definition 4.1, which is needed in lemma 4.4 to repeatedly integrate by parts; this property, which is paramount for handling carriers with slowly-varying shapes, is trivially satisfied for fixed-shape carriers as in [Sur+19a].

Let $g(t,\sigma)$ be a function of two variables; informally speaking, t represents the slow timescale and σ the fast timescale. We will often use the convenient notation $g_\varepsilon(t) := g(t, \frac{t}{\varepsilon})$. The function g is 1-periodic in the second variable if $g(t,\sigma+1) = g(t,\sigma)$ for all t. Its mean in the second variable is the function $\overline{g}(t) := \int_0^1 g(t,\sigma)d\sigma$. For brevity, we will usually omit the phrase "in the second variable". If g is 1-periodic with zero mean, any of its primitives (in the second variable) is also 1-periodic, in particular its zero-mean primitive $g^{(-1)}(t,\sigma) := \int_0^\sigma g(t,\tau)d\tau - \int_0^1 \int_0^\zeta g(t,\tau)d\tau d\zeta$. Likewise, $g^{(-k-1)}$ denotes the zero-mean primitive of $g^{(-k)}$. We say g is Lipschitz (in the first argument) if $\|g(t_1,\sigma) - g(t_2,\sigma)\| \le L\|t_1 - t_2\|$ for some L independent of t_1, t_2 and σ.

Finally, we introduce the $\mathcal{A}_k$ regularity property.

Definition 4.1 ($\mathcal{A}_k$ property)**.** Let $g(t,\sigma)$ be 1-periodic with zero mean. It is said to be $\mathcal{A}_k$, $k \ge 1$, if $g^{(-k)}$ is $k-1$ times differentiable in the first variable, with bounded derivatives at all orders, and $\partial_1^{k-1} g^{(-k)}$ Lipschitz.

A typical $\mathcal{A}_k$ function encountered in practice is $g(t,\sigma) = \operatorname{sign}(u(t) - \mathrm{w}(\sigma)) - 2u(t) + 1$ where $\mathrm{w}(\sigma) := \sigma \mod 1$; $u(t) \in (0,1)$ represents the PWM duty cycle and is assumed $k-1$ times differentiable, with bounded derivatives at all orders, and $u^{(k-1)}$ Lipschitz.

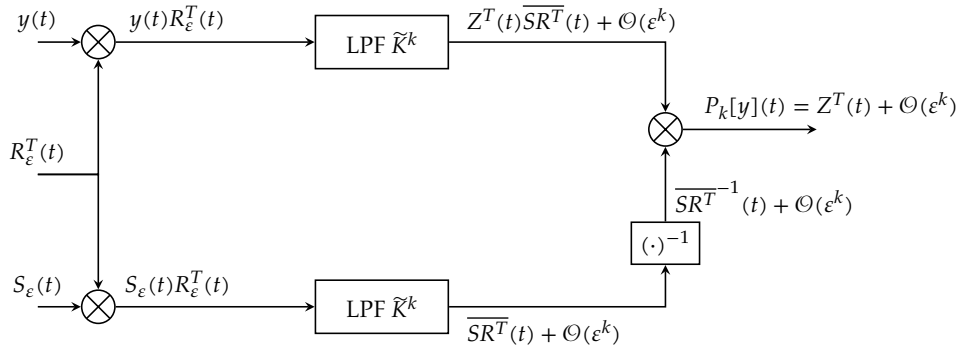

Figure 4.1: The demodulation procedure.

It is easy to show that if on the one hand $g(t,\sigma)$ is $\mathcal{A}_k$, and on the other hand $z(t)$ is $k-1$ times differentiable, with bounded derivatives at all orders, and $z^{(k-1)}$ Lipschitz, then the product zg is also $\mathcal{A}_k$.

4.3 The demodulation procedure

The demodulation procedure for an error of order ε^k consists of multiplications by a suitable demodulating basis $R := (r_1, \dots, r_n)^T$, followed by a bank of low-pass finite impulse response filters with kernel $\widetilde{K}^k$; see section 4.3.1 for a discussion of how to select R.

The kernel $\widetilde{K}^k$ is a "compensated" k-times iterated moving average, namely a suitable linear combination of shifted instances of K^k, where the kernel K^k is defined recursively by $K^1 := \frac{1}{\varepsilon}\mathbb{1}_{[0,\varepsilon]}$ and $K^k := K^{k-1} * K$, see e.g. [Aubo5, chapter 6.7] for explicit expressions. For instance for $k = 3$, the linear combination is

$$\widetilde{K}^3(t) := \tfrac{17}{4}K^3(t) - 5K^3(t-\varepsilon) + \tfrac{7}{4}K^3(t-2\varepsilon),$$

see section 4.3.2 for more details.

Figure 4.1 illustrates the whole demodulation procedure:

- $y(t)$ is multiplied by $R_\varepsilon^T(t)$, and filtered by $\widetilde{K}_k$; the result, $\left(\widetilde{K}^k * (yR_\varepsilon^T)\right)(t)$, turns out to be $Z^T(t)\overline{SR^T}(t) + \mathcal{O}(\varepsilon^k)$, where $Z := (z_1, \dots, z_n)^T$ is the vector signal to recover
- the modulating basis $S := (s_1, \dots, s_n)^T$ is also multiplied by $R_\varepsilon^T(t)$, and filtered by $\widetilde{K}_k$; the result, $\left(\widetilde{K}^k * (S_\varepsilon R_\varepsilon^T)\right)(t)$, turns out to be $\overline{SR^T}(t) + \mathcal{O}(\varepsilon^k)$
- finally, $\left(\widetilde{K}^k * (yR_\varepsilon^T)\right)(t)$ is multiplied by the inverse of the matrix $\left(\widetilde{K}^k * (S_\varepsilon R_\varepsilon^T)\right)(t)$; the result, $\left(\widetilde{K}^k * (yR_\varepsilon^T)\right)(t) \times \left(\widetilde{K}^k * (S_\varepsilon R_\varepsilon^T)\right)^{-1}(t)$, is as desired $Z^T(t) + \mathcal{O}(\varepsilon^k)$.

As pointed out in the introduction, this demodulation scheme is at first sight not completely surprising. What is much less obvious is that the overall demodulation error is indeed of order ε^k.

4.3.1 Demodulation of multiplexed signals – Main result

We assume that the s_i's are independent outside the subset D_t containing the support of the disturbance $d(t,\cdot)$, i.e. that the $\check{s}_i$'s defined by $\check{s}_i(t,\sigma) := (1-\mathbb{1}_{D_t})(\sigma)s_i(t,\sigma)$ are linearly independent. We can thus choose the demodulating basis $R := (r_1,\dots,r_n)^T$ such that $Rd = 0$ and $\overline{SR^T}$ is invertible, where $S := (s_1,\dots,s_n)^T$ is the modulating basis; one simple choice is for instance $R(t,\sigma) := (1-\mathbb{1}_{D_t}(\sigma))S(t,\sigma)$. A delicate point is to select R also such that $SR^T - \overline{SR^T}$ is $\mathcal{A}_k$, provided of course that D_t is "well-behaved" (for instance a finite union of intervals with sufficiently regular moving bounds). For simplicity, we just assume this is the case (and check it a posteriori in the numerical experiments of section 4.4). Finally, we assume the z_i's are $k-1$ times differentiable, with bounded derivatives at all orders, and $z_i^{(k-1)}$ Lipschitz, so that $z_i(SR^T - \overline{SR^T})$ is also $\mathcal{A}_k$.

Theorem 4.1. *$Z := (z_1,\dots,z_n)^T$ can be recovered to order ε^k from y by the causal process P_k defined by*

$$P_k[y](t) := \left(\widetilde{K}^k * (yR_\varepsilon^T)\right)(t) \times \left(\widetilde{K}^k * (S_\varepsilon R_\varepsilon^T)\right)^{-1}(t).$$

In other words, $Z^T(t) = P_k[y](t) + \mathcal{O}(\varepsilon^k)$.

4.3.2 Proof of theorem 4.1

Rewriting (4.1) as

$$y(t) = Z^T(t)S(t,\tfrac{t}{\varepsilon}) + d(t,\tfrac{t}{\varepsilon}) + \mathcal{O}(\varepsilon^k),$$

right-multiplying by R_ε^T and convolving with K^k yields

$$\begin{aligned}\left(K^k * (yR_\varepsilon^T)\right)(t) &= \left(K^k * (Z^T S_\varepsilon R_\varepsilon^T)\right)(t) + \mathcal{O}(\varepsilon^k)\\ &= \left[K^k * \left(Z^T(S_\varepsilon R_\varepsilon^T - \overline{SR^T})\right)\right](t) + \left(K^k * (Z^T\overline{SR^T})\right)(t) + \mathcal{O}(\varepsilon^k)\\ &= \left(K^k * (Z^T\overline{SR^T})\right)(t) + \mathcal{O}(\varepsilon^k);\end{aligned}$$

to obtain the last line, we have applied Lemma 4.4 with $g(t,\sigma) := Z^T(t)(S(t,\sigma)R^T(t,\sigma) - \overline{SR^T}(t))$, which is by construction zero-mean and $\mathcal{A}_k$. The result obviously holds also if $K^k(t)$ is replaced by the shifted kernel $\tau_T K^k(t) := K^k(t-T)$.

On the other hand, theorem 4.5 [Sur+19b, Theorem 1] asserts that a $\mathcal{C}^k$-function φ with bounded $\varphi^{(k)}$ is left unchanged to order ε^k by a suitable linear combination $\widetilde{K}^k$ of the shifted kernels $\tau_{i\varepsilon}K^k$, $i = 0,\dots,k-1$, i.e. $(\widetilde{K}^k * \varphi)(t) = \varphi(t) + \mathcal{O}(\varepsilon^k)$. For instance,

$$\begin{aligned}\widetilde{K}^1(t) &:= K^1(t)\\ \widetilde{K}^2(t) &:= 2K^2(t) - K^2(t-\varepsilon)\\ \widetilde{K}^3(t) &:= \tfrac{17}{4}K^3(t) - 5K^3(t-\varepsilon) + \tfrac{7}{4}K^3(t-2\varepsilon).\end{aligned}$$

Actually, we must slightly extend the result to the case where φ is $k-1$ times differentiable with $\varphi^{(k-1)}$ Lipschitz, which we omit here. As a consequence,

$$\begin{aligned}\left(\widetilde{K}^k * (yR_\varepsilon^T)\right)(t) &= \left(\widetilde{K}^k * (Z^T\overline{SR^T})\right)(t) + \mathcal{O}(\varepsilon^k)\\ &= Z^T(t)\overline{SR^T}(t) + \mathcal{O}(\varepsilon^k).\end{aligned}$$

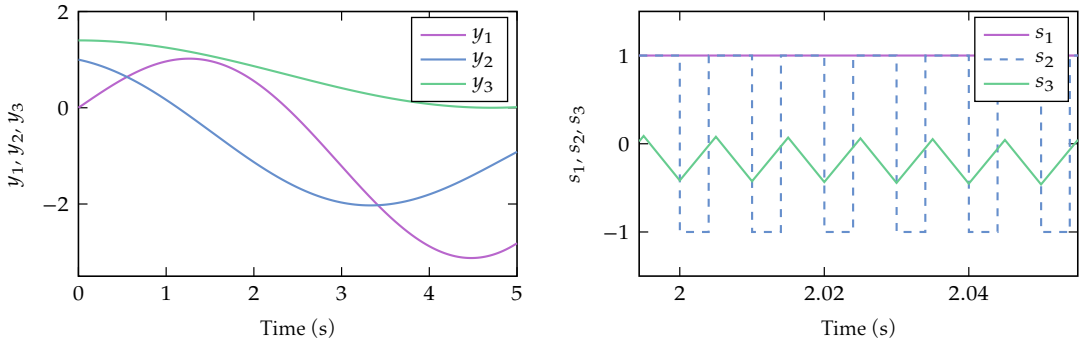

(a) $z_1(t), z_2(t), z_3(t)$ (b) $s_1(t), s_2(t), s_3(t)$ (zoom)

Figure 4.2: Encoded signals z_i (left), carriers s_i (right).

Since $\overline{SR^T}(t)$ is invertible, $Z(t)$ can be recovered to order ε^k.

To make the process truly implementable in practice, notice $\overline{SR^T}(t)$ can be computed to order ε^k by

$$\left(\widetilde{K}^k * (S_\varepsilon R_\varepsilon^T)\right)(t) = \overline{SR^T}(t) + \mathcal{O}(\varepsilon^k),$$

which is an instance of the previous equation with $Z = \begin{pmatrix} 1 & 1 & \cdots & 1 \end{pmatrix}^T$.

In conclusion, $Z(t)$ is recovered to order ε^k by

$$\begin{aligned} P_k[y](t) &:= \left(\widetilde{K}^k * (yR_\varepsilon^T)\right)(t) \times \left(\widetilde{K}^k * (S_\varepsilon R_\varepsilon^T)\right)^{-1}(t) \\ &= Z^T(t) + \mathcal{O}(\varepsilon^k), \end{aligned}$$

where the process P_k is causal since the kernel $\widetilde{K}^k$ is supported on $[0, k\varepsilon] \subset \mathbb{R}^+$.

4.3.3 Characteristic powers and $\mathcal{A}_k$-signals properties

This subsection is quite technical and can be skipped without disturbing the flow of ideas. Its goal is to establish Lemma 4.4, which is instrumental in the proof of Theorem 4.1. Lemma 4.4 relies on Lemma 4.3, which itself relies on Lemma 4.2. Lemmas 4.4 and 4.3 are in some sense properties of the convolution kernel K^k, whereas Lemma 4.2 extends to our context a classical result of finite-differences calculus. Notice the use of the $\mathcal{A}_k$ property when integrating by parts in Lemma 4.4, which is the main trick to extend the ideas of [Sur+19b] to slowly-moving carriers.

Define the k^{th}-order backward difference $\Delta^k g_\varepsilon$ of the function $g_\varepsilon(t) := g(t, \frac{t}{\varepsilon})$ by

$$(\Delta^k g_\varepsilon)(t) := \sum_{i=0}^{k} (-1)^i \binom{k}{i} g_\varepsilon(t - i\varepsilon).$$

On the other hand, recall that K^k is $k-1$ times differentiable, with compact support for all the derivatives. As for $(K^k)^{(k)}$, it can be defined in the distributional sense, and is a linear combination of Dirac delta functions, and in particular also has compact support; for instance, $(K^1)^{(1)} = \frac{1}{\varepsilon}(\delta_0 - \delta_\varepsilon)$.

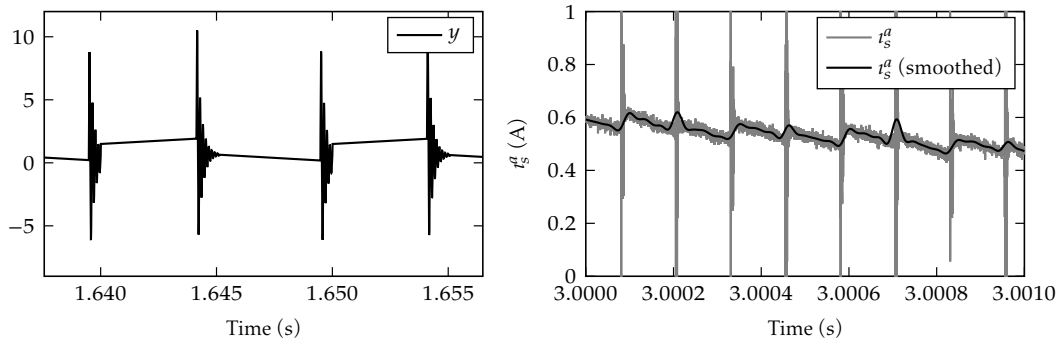

(a) Synthetic data (b) Stator current i_s^a

Figure 4.3: Composite signal $y(t)$ (zoom).

Lemma 4.2. *Let $g(t,\sigma)$ be 1-periodic, and $k-1$ times differentiable in the first variable with $\partial_1^{(k-1)} g$ Lipschitz. Then $(\Delta^k g_\varepsilon)(t) = \mathcal{O}(\varepsilon^k)$.*

Proof. By the Lipschitz form of Taylor's formula [ESD90, (2.1)],

$$g(t+\mu,\sigma) = \sum_{j=0}^{k-1} \frac{\mu^j}{j!} \partial_1^j g(t,\sigma) + \mu^k \rho_t(\mu,\sigma),$$

where the remainder ρ_t is $\mathcal{O}(1)$ since it satisfies

$$\mu\rho_t(\mu,\sigma) = \frac{1}{(k-2)!} \int_0^1 (1-\tau)^{k-2} \times \left(\partial_1^{k-1} g(t+\mu\tau,\sigma) - \partial_1^{k-1} g(t,\sigma)\right) d\tau.$$

Applying this to $g(t-i\varepsilon, \frac{t-i\varepsilon}{\varepsilon}) = g(t-i\varepsilon, \frac{t}{\varepsilon})$ since g is 1-periodic yields

$$\begin{aligned}(\Delta^k g_\varepsilon)(t) &= \sum_{i=0}^{k} (-1)^i \binom{k}{i} g(t-i\varepsilon, \tfrac{t-i\varepsilon}{\varepsilon}) = \sum_{i=0}^{k} (-1)^i \binom{k}{i} \left(\sum_{j=0}^{k-1} \frac{(-i\varepsilon)^j}{j!} \partial_1^j g(t, \tfrac{t}{\varepsilon}) + \mathcal{O}(\varepsilon^k) \right) \\ &= \sum_{j=0}^{k-1} \frac{(-\varepsilon)^j}{j!} \partial_1^j g(t, \tfrac{t}{\varepsilon}) \sum_{i=0}^{k} (-1)^i \binom{k}{i} i^j + \mathcal{O}(\varepsilon^k).\end{aligned}$$

As $\sum_{i=0}^{k} (-1)^i \binom{k}{i} i^j = 0$, see [Rui96, Cor. 2], this gives the desired result. □

Lemma 4.3. *Let $g(t,\sigma)$ be 1-periodic, and $k-1$ times differentiable in the first variable with $\partial_1^{(k-1)} g$ Lipschitz. Then $((K^k)^{(k)} * g_\varepsilon)(t) = \mathcal{O}(1)$.*

Proof. We first prove by induction that $(K^k)^{(k)} * g_\varepsilon = \frac{1}{\varepsilon^k} \Delta^k g_\varepsilon$. We have $(K^1)' * g_\varepsilon = \frac{1}{\varepsilon}(\delta_0 - \delta_\varepsilon) * g_\varepsilon = \frac{1}{\varepsilon} \Delta_1 g_\varepsilon$. Assuming the property holds at rank k,

$$\begin{aligned}(K^{k+1})^{(k+1)} * g_\varepsilon &= (K^k * K^1)^{(k+1)} * g_\varepsilon = (K^k)^{(k)} * (K^1)' * g_\varepsilon \\ &= \frac{1}{\varepsilon^k} \Delta^k ((K^1)' * g_\varepsilon) = \frac{1}{\varepsilon^k} \Delta^k \Big(\frac{\Delta_1 g_\varepsilon}{\varepsilon} \Big) \\ &= \frac{1}{\varepsilon^{k+1}} \Delta_{k+1} g_\varepsilon.\end{aligned}$$

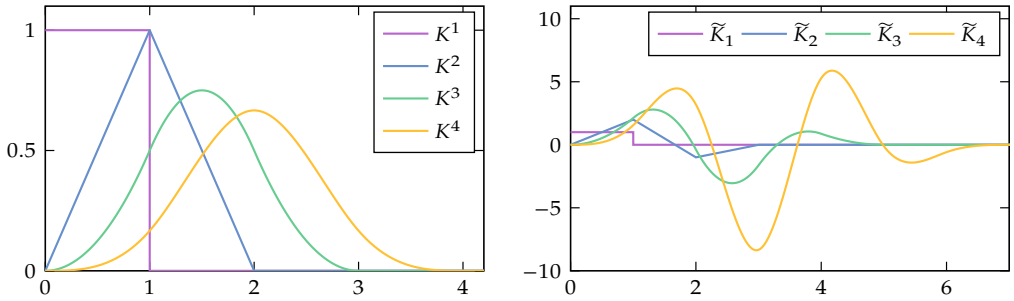

Figure 4.4: Characteristic powers K^k (left), reconstruction kernels $\widetilde{K}^k$ (right) for $k = 1, \dots, 4$.

To obtain the second equality, we have repeatedly used $(T * S)' = T' * S = T * S'$ (with T and S piecewise absolutely continuous). Applying Lemma 4.2, we eventually find $((K^k)^{(k)} * g_\varepsilon)(t) = \frac{1}{\varepsilon^k}\Delta^k g_\varepsilon(t) = \frac{1}{\varepsilon^k}\mathcal{O}(\varepsilon^k) = \mathcal{O}(1)$, thus concluding the proof. □

Lemma 4.4. *Let g be $\mathcal{A}_k$. Then $(K^k * g_\varepsilon)(t) = \mathcal{O}(\varepsilon^k)$.*

Proof. We sketch the proof for $k = 3$, the general result following by induction. Notice that by assumption $g^{(-3)}$ is twice differentiable in the first variable with $\partial_1^2 g^{(-3)}$ Lipschitz, which will be used each time Lemma 4.3 is invoked.

We first prove $\left((K^3)'' * (g^{(-2)})_\varepsilon\right)(t) = \mathcal{O}(\varepsilon)$. Starting from

$$\left((g^{(-3)})_\varepsilon\right)' = (\partial_1 g^{(-3)})_\varepsilon + \frac{1}{\varepsilon}(\partial_2 g^{(-3)})_\varepsilon = (\partial_1 g^{(-3)})_\varepsilon + \frac{1}{\varepsilon}(g^{(-2)})_\varepsilon,$$

we find after convolving with $(K^3)''$ and integrating by parts

$$(K^3)'' * (g^{(-2)})_\varepsilon = \varepsilon (K^3)''' * (g^{(-3)})_\varepsilon - \varepsilon (K^3)'' * (\partial_1 g^{(-3)})_\varepsilon;$$

the boundary terms vanish since $(K^3)''$ has compact support. The first term is $\mathcal{O}(\varepsilon)$ by Lemma 4.3. Using $(K^3)'' = (K^1 * K^2)'' = K^1 * (K^2)''$, the second term reads $\varepsilon K^1 * \left((K^2)'' * (\partial_1 g^{(-3)})_\varepsilon\right)$, hence is also $\mathcal{O}(\varepsilon)$ by Lemma 4.3. The sum of the two terms is therefore also $\mathcal{O}(\varepsilon)$.

We next prove $\left((K^3)' * (g^{(-1)})_\varepsilon\right)(t) = \mathcal{O}(\varepsilon^2)$. Indeed, using successively

$$(g^{(-1)})_\varepsilon = \varepsilon (g^{(-2)})'_\varepsilon - \varepsilon (\partial_1 g^{(-2)})_\varepsilon$$
$$(\partial_1 g^{(-2)})_\varepsilon = \varepsilon (\partial_1 g^{(-3)})'_\varepsilon - \varepsilon (\partial_1^2 g^{(-3)})_\varepsilon$$

yields

$$(g^{(-1)})_\varepsilon = \varepsilon (g^{(-2)})'_\varepsilon - \varepsilon^2 (\partial_1 g^{(-3)})'_\varepsilon + \varepsilon^2 (\partial_1^2 g^{(-3)})_\varepsilon.$$

Convolving with $(K^3)'$ and integrating by parts,

$$(K^3)' * (g^{(-1)})_\varepsilon = \varepsilon (K^3)'' * (g^{(-2)})_\varepsilon - \varepsilon^2 (K^3)'' * (\partial_1 g^{(-3)})_\varepsilon + \varepsilon^2 (K^3)' * (\partial_1^2 g^{(-3)})_\varepsilon;$$

the boundary terms vanish since $(K^3)'$ has a bounded support. We already know the first two terms are $\mathcal{O}(\varepsilon^2)$. Using $(K^3)' = (K^2 * K^1)' = K^2 * (K^1)'$, the last term reads $\varepsilon^2 K^2 * \left((K^1)' *\right.$

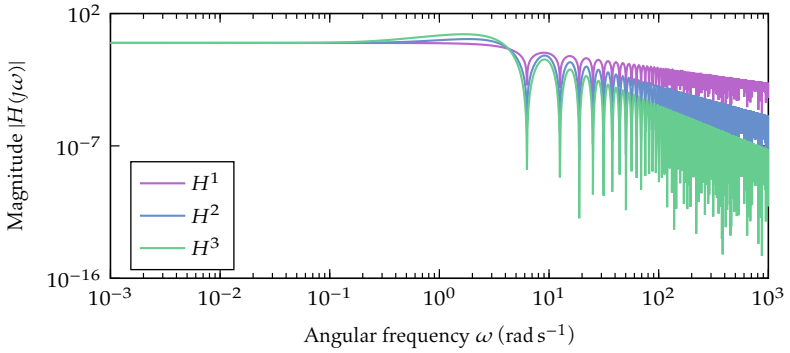

Figure 4.5: Bode magnitude plot of H^1 (purple), H^2 (blue) and H^3 (green).

$(\partial_1^2 g^{(-3)})_\varepsilon\big)$, hence is also $\mathcal{O}(\varepsilon^2)$ by lemma 4.3. The sum of the three terms is therefore also $\mathcal{O}(\varepsilon^2)$.

We finally prove $(K^3 * g_\varepsilon)(t) = \mathcal{O}(\varepsilon^3)$. Indeed, using successively

$$\begin{aligned} g_\varepsilon &= \varepsilon (g^{(-1)})'_\varepsilon - \varepsilon (\partial_1 g^{(-1)})_\varepsilon \\ (\partial_1 g^{(-1)})_\varepsilon &= \varepsilon (\partial_1 g^{(-2)})'_\varepsilon - \varepsilon (\partial_1^2 g^{(-2)})_\varepsilon \\ (\partial_1^2 g^{(-2)})_\varepsilon &= \varepsilon (\partial_1^2 g^{(-3)})'_\varepsilon - \varepsilon (\partial_1^3 g^{(-3)})_\varepsilon, \end{aligned}$$

we find

$$g_\varepsilon = \varepsilon (g^{(-1)})'_\varepsilon - \varepsilon^2 (\partial_1 g^{(-2)})'_\varepsilon + \varepsilon^3 (\partial_1^2 g^{(-3)})'_\varepsilon - \varepsilon^3 (\partial_1^3 g^{(-3)})_\varepsilon.$$

Convolving with K^3 and integrating by parts,

$$K^3 * g_\varepsilon = \varepsilon (K^3)' * (g^{(-1)})_\varepsilon - \varepsilon^2 (K^3)' * (\partial_1 g^{(-2)})_\varepsilon + \varepsilon^3 (K^3)' * (\partial_1^2 g^{(-3)})_\varepsilon - \varepsilon^3 K^3 * (\partial_1^3 g^{(-3)})_\varepsilon;$$

the boundary terms vanish since K^3 has a bounded support. We already know the first and third terms are $\mathcal{O}(\varepsilon^3)$. The second term reads

$$\begin{aligned} \varepsilon^2 (K^3)' * (\partial_1 g^{(-2)})_\varepsilon &= \varepsilon^3 (K^3)' * (\partial_1 g^{(-3)})'_\varepsilon - \varepsilon^3 (K^3)' * (\partial_1^2 g^{(-3)})_\varepsilon \\ &= \varepsilon^3 (K^3)'' * (\partial_1 g^{(-3)})_\varepsilon - \varepsilon^3 (K^3)' * (\partial_1^2 g^{(-3)})_\varepsilon \\ &= \varepsilon^3 K^1 * \big((K^2)'' * (\partial_1 g^{(-3)})_\varepsilon\big) - \varepsilon^3 (K^2)' * \big((K^1)' * (\partial_1^2 g^{(-3)})_\varepsilon\big), \end{aligned}$$

and is also $\mathcal{O}(\varepsilon^3)$ by using Lemma 4.3 twice. Finally, by Young's convolution inequality, the fourth term satisfies

$$\| \varepsilon^3 K^3 * \partial_1^3 g^{(-3)} \|_\infty \leq \varepsilon^3 \| K^3 \|_1 \| \partial_1^3 g^{(-3)} \|_\infty,$$

hence is also $\mathcal{O}(\varepsilon^3)$; notice $\partial_1^3 g^{(-3)}$ is bounded by assumption, and so is K^3. The sum of the four terms is therefore also $\mathcal{O}(\varepsilon^3)$, which concludes the proof. □

4.3.4 Identity reconstruction from shifted iterated moving averages

The strength of lemma 4.4 lies in the mitigation of $\mathcal{A}_k$ signals up to the k^{th} order in ε. This result is particularly useful for canceling the periodic (in the second argument) terms, but

fails at fully recovering its input, that is, recovering y from $y * K^k$. One way to achieve this recovery consists in considering linear combinations of shifted convolutions $y * \tau_{i\varepsilon}K^k$. Theorem 4.5 details the technique to select the coefficients of such a linear combination to yield the input signal y. Simply put, the operator P defined in the theorem is the identity with an approximation error in $\mathcal{O}(\varepsilon^k)$. This result is a generalization of lemma 2.9.

Theorem 4.5. *Let φ be C^k with $\varphi^{(k)}$ bounded. There exists a sequence $(\alpha_i^k)_{0\leq i\leq k-1} \in \mathbb{Q}^k$ (specified in the proof and in table 4.1 for $k = 1, \dots, 6$) such that*

$$P^k[\varphi](t) := \sum_{i=0}^{k-1} \alpha_i^k \varphi * K^k(t - i\varepsilon) = \varphi(t) + \mathcal{O}(\varepsilon^k).$$

Proof. Let first compute the convolution product $\varphi * K^k$. Considering the k^{th}-order Taylor expansion of φ, with the remainder being bounded by hypothesis, it reads

$$\begin{aligned}\varphi * K(t) &= \frac{1}{\varepsilon}\int_0^\varepsilon \varphi(t-\sigma)\,d\sigma = \frac{1}{\varepsilon}\int_0^\varepsilon \left[\sum_{i=0}^{k-1} \frac{(-\sigma)^i}{i!}\varphi^{(i)}(t)\right] d\sigma + \mathcal{O}(\varepsilon^k) \\ &= \sum_{i=0}^{k-1} \varepsilon^i a_{0,i}^1 \varphi^{(i)}(t) + \mathcal{O}(\varepsilon^k), \end{aligned} \tag{4.2}$$

where the coefficients $a_{0,i}^1$ satisfy for $0 \leq i \leq k-1$, $a_{0,i}^1 := (-1)^i/(i+1)!$. The expression for $\varphi * K^2$ is directly obtained by applying K to (4.2), namely

$$\begin{aligned}\varphi * K^2(t) = (\varphi * K) * K(t) &= \sum_{i_1=0}^{k-1} \varepsilon^{i_1} a_{0,i_1}^1 \varphi^{(i_1)} * K(t) + \mathcal{O}(\varepsilon^k) \\ &= \sum_{i_1=0}^{k-1} \varepsilon^{i_1} a_{0,i_1}^1 \sum_{i_2=0}^{k-1-i_1} \varepsilon^{i_2} \frac{(-1)^{i_2}}{(i_2+1)!}\varphi^{(i_1+i_2)}(t) + \mathcal{O}(\varepsilon^k) \\ &= \sum_{i=0}^{k-1} \varepsilon^i a_{0,i}^2\, \varphi^{(i)}(t) + \mathcal{O}(\varepsilon^k),\end{aligned}$$

where the second line is obtained through the application of Taylor expansion (4.2) to each summed terms. Notice also that the application of K to the uniform remainder $\mathcal{O}(\varepsilon^k)$ still yields a $\mathcal{O}(\varepsilon^k)$ term, as K is bounded with compact support. The coefficients $a_{0,i}^2$ are defined for $0 \leq i \leq k-1$ by

$$a_{0,i}^2 := \sum_{j=0}^{i} \frac{(-1)^{i-j}}{(i-j+1)!} a_{0,j}^1.$$

This computational process can be iterated to obtain the expression of the convolution product between φ and the k^{th}-order convolution kernel K^k, that is

$$\varphi * K^k(t) = \sum_{i=0}^{k-1} \varepsilon^i a_{0,i}^k \varphi^{(i)}(t) + \mathcal{O}(\varepsilon^k),$$

where $a_{0,i}^k$ is defined, for $0 \leq i \leq k-1$, by induction as follows

$$a_{0,i}^k := \sum_{j=0}^{i} \frac{(-1)^{i-j}}{(i-j+1)!} a_{0,j}^{k-1}.$$

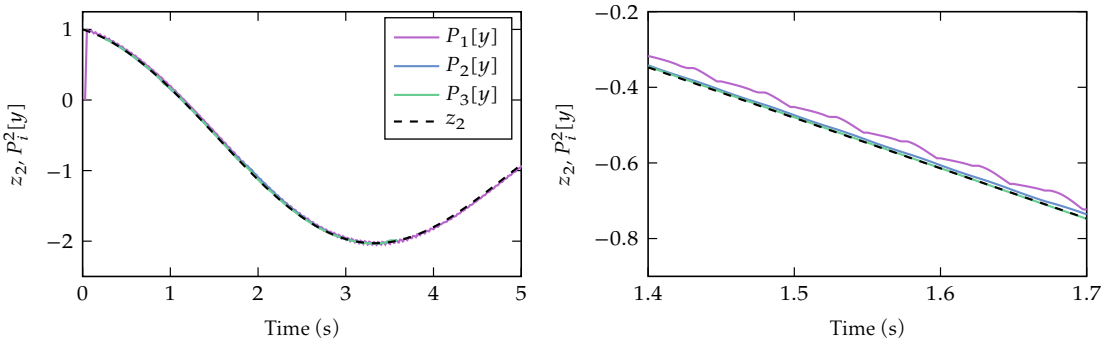

(a) y_2, $P_2^i(y)$ (b) Zoom on 4.6a

Figure 4.6: Component z_2 (black, dashed) and its estimates at order one $P_2^1(y)$ (purple), two $P_2^2(y)$ (blue) and three $P_2^3(y)$ (green) with $\varepsilon = 0.05$.

To reconstruct φ from $\varphi * K$, consider first its expression delayed by a factor $l\varepsilon$ with $l = 0, \dots, k-1$

$$\varphi * K^k(t - l\varepsilon) = \sum_{i=0}^{k-1} \varepsilon^i a_{0,i}^k \varphi^{(i)}(t - l\varepsilon) + \mathcal{O}(\varepsilon^k) = \sum_{i=0}^{k-1} \varepsilon^i a_{l,i}^k \varphi^{(i)}(t) + \mathcal{O}(\varepsilon^k),$$

where the second identity is once again obtained by Taylor expansion. Also, the coefficients $a_{l,i}^k$ read for $0 \leq l, i \leq k-1$,

$$a_{l,i}^k := \sum_{j=0}^{i} \frac{(-l)^{i-j}}{(i-j)!} a_{0,j}^k. \tag{4.3}$$

A suitable linear combination of shifted $\varphi * K^k$ recovers φ with an accuracy in ε^k. Indeed, define $\mathfrak{M}^k(\varphi)(t) = \big(\varphi * K^k(t - i\varepsilon)\big)_{0 \leq i \leq k-1}$ the concatenation of $\varphi * K^k(t)$ and its delayed evaluations, $\mathfrak{A}^k := (a_{l,i}^k)_{0 \leq l,i \leq k-1}$ defined by equation (4.3) and $\Phi(t) := (\varepsilon^i \varphi^{(i)})_{0 \leq i \leq k-1}$ the "Taylor expansion basis". Then from the previous calculations,

$$\mathfrak{M}^k(\varphi)(t) = \mathfrak{A}^k \Phi(t) + \mathcal{O}(\varepsilon^k).$$

Assume the matrix $\mathfrak{A}^k$ is invertible, and define $\alpha^k = (\alpha_i^k)_{0 \leq i \leq k-1}$ such that

$$\alpha^k \mathfrak{A}^k = \begin{pmatrix} 1 & 0 & \dots & 0 \end{pmatrix}.$$

The first coefficient of $\Phi(t)$ is simply $\varphi(t)$, meaning that

$$\alpha^k \mathfrak{M}^k(\varphi)(t) = \alpha^k \mathfrak{A}^k \Phi(t) + \mathcal{O}(\varepsilon^k) = \varphi(t) + \mathcal{O}(\varepsilon^k).$$

This identity reads $(\varphi * \widetilde{K}^k)(t) = \varphi(t) + \mathcal{O}(\varepsilon^k)$, where $\widetilde{K}^k$ is the k^{th}-order reconstruction kernel

$$\widetilde{K}^k(t) := \sum_{i=0}^{k-1} \alpha_i^k K^k(t - i\varepsilon).$$

For $k = 1, \dots, 6$, $\mathfrak{A}^k$ explicitly reads

$$\mathfrak{A}^1 = \begin{pmatrix} 1 \end{pmatrix}, \quad \mathfrak{A}^2 = \begin{pmatrix} 1 & -1 \\ 1 & -2 \end{pmatrix}, \quad \mathfrak{A}^3 = \begin{pmatrix} 1 & -3/2 & 5/4 \\ 1 & -5/2 & 13/4 \\ 1 & -7/2 & 25/4 \end{pmatrix},$$

$$\mathfrak{A}^4 = \begin{pmatrix} 1 & -2 & 13/6 & -5/3 \\ 1 & -3 & 14/3 & -5 \\ 1 & -4 & 49/6 & -34/3 \\ 1 & -5 & 38/3 & -65/3 \end{pmatrix}, \quad \mathfrak{A}^5 = \begin{pmatrix} 1 & -5/2 & 10/3 & -25/8 & 331/144 \\ 1 & -7/2 & 19/3 & -63/8 & 1087/144 \\ 1 & -9/2 & 31/3 & -129/8 & 2767/144 \\ 1 & -11/2 & 46/3 & -231/8 & 5947/144 \\ 1 & -13/2 & 64/3 & -377/8 & 11347/144 \end{pmatrix},$$

$$\mathfrak{A}^6 = \begin{pmatrix} 1 & -3 & 19/4 & -21/4 & 1087/240 & -259/80 \\ 1 & -4 & 33/4 & -35/3 & 3047/240 & -679/60 \\ 1 & -5 & 51/4 & -265/12 & 4175/143 & -1507/48 \\ 1 & -6 & 73/4 & -75/2 & 14047/240 & -2959/40 \\ 1 & -7 & 99/4 & -707/12 & 10301/97 & -12828/83 \\ 1 & -8 & 129/4 & -262/3 & 42887/240 & -8839/30 \end{pmatrix}. \tag{4.4}$$

Solving $\alpha^k \mathfrak{A}^k = \begin{pmatrix} 1 & 0 & \dots 0 \end{pmatrix}$ provides the coefficients α_i^k; table 4.1 eventually gathers these values. □

4.3.5 Sensitivity to noise of the designed estimator

In practical applications, the measurement y is always corrupted by noise on top of the physical disturbance d. Windowing the disturbances by selecting a suited demodulation basis R proved to cancel the harmful effects of d on the y. Still, the demodulation properties with respect to the noise has not been examined yet. To do so, consider the signal y as in (4.1) perturbed by an Additive White Gaussian Noise (AWGN) ν with Power Spectral Density PSD$[\nu]$

$$y(t) = \sum_{i=0}^{N} z_i(t) s_i(t, \tfrac{t}{\varepsilon}) + d(t, \tfrac{t}{\varepsilon}) + \nu + \mathcal{O}(\varepsilon^n).$$

Demodulating the components z_l from this measurement introduces an additive white noise ν_l^k in the expression of the estimate $P_l^k[y]$ of z_l. Specifically, the PSD of ν_l^k is

$$\text{PSD}[\nu_l^k](\omega) = \text{PSD}[\nu\xi_l](\omega) |H^n(\jmath\omega)|^2,$$

where $\xi_l := [R_\varepsilon^T (\overline{SR^T})^{-1}]_l$ is the l^{th} function coefficient of the matrix $R_\varepsilon^T (\overline{SR^T})^{-1}$, for $l = 1, \dots, n$, and H^k is the transfer function associated to K_k whose expression is

$$H^k(\jmath\omega) := \text{sinc}^k\left(\frac{\varepsilon\omega}{2}\right) \exp\left(\frac{-\jmath k\varepsilon\omega}{2}\right) \sum_{l=0}^{k-1} \alpha_l^k \exp\left(-\jmath l\varepsilon\omega\right).$$

Along the lines of [Com+16a], since ν and ξ_l are independent (the latter being purely deterministic), $\nu\xi_l$ behaves as a Gaussian white noise with PSD$[\nu\xi_l] = \overline{\xi_l^2}PSD[\nu]$. The functions ξ_l directly depends on the inverse of matrix $\overline{SR^T}$, meaning its condition number characterizes the estimate properties regarding the additive noise ν. A better condition number κ limits the magnitudes of the signals ξ_l, thereby reducing the noise PSD in the estimate. Selecting a

Table 4.1: Coefficients α^k of the reconstruction kernel for $k = 1, \dots, 6$

k	α_0^k	α_1^k	α_2^k	α_3^k	α_4^k	α_5^k
1	1					
2	2	-1				
3	17/4	-5	7/4			
4	28/3	$-109/6$	40/3	$-7/2$		
5	3013/144	$-2089/36$	1589/24	$-1279/36$	1069/144	
6	1903/40	$-19557/113$	16247/60	$-8877/40$	11269/120	$-781/48$

suitable demodulation basis turns out to be of utmost importance, both for discarding the disturbance d and mitigating the noise corruption.

The Bode plots of H^k, given in Fig. 4.5, show that the PSD of the noise is slightly amplified at low frequencies as k increases. Indeed, the reconstruction kernel $\widetilde{K}_k$ describes an active filter whose gains increase with the kernel order k, as described by table 4.1 and the graphical representation 4.4. This stems from the poor conditioning of the matrices (4.4) to invert in order to derive the full kernel $\widetilde{K}_k$. In practice, we restrict to orders lower than three to extract Z from the measurement y.

4.4 Numerical experiments

4.4.1 Scenario

We illustrate the error analysis of Theorem 4.1 with numerical experiments for $k = 1, 2, 3$. Consider the composite signal y defined on $[0, 5]$ by

$$y(t) = z_1(t)s_1(t, \tfrac{t}{\varepsilon}) + z_2(t)s_2(t, \tfrac{t}{\varepsilon}) + z_3(t)s_3(t, \tfrac{t}{\varepsilon}) + d(t, \tfrac{t}{\varepsilon}),$$

with encoded signals z_1, z_2, z_3 (see Fig. 4.2a) and carriers s_1, s_2, s_3 (see Fig. 4.2b)

$$\begin{aligned} z_1(t) &:= 2\sin(t) - 1.5\sin(\tfrac{t}{2}), & s_1(t,\sigma) &:= 1, \\ z_2(t) &:= \cos(t) - 1.2\sin(\tfrac{t}{4}), & s_2(t,\sigma), &:= \operatorname{sign}(\tfrac{t}{20} + \mathrm{w}(\sigma) - 0.5), \\ z_3(t) &:= 1.4\cos(\tfrac{t}{3})^2 & s_3(t,\sigma) &:= \cos(t) + \mathrm{w}(\sigma)\mathbb{1}_{[0,0.5]}(\mathrm{w}(\sigma)) \\ & & &\quad +(1-\mathrm{w}(\sigma))\mathbb{1}_{[0.5,1]}(\mathrm{w}(\sigma)), \end{aligned}$$

where $\mathrm{w}(\sigma) := \sigma \mod 1$. The support of the disturbance $d(t, \cdot)$ is

$$D_t := D_{1,t} \cup D_{2,t} = [f(t) - \tfrac{1}{20}, f(t) + \tfrac{1}{20}] \cup [g(t) - \tfrac{1}{20}, g(t) + \tfrac{1}{20}],$$

with $f(t) := \frac{1}{2}(1 + \sin(t))$ and $g(t) := \frac{1}{2}(1 + \cos(t))$; hence, on a window of length ε between 10 % (when the two intervals $D_{1,t}$ and $D_{2,t}$ coincide) and 20 % (when the two intervals are disjoint) of the signal is corrupted. The disturbance d itself is defined as follows: consider $\tilde{\tau} := \varepsilon^{-1}(t/\varepsilon \mod 1)$, τ_1 and τ_2 such that

$$\tau_1 = 10(\tilde{\tau} \bmod f(t) - 1/20)\mathbb{1}_{D_1}(t), \qquad \tau_2 = 10(\tilde{\tau} \bmod g(t) - 1/20)\mathbb{1}_{D_2}(t).$$

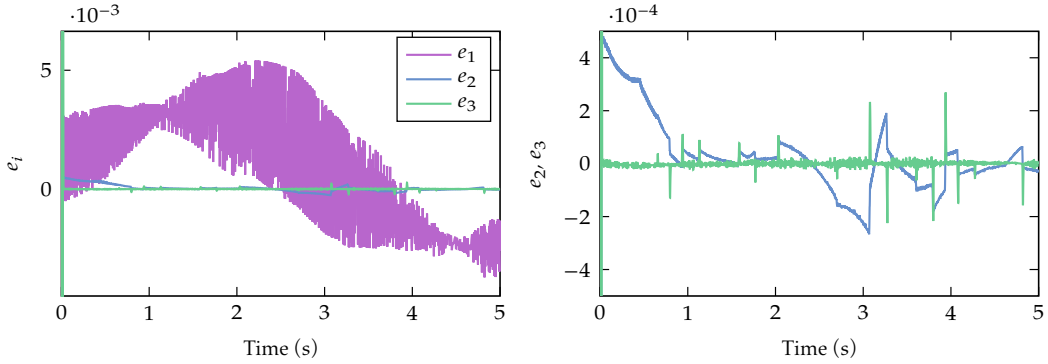

Figure 4.7: Errors $e_k(t)$ for $\varepsilon = 10^{-2}$: full view (left), zoom (right).

The disturbance reads $d = d_1 + d_2$ with

$$d_1 = 10\exp(-5\tau_1)\sin(50\tau_1), \qquad d_2 = 10\exp(-5\tau_2)\sin(50\tau_2).$$

The partial disturbance d_1 (resp. d_2) is only active on $D_{1,t}$ (resp. $D_{2,t}$); such a definition for d tries to replicate the experimental observations, see Fig 4.3b. Fig 4.3a displays the resulting signal y, with the spikes caused by d clearly visible.

We select the simplest demodulating basis that is zero on D_t, namely $R(t,\sigma) := (1 - 1_{D_t}(\sigma))S(t,\sigma)$; tedious but routine computations show $SR^T - \overline{SR^T}$ is $\mathcal{A}_k$ for $k = 1,2,3$. We check numerically that $\overline{SR^T}(t)$ is invertible by plotting its condition number κ, see Fig. 4.8: indeed, $\overline{SR^T}(t)$ is always well-conditioned, except during the filter initialization.

4.4.2 Asymptotic behavior of the error

We focus on the recovery of z_2, since it is modulated by the least regular carrier. We consider the error $e_k(t) := z_2(t) - P_k^2[y](t)$, where $P_k^2[y]$ denotes the second component of $P_k[y]$. For ε fixed, the error decreases as anticipated with k, see Fig 4.7. To study the asymptotic behavior as a function of ε, we consider the L_2-error $\|e_k\| := (\int_1^5 (e_k(t))^2 dt)^{\frac{1}{2}}$; the first second of data is discarded to ensure the filters are well initialized. As anticipated, the plots in log scale are straight lines with slopes equal to the orders of the estimates, see Fig. 4.9.

4.5 Conclusion

We have proposed a demodulation procedure to recover analog signals encoded by multiple carriers with slowly-varying shapes. Though the procedure is not completely surprising at first sight, proving that the overall demodulation error is arbitrarily small is not obvious. Arguably, the framework is somewhat peculiar, which explains why no similar work seems to exist in the literature. Nevertheless, the result is exactly what we need for the application we have in mind, namely the "sensorless" control of AC electric motors at or near standstill. In this application, the composite signal y to be decoded is the (vector) current in the motor,

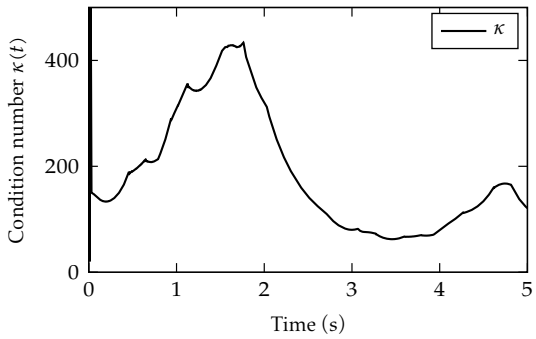

Figure 4.8: Condition number $\kappa(t)$ of matrix $\overline{SR^T}(t)$.

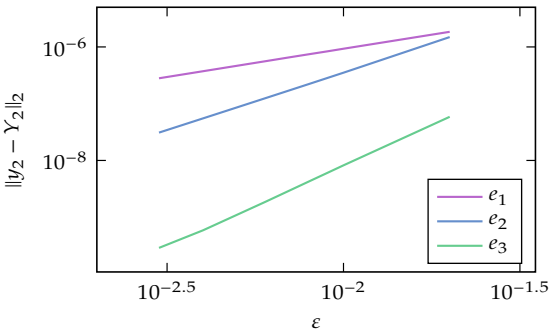

Figure 4.9: L^2-error $\|e_k\|$ as a function of ε.

the motor itself acting as a multicarrier modulator when fed by a PWM inverter; a suitable processing of the demodulated signal then yields the rotor angle, which is needed to accurately control the motor.

Chapter 5

Synchronous demodulation over Sigma-Delta modulators

This chapter is an extension of *Error Estimates in Second-Order Continuous-Time Sigma-Delta Modulators* [SCM21b], published in the Proceedings of ICASSP 2021.

Résumé Afin de capter les effets induits par l'injection endogène sur les courants mesurés — et donc récupérer les mesures virtuelles —, il est nécessaire d'avoir un Convertisseurs Analogique-Numérique (CAN) rapide possédant une fréquence d'échantillonnage supérieure à la fréquence MLI. Les variateurs de vitesse modernes sont aujourd'hui équipés d'un CAN Sigma-Delta (ΣΔ) qui suréchantillonne le signal analogique à une fréquence largement supérieure à celle de la MLI, mais qui en contrepartie ne produit qu'un flux binaire. Demeure alors la question de la possibilité de récupérer l'information contenue dans le ripple de courant non pas à partir des données analogiques, mais en utilisant uniquement ce flux binaire ΣΔ. Bien que l'analyse théorique de l'erreur de reconstruction — et donc de démodulation — pour les modulateurs Sigma-Delta à temps discret utilisant des filtres « sinc » standards soit bien établie, les résultats relatifs à leur équivalent continu ou à l'utilisation de filtres de reconstruction généraux restent rares. Ce chapitre fournit des estimations d'erreur pour des modulateurs Sigma-Delta d'ordre quelconque en temps continu et en temps discret, en utilisant une large classe de filtres passe-bas qui réalisent une détection synchrone sur le flux binaire en sortie. Dans le cas continu, une discrétisation de l'estimation est également proposée afin de permettre une implémentation numérique sur un microprocesseur ou un FPGA. Ce chapitre se conclut par une validation numérique des résultats proposés.

Abstract To capture the effects induced by the endogenous injection on the measured currents —and thus to recover the virtual measurements—, a high-rate Analog-to-Digital Converter (ADC) with a sampling frequency higher than the PWM frequency is required. Modern Variable-Frequency Drives are now equipped with an oversampling Sigma-Delta (ΣΔ) ADC operating at many-times the PWM frequency, but only producing a bitstream in return. The question therefore remains about recovering the information contained in the current ripple not from the analog data, but only from this ΣΔ bitstream. Although theoretical analysis of the reconstruction error —and hence demdoulation— for discrete-time ΣΔ modulators using standard sinc filters is well-established, results pertaining to their continuous counterpart or to the use of general reconstruction filter remain scarce. This

chapter provides error estimates for both continuous-time and discrete-time k^{th}-order Sigma-Delta modulators using a broad class of low-pass filters in order to achieve synchronous detection or matched filtering. In the continuous case, a discretization of the estimate is also derived to allow an actual implementation on a Digital Signal Processor (DSP) or an Field Programmable Gate Array (FPGA). The whole theory is validated by numerical experiments.

5.1 Introduction

Introduced first by Inose and Yasude [IYM62; IY63], Sigma-Delta ($\Sigma\Delta$) modulation is currently a popular technique used in high-accuracy Analog-to-Digital converters (ADC), finding applications in numerous areas, going from the processing of audio signals [YSS04; RW97; Pav+08; Luo+13] to its use in integrated circuits for wireless communications [RCK93; PTS02]. Compared to standard Nyquist-rate converters, $\Sigma\Delta$ converters possess a lower sensitivity to implementation imperfections such as components mismatch. Despite their 1-bit quantization process, they also achieve high resolution through the oversampling of the signal input and noise shaping [CT92; ASS96]. Traditionally, these converters are followed by both a digital low-pass filter and a decimator to realize high resolution conversion [Hog81], thus raising the question of the reconstruction error. For k^{th}-order discrete-time $\Sigma\Delta$ modulators, instantaneous error estimate in $\mathcal{O}(1/N^k)$ are obtained Daubechies et al. [DD03] and Güntürk [Gun03; GT04] for a time-varying input, where N is the oversampling ratio, using for example a sinc^{k+1} filter for the reconstruction [Tha01]. For continuous-time $\Sigma\Delta$ (CT-$\Sigma\Delta$) modulators, which deliver more power-efficient operations than their discrete-time equivalent as well as higher sampling rates [OG06; ST05; SP08], such general results remain partial, however. To provide tools for the design of continuous-time modulators, equivalence results between CT and DT-$\Sigma\Delta$ might be harnessed [SZ96] to derive this type of estimate. In [SCM21b], the theoretical analysis for second-order CT-$\Sigma\Delta$ modulators is conducted by a straightforward approach, yielding the same estimate as in the discrete case.

While estimates are known when the reconstruction filter is a sinc^k or ideal brick-wall filter, the sole use of these two low-pass filters is restrictive for specific applications. Achieving synchronous detection through a $\Sigma\Delta$ modulator (see Fig. 5.1, for instance, requires ad hoc filtering technique, generally by exploiting the properties of the input signal. The same question emerges for the design of matched filters on the output $\Sigma\Delta$-bitstream [Tur60].

This problem also arises in motor control: $\Sigma\Delta$ converters are widely used to retrieve the phase currents as they provide galvanic insulation [Sor15]. The currents carry information on the rotor position if correctly filtered [SCM21a]: indeed, the Pulse-Width Modulation (PWM) of the input voltage creates ripples in the current measurements [Sur+20a] that can be extracted through a demodulation procedure using a homodyne detection based on iterated moving averages [Sur+19a]. This operation cannot be easily conducted directly on the analog currents prior to A/D conversion (as it requires to compute the product of two analog signals), and requires a proper process on the $\Sigma\Delta$ output bitstream. Therefore, knowing the reconstruction error of the $\Sigma\Delta$ modulator is of utmost importance for this type of application, when the filter is no more a simple sinc filter.

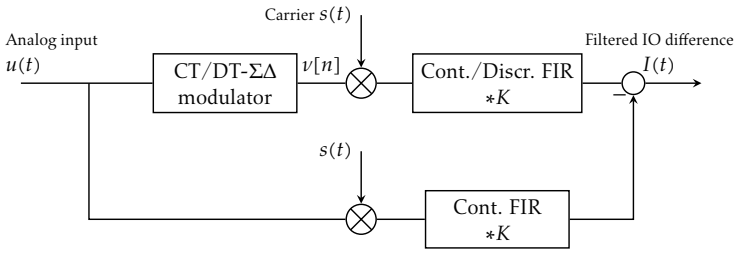

Figure 5.1: Synchronous detection over a ΣΔ modulator.

This chapter tackles the problem of synchronous detection through both continuous and discrete-time ΣΔ modulators. Error estimates are obtained for a more general class of reconstruction filters than the traditional sinc. Noise, as well as stability analyses are otherwise beyond the scope of this chapter: to this extent, every CT/DT-ΣΔ modulator is supposed to be stable for the considered class of inputs.

The outline of this chapter is the following: we first show that for a k^{th}-order DT-ΣΔ modulator in feedforward form, we can obtain an error in $\mathcal{O}(1/N^k)$ with an adequate filtering process, thus realizing the synchronous detection through the DT-ΣΔ. This result is then obtained for CT-ΣΔ modulators also in feedforward form. Such a result is slightly refined with in the continuous case with the help of a generalized version of the Riemann-Lebesgue lemma. In section 5.4, weaker results on feedback structures as well as on the filtering by an IIR are derived. In section 5.5, the continuous filtering procedure is discretized to allow an actual implementation on a Digital Signal Processor (DSP) or an FPGA. We wrap up the whole theory by numerical validations in section 5.6.

5.2 Estimate for DT-ΣΔ modulators in feedforward form

In the following, $u \in [-1,1]$ denotes the input of the modulator, $\tilde{v}[n] \in \{0,1\}$ its output bitstream (see Fig. 6.6) and $v[n] := -1 + 2\tilde{v}[n] \in \{-1,1\}$ the scaled output, $x_{1,2,\dots,k}$ the states of the modulator with k the order of the modulator, T_s is the modulator sampling time such that $N := 1/T_s$, the oversampling ratio, is an integer. Thus the function v is constant on $[jT_s, (j+1)T_s)$ for $j \in \mathbb{N}$.

Throughout this chapter, estimates are often expressed with the notation $\mathcal{O}$, denoting the "big O" of analysis, i.e. $f(t,\varepsilon) = \mathcal{O}(\varepsilon)$ if there exists $K(t) > 0$ independent of ε such that $\|f(t,\varepsilon)\| \leq K(t)\varepsilon$. If additionally, K is independent of t, we write $f(t,\varepsilon) = \mathcal{O}_\infty(\varepsilon)$. Likewise, the notation o is the "small o" of analysis, i.e. $f(t,\varepsilon) = o(\varepsilon)$ if $\|f(t,\varepsilon)\| \leq \varepsilon g(t,\varepsilon)$ where $\lim_{\varepsilon\to 0} g(t,\varepsilon) = 0$. If g is independent of t, we write $f(t,\varepsilon) = o_\infty(\varepsilon)$.

Also, all the modulators will be assumed stable, i.e. the states x_i, $i = 1,\dots,k$ defined in (5.1) and (5.8) remain bounded for both DT and CT-ΣΔ; comprehensive considerations on stability are discussed e.g. in [HZ93; DD03; AP87]. This chapter otherwise does not study the properties and effects of the quantizer, the latter being solely assumed to output a bitstream v.

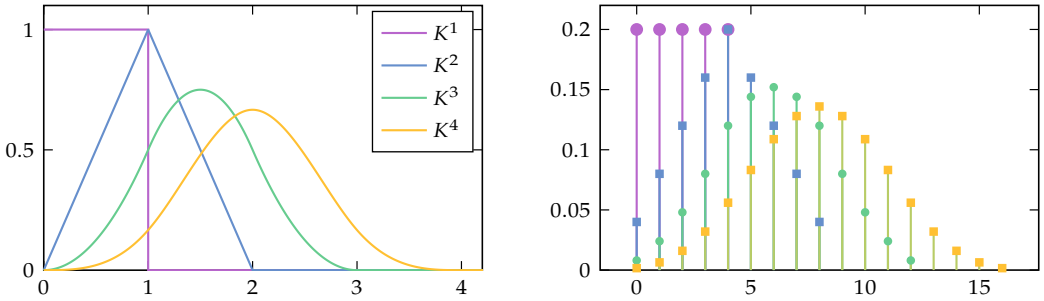

Figure 5.2: Continuous (left) and discretized FIR filters K^k (right, on five points) for $k = 1, 2, 3, 4$ (purple, blue, green, red respectively).

5.2.1 Discrete state-space model of the modulator

The state-space model of a discrete-time k^{th}-order ΣΔ modulator in the feedforward form reads for $j \geq 0$

$$x_1[j+1] = x_1[j] + \beta[j] \tag{5.1a}$$
$$x_i[j+1] = x_i[j] + x_{i-1}[j], \qquad i = 2, \dots, k \tag{5.1b}$$
$$y[j] = \sum_{l=1}^{n} b_l x_l[j], \tag{5.1c}$$

where $x_1[j] := x_1(jT_s)$, and $\beta[j] := u[j] - v[j]$. We start by defining the discrete convolution kernel K^k as follows

$$K^1[j] := \begin{cases} \frac{1}{N} & j = 0, \dots, N-1 \\ 0 & \text{otherwise,} \end{cases} \qquad K^k := (K^1)^{*k} = K^1 * \dots * K^1,$$

where $\cdot^{*k}$ denotes the convolution power; the sampling period is the one of the modulator, namely T_s. For $k = 2$, the kernel K^2 describes the triangular, or Bartlett kernel [BT58], and for $k = 4$, the convolution of the triangle with itself K^4 defines the de la Vallée Poussin (or Parzen) kernel [Har78; Par61]. More generally, the characteristic powers define the so-called Kolmogorov-Zurbenko filters [Zur91; YZ10], also known as the sinc^k filter, and can be seen as a discretization of the continuous B-spline kernels, see figure 5.2.

The synchronous demodulation estimate is encapsulated in theorem 5.1: if the modulating signal s is $\mathcal{C}^k$, then the filtered error is in $\mathcal{O}(1/N^k)$. This estimate is made uniform if additionally, the derivatives of s are bounded. This requirement might seem restrictive, but in practice, periodic signals are employed in modulation processes, hence only assuming the regularity of s gives the desired properties on s and its derivatives.

Theorem 5.1. *Assume s is $\mathcal{C}^k$ such that $s^{(i)}$ is bounded for $i = 0, \dots, k$. Then the following (uniform) estimate holds*

$$\beta s * K^k = \mathcal{O}_\infty(1/N^k).$$

The proof is divided into two parts: first, we prove the result holds for $s = 1$, then we tackle

the synchronous detection issue, by considering a generic signal s satisfying the hypotheses of theorem 5.1.

5.2.2 Standard filtering process (with $s = 1$)

In this subsection, the well-known estimate on k^{th}-order is derived. The next subsection will be dedicated to the synchronous detection using an exogenous signal s.The following proof mainly relies on the basic summation by parts

Lemma 5.2 (Summation by parts)**.** *Consider two sequences $\{a_j\}$ and $\{b_j\}$. Then*

$$\sum_{j=m}^{n} a_j(b_{j+1} - b_j) = a_n b_{n+1} - a_m b_m - \sum_{j=m+1}^{n} b_j(a_j - a_{j-1}).$$

By definition, the discrete convolution of the input-output difference β with K^k reads

$$\beta * K^k[n] := \sum_{j=-\infty}^{+\infty} \beta[n-j]K^k[j]. \tag{5.2}$$

Based on the state-space model of the modulator (see equation (5.1a)), $\beta[j]$ satisfies

$$\beta[j] = x_1[j+1] - x_1[j].$$

Therefore, replacing $\beta[n-j]$ by the previous identity in (5.2) and using the summation by parts between $j = -k$ and $j = kN + k$ (this last bound is so defined because of the non-zero $(kN+k)^{\text{th}}$ terms arising below, see especially equation (5.4)) yields

$$\beta * K^k[n] = x_1[n - kN - k + 1]K^k[kN + k] - x_1[-k]K^k[-k] - \sum_{j=-k+1}^{kN+k} x_1[n-j]\Delta K^k[j],$$

where $\Delta K^k[j] := K^k[j] - K^k[j-1]$ is the finite backward difference. The selected kernel K^k is such that $K^k[-k] = K^k[kN+k] = 0$, thus canceling the first two terms in the previous equation. Besides, the discrete state-space of the ΣΔ modulator (see equation (5.1b)) in a pure feedforward form provides the following expression for $x_i[j]$

$$x_i[j] = x_{i+1}[j+1] - x_{i+1}[j], \qquad k = 1, \dots, k-1.$$

By a straightforward induction, and using that for $j \leq n-1$, $\Delta^j K^k[-k+j] = \Delta^j K^k[kN+k] = 0$, the convolution reduces to

$$\beta * K^k[n] = (-1)^k \sum_{j=0}^{kN-k} x_k[n-j]\Delta^k K^k[j]. \tag{5.3}$$

We now turn to the computation of the coefficients $\Delta^k K^k[j]$. The z-transform of the sinc^k kernel of order k and length N verifies [Zur91]

$$\sum_{r=0}^{+\infty} z^r K^k[r] = \frac{1}{N^k}\left(1 + z + \dots + z^{N-1}\right)^k.$$

By definition of the k-fold composition of the backward difference Δ^k,

$$\Delta^k K^k[m] = \sum_{j=0}^{k} (-1)^j \binom{k}{j} K^k[m-j].$$

Which means the z-transform of $\Delta^k K^k$ satisfies

$$\sum_{r=0}^{+\infty} z^r \Delta^k K^k[r] = \frac{1}{N^k} \sum_{j=0}^{k} (-1)^j \binom{k}{j} z^j \left(1 + z + \ldots + z^{N-1}\right)^k.$$

Using the classical result

$$\sum_{j=0}^{k} (-1)^j \binom{k}{j} z^j = (1-z)^k,$$

the z-transform of $\Delta^k K^k$ reduces to

$$\sum_{r=0}^{+\infty} z^r \Delta^k K^k[r] = \frac{1}{N^k}(1-z^N)^k.$$

The development of the previous right-hand side, followed by identification of the z powers finally gives, for $j = 0, \ldots, k$

$$\Delta^k K^k[jN] = \frac{(-1)^j}{N^k} \binom{k}{j}, \tag{5.4}$$

and 0 otherwise. Ultimately, since the modulator is stable, $\|x_n\|_\infty < +\infty$, replacing the identities (5.4) in (5.3) yields the following filtered-input filtered-output difference

$$\|\beta * K^k\|_\infty \leq \frac{2^k}{N^k} \|x_n\|_\infty, \tag{5.5}$$

where $\beta = u - v$. The progression of the proof suggests that the estimate (5.5) (in ℓ^∞ norm) stays valid for any FIR K^k such that the k^{th}-order backward difference $\Delta^k K^k$ is non-zero for a finite number (independent of N) of coefficients, and of amplitude dominated by $1/N^k$. The sinc^k filter then appears as a particular instance of this type of filter, with $k+1$ coefficients of $\Delta^k K^k$ being non-zero. Besides, nonlinear filters can also be used to fasten the error decay rate [TV94; Tha96], even if they are seldom used, as they drastically complexify the actual implementation.

5.2.3 Synchronous detection through a DT-ΣΔ modulator

The exogenous signal s is henceforth taken into account in the derivation of the error estimate. Equation (5.3) now reads,

$$\beta s * K^k[n] = (-1)^k \sum_{j=0}^{kN-k} x_k[n-j] \Delta^k (s_n K^k)[j], \tag{5.6}$$

with $s_n[j] := s[n-j]$ and $\beta = u - v$ the input-output difference. Owing to Leibniz rule for finite differences, the k-fold finite differences in (5.6) satisfies

$$\Delta^k (s_n K^k)[j] = \sum_{i=0}^{k} \binom{k}{i} \Delta^i s_n[j] \Delta^{k-i} K^k[j-i]. \tag{5.7}$$

We seek to bound each of the terms in the sum (5.7), starting by $i = 1, \ldots, k$ (temporarily excluding the first term $i = 0$). Using Taylor-Lagrange formula, there exists $t_l \in [(j-l)T_s, jT_s]$

for $l = 1, \dots, i$ such that (see [Sur+19a, proof of lemma 1] for instance)

$$\Delta^i s_n[j] = \frac{(-1/N)^i}{i!} \sum_{l=0}^{i} \binom{i}{l} l^i s_n^{(i)}(t_l).$$

For $1 \leq i \leq k$, there exists a constant $C_i > 0$ such that the $k-i$-fold finite difference applied on the B-spline K^k reads

$$\left|\Delta^{k-i} K^k[j-i]\right| \leq \frac{C_i}{N^{k-i+1}}.$$

Setting $\widetilde{C}_i := C_i \sum_{l=0}^{i} \binom{i}{l} l^i / i!$, the terms under the sum symbol in (5.7) for $i = 1, \dots, k$ verify [Sur+19a]

$$\left|\Delta^i s_n[j] \Delta^{k-i} K^k[j-i]\right| \leq \frac{\widetilde{C}_i}{N^{k+1}} \sup_{t \in [(n-j)T_s, (n-j+i)T_s]} |s^{(i)}(t)|.$$

Besides, for $i = 0$ in (5.7), the expression for $\Delta^k K^k$ is given by (5.4). The convolution (5.6) then reads

$$\left|\beta s * K^k[n]\right| \leq \frac{kN+k+1}{N^{k+1}} \|x_k\|_\infty \sum_{i=1}^{k} \widetilde{C}_i \binom{k}{i} \sup_{[(n-kN)T_s, nT_s]} |s^{(i)}| + \frac{2^k}{N^k} \|x_k\|_\infty \sup_{[(n-kN)T_s, nT_s]} |s|,$$

where the first term is bounded using the previous estimates for $i = 1, \dots, k$, and the second term stems from the summation of the (absolute) coefficients given in (5.4), giving 2^k. If all the derivatives of s are bounded, then the estimate holds uniformly, i.e. there exists $B > 0$ independent of N, x_k and s such that

$$\left\| \beta s * K^k \right\|_\infty \leq \frac{B}{N^k} \|x_k\|_\infty \max_{i=0,\dots,k} \|s^{(i)}\|_\infty;$$

in other words, $\beta s * K^k = \mathcal{O}_\infty(1/N^k)$.

5.3 Estimate for CT-ΣΔ modulators in feedforward form

5.3.1 A first estimate

The previous section derived an error estimate for DT-ΣΔ modulators by considering an homodyning-type filtering process (subsection 5.2.3) which consists in multiplying the kernel by the exogenous signal s. This signal is often all or part of the input signal, as in standard demodulation procedures. The same type of estimate is derived in this section for CT-ΣΔ modulators. We consider a single-stage k^{th}-order continuous ΣΔ modulator as depicted in figure 5.3 The state-space model of this modulator is

$$\frac{1}{N}\dot{x}_1(\tau) = u(\tau) - v(N\tau) \tag{5.8a}$$

$$\frac{1}{N}\dot{x}_{i+1}(\tau) = x_i(\tau) - a_i v(N\tau), \qquad i = 1, \dots, k-1 \tag{5.8b}$$

$$y(\tau) = \sum_{i=1}^{k} b_i x_i(\tau), \tag{5.8c}$$

with $N := 1/T_s$ (not necessarily taking integer values for the continuous case). Again, $\beta(\tau) := u(\tau) - v(N\tau)$ is the input-output difference. In this section, we consider a modulator in pure

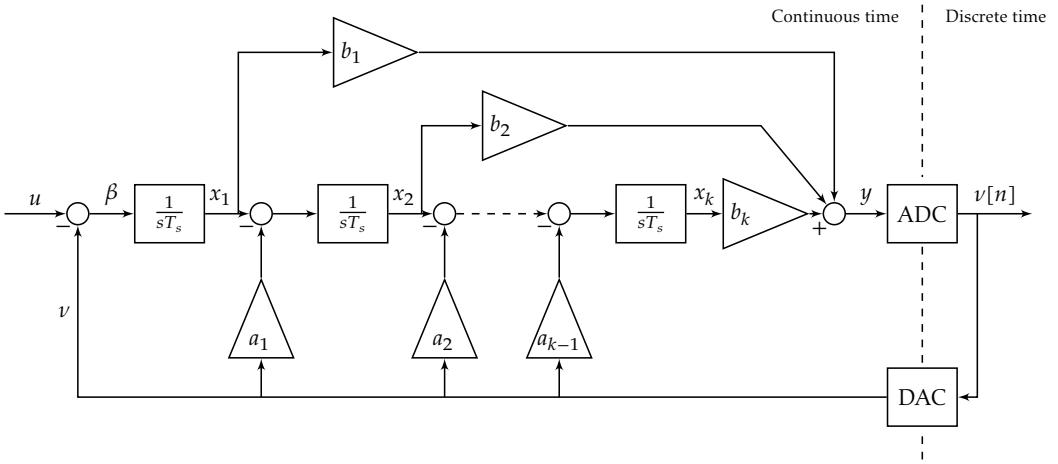

Figure 5.3: Single-stage k^{th}-order CT-ΣΔ with weighted feedback coefficients $(a_1, \dots, a_{k-1})$ and feedforward coefficients $(b_1, \dots, b_k)$.

feedforward form; the weighted feedback coefficients all being zero, i.e. $b_i = 0$ for $i = 1, \dots, k$. The objective is to complete the previous result pertaining to the discrete convolution of the ΣΔ input-output difference with a kernel K^k. A first result is given by

Theorem 5.3. *Consider a single-stage k^{th}-order continuous ΣΔ modulator with feedforward coefficients $(b_1, \dots, b_k)$ and no weighted feedback, i.e. $a_i = 0$ for $i = 1, \dots, k-1$. Let K^k be a C^k kernel whose support is $[0, k]$, and such that $(K^k)^{(j)}(0) = (K^k)^{(j)}(k)$ for $j = 0, \dots, n-1$; and consider a C^k signal s such that s and its derivatives $s^{(i)}$ for $i = 0, \dots, k$ are bounded. Then the filtered error $I(t)$, as depicted in figure 5.1 verifies the uniform estimate*

$$I(t) := \int_{\mathbb{R}} \beta(\sigma) s(\sigma) K_t^k(\sigma)\, d\sigma = \mathcal{O}_\infty(1/N^k), \tag{5.9}$$

with $K_t^k(\sigma) = K^k(t - \sigma)$.

Proof. For the feedforward structure, a k^{th}-order primitive of $u(\tau) - v(\tau)$ is $\beta^{(-k)}(\tau) = \frac{1}{N^k} x_k$. Indeed, $\frac{1}{N^k} \dot{x}_k(\tau) = \frac{1}{N^{k-1}} x_{k-1}(\tau)$ (see (5.8b)). Iterating this process yields $\frac{1}{N^k} x_n^{(k)}(\tau) = u(\tau) - v(\tau)$. Successive integration by parts on $I(t)$ then yields

$$I(t) = (-1)^k \int_{t-k}^{t} \beta^{(-k)}(\sigma) f_t^{(k)}(\sigma)\, d\sigma,$$

with $f_t(\sigma) := s(\sigma) K_t^k(\sigma)$. Since the modulator is stable, x_n is bounded, and $\| \beta^{(-k)}(\sigma) \|_\infty \leq \| x_k \|_\infty / N^k$. Consequently $I(t) = \mathcal{O}(1/N^k)$. With the additional hypothesis on s, f_t is bounded (independently of t) by Leibniz's rule. Therefore, the previous estimate is uniform, i.e. $I(t) = \mathcal{O}_\infty(1/N^k)$, thus concluding the proof. □

5.3.2 Error estimate refinement for CT-ΣΔ modulators

Under additional hypotheses on both the final state of the modulator x_k and the exogenous signal s, a better estimate can be obtained for CT-ΣΔ modulators. This result is encapsulated

in theorem 5.6: for CT-ΣΔ modulators in pure feedforward form, instead of dominating the estimate by $1/N^k$, it is made negligible still in front of $1/N^k$. The first step of the proof consists in exhibiting a function whose k^{th}-order derivative is the input-output difference. For feedforward structures, this function is simply the last state x_k. Therefore, if we assume x_k admits a generalized mean as subsequently defined, theorem 5.6 refines the estimate obtained in the previous section.

Definitions, preliminary results

We start by collecting the required technical definitions and lemmas. In the following, if a function $f \in L^\infty[0,+\infty)$ has a primitive that has a generalized mean, we will write $f^{(-1)}$ the zero-(generalized)-mean primitive of f, namely

$$f^{(-1)}(t) := \int_0^t f(s)\,ds - \lim_{T\to+\infty} \frac{1}{T}\int_0^T \int_0^\sigma f(s)\,ds\,d\sigma.$$

By induction, we also define for $j \geq 1$ the zero-mean primitive $f^{(-j-1)}$ of $f^{(-j)}$ if the latter has a generalized mean. Notice a bounded function on $[0,+\infty)$ does not necessarily has a generalized mean. Consider for instance $f(t) := \cos(\ln(t)) - \sin(\ln(t))$, whose primitive on $(0,+\infty)$ is $F(t) = t\cos(\ln(t))$. Therefore, $\frac{1}{t}\int_0^t f(s)\,ds = \cos(\ln(t))$, which does not converge when $t \to +\infty$.

The proof in subsection 5.5 relies on the application of a generalization of the classical Riemann-Lebesgue lemma

Lemma 5.4 (Generalized Riemann-Lebesgue lemma [Kah80])**.** *Consider $\beta \in L^\infty[0,+\infty)$ such that β has a mean value $\overline{\beta}$, with*

$$\overline{\beta} := \lim_{T\to+\infty} \frac{1}{T}\int_0^T \beta(t)\,dt.$$

Then for every $f \in L^1[0,+\infty)$,

$$\lim_{N\to+\infty} \int_0^{+\infty} \beta(Nt) f(t)\,dt = \overline{\beta}\int_0^{+\infty} f(t)\,dt.$$

The signal s is assumed to be either AC^k or piecewise AC^k, as defined below, as well as a rewriting of the integration by parts for piecewise AC^0 functions.

Definition 5.1 (AC^p functions)**.** A function $f : I \subset \mathbb{R} \to \mathbb{R}$ is AC^p on an interval I if it is p-times differentiable and its p^{th}-order derivative $f^{(p)}$ is absolutely continuous. It is piecewise AC^p if f is p-times differentiable and $f^{(p)}$ is piecewise absolutely continuous.

Lemma 5.5 (Integration by parts for piecewise AC^0 functions)**.** *Consider $f \in L^1[a,b]$ with $-\infty \leq a < b \leq +\infty$, F a primitive of f, and g a piecewise AC^0 function. Write $I = \cup_{0\leq i\leq m}[x_i, x_{i+1}]$, with $a = x_0 < x_1 < \ldots < x_m = b$, such that g is AC^0 on each $[x_i, x_{i+1}]$. g being piecewise AC^0, it is differentiable almost everywhere, and we note g' this derivative. Then*

$$\int_a^b f(\sigma)g(\sigma)\,d\sigma = \sum_{i=0}^{m-1}\left[F(x_{i+1}^-)g(x_{i+1}^-) - F(x_i^+)g(x_i^+)\right] - \int_a^b F(\sigma)g'(\sigma)\,d\sigma.$$

Refined estimate

The input-output difference $\beta(N\tau) := u(\tau) - v(N\tau)$ has a generalized mean $\overline{\beta}$, and for $j \leq k-1$, $\beta^{(-j)}$, the zero-mean primitive of $\beta^{-(j-1)}$ is also well-defined and verifies $\beta^{(-j)}(N\tau) = x_j$. Indeed, based on the state-space model (5.8b), x_j is the primitive of x_{j-1} for $2 \leq j \leq k$. Integrating (5.8b) from 0 to t gives

$$\frac{1}{t}\int_0^t x_j(\tau)\,d\tau = \frac{x_{j+1}(t) - x_{j+1}(0)}{Nt}.$$

The ΣΔ modulator is assumed to be stable, therefore x_{j+1} is bounded. Taking the limit when $t \to +\infty$ of both sides yields $\overline{x}_j = 0$, meaning $\beta^{(-j)} = x_j$. A primitive of $\beta^{-(-k-1)}$ is ultimately given by x_k. However, even if x_k is bounded by hypothesis, it does not necessarily admit a generalized mean as previously mentioned. As the bounded functions without generalized mean seem to be very particular, we will assume it does not hold for x_k, namely, $\beta^{(-k)} = x_k$ is the zero-mean primitive of $\beta^{(-(k-1))}$. We now state the refined result —theorem 5.6— based on the previous definitions and lemmas.

Theorem 5.6. *Consider K^k a AC^{k-1} kernel whose support is $[0,k]$, and such that $(K^k)^{(j)}(0) = (K^k)^{(j)}(k)$ for $j = 0,\dots,k-1$. If s is AC^{k-1}, then for $t \geq 0$,*

$$I(t) := \int_{\mathbb{R}} \beta(N\sigma)s(\sigma)K^k(t-\sigma)\,d\sigma = o(1/N^k). \tag{5.10}$$

If s is only piecewise AC^{k-1}, then for $t \geq 0$, $I(t) = \mathcal{O}_\infty(1/N^k)$. If s and all its derivatives, $s^{(i)}$ for $i = 0,\dots,k$, are bounded, then the first estimate (5.10) is uniform, i.e. $I(t) = o_\infty(1/N^k)$.

In other words, the instantaneous difference between the filtered input and the filtered output is in $o(1/N^k)$ under some regularity assumptions on the kernel K^k.

Proof. If s is AC^{k-1} (resp. piecewise AC^{k-1}), then $f_t : \sigma \mapsto s(\sigma)K^k(t-\sigma)$ is also AC^{k-1} (resp. piecewise AC^{k-1}). In any case, f_t is differentiable with support $[t-k,t]$ and a basic integration by parts gives

$$I(t) = \frac{1}{N}[\beta^{(-1)}(Nt)f_t(t) - \beta^{(-1)}(N(t-k))f_t(t-k)] - \frac{1}{N}\int_{t-k}^t \beta^{(-1)}(N\sigma)f_t'(\sigma)\,d\sigma,$$

where the first term is zero since $f_t(t) = f_t(t-k) = 0$.

We write $t-k = \sigma_0 < \dots < \sigma_m = t$ the locations of the loss of regularity of s. Repeating the integration by parts, given by lemma 5.5, yields

$$\begin{aligned} I(t) = &-\frac{(-1)^k}{N^k}\sum_{i=0}^{m-1}\left[\beta^{(-k)}(N\sigma_{i+1}^-)f_t^{(k-1)}(\sigma_{i+1}^-) - \beta^{(-k)}(N\sigma_i^+)f_t^{(k-1)}(\sigma_i^+)\right] \\ &+\frac{(-1)^k}{N^k}\int_{t-k}^t \beta^{(-k)}(N\sigma)f_t^{(k)}(\sigma)\,d\sigma. \end{aligned} \tag{5.11}$$

Since $f_t^{(k-1)}$ is absolutely continuous, it admits a derivative almost everywhere. Thus, the limit of the integral term in (5.11), by lemma 5.4, is

$$\lim_{N\to+\infty}\int_0^{+\infty}\beta^{(-k)}(N\sigma)f_t^{(k)}(\sigma)\,d\sigma = \overline{\beta^{(-k)}}\int_0^{+\infty}f_t^{(k)}(\sigma)\,d\sigma = 0,$$

i.e. $\frac{1}{N^k}\int_{t-k}^{t}\beta^{(-k)}(N\sigma)f_t^{(k)}(\sigma)\,d\sigma = o(1/N^k)$. If f is AC^{k-1}, the sum in (5.11) is zero since $f_t^{(k-1)}(t) = f_t^{(k-1)}(t-k) = 0$; therefore $I(t) = o(1/N^k)$. Otherwise the sum in (5.11) is non-necessarily zero, and $I(t) = \mathcal{O}(1/N^k)$. With the additional hypothesis on s, f_t is bounded (independently of t) by Leibniz's rule. Therefore, the previous limit is uniform, concluding the proof. □

At first sight, the writing of $\beta(Nt)$ might seem artificial. Nonetheless, it is worth noting that the inner states of the modulator are also fast-varying. Besides, without such a writing, the j^{th}-order zero-mean primitive of $u - v$ is given by $\frac{1}{N^j}x_j$ when there is no feedback coefficients. The detailed computations in the proof of theorem 5.6 then holds, with a multiplying factor $1/N^j$, as detailed in subsection 5.3.1, which is equivalent to the designed proof. Here, the obtained result is slightly more accurate, as when the regularity assumptions are satisfied, we have an estimate in $o(1/N^k)$ instead of $\mathcal{O}(1/N^k)$.

5.4 Weaker estimates

5.4.1 Estimate for feedback ΣΔ modulators

We now consider a CT-ΣΔ modulator with weighted feedback. For the feedback structure, a primitive of the input-output difference is given by

$$\beta^{(-k)} = \frac{x_k}{N^k} + \sum_{j=1}^{k-1}\frac{a_{k-j}}{N^{k-j}}\nu^{(-j)},$$

where $\nu^{(-j)}$ is a primitive of $\nu^{-(j-1)}$. Replacing $\beta^{(-k)}$ by the previous expression in (5.9) only yields $I(t) = \mathcal{O}(1/N)$, the estimate being uniform if the $\nu^{(-j)}$ are bounded. However, it appears in the expression of $\beta^{(-k)}$ that if $a_1 = 0$, $I(t) = \mathcal{O}(1/N^2)$ is likewise obtained.

5.4.2 Demodulation with an IIR filter

A great part of the prior proofs resides in the finiteness of the convolution kernel through the successive use of integration by parts. This technique is nonetheless limited when it comes to IIR filtering. To illustrate this, consider equation (5.10) with a kernel K whose support is not finite. Notice first that additional assumptions on the integrand are required so that $I(t)$ is well-defined. If $K = 1$ and $s = 1$ on $[0, +\infty)$ for instance, β should be integrable on $[0, +\infty)$, which is not guaranteed by the modulator stability only. To have a guess on the behavior of $I(t)$ with respect to N, we start by integrating on $[0, A]$ for $A > 0$:

$$I(t) = \frac{1}{N}\left[\beta^{(-1)}(NA)f_t(A) - \beta^{(-1)}(0)f_t(0)\right] - \frac{1}{N}\int_0^A \beta^{(-1)}(N\sigma)f_t'(\sigma)\,d\sigma.$$

Although the first term $\beta^{(-1)}(NA)$ is bounded, it does not necessarily converge when A tends to $+\infty$. As for the integral term, if we assume f_t' is integrable,

$$\left\|\frac{1}{N}\int_0^A \beta^{(-1)}(N\sigma)f_t'(\sigma)\,d\sigma\right\| \leq \frac{1}{N}\|\beta^{(-1)}\|_\infty\|f_t'\|_1.$$

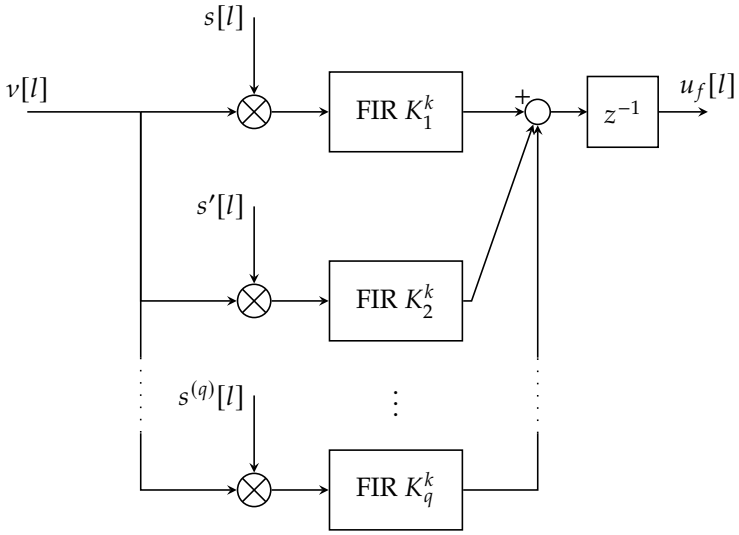

Figure 5.4: Actual implementation of the filter.

5.5 Discrete implementation

While theorem 5.6 provides a theoretical estimate of the filtered input-filtered output difference for CT-ΣΔ modulators, it is of lesser relevance when it comes to the online processing of the ΣΔ-bitstream. Indeed, this bitstream lies in the digital realm; the error $I(t)$ computes a continuous convolution with a fast-varying discrete signal v and, even though it is mathematically well defined, is not in practice desirable, let alone doable. What is effectively done is a discretization of the process described by theorem 5.6.

An immediate yet naive strategy might consists in directly discretizing the convolution product described by (5.10). Nevertheless, such an approximation introduces an error in $\mathcal{O}(1/N)$ given by a straighforward application of Young's inequality, thus burying the accuracy of the estimate provided by theorem 5.6. A more subtle approach consists in discretizing the kernel K and discretely convolving with the ΣΔ bitstream v multiplied by s. When the signal s is constant, this computation is rigorously equivalent to the continuous one since the ΣΔ bitstream is a staircase function. Nevertheless, when s is time-varying, a discretization error is introduced.

This section is devoted to the design of FIR filters approaching the continuous convolution: the knowledge of the signal s and its derivatives is leveraged to improve the accuracy of the discretized convolution: theorem 5.7 encapsulates this result. In the following, we adopt the same notation as in the discrete case, namely, for $l \in \mathbb{N}$, we write $\tau_l := l/N$, and for every function f, $f[l] := f(\tau_l)$. The timestep between two consecutive values is therefore $\Delta\tau = T_s$, which is the time interval where the ΣΔ bitstream is constant. We also consider the filtered output v_f defined by

$$v_f(t) := \int_{-\infty}^{+\infty} v(N\sigma)s(\sigma)K^k(t-\sigma)\,d\sigma.$$

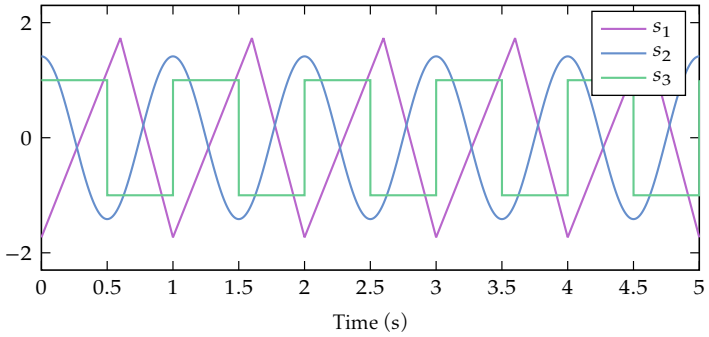

Figure 5.5: Signals s_i, $i = 1, 2, 3$.

Theorem 5.7. *Assume the signal s is q-times differentiable, with $s^{(q)}$ Lipschitz. For $j = 0, \dots, q$, we define the following FIR coefficients: for $i \in \{0, \dots, kN-1\}$,*

$$K_j^k[i] := \int_{\frac{i}{N}}^{\frac{i+1}{N}} \frac{(\frac{i+1}{N} - \sigma)^j}{j!} K^k(\sigma)\, d\sigma, \tag{5.12}$$

and $K_j^k[i] = 0$ otherwise. Then the following estimate holds

$$\sum_{j=0}^{q} (\tau(\nu s^{(j)}) * K_j^k)[l] = \nu_f[l] + \mathcal{O}\Big(\frac{1}{N^{q+1}}\Big), \tag{5.13}$$

where $\tau(f)[l] := f[l-1]$ is the unit delay, and $(f * g)[l] = \sum_{i \in \mathbb{Z}} f[i] g[l-i]$ is the discrete convolution. In other words, there exists a discrete, causal FIR filter whose coefficients can be computed offline and yielding $\nu_f[l]$ with an accuracy in $\mathcal{O}(1/N^{q+1})$.

Proof. The $\Sigma\Delta$ output bitstream $\nu(N\tau)$ is constant on each interval $[i/N, (i+1)/N)$, $i \in \mathbb{N}$. Therefore, splitting the integral $I(t)$ into kN subintervals and integrating on each yields

$$\begin{aligned} \nu_f[l] &= \int_0^k K^k(\sigma)\nu(N(\tau_l - \sigma))s(\tau_l - \sigma)\, d\sigma = \sum_{i=0}^{kN-1} \int_{\frac{i}{N}}^{\frac{i+1}{N}} K^k(\sigma)\nu(N(\tau_l - \sigma))s(\tau_l - \sigma)\, d\sigma \\ &= \sum_{i=0}^{kN-1} \nu[l-i-1] \int_{\frac{i}{N}}^{\frac{i+1}{N}} K^k(\sigma) s(\tau_l - \sigma)\, d\sigma. \end{aligned}$$

No approximation is made in the previous computations as ν is held constant on each interval. This expression could give birth to an actual FIR filter yielding exactly $\nu_f[l]$ by computing the integral terms for $i = 0, \dots, kN-1$. These computations however have to be conducted at every timestep, as the signal s is time-varying. The online computation of these integrals is thereby highly demanding in CPU/FPGA resources.

Instead, we compute an approximation of these kN integrals. For this purpose, consider the Lipschitz form of Taylor's formula (see for example [ESD90, (2.1)])

$$g(t+\mu) = \sum_{j=0}^{q} \frac{\mu^j}{j!} g^{(j)}(t) + \mu^{q+1} \rho_t(\mu), \tag{5.14}$$

where the remainder $\rho_t(\mu)$ satisfies

$$\mu\rho_t(\mu) = \frac{1}{(q-1)!}\int_0^1 (1-\tau)^{q-1}(g^{(q)}(t+\mu\tau) - g^{(q)}(t))\,d\tau.$$

With $t = \tau_l - \frac{i+1}{N}$ and $\mu = \frac{i+1}{N} - \sigma$, the application of equation (5.14) to the signal s reads

$$\begin{aligned} s(\tau_l - \sigma) &= s(\tau_l - \tfrac{i+1}{N} + \tfrac{i+1}{N} - \sigma) \\ &= s[l-i-1] + \sum_{j=0}^{q} \frac{(\frac{i+1}{N} - \sigma)^j}{j!} s^{(j)}[l-i-1] + (\tfrac{i+1}{N} - \sigma)^{q+1}\rho(\tfrac{i+1}{N} - \sigma). \end{aligned}$$

We start by estimating the magnitude of the remainder. If L is the Lipschitz constant of $g^{(q)}$, the remainder ρ_t satisfies the following inequality for every $\mu \in \mathbb{R}$

$$|\,\mu\rho_t(\mu)\,| \leq \frac{L|\mu|}{(q-1)!}\int_0^1 \tau(1-\tau)^{q-1}\,d\tau;$$

that is, for every t and with $M := \frac{L}{(q-1)!}\int_0^1 \tau(1-\tau)^{q-1}\,d\tau$,

$$\left|(\tfrac{i+1}{N} - \sigma)^{q+1}\rho(\tfrac{i+1}{N} - \sigma)\right| \leq M(\tfrac{i+1}{N} - \sigma)^{q+1}.$$

Consequently,

$$\begin{aligned} \left|\int_{\frac{i}{N}}^{\frac{i+1}{N}} \Big(\frac{i+1}{N} - \sigma\Big)^{q+1}\rho\Big(\frac{i+1}{N} - \sigma\Big)\,d\sigma\right| &\leq \|\rho_t\|_\infty \int_{\frac{i}{N}}^{\frac{i+1}{N}} \Big(\frac{i+1}{N} - \sigma\Big)^{q+1}\,d\sigma \\ &\leq \frac{M}{q+2} \times \frac{1}{N^{q+2}}, \end{aligned}$$

which means the remainder $(\frac{i+1}{N} - \sigma)^{q+1}\rho(\frac{i+1}{N} - \sigma)$ is $\mathcal{O}(1/N^{q+2})$. When summed for $i = 0, \dots, kN-1$, it becomes $\mathcal{O}(1/N^{q+1})$. For $j = 0, \dots, q$, using equation (5.12)

$$\int_{\frac{i}{N}}^{\frac{i+1}{N}} K^k(\sigma)s^{(j)}[l-i-1]\frac{(\frac{i+1}{N} - \sigma)^j}{j!}\,d\sigma = s^{(j)}[l-i-1]K_j^k[i].$$

Finally, $v_f[l]$ reads

$$v_f[l] = \sum_{i=0}^{kN-1} v[l-i-1]\sum_{j=0}^{q} s^{(j)}[l-i-1]K_j^k[i] + \mathcal{O}\Big(\frac{1}{N^{q+1}}\Big).$$

This expression boils down to a sum of discrete convolutions, i.e. equation (5.13), thus concluding the proof. □

Notice that if s is a constant signal, $v_f[l] = v * K_0^k$ is simply a discretization of $v * K^k$, and the FIR implementation does not introduce any additional error. The estimate (5.13) is also independent from the ΣΔ order as the only property required is that the bitstream is held constant on each $[i/T_s, (i+1)/T_s)$. Thereby the result stays valid when replacing the bitstream v by any staircase function constant on each $[i, i+1)$.

Put simply, theorem 5.7 states the existence of an implementable digital processing of the ΣΔ-bitstream that realizes the continuous convolution described by theorem 5.6, with an additional $\mathcal{O}(1/N^{q+1})$ error under the regularity assumptions of the theorem on s. As a result, under the assumptions of theorem 5.7, the discretization error is negligible in front of the

continuous error estimate, meaning the actual implementation of the FIR filter does not introduce a significant approximation error. Nonetheless, the procedure requires the knowledge of s and its derivatives, which may hinder the filtering process if only approximations of the derivatives are known.

The strength of this method lies in the offline computation of the coefficients K_j^k that inherently depends on the kernel choice K^k. A well-known class of kernels satisfying the hypotheses of theorem 5.6 is the B-splines $K^k = 1_{[0,1]}^{(*k)}$, whose support is $[0,k]$. For such K^k, the associated FIR filter kernels are given in appendix 5.8.

5.6 Numerical results

5.6.1 Second-order CT-ΣΔ in feedforward structure

The estimates are now validated on numerical examples. We consider the second-order modulator of figure 5.3 with $b_1 = 3/2$ and $b_2 = 1$ (this example being thoroughly treated in Surroop et al. [SCM21b]). The tests are conducted with three different inputs $u_i(t) := z(t)s_i(t)$, with $z(t) := 0.04\cos(\frac{t}{12}) - 0.06\sin(\frac{t}{4\pi})$, and

$$s_1(t) := \frac{1}{\sqrt{0.03}}\left(\tau 1_{[0,0.6]}(\tau) + 1.5(1-\tau)1_{]0.6,1]}(\tau) - 0.3\right),$$
$$s_2(t) := \sqrt{2}\cos(2\pi\tau), \qquad s_3(t) := 1_{[0,0.5]}(\tau) - 1_{]0.5,1]}(\tau),$$

where $\tau = \mathrm{mod}(t)$ and $t \in [0,25]$. Illustrated in figure 5.5, the s_i's are respectively piecewise AC^1 (s_1), AC^1 (s_2) and discontinuous (s_3), and such that $\|s_i\|_2 = 1$. A kernel satisfying the hypotheses of theorem 5.6 is the convolution power of the characteristic function $1_{[0,1]}$, $K^3 := 1_{[0,1]} * 1_{[0,1]} * 1_{[0,1]}$, as $\mathrm{supp}\, K^3 = [0,3]$ and $K^3(0) = K^3(3) = (K^3)'(0) = (K^3)'(3) = 0$ (see for example [Aub05]); this kernel corresponds to a triple moving average.

Define $\hat{z}$ (resp $\hat{z}_{\Sigma\Delta}$) the filtered input (resp. output) as

$$\hat{z}(t) := \int_0^{+\infty} u(\sigma)s(\sigma)K^3(t-\sigma)\,d\sigma, \qquad \hat{z}_{\Sigma\Delta}(t) := \int_0^{+\infty} v(\sigma)s(\sigma)K^3(t-\sigma)\,d\sigma,$$

so that $I(t) = \hat{z}(t) - \hat{z}_{\Sigma\Delta}(t)$.

To confirm the asymptotic behavior described by theorem 5.6, the same simulation is carried out for each input u_i and for different oversampling ratio values N; for each numerical experiment, the L^2-error $\|I\|_2 := (\int_1^{25} I(\sigma)^2\,d\sigma))^{1/2}$ is computed (the first second in the error definition is discarded to initialize the filters). Figure 5.6a shows these behaviors for the three considered inputs u_i and validates the approximation orders. Indeed, when $s = s_1$ is piecewise AC^1, the approximation order is in $\mathcal{O}(1/N^2)$; it is slightly better when $s = s_1$ is AC^1, with $\|I\|_2 = \mathcal{O}(1/N^{2.3}) = o(1/N^2)$; when $s = s_3$ is discontinuous, we only have an estimate in $\mathcal{O}(1/N)$.

5.6.2 Third-order CT-ΣΔ in feedforward structure

The same tests are conducted on a display of third-order CT-ΣΔ in feedforward structure. This modulator is designed thanks to Richard Schreier's Delta-Sigma MATLAB toolbox [Sch17]: the

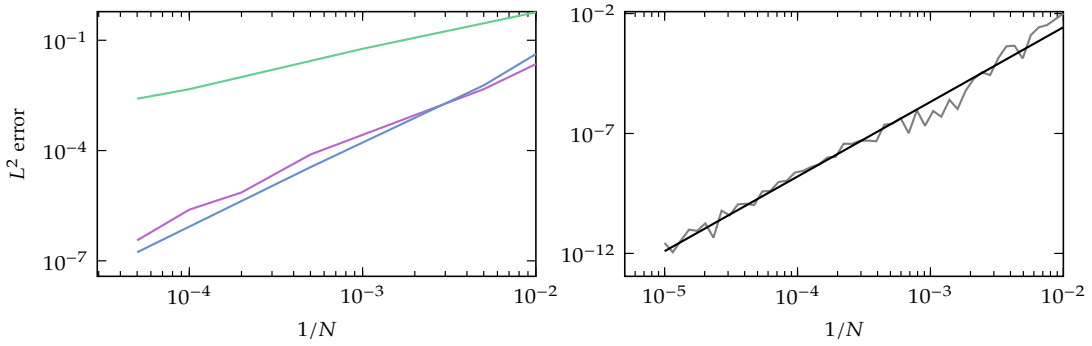

(a) Second-order modulator

(b) Third-order modulator (slope=3.11)

Figure 5.6: L^2 error for second (left) and third-order (right) CT-ΣΔ in feedforward form.

coefficients are set to $b_1 = 4.63 \times 10^{-1}$, $b_2 = 1.13 \times 10^{-1}$, $b_3 = 1.38 \times 10^{-2}$, with $a_1 = a_2 = 0$. We test the estimate this time for u_2, with s_2 being AC^2: figure 5.6b shows the behavior of the error, with an asymptotic slope around 3.1, and confirms the validity of the estimate.

5.6.3 Discretization error

We now validate the discretization error given by theorem 5.7. Still using the input u_2, we compare the continuous convolution to the sum of discrete convolutions described by (5.13). The asymptotic error is displayed in figure 5.7: the slope is equal to 1 when only the value of s_2 is used in the discretization scheme; equal to 2 when both s_2 and its derivative s_2' are taken into account, and finally equal to 3 when s_2, s_2' and $s_2^{(2)}$ are available. These asymptotic behaviors validates the estimate provided by theorem 5.7.

5.6.4 Using an IIR filter

The different results exploit the finiteness of the kernel support. When this assumption is dropped, only a $\mathcal{O}(1/N)$ estimate can be derived along the lines of the proof in section 5.3. Figure 5.8 shows this estimate is reached for a basic first-order low-pass filter with transfer function $H(s) = \frac{1}{1+s}$, still on a third-order (feedforward) CT-ΣΔ.

5.7 Conclusion

In this chapter, a method has been presented to demodulate a signal through a ΣΔ modulator with an accuracy increasing with the modulator order. The proposed method applies for both discrete and continuous modulators, and guarantees the validity of the aforementioned estimate under some regular properties on the carrier signal. In the continuous case, the estimate is discretized so as to be implemented in a DSP: still with suitable hypotheses on the carrier, the error introduced by the discretization shares the same order of magnitude as the original continuous estimate.

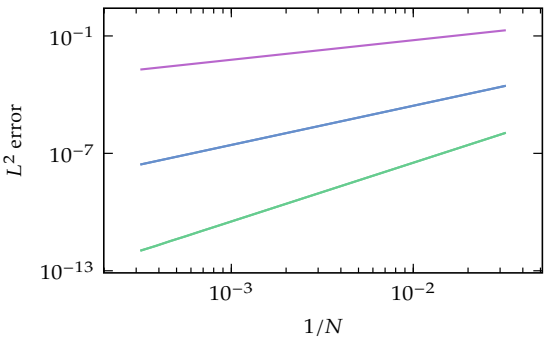

Figure 5.7: L^2-error of the discretization process for $k = 1$ (purple), 2 (blue), 3 (green). Slopes respectively equal to 1, 2, 3.

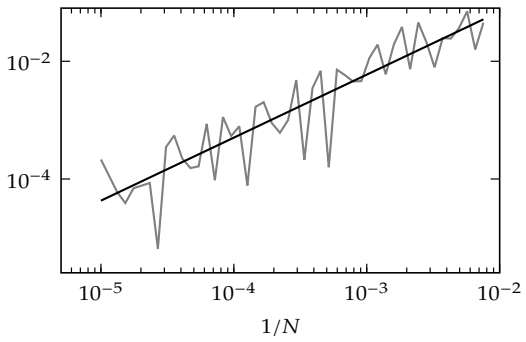

Figure 5.8: Asymptotic behavior of the error (slope=1) using a IIR filter.

5.8 Appendix: FIR filters coefficients

The FIR filter coefficients computed in the proof of theorem 5.7 are gathered in this appendix when K^k is a B-spline. We remind the general expression of the discretized kernels

$$K_j^k[i] := \int_{\frac{i}{N}}^{\frac{i+1}{N}} \frac{(\frac{i+1}{N} - \sigma)^j}{j!} K^k(\sigma)\, d\sigma.$$

The continuous kernels are $K^k = 1_{[0,1]}^{(*k)}$ $(k = 1, 2, 3)$, and the FIR coefficients are the following. For $i < 0$ and $i \geq kN$, $K_{1,2,3}^k[i] = 0$. For $k = 1$,

$$K_1^1[i] = \frac{1}{N}, \qquad K_2^1[i] = \frac{1}{2N^2}, \qquad K_3^1[i] = \frac{1}{6N^3}.$$

For $k = 2$, $i = 0, \dots, N-1$ (left) and $i = N, \dots, 2N-1$ (right),

$$\begin{aligned} K_1^2[i] &= \frac{2i+1}{2N^2}, & K_1^2[i] &= -\frac{2i-4N+1}{2N^2}, \\ K_2^2[i] &= \frac{3i+1}{6N^3}, & K_2^2[i] &= -\frac{3i-6N+1}{6N^3}, \\ K_3^2[i] &= \frac{4i+1}{24N^4}, & K_3^2[i] &= -\frac{4i-8N+1}{24N^4}. \end{aligned}$$

For $k = 3$, $i = 0, \dots, N-1$ (left), $i = N, \dots 2N-1$ (right)

$$\begin{aligned} K_1^3[i] &= \frac{3i^2+3i+1}{6N^3}, & K_1^3[i] &= -\frac{6i+9N^2+6i^2-18Ni-9N+2}{6N^3}, \\ K_2^3[i] &= \frac{6i^2+4i+1}{24N^4}, & K_2^3[i] &= -\frac{4i+9N^2+6i^2-18Ni-6N+1}{12N^4}, \\ K_3^3[i] &= \frac{10i^2+5i+1}{120N^5}, & K_3^3[i] &= -\frac{10i+30N^2+20i^2-60Ni-15N+2}{120N^5}. \end{aligned}$$

For $k = 3$, $i = 2N, \dots, 3N - 1$,

$$K_1^3[i] = \frac{3i + 27N^2 + 3i^2 - 18Ni - 9N + 1}{6N^3},$$
$$K_2^3[i] = \frac{4i + 54N^2 + 6i^2 - 36Ni - 12N + 1}{24N^4},$$
$$K_3^3[i] = \frac{5i + 90N^2 + 10i^2 - 60Ni - 15N + 1}{120N^5}.$$

Chapter 6
Sensorless rotor position estimation by endogenous signal injection

This chapter collects the results from two papers: one published in the proceedings of IECON20 under the title *Sensorless rotor position estimation by PWM-induced signal injection* [Sur+20b], the other in the proceedings of IEMDC21 under the title *Towards an industrially implementable PWM-injection scheme* [SCM21c].

Résumé Les différentes théories développées précédemment sont maintenant réunies pour l'étude expérimentale de l'injection de signal endogène appliquée à un PMSM. Jusqu'à aujourd'hui, les méthodes d'estimation sans capteur reposant sur l'excitation MLI exploitent principalement la modification du schéma de calcul de la MLI, par une injection de séquences de test par exemple. Des capteurs de dérivée de courant ou des convertisseurs analogiques-numériques à suréchantillonnage de haute précision sont généralement nécessaires pour extraire précisément le ripple de courant et donc implémenter ces stratégies d'estimation. D'un point de vue industriel, ces dispositifs ne sont cependant pas standards, car coûteux, complexes à mettre en œuvre, ce qui revient à remplacer le capteur de position par un autre. Ce chapitre traite de l'estimation de la position du rotor à basse vitesse sans modifier le schéma de calcul de la MLI, et ce, sans capteur supplémentaire. Ceci est réalisé en extrayant la position du ripple induit par la MLI directement du flux binaire Sigma-Delta. Cette méthode peut également être couplée à un schéma de porteuses décalées (PSC-PWM) afin d'améliorer la précision des estimations produites. Les résultats numériques et expérimentaux parachèvent l'étude, valident la stratégie d'estimation sans capteur proposée, et mettent en évidence les difficultés propres au contrôle moteur, à savoir le rôle de la saturation magnétique ainsi que les pertes de rang de la base de démodulation.

Abstract The theories developed in this thesis are now collected to study the endogenous signal injection technique applied to PMSM. Up to now, sensorless estimation methods based on PWM excitation mainly exploit the modification of the PWM computation scheme, through the injection of the so-called test sequences for example. Current derivative sensors or high-precision oversampling Analog-to-Digital converters are usually required to accurately extract the current ripple and thus implement these estimation strategies. From an industrial point of view, however, these devices are not standard, as they are expensive, greatly complexify the implementation, and finally replace the position sensor by another one. This chapter

deals with the rotor position estimation at low speed without modifying the computational scheme of the PWM, nor bringing an additional sensor. This is realized by extracting the ripple position induced by the PWM directly from the Sigma-Delta bitstream. This method can also be coupled to a phase-shifted carrier scheme (PSC-PWM) to improve the accuracy of the estimates. Numerical and experimental results complete the study, validate the proposed sensorless estimation strategy, and highlight the difficulties specific to motor control, namely the role of magnetic saturation and the demodulation basis rank losses.

6.1 Introduction

Sensorless control of Permanent Magnet Synchronous Motors has known a great impetus in the last decade, and still remains a challenging task. Numerous strategies have been tailored to estimate the rotor position without mechanical encoder, only from the input voltages and output currents. They are mainly classified into two categories: fundamental excitation and saliency strategies. While the former describes model-based methods [Gen+10; Lee+10; BP18; KSL11; KKK03; KG06], —suited for the medium to high-speed range, namely over 10% to 15% of the rated speed [FSO92]— and do not overcome the underlying observability issues at low speed, the latter focuses on the motor response to high-frequency signals, and are adapted to estimate the position in the low-speed range. Among the saliency methods is found the traditional signal injection introduced by Jansen and Lorentz [JL95], which consists in superimposing a fast-varying signal to the control law to create position-dependent current ripples. Thanks to the machine's saliency —either geometrical or induced by magnetic saturation—, these ripples gives access to the rotor position, if correctly decoded. This method though comes with potential drawbacks, such as the introduction of acoustic noise in the device [Jun+11], the excitation of unmodelled dynamics [Åst84], and the inherent limitations of the injection frequency by the inverter, which may distort the injected wave, should its frequency be too close from the PWM one.

PWM excitation methods —a subclass of saliency methods— bypass the limitations imposed by the inverter by modifying the PWM scheme. This line of research has been pioneered by Schrödl's INFORM —Indirect Flux detection by Online Reactance Measurements— method [Sch96], which consists in injecting the so-called test sequences, modulating the PWM zero sequence to introduce special current harmonics during the measurement period [Sch96; WM02]. It turns out the PWM switchings naturally also introduce high-frequency harmonics that act like a traditional injection; such a natural harmonic method has been instigated for example by Ogasawara and Akagi [OA98]. But whatever the scheme, the problem of estimating the rotor position more or less amounts to estimating the slope of the triangular-shaped current ripple. This could be done with specific current derivative sensors [Sch96] such as Rogowski coils for instance [Gao+07], which are experimental devices not found on industrial devices, and most of the time, expensive. On the other hand with regular current sensors, the slope can be estimated by the difference between two current samples [WX04; LKH03]. But with only a couple of points per PWM signal edge, the estimate is easily corrupted by noise. To achieve better accuracy, a high resolution and high speed sampling ADC is required [Lan+13].

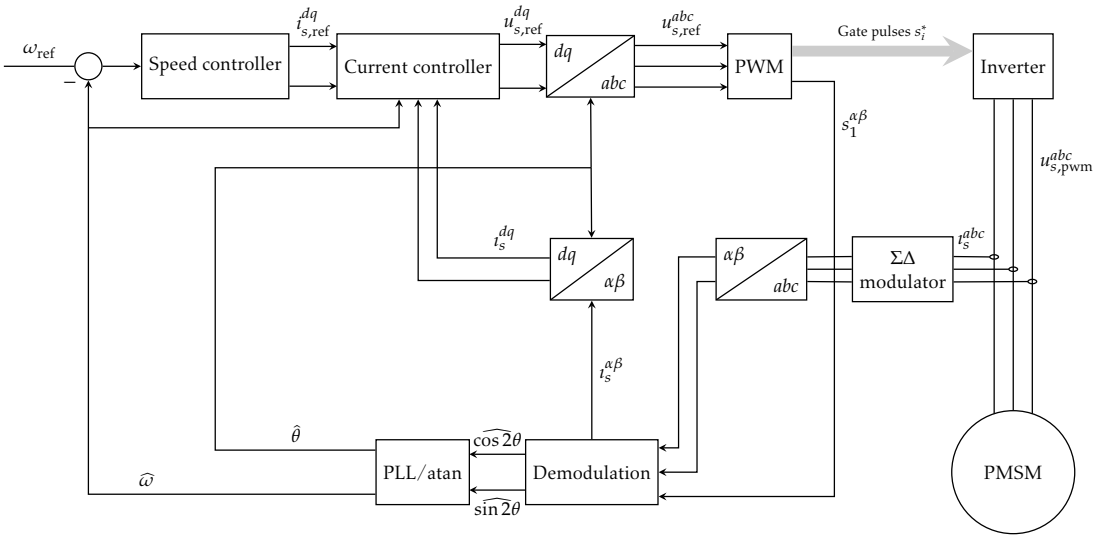

Figure 6.1: Diagram of the proposed control scheme. In this chapter, the rotor position is recovered outside the feedback loop.

In this chapter, building on ideas developed in the previous chapters, we propose and test a scheme to estimate the rotor position of a PMSM that exploits (nearly) all the information in the natural PWM-induced ripple —hence is much more robust than two-point slope estimation—, and that is moreover compatible with an industrial drive hardware. The hardware comprises usual current sensors connected to 1-bit ΣΔ modulators, and an FPGA processing the modulators bitstreams. This configuration is common in recent industrial drives, where the modulators serve both for galvanic insulation and as the first stage of a ΣΔ ADC [Sor15; SOO19b; SOO19a]; the FPGA implements the necessary signal processing (usually sinc and decimation filters) to form a complete ΣΔ ADC. The proposed scheme extracts the rotor position directly from the modulators bitstreams by a kind of generalized sinc filter, and can be programmed on the FPGA without further modifications. Additionally, an alternative scheme realized by replacing the standard PWM by Phase Shifted Carrier Pulse Width Modulation (PSC-PWM) [Has+17], is proposed to improve the demodulation procedure. In fact, the method proves to be compatible with both space vector and voltage level based modulation algorithms, with either a single or several carriers.

The chapter runs as follows: section 6.2 recalls the main steps to extract the rotor position directly from the Sigma-Delta modulator bitstream; section 6.3 describes the position recovery from the virtual measurement; finally, section 6.4 illustrates the good behavior of the method on experimental and simulation data.

6.2 Virtual measurement for the PMSM

6.2.1 Model of the PWM-fed PMSM

Consider the state-space model of a PMSM in the field-oriented dq-frame

$$\frac{d\phi_s^{dq}}{dt} = u_s^{dq} - R_s i_s^{dq} - \omega \mathcal{J} \phi_s^{dq} \tag{6.1a}$$

$$\frac{J}{n}\frac{d\omega}{dt} = n i_s^{dq^T} \mathcal{J} \phi_s^{dq} - T_l \tag{6.1b}$$

$$\frac{d\theta}{dt} = \omega, \tag{6.1c}$$

as developed in chapter 1. For simplicity, we momentarily assume no magnetic saturation, i.e. linear current-flux relations

$$L_d i_s^d = \phi_s^d - \phi_m, \qquad L_q i_s^q = \phi_s^q. \tag{6.2a}$$

The input is the voltage u_s^{abc} through the relation $u_s^{dq} = \mathcal{R}(-\theta)\mathcal{C}u_s^{abc}$, where $\mathcal{R}(\theta) := \left(\begin{smallmatrix} \cos\theta & -\sin\theta \\ \sin\theta & \cos\theta \end{smallmatrix}\right)$ is the rotation matrix with angle θ and $\mathcal{C} := \sqrt{\frac{2}{3}}\left(\begin{smallmatrix} 1 & -1/2 & -1/2 \\ 0 & \sqrt{3}/2 & -\sqrt{3}/2 \end{smallmatrix}\right)$ is the Concordia transformation. As we are concerned with sensorless control, the only measurement is the current $i_s^{abc} = \mathcal{C}^T\mathcal{R}(\theta)i_s^{dq}$, or equivalently $i_s^{\alpha\beta} = \mathcal{R}(\theta)i_s^{dq}$ since $i_s^a + i_s^b + i_s^c = 0$ (we assume the motor is star connected, see Fig. 1.2).

The impressed voltage is the PWM encoding $u_{\text{pwm}}^{abc}(t)$ of $u_s^{abc}(t)$; it can be written as

$$u_{\text{pwm}}^{abc}(t) = u_s^{abc}(t) + s_0^{abc}\Big(u_s^{abc}(t), \frac{t}{T_{\text{pwm}}}\Big),$$

where $s_0^{abc}(u_s^{abc}(t), \frac{t}{\varepsilon}) := u_{\text{pwm}}^{abc}(t) - u_s^{abc}(t)$ and T_{pwm} is the PWM period. Defined in this way, s_0^{abc} is 1-periodic with zero mean in the second argument; it can be seen as a rectangular injection signal (Fig. 3.2, left), depending on u_s^{abc}, and induced by the PWM that creates a (nearly) triangular current ripple (Fig. 3.2, right).

6.2.2 Virtual measurement for the PMSM

Slightly generalizing the second-order averaging analysis of chapter 3 to the multiple-input multiple-output case, the effect of PWM-induced signal injection can be analyzed as follows. Consider the system

$$\dot{x} = f(x) + G(u + s_0(u, \tfrac{t}{\varepsilon})),$$
$$y = h(x),$$

where u is the control input, y is the measured output, ε is the PWM period, and s_0 is 1-periodic with zero mean in the second argument. The averaging theory could be generalized to the case where the matrix G becomes state-dependent, without loss of generality. For this system, the measured output then reads

$$y(t) = h(\bar{x}(t)) + \varepsilon h'(\bar{x}(t))Gs_1(u(t), \tfrac{t}{\varepsilon}) + \mathcal{O}(\varepsilon^2),$$

where $\overline{x}(t)$ is the solution of the system *without injection* $\dot{\overline{x}} = f(\overline{x}) + Gu$, and s_1 is the zero-mean primitive in the second argument of s_0. Figure 3.2 illustrates typical signals $s_0(u,\cdot)$ for fixed u and their zero-mean primitive $s_1(u,\cdot)$. The quantity $\varepsilon h'(\overline{x}(t))Gs_1(u(t),\frac{t}{\varepsilon})$ is the ripple caused on the output y by the excitation signal $s_0(u(t),\frac{t}{\varepsilon})$; though small, it contains valuable information when properly processed. To fully exploit the PWM-induced ripple, define the so-called virtual measurement $y_v := \varepsilon h'(\overline{x}(t))G\mathcal{A}(u(t))$, where the matrix $\mathcal{A}(v)$, which can be computed online, is defined by $\mathcal{A}(v) := \int_0^1 s_1(v,\tau)s_1(v,\tau)^T\,d\tau$. This virtual measurement is defined so that y_v encompasses the same knowledge as $h'(\overline{x})Gs_1$, in the sense that $\mathcal{A}$ shares the same rank as the set of s' components. Besides, the *actual measurement* $h(\overline{x}(t))$ and the *virtual measurement* $y_v(t)$ can be extracted from the physical measurement $y(t)$ with an accuracy of order ε^2, see subsection 6.2.3.

For the PMSM (6.1) with actual measurement $\imath_s^{\alpha\beta}$, $h(\overline{x}(t)) = \overline{\imath_s^{\alpha\beta}}$, and the virtual measurement $h'(\overline{x}(t))Gs_1(u(t),\frac{t}{\varepsilon})$ boils down to

$$\begin{bmatrix}\mathcal{R}(\bar\theta)\begin{pmatrix}\frac{1}{L_d} & 0\\ 0 & \frac{1}{L_q}\end{pmatrix} & 0_{2\times1} & \mathcal{R}'(\bar\theta)\imath_{dq}\end{bmatrix}\begin{bmatrix}\mathcal{R}(-\bar\theta)\mathcal{C}s_1^{abc}\\ 0_{1\times2}\\ 0_{1\times2}\end{bmatrix} = \mathcal{S}(\bar\theta)s_1^{\alpha\beta},$$

where $\mathcal{S}(\theta)$ is the saliency matrix

$$\mathcal{S}(\bar\theta) := \frac{L_d+L_q}{2L_dL_q}\begin{pmatrix}1+\frac{L_q-L_d}{L_d+L_q}\cos2\bar\theta & \frac{L_q-L_d}{L_d+L_q}\sin2\bar\theta\\ \frac{L_q-L_d}{L_d+L_q}\sin2\bar\theta & 1-\frac{L_q-L_d}{L_d+L_q}\cos2\bar\theta\end{pmatrix}, \tag{6.3}$$

and $s_1^{\alpha\beta} := \mathcal{C}s_1^{abc}$. Therefore $y_v := \varepsilon\mathcal{S}(\bar\theta)\mathcal{A}^{\alpha\beta}(u(t))$ with $\mathcal{A}^{\alpha\beta} := \int_0^1 s_1^{\alpha\beta}(v,\tau)s_1^{\alpha\beta}(v,\tau)^T\,d\tau$. As noticed earlier, this matrix $\mathcal{A}^{\alpha\beta}$ is invertible if s_1^α and s_1^β are independent; rank one if they are colinear and rank zero if they are both zero. For this system, the actual measurement reads $h(\overline{x}(t)) = \overline{\imath_s^{\alpha\beta}}$ and the virtual measurement is $y_v(t) = \varepsilon\mathcal{S}(\bar\theta)\mathcal{A}^{\alpha\beta}(u(t))$. If the motor is geometrically salient, i.e. if L_d and L_q are sufficiently different, the rotor position $\theta(t)$ can then be computed from $y_v(t)$ and $\mathcal{A}^{\alpha\beta}(u_s^{abc}(t))$, see section 6.3 for details [Sur+19a].

6.2.3 Virtual measurement extraction

The demodulation process to estimate $y_v(t)$ and $\mathcal{A}^{\alpha\beta}(u_s^{abc}(t))$ is as follows, see chapter 4 for a detailed analysis:

1. define the kernel filter $\phi(t) := 2K(t) - K(t-\varepsilon)$ (see Fig. 4.4), where $K := \frac{1}{\varepsilon^2}1_{[0,\varepsilon]} * 1_{[0,\varepsilon]}$ ($*$ denoting the convolution product) is the kernel of a double moving average with window $[t-\varepsilon, t]$; it is but a "corrected" sinc2 filter similar to the second stage of a $\Sigma\Delta$ ADC.

2. filter with ϕ the known signal $s_1^{\alpha\beta}(u_s^{abc}(t),\frac{t}{\varepsilon})s_1^{\alpha\beta^T}(u_s^{abc}(t),\frac{t}{\varepsilon})$; this yields $\mathcal{A}^{\alpha\beta}(u_s^{abc}(t))$ with an $\mathcal{O}(\varepsilon^2)$ error.

3. filter with ϕ the measured signal $\imath_s^{\alpha\beta}(t)$; this yields $\overline{\imath_s^{\alpha\beta}}(t)$ with an $\mathcal{O}(\varepsilon^2)$ error.

4. filter with ϕ the known signal $(\imath_s^{\alpha\beta}(t) - \overline{\imath_s^{\alpha\beta}}(t))s_1^{\alpha\beta^T}(u_s^{abc}(t), \frac{t}{\varepsilon})$; this yields $y_v(t)$ with an $\mathcal{O}(\varepsilon^2)$ error.

This procedure is encapsulated in the following equations: $\imath_s^{\alpha\beta}$ is recovered through $(\imath_s^{\alpha\beta} * \phi)(t) = \overline{\imath_s^{\alpha\beta}}(t) + \mathcal{O}(\varepsilon^2)$. As for the virtual measurement y_v, the subsequent result holds

$$\begin{aligned}\left[(\imath_s^{\alpha\beta} - \overline{\imath_s^{\alpha\beta}})s_1^{\alpha\beta^T}\right] * \phi &= \varepsilon\mathcal{S}(\bar{\theta})(s_1^{\alpha\beta}s_1^{\alpha\beta^T} * \phi) + \mathcal{O}(\varepsilon^2)\\ &= \varepsilon\mathcal{S}(\bar{\theta})\overline{s_1^{\alpha\beta}s_1^{\alpha\beta^T}} + \mathcal{O}(\varepsilon^2)\\ &= y_v + \mathcal{O}(\varepsilon^2).\end{aligned}$$

The whole procedure is represented in figure 6.1. The rotor position is extracted from the virtual measurement using the two demodulation procedures fleshed out in section 6.3, thus providing an estimate $\hat{\theta}$ of θ with an $\mathcal{O}(\varepsilon)$ error.

6.2.4 Processing directly the Sigma-Delta bitstream

Using the results developed in chapter 5, it turns out that, if the demodulation process of subsection 6.2.3 is applied directly to the bitstream $\imath_{s,\Sigma\Delta}^{\alpha\beta} \in \{0,1\}$ output by a continuous or discrete second-order $\Sigma\Delta$, then the estimation of the virtual output y_v is the same as if it were applied directly to the (unavailable) analog measurement $\imath_s^{\alpha\beta}$, up to an error $\mathcal{O}(1/N^j)$, where $N := \varepsilon/T_s$ is the modulator oversampling ratio, with T_s the modulator sampling time. Simply put, the synchronous detection over $\Sigma\Delta$ modulators only differs by a factor $\mathcal{O}(1/N^j)$ from the detection on the analog input. The total error with respect to the true y_v is therefore $\mathcal{O}(\varepsilon^2) + \mathcal{O}(1/N^j)$. If the signal $s_1^{\alpha\beta}s_1^{\alpha\beta^T}$ is continuous, which holds for the presented application, then $j = 2$; if this signal presents discontinuities, we have only $j = 1$.

6.3 Extracting θ from the virtual measurement

Extracting the rotor position θ from y_v depends on the rank of the 2×2 matrix $\mathcal{A}^{\alpha\beta}(u_s^{abc})$. The structure of this matrix, hence its rank, depends on the specifics of the PWM employed. After recalling the basics of single-phase PWM, we study two cases: standard three-phase PWM with a single carrier, and three-phase PWM with interleaved carriers, i.e. PSC-PWM.

6.3.1 Single-phase PWM

We recapitulate here the discussion conducted in section 3.2. In standard sinusoidal PWM with period ε and range $[-u_m, u_m]$, the input signal u is compared to the ε-periodic triangular carrier

$$c(t) := \begin{cases} u_m + 4\,\mathrm{w}(\frac{t}{\varepsilon}) & \text{if } -\frac{u_m}{2} \le \mathrm{w}(\frac{t}{\varepsilon}) \le 0\\ u_m - 4\,\mathrm{w}(\frac{t}{\varepsilon}) & \text{if } 0 \le \mathrm{w}(\frac{t}{\varepsilon}) \le \frac{u_m}{2};\end{cases}$$

the 1-periodic function $\mathrm{w}(\sigma) := u_m \bmod(\sigma + \frac{1}{2}, 1) - \frac{u_m}{2}$ wraps the normalized time $\sigma = \frac{t}{\varepsilon}$ to $[-\frac{u_m}{2}, \frac{u_m}{2}]$. If u varies slowly enough, it crosses the carrier c exactly once on each rising and

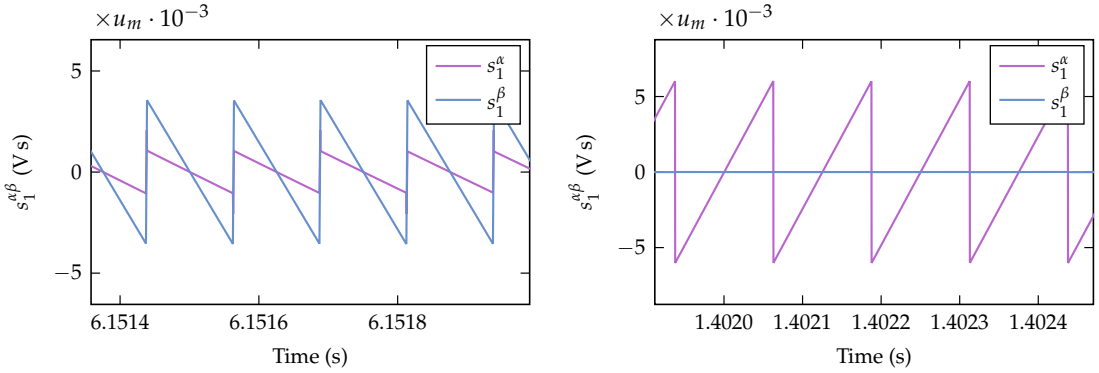

Figure 6.2: Signals $s_1^{\alpha\beta}$ for single-carrier PWM (simulation data): nondegenerate (left), degenerate (right).

falling ramp, at times $t_1^u < t_2^u$ such that

$$u(t_1^u) = u_m + 4\,\mathrm{w}\Big(\frac{t_1^u}{\varepsilon}\Big), \quad u(t_2^u) = u_m - 4\,\mathrm{w}\Big(\frac{t_2^u}{\varepsilon}\Big).$$

The PWM-encoded signal is therefore given by

$$u_{\mathrm{pwm}}(t) = \begin{cases} u_m & \text{if } -\frac{u_m}{2} < \mathrm{w}(\frac{t}{\varepsilon}) \le \mathrm{w}(\frac{t_1^u}{\varepsilon}) \\ -u_m & \text{if } \mathrm{w}(\frac{t_1^u}{\varepsilon}) < \mathrm{w}(\frac{t}{\varepsilon}) \le \mathrm{w}(\frac{t_2^u}{\varepsilon}) \\ u_m & \text{if } \mathrm{w}(\frac{t_2^u}{\varepsilon}) < \mathrm{w}(\frac{t}{\varepsilon}) \le \frac{u_m}{2}. \end{cases}$$

Fig. 3.1b illustrates the signals u, c and u_{pwm}. The function

$$\begin{aligned} \mathcal{M}(u,\sigma) &:= \begin{cases} u_m & \text{if } -2u_m < 4\,\mathrm{w}(\sigma) \le u - u_m \\ -u_m & \text{if } u - u_m < 4\,\mathrm{w}(\sigma) \le u_m - u \\ u_m & \text{if } u_m - u < 4\,\mathrm{w}(\sigma) \le 2u_m \end{cases} \\ &= u_m + u_m \operatorname{sign}(u - u_m - 4\,\mathrm{w}(\sigma)) + u_m \operatorname{sign}(u - u_m + 4\,\mathrm{w}(\sigma)), \end{aligned}$$

which is obviously 1-periodic and with mean u with respect to its second argument, therefore completely describes the PWM process since $u_{\mathrm{pwm}}(t) = \mathcal{M}(u(t), \frac{t}{\varepsilon})$.

The induced zero-mean probing signal is then

$$\begin{aligned} s_0(u,\sigma) &:= \mathcal{M}(u,\sigma) - u \\ &= u_m - u + u_m \operatorname{sign}(\tfrac{u-u_m}{4} - \mathrm{w}(\sigma)) + u_m \operatorname{sign}(\tfrac{u-u_m}{4} + \mathrm{w}(\sigma)), \end{aligned}$$

and its zero-mean primitive in the second argument is

$$s_1(u,\sigma) := (1 - \tfrac{u}{u_m})\,\mathrm{w}(\sigma) - \Big|\tfrac{u-u_m}{4} - \mathrm{w}(\sigma)\Big| + \Big|\tfrac{u-u_m}{4} + \mathrm{w}(\sigma)\Big|.$$

The signals s_0, s_1 are displayed in Fig. 3.2. Notice that, by construction, $s_0(\pm u_m, \sigma) = 0$ and $s_1(\pm u_m, \sigma) = 0$, so there is no ripple, hence no usable information, at the PWM limits.

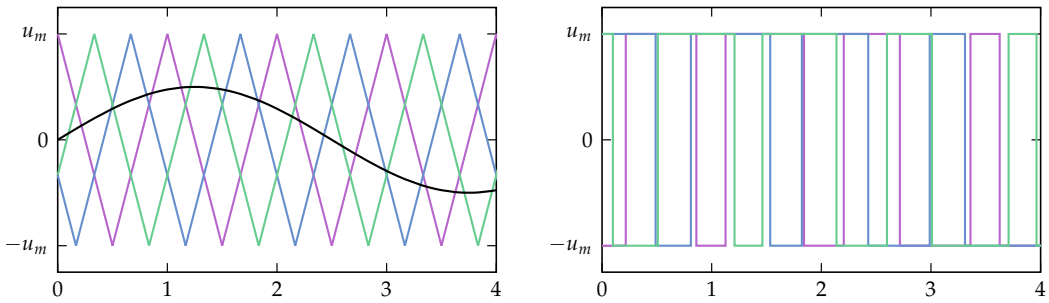

Figure 6.3: Interleaved carriers (purple, blue, green: left). The same reference (black) produces different PWM signals (right).

6.3.2 Three-phase PWM with single carrier

In three-phase PWM with single carrier, each component u_s^k, $k \in \{a, b, c\}$, of u_s^{abc} is compared to the same carrier, yielding

$$s_0^k(u_s^{abc}, \sigma) := s_0(u_s^k, \sigma), \qquad s_1^k(u_s^{abc}, \sigma) := s_1(u_s^k, \sigma),$$

with s_0 and s_1 as in single-phase PWM. This is the most common PWM in industrial drives as it is easy to implement and ensures a reduced zero-sequence voltage. For such a PWM scheme, the rank of the matrix $\mathcal{A}^{\alpha\beta}$ regularly drops from two to one (see subsection 6.3.5), thus demands a tailored demodulation procedure to get round these invertibility losses, see subsection 6.3.4. Fig. 6.2 displays examples of the shape of $s_1^{\alpha\beta}$, in the rank 2 case (left), and in the rank 1 (right) case where $u_s^c = u_s^b \neq u_s^a$.

6.3.3 Three-phase PWM with interleaved carriers

At the cost of a more complicated implementation, it turns out that a PSC-PWM, i.e. a scheme with (regularly) interleaved carriers offers several benefits over single-carrier PWM. In this scheme, each component of u_s^{abc} is compared to a shifted version of the same triangular carrier (with shift 0 for axis a, 1/3 for axis b, and 2/3 for axis c), yielding

$$\begin{aligned}
s_0^a(u_s^{abc}, \sigma) &:= s_0(u_s^a, \sigma), & s_1^a(u_s^{abc}, \sigma) &:= s_1(u_s^a, \sigma),\\
s_0^b(u_s^{abc}, \sigma) &:= s_0(u_s^b, \sigma - \tfrac{1}{3}), & s_1^b(u_s^{abc}, \sigma) &:= s_1(u_s^b, \sigma - \tfrac{1}{3}),\\
s_0^c(u_s^{abc}, \sigma) &:= s_0(u_s^c, \sigma - \tfrac{2}{3}), & s_1^c(u_s^{abc}, \sigma) &:= s_1(u_s^c, \sigma - \tfrac{2}{3}).
\end{aligned}$$

Fig. 6.3 illustrates the principle of this scheme, where a same input signal is converted into three different PWM outputs, one for each phase. Fig. 6.4 displays an example of the shape of $s_1^{\alpha\beta}$, which always more or less looks like two signals in quadrature. Here, $\mathcal{A}^{\alpha\beta}$ remains invertible, on the contrary to the synchronized case, thus allowing the use, without restriction, of its inverse to recover the rotor position from the virtual measurement, see subsection 6.3.4.

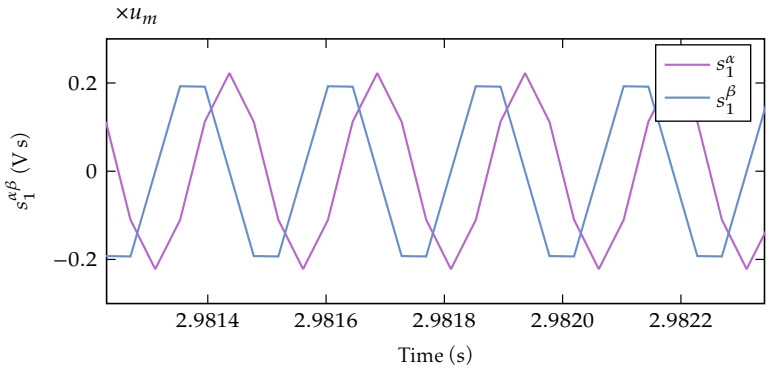

Figure 6.4: $s_1^{\alpha\beta}$ for interleaved PWM (simulation data).

6.3.4 Demodulation procedure

Synchronized carriers As the rank 1 situation very often occurs —six times per electrical turn at steady state as described in subsection 6.3.5— for single-carrier PWM, it must be handled by the procedure for extracting θ from the virtual measurement $y_v = \varepsilon \mathcal{S}(\theta).\mathcal{A}^{\alpha\beta}(u^{abc})$ (see section 6.2). Similarly to the extraction described in subsection 2.5.5, this can be done by a linear least squares method, thanks to the particular structure of the saliency matrix $\mathcal{S}(\theta)$ defined by (6.3). Setting

$$\begin{pmatrix} \lambda & \mu \\ \mu & \nu \end{pmatrix} := \mathcal{A}^{\alpha\beta}(u^{abc}), \qquad \begin{pmatrix} y_{11} & y_{12} \\ y_{21} & y_{22} \end{pmatrix} := \frac{2L_dL_q}{L_d+L_q}\frac{y_v}{\varepsilon},$$

and $L := \frac{L_d+L_q}{L_q-L_d}$, we can rewrite the virtual measurement expression $\varepsilon \mathcal{S}(\theta).\mathcal{A}^{\alpha\beta}(u^{abc})$ as the following linear system in $\cos 2\theta$ and $\sin 2\theta$

$$\underbrace{\begin{pmatrix} \lambda & \mu \\ \mu & \nu \\ -\mu & \lambda \\ -\nu & \mu \end{pmatrix}}_{:=P} \begin{pmatrix} \cos 2\theta \\ \sin 2\theta \end{pmatrix} = L \underbrace{\begin{pmatrix} y_{11}-\lambda \\ y_{12}-\mu \\ y_{21}-\mu \\ y_{22}-\nu \end{pmatrix}}_{:=d}.$$

The least-square solution of this (consistent) overdetermined linear system is

$$\begin{aligned} \begin{pmatrix} \cos 2\theta \\ \sin 2\theta \end{pmatrix} &= L[P^TP]^{-1}P^Td = \frac{L}{\lambda^2+2\mu^2+\nu^2}P^Td \\ &= \frac{L}{\lambda^2+2\mu^2+\nu^2}\begin{pmatrix} \lambda y_{11}+\mu(y_{12}-y_{21})-\nu y_{22}-\lambda^2+\nu^2 \\ \mu(y_{11}+y_{22})+\nu y_{12}+\lambda y_{21}-2\mu(\lambda+\nu) \end{pmatrix}. \end{aligned}$$

Estimates $\widehat{\cos 2\theta}, \widehat{\sin 2\theta}$ for $\cos 2\theta, \sin 2\theta$ are obtained with the same formulas, using $\hat{y}_{ij}$ instead of the actual y_{ij} the estimated

$$\begin{pmatrix} \hat{y}_{11} & \hat{y}_{12} \\ \hat{y}_{21} & \hat{y}_{22} \end{pmatrix} := \frac{2L_dL_q}{L_d+L_q}\frac{\hat{y_v}}{\varepsilon} = \frac{2L_dL_q}{L_d+L_q}\frac{y_v}{\varepsilon} + \mathcal{O}(\varepsilon).$$

We thus have

$$\begin{aligned}\widehat{\cos 2\theta} &:= L\frac{\lambda\hat{y}_{11} + \mu(\hat{y}_{12} - \hat{y}_{21}) - \nu\hat{y}_{22} - \lambda^2 + \nu^2}{\lambda^2 + 2\mu^2 + \nu^2}\\ &= \cos 2\theta + \mathcal{O}(\varepsilon),\\ \widehat{\sin 2\theta} &:= L\frac{\mu(\hat{y}_{11} + \hat{y}_{22}) + \nu\hat{y}_{12} + \lambda\hat{y}_{21} - 2\mu(\lambda + \nu)}{\lambda^2 + 2\mu^2 + \nu^2}\\ &= \sin 2\theta + \mathcal{O}(\varepsilon).\end{aligned}$$

Finally, we get an estimate $\hat{\theta}$ of θ by

$$\hat{\theta} := \frac{1}{2}\operatorname{atan2}(\widehat{\sin 2\theta}, \widehat{\cos 2\theta}) + k\pi = \theta + \mathcal{O}(\varepsilon),$$

where $k \in \mathbb{N}$ is the number of turns. Due to the nonlinear nature of atan2, chattering might occur at every half-turn in the presence of noise, thus hindering the estimate use in a feedback loop. This issue is simply solved by using a basic Quadrature-Component Q-PLL [ZL16] to recover the position from the sine and cosine estimates.

Interleaved carriers For PSC-PWM, even when two, or even three, components of u_s^{abc} are equal, $\mathcal{A}^{\alpha\beta}(u^{abc})$ remains invertible (except of course at the PWM limits), since each component has, because of the interleaving, a different PWM pattern. It is therefore possible to recover all four entries of the saliency matrix $\mathcal{S}(\theta)$ by

$$\widehat{\mathcal{S}(\theta)} := \hat{y}_v \cdot [\mathcal{A}^{\alpha\beta}(u^{abc})]^{-1} = \mathcal{S}(\theta) + \mathcal{O}(\varepsilon).$$

Notice now that thanks to the structure of $\mathcal{S}(\theta) = (s_{ij})_{ij}$, the rotor angle θ can be computed from the matrix entries by

$$s_{12} + s_{21} = \frac{L_q - L_d}{L_d L_q}\sin 2\theta, \quad s_{11} - s_{22} = \frac{L_q - L_d}{L_d L_q}\cos 2\theta,$$
$$\theta = \frac{1}{2}\operatorname{atan2}(s_{12} + s_{21}, s_{11} - s_{22}) + k\pi,$$

where $k \in \mathbb{N}$ is the number of turns. An estimate $\hat{\theta}$ of θ can therefore be computed from the entries $(\hat{s}_{ij})_{ij}$ of $\widehat{\mathcal{S}(\theta)}$ by

$$\hat{\theta} = \frac{1}{2}\operatorname{atan2}(\hat{s}_{12} + \hat{s}_{21}, \hat{s}_{11} - \hat{s}_{22}) + k\pi = \theta + \mathcal{O}(\varepsilon),$$

without requiring the knowledge of the magnetic parameters L_d and L_q, which is indeed a nice practical feature. Also, shifting the carriers enhances the amplitude of $s_1^{\alpha\beta}$ compared to the synchronized scheme, see figures 6.2 and 6.4. While a greater current ripple amplitude is detrimental in many industrial applications, it helps in achieving a better estimate resolution. Instead of considering phase-shifted carriers, a trade-off could be to slightly shift the carriers, so that the matrix $\mathcal{A}^{\alpha\beta}$ keeps its properties while inducing reduced current ripples.

6.3.5 Properties of matrix $\mathcal{A}^{\alpha\beta}$ for single-carrier PWM

Rank one The demodulation procedure when the matrix $\mathcal{A}^{\alpha\beta}(u_s^{abc})$ is invertible is straightforward, and does not require the prior knowledge of the d- and q-axis inductances. For a

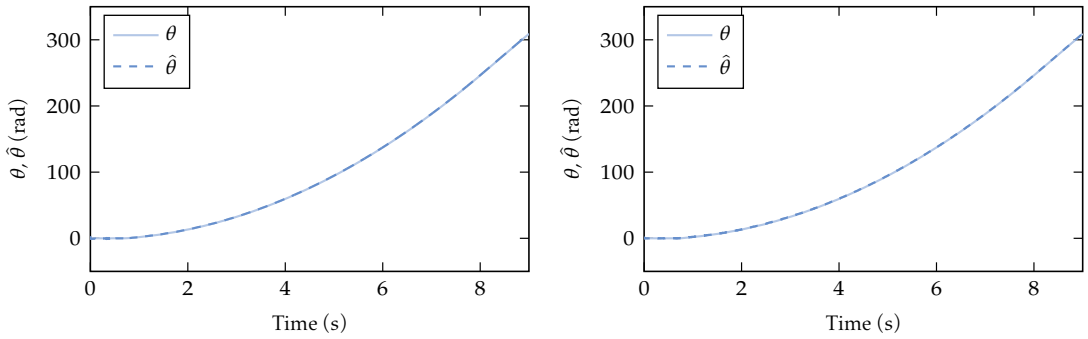

(a) Actual rotor position θ and its estimate $\hat{\theta}$ at 100 % of rated torque.

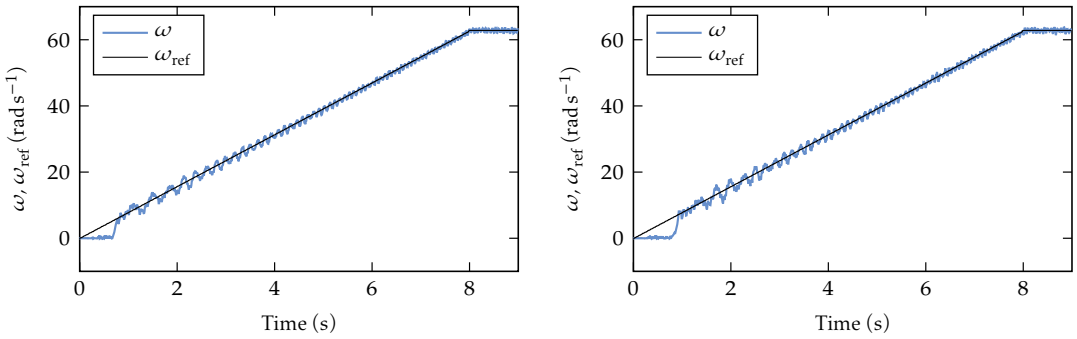

(b) Rotor speed ω and its reference ω_{ref} at 100 % of rated torque.

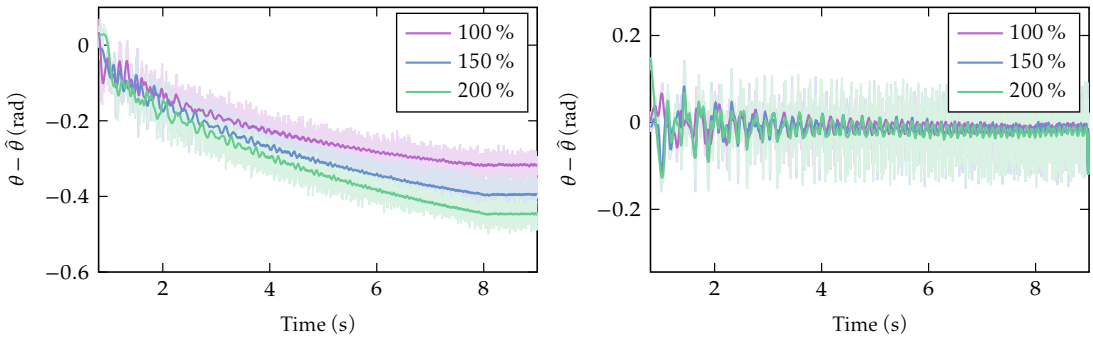

(c) Error $\theta - \hat{\theta}$ (rad) at 100 % (purple), 150 % (blue) and 200 % (green) of rated torque: actual (pale) and filtered (dark) data.

Figure 6.5: Experimental results: standard PWM (left), PSC-PWM (right).

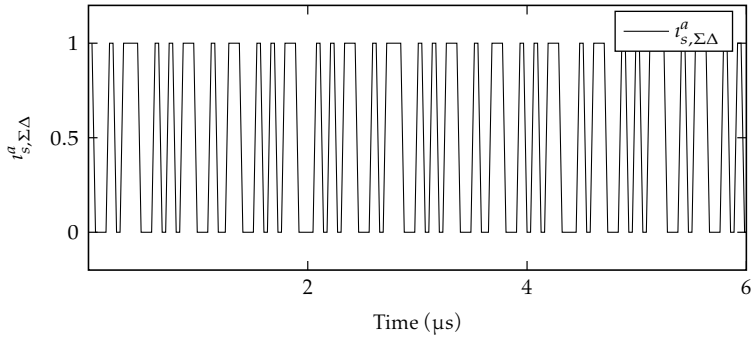

Figure 6.6: Sigma-Delta encoding $i^a_{s,\Sigma\Delta}$ of the stator current i^a_s.

single-carrier PWM-scheme though, this property does not always hold, as the rank regularly drops to one, namely when two components of u_s^{abc} are equal, which happens six times per electrical turn at steady state.

Indeed, without loss of generality, assume $u_s^a = u_s^b$. Then $s_1^a(u_s^a, t) = s_1^b(u_s^b, t)$. Applying Concordia's transformation to s_1^{abc} then yields

$$s_1^{\alpha\beta}(u,t) := \mathcal{C}s_1^{abc}(u_s^{abc}, \tfrac{t}{\varepsilon}) = \sqrt{\frac{2}{3}}\begin{pmatrix} 1/2 \\ \sqrt{3}/2 \end{pmatrix}(s_1^b(u_s^b,t) - s_1^c(u_s^c,t)).$$

This means s_1^α and s_1^β are colinear, so $\operatorname{rank}\mathcal{A}^{\alpha\beta} = 1$. Conversely, assume the three input voltages are different, namely $u^i \neq u^j$ for $i \neq j$. Then s_1^a, s_1^b and s_1^c are necessarily independent, as their commutation moments differ. Indeed, the three signals $s_1^i(u_s^i, \cdot)$ are periodic triangles, they are colinear if and only if their vertices share the same t-axis coordinate. Therefore, s_1^α and s_1^β are independent, meaning $\det \mathcal{A}^{\alpha\beta} \neq 0$.

Rank zero The rank of the matrix $\mathcal{A}^{\alpha\beta}(u^{abc})$ degenrates to 0 and consequently position recovery thanks to the modulation-induced current ripple is not possible, in only two cases:

— When $u_s^a = u_s^b = u_s^c$.

— When $\{u_s^a, u_s^b, u_s^c\} = \{u_m, \pm u_m, -u_m\}$.

The second case occurs only when over-modulation [HLK92] is used and at very high speed when the position of the rotor of the PMSM can be estimated without resorting to transient methods.

In steady state, when $u_s^a = u_s^b = u_s^c$, the two first equations of (6.1) under the linear current-flux relation read

$$0 = -R_s i_s^d + \omega L_q i_s^q \tag{6.5a}$$
$$0 = -R_s i_s^q - \omega L_d i_s^d - \omega \phi_m \tag{6.5b}$$

and the electromagnetic torque reads

$$T_e = n i_s^q \phi_m + n(L_d - L_q) i_s^d i_s^q.$$

Table 6.1: Rated parameters

Rated power	400 W	Number of pole pairs n	2
Rated voltage (RMS)	400 V	Stator resistance R_s	4.25 Ω
Rated current (RMS)	1.66 A	d-axis inductance L_d	43.25 mH
Rated speed	1800 RPM	q-axis inductance L_q	69.05 mH
Rated torque	2.12 N m	Permanent magnet flux linkage ϕ_m	0.277 Wb

Inverting (6.5), we can obtain the stator currents in dq-frame and show that they verify

$$\left(\imath_s^d + \frac{1}{2}\frac{\phi_m}{L_d}\right)^2 + (\imath_s^q)^2\frac{L_q}{L_d} = \left(\frac{1}{2}\frac{\phi_m}{L_d}\right)^2,$$

which is the equation of an ellipsis of radii ϕ_m/L_d and $\phi_m/\sqrt{L_dL_q}$ tangent to the vertical axis in 0. Thanks to the degree of freedom we have in the realization of T_e, by carefully adapting the current trajectory, we can always avoid this case. For instance, setting $\imath_s^d > 0$ will ensure that we never have $u_s^a = u_s^b = u_s^c$. Otherwise, we may fall in this case, when

$$T_e = -n\frac{\phi_m^2}{L_d}\left(\frac{R_s}{L_d}\omega\right)\frac{\frac{R_s^2}{L_q^2} + \omega^2}{\left(\frac{R_s^2}{L_dL_q} + \omega^2\right)^2}.$$

In the speed-torque plane, this relation describes a curve going through the origin and staying in the two generator quadrants. Hence, position estimation may not be always possible in the low speed range, if the currents are not appropriately selected.

6.4 Numerical and experimental results

6.4.1 Scenario and experimental results

The whole approach is validated experimentally on a salient PMSM with rated parameters given in table 6.1. The ΣΔ modulator is a Broadcom ACPL-798J [Bro] with a sampling frequency $T_s^{-1} := 15\,\text{MHz}$; the PWM frequency is $\varepsilon^{-1} := 4\,\text{kHz}$, thereby the oversampling ratio $N = \varepsilon/T_s = 3750$. Due to its very high frequency, processing the ΣΔ bitstream in real time will ultimately require to use an FPGA. However, to validate the theory without resorting to FPGA programming, we recorded simultaneously at 31.25 MHz the analogue value of the bus voltage, the ΣΔ bitstreams (see e.g. Fig. 6.6) and the six gate control signals using a mixed signal oscilloscope (Picoscope 3206D MSO). For comparison purposes we also recorded the digital encoder output signals, so that we can get the real position of the rotor.

In the test scenario, the motor starts at rest and slowly accelerates from 0 to 10 Hz (electrical) in approximately 8 s. The experiment is performed with three different load torques, namely about 100 %, 150 % and 200 % of the rated torque, for standard PWM. The results are displayed in Fig. 6.5; they are very satisfying, though with errors larger than expected, and increasing with the load torque. The reason for this behavior is most probably the effect of magnetic

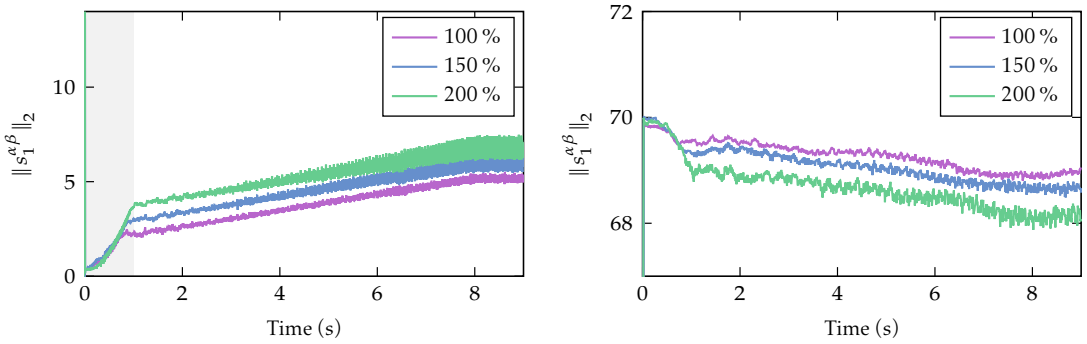

(a) Experimental, standard PWM

(b) Experimental, PSC-PWM

Figure 6.7: RMS value of $s_1^{\alpha\beta}$ (experimental values).

saturation, not taken into account in the rotor position extraction procedure of subsection 6.3.4.

The method is further validated for PSC-PWM-controlled PMSM. The results are displayed in Fig. 6.5, and exhibit a reduced position error compared to the standard scheme estimate. The amplitude of the ripple $s_1^{\alpha\beta}$ is stronger, achieves better resolution than its synchronized correlative: when $\| s_1^{\alpha\beta} \|_2$ remains weak for standard PWM (see Fig. 6.7a, especially during the first second), using different carriers greatly enhances this norm (Fig. 6.7b), thus guaranteeing the procedure validity during the whole scenario duration. The natural downsides of shifted-carriers PWM are twofold: the acoustic noise the carrier shifting introduces and the strong current and torque ripple which might be harmful for high-performance applications.

6.4.2 Role of magnetic saturation and numerical results

Saturated current-flux relation

When operating at medium to high speed, namely above 10 % of the rated speed, linear current-flux relations are accurate enough for control purposes. At low speed though, the linear model fails to capture magnetic saturation and cross-coupling, thereby deteriorating the control model accuracy [Com+17]. Recently, macroscopic approaches based on the machine symmetries and energy considerations have been proposed to modelize the motor nonlinearities due to magnetic saturation [Jeb+16; Jeb+14]. Following this way, the magnetic energy can be described by a fourth-order function $\mathcal{H}_m^{dq}$ of the form (see [Jeb+11] for further details)

$$\begin{aligned}\mathcal{H}_m^{dq}(\phi_s^{dq}) := {} & p_{10}\phi_s^d + p_{20}(\phi_s^d - \phi_m)^2 + p_{30}(\phi_s^d - \phi_m)^3 + p_{40}(\phi_s^d - \phi_m)^4 + p_{02}(\phi_s^q)^2 + p_{04}(\phi_s^q)^4 \\ & + p_{12}(\phi_s^d - \phi_m)(\phi_s^q)^2 + p_{22}(\phi_s^d - \phi_m)^2(\phi_s^q)^2,\end{aligned}$$

where the coefficients p_{ij} are magnetic parameters to be identified, using for example the classic signal injection technique in the locked-rotor position. The magnetization current-flux

Table 6.2: Estimated magnetic parameters

p_{02}	p_{04}	p_{10}	p_{12}	p_{20}	p_{22}	p_{30}	p_{40}
6.6680	−0.5198	0.0391	1.0922	11.0815	22.1409	18.7946	68.6069

curves eventually reads

$$\begin{aligned} \imath_s^d &= \frac{\partial \mathcal{H}_m^{dq}}{\partial \phi_s^d}(\phi_s^{dq}) = p_{10} - 2p_{20}(\phi_s^d - \phi_m) + 3p_{30}(\phi_s^d - \phi_m)^2 \\ &\qquad + p_{12}(\phi_s^q)^2 + 4p_{40}(\phi_s^d - \phi_m)^3 + 2p_{22}(\phi_s^d - \phi_m)(\phi_s^q)^2 \\ \imath_s^q &= \frac{\partial \mathcal{H}_m^{dq}}{\partial \phi_s^q}(\phi_s^{dq}) = 2p_{02}\phi_s^q + 2p_{12}(\phi_s^d - \phi_m)\phi_s^q + 2p_{22}(\phi_s^d - \phi_m)^2\phi_s^q + 4p_{04}(\phi_s^q)^3. \end{aligned}$$

The saturated current-flux relations define another mapping h for the output currents that modifies the virtual measurement structure. More specifically, the saliency matrix turns out to depend on the flux linkages due to the polynomial terms in the expression of $\imath_s^{dq}$. This difference between the linear and saturated saliency matrices may ultimately corrupt the estimate quality.

Numerical results

To substantiate the magnetic saturation role in the error estimate discrepancies for the synchronized scheme, we have run the same scenario in simulation with and without a model of magnetic saturation. The saturation model is previously described, with magnetic parameters gathered for the considered PMSM in table 6.2. With the saturation model (Fig. 6.9), the error has approximately the same shape and value as in the experiment; whereas without the saturation model (Fig. 6.8), the error substantially decreases and is independent of the load torque as expected. Notice that it is conceivable to take into account magnetic saturation in our approach, along the lines of [Jeb+16] for forced injection. This would mean using a more complicated saliency matrix $\mathcal{S}$, together with a more complicated rotor position extraction scheme; other than that, the demodulation procedure would remain the same, and the error due to the ΣΔ modulator would be unchanged.

6.4.3 Masking the current transients

Due to parasitic effects in industrial drives, and especially the discharge of parasitic capacitances in the Insulated-Gate Bipolar Transistors (IGBT), the measured currents are heavily corrupted by huge spikes, see figure 6.10a. These transients occur at every inverter commutation, i.e. six times per PWM period (twice per phase), and bring about the loss of 10 to 20 % of the signal per period. The procedure to recover the rotor position from the currents could eventually be hindered by these inverter non-idealities, and thus needs to be adapted to take them into account.

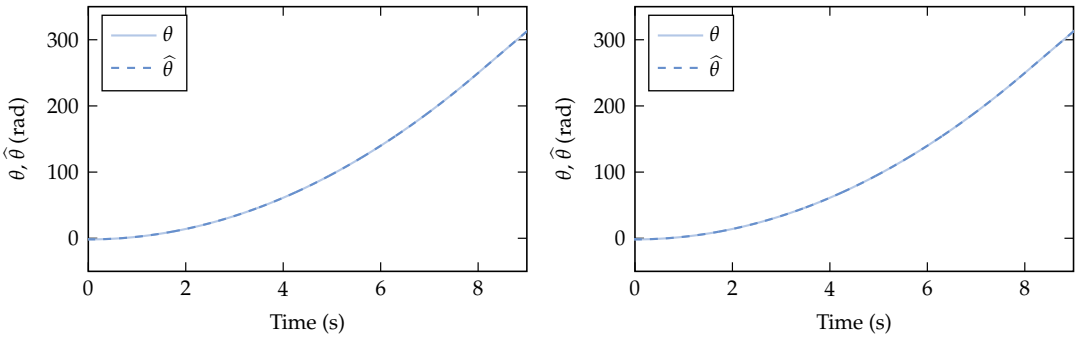

(a) Actual rotor position θ and its estimate $\hat{\theta}$ at 100 % of rated torque.

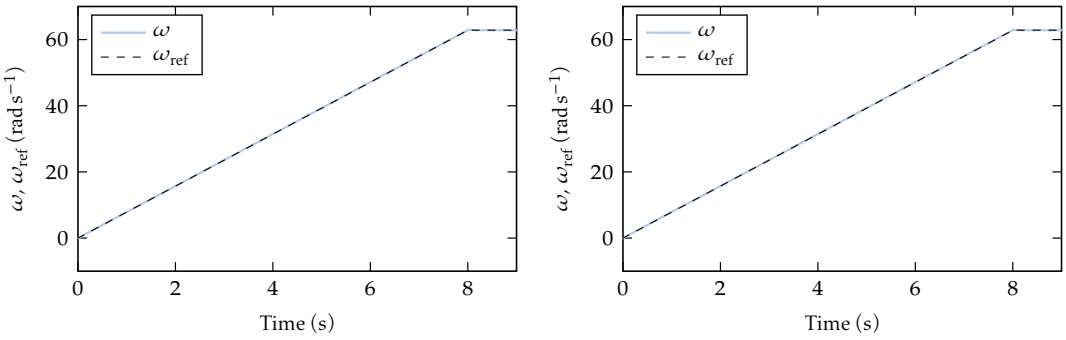

(b) Actual rotor speed ω at 100 % of rated torque.

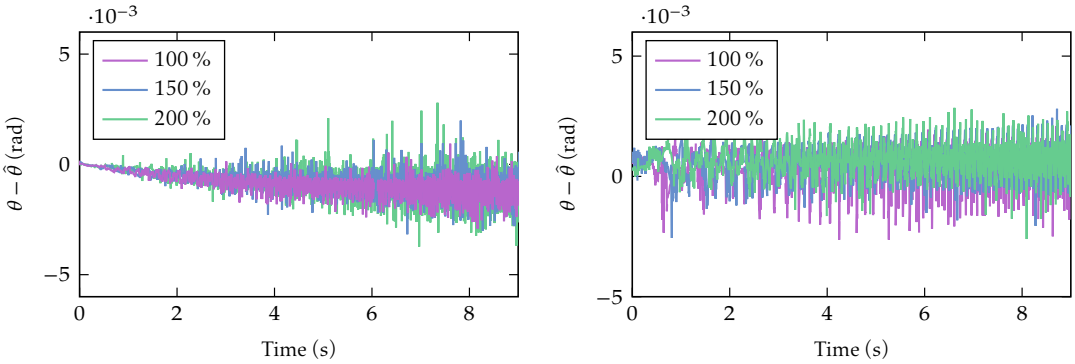

(c) Error $\theta - \hat{\theta}$ (rad) at 100 % (purple), 150 % (blue) and 200 % (green) of rated torque.

Figure 6.8: Test scenario, numerical results, without magnetic saturation model: synchronized carriers (left), PSC-PWM (right).

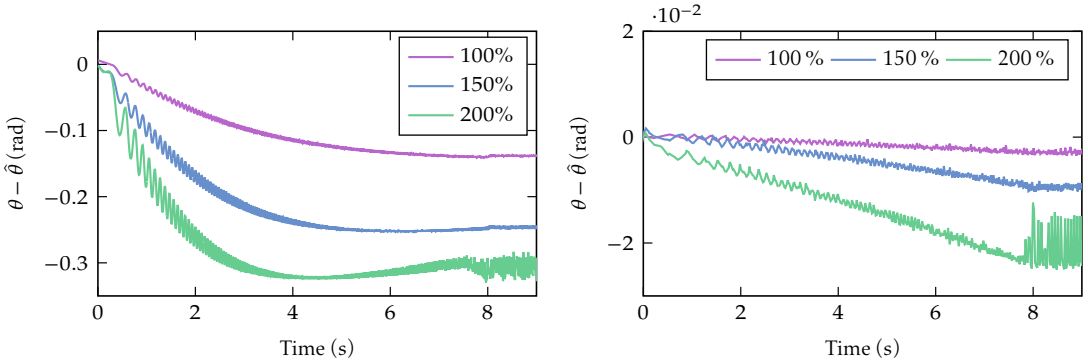

(a) Standard PWM (b) PSC-PWM

Figure 6.9: Error $\theta - \hat{\theta}$ (rad) at 100 % (purple), 150 % (blue) and 200 % (green) of rated torque; numerical results with magnetic saturation model: standard PWM (left), PSC-PWM (right).

To achieve this, the virtual measurement extraction detailed in subsection 6.2.2 is slightly modified. Since the moments the spikes are observed are approximately known, we can define the window c with $c(u_s^{abc}, \tau) = 0$ when the perturbation is active, 1 otherwise. The rectangular masking window c, synchronized with the PWM commutations, simply discards the corrupted data. Define also the new *demodulation basis* $r(u_s^{abc}, \tau) := s_1^{\alpha\beta}(u_s^{abc}, \tau)c(u_s^{abc}, \tau)$, and the new matrix $\mathcal{A}_r^{\alpha\beta}$:

$$\mathcal{A}_r^{\alpha\beta}(v^{abc}) := \int_0^1 s_1(v^{abc}, \tau) r^T(v^{abc}, \tau)\, d\tau - \frac{1}{\bar{c}} \int_0^1 r(v^{abc}, \tau)\, d\tau \int_0^1 r^T(v^{abc}, \tau)\, d\tau,$$

where $\bar{c} := \int_0^1 c(v^{abc}, \tau)\, d\tau$. Notice that if $c := 1$, then $r = s$ and the matrix $\mathcal{A}^{\alpha\beta}$ remain the same as in subsection 6.2.2. The new procedure now reads

2. filter with ϕ the known signal $c(u_s^{abc}(t), \frac{t}{\varepsilon})$, this yields $\bar{c}$ with an $\mathcal{O}(\varepsilon^2)$ error.
3. filter with ϕ the known signal $(\imath_s^{\alpha\beta} c)/\bar{c}$; this yields $\overline{\imath_s^{\alpha\beta}}$ with an $\mathcal{O}(\varepsilon)$ error.
4. filter with ϕ the known signal $(\imath_s^{\alpha\beta} - \overline{\imath_s^{\alpha\beta}}) r^T(u_s^{abc}(t), \frac{t}{\varepsilon})$, this yields $y_v(t) = \varepsilon S(\bar{\theta}) \mathcal{A}_r^{\alpha\beta}$ with an $\mathcal{O}(\varepsilon^2)$ error.

From here, the position extraction based on a least-square method from the virtual measurement y_v follows as in section 6.3 with the replacement of the matrix $\mathcal{A}^{\alpha\beta}$ by $\mathcal{A}_r^{\alpha\beta}$. This method has been applied both numerically and experimentally, but did not show any major improvements compared to the results displayed in subsection 6.4.1. This might stem from the very particular shapes of the current disturbances, namely damped oscillations that are ultimately mitigated by the low-pass filtering of the currents (using the kernel ϕ). This theory however turns out to be particularly effective to discard stronger disturbances, which would otherwise corrupt the whole procedure.

Under the light of section 6.2.4, the demodulation basis c can be tailored to improve the demodulation error over the $\Sigma\Delta$ encoding of the currents. With the rectangular window, $\Sigma\Delta$

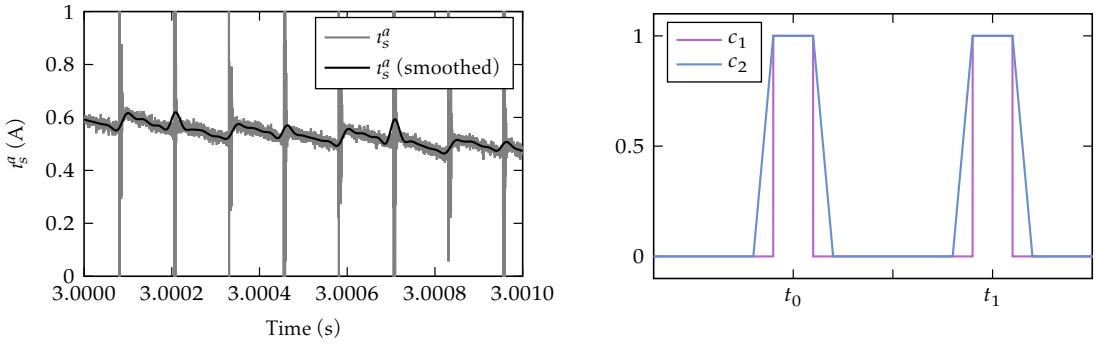

(a) Measured current i_s^a (experimental data)

(b) Masking windows

Figure 6.10: Rectangular and trapezoidal masking windows c_1 and c_2 centered on the perturbation times t_0 and t_1 (right) to mitigate the parasitic capacitances discharges (left).

modulation introduces an $\mathcal{O}(1/\varepsilon)$ error due to the discontinuous nature of $s_1^{\alpha\beta} r^T$. Replacing c by a trapezoidal window (see Fig. 6.10), so that $s_1^{\alpha\beta} r^T$ becomes continuous, eventually reduces this modulation error to a $\mathcal{O}(1/\varepsilon^2)$.

6.5 Conclusion

We have presented a method to estimate the rotor position of a PWM-fed PMSM from the ripple created by the PWM itself, without the need for an external probing signal. The method is compatible with the hardware found in recent industrial drives, i.e. comprising $\Sigma\Delta$ modulators and an FPGA. Notice that on such drives the primary role of the modulators and FPGA are to act as complete multibit ADCs with moreover galvanic insulation provided by the modulators; the proposed procedure can overall be seen as an enhanced multibit ADC, providing not only the actual output, but also the virtual measurement and in turn the rotor position. The procedure could also be seen as a kind of software sensor for measuring the slope of the current ripple. But it is much more general than that, in the sense than it can in theory accommodate any modulation scheme with e.g. a multilevel inverter or Space-Vector PWM, and not only classical PWM with a standard two-level inverter; the only thing to change is the expression of the modulation function s_0^{abc} of section 6.2, and of its zero-mean primitive s_1^{abc}.

Conclusion and perspectives

La commande sans capteur des moteurs électriques à basse vitesse demeure une problématique industrielle à la fois complexe et fertile. Ce travail de thèse s'est attaché à démontrer la validité théorique et expérimentale d'une méthode d'estimation de la position du rotor sans capteur mécanique, reposant uniquement sur les grandeurs électriques mesurées. Contrairement aux méthodes originelles exploitant la réponse induite par une excitation exogène à haute fréquence, il a été mis en évidence que l'onduleur qui convertit les entrées analogiques en signaux modulés par largeur d'impulsions introduit des harmoniques qui agissent comme une injection de signal endogène.

La théorie de la moyennisation s'est avérée être un outil mathématique particulièrement puissant dans l'étude des effets des injections endogène et exogène, notamment dans l'obtention d'une expression analytique desdites réponses induites. Dans le cas de l'injection externe, la moyennisation a été poussée jusqu'à l'ordre trois, mettant en lumière la possibilité de récupérer en toute généralité deux mesures virtuelles supplémentaires par rapport à une analyse à l'ordre deux. Satisfaisante théoriquement, cette technique présente toutefois des limites quant à sa réalisation pratique telles que l'amplitude réduite des deux signaux additionnels ou la corruption de ces derniers par le bruit de mesure. Ce travail a néanmoins posé les bases d'une théorie qui a été adaptée au traitement de systèmes hybrides contrôlés par des entrées MLI ; à cet égard, il est apparu que l'injection endogène induit la même forme de réponse que l'injection de signal externe, ouvrant donc les mêmes possibilités d'extraction d'une mesure virtuelle.

Que ce soit pour l'injection exogène ou endogène, l'information contenue dans l'excitation induite dans la sortie mesurée doit y être extraite. Pour ce faire, une théorie de la démodulation de signaux multiplexés par des porteuses à deux échelles de temps, spécialement adaptée aux spécificités des signaux moteurs, a été développée. Celle-ci se résume par une combinaison de filtres passe-bas, permettant de séparer chacune des composantes du signal multiplexé avec une précision arbitraire. Cette théorie a au départ été développée en supposant disponibles les sorties analogiques, une hypothèse qui n'est cependant pas vérifiée dans un contexte industriel, où les courants sont encodés numériquement par un modulateur Sigma-Delta. Seul un flux binaire à très haute fréquence est alors disponible en sortie, soulevant alors la question de la validité dans ce cadre de la démarche proposée sur les signaux analogiques. Il est apparu que la même procédure de démodulation analogique s'appliquait au flux binaire en sortie du Sigma-Delta, avec un terme d'erreur supplémentaire qui dépend à la fois de l'ordre du modulateur, du sur-échantillonnage et de sa structure.

Reposant sur ces deux fondements théoriques que sont la moyennisation pour l'obtention

de l'expression analytique de la perturbation induite par la MLI et la démodulation de signaux multiplexés en sortie d'un modulateur Sigma-Delta pour récupérer cette information, l'extraction de la position du rotor a été validée sur des données expérimentales. L'étude d'un modèle de MSAP a révélé des difficultés propres au contrôle moteur, à savoir la présence de transitoires de courant à chaque commutation des IGBT ou les pertes de rang de la Gramienne utilisée pour la démodulation. De cette dernière particularité est venue l'idée de décaler les porteuses de la MLI afin de garantir à la fois l'inversibilité et une grande amplitude de cette Gramienne, garantissant ainsi la présence de la perturbation portant l'information de position. Même si cette méthode garantit une bonne estimation de la position, elle requiert des modifications logicielles de très bas niveau et introduit par ailleurs un certain bruit acoustique. En gardant le schéma de MLI avec une seule porteuse, les erreurs de position deviennent non négligeables, mais sont consistantes avec les résultats numériques, et témoignent du rôle de la saturation magnétique ainsi que de la taille de l'excitation qui reste faible à basse vitesse.

Une extension naturelle de l'étude ici menée consisterait à tester la stratégie d'estimation en boucle fermée, c'est-à-dire en utilisant la position estimée dans la boucle de contrôle. Des prémices de résultats numériques confirment la faisabilité d'un tel schéma de contrôle, mais nécessitent une vérification expérimentale pour parachever la validation de ce schéma de contrôle sans capteur.

Sensorless control of electric motors at low speed remains a complex and fertile industrial problem. This thesis aimed at demonstrating the theoretical and experimental validity of a sensorless rotor position estimation method, based solely on the measured electrical quantities. In contrast to the original methods exploiting the response induced by an exogenous high-frequency excitation, it was shown that the inverter that converts the analog inputs into Pulse-Width Modulated signals introduces harmonics that act as a natural signal injection.

Averaging theory has proven to be a particularly powerful mathematical tool in the study of the effects of exogenous and endogenous injection, especially in obtaining an analytical expression of the said induced responses. In the exogenous injection case, averaging computations were taken to the third order, highlighting the possibility of recovering in full generality two additional virtual measurements compared to a second order analysis. Although theoretically satisfactory, this technique has limitations in terms of practical implementation, such as the reduced amplitude of the two additional signals or their corruption by measurement noise. This work has nevertheless laid the foundations of a theory that has been adapted to the processing of hybrid systems controlled by PWM inputs; in this regard, it has been shown that endogenous injection induces the same response pattern as external signal injection, thus opening up the same possibilities of extracting a virtual measurement.

For both exogenous and endogenous injection, the information contained in the induced excitation in the measured output must be extracted. For this purpose, a theory of the demodulation of multiplexed signals with slowly-varying carriers, specially adapted to the specificities of motor signals, has been developed. This boils down to a suitable combination of low-pass

filters that separates each component of the multiplexed signal with an arbitrary accuracy. This theory was initially developed assuming the availability of analog outputs, an assumption that is not satisfied in an industrial context, where the currents are digitally encoded by a Sigma-Delta modulator. Only a very high frequency bitstream is then available at the output, raising the question of the validity in this context of the proposed approach for analog signals. It appeared that the same analog demodulation procedure applied to the Sigma-Delta output bitstream, with an additional error term that depends on the modulator order, its structure and the oversampling ratio.

Based on these two theoretical foundations, namely averaging to obtain the analytical expression of the disturbance induced by the PWM and the demodulation of multiplexed signals encoded by a Sigma-Delta modulator to recover this information, the extraction of the rotor position was validated on experimental data. The study of a PMSM model brought the light to difficulties that are specific to motor control, namely the presence of current transients at each switching of the IGBTs or the rank losses of the Gramian used for the demodulation. From this last peculiarity came the idea of shifting the carriers of the PWM to guarantee both the invertibility and a large amplitude of this Gramian, thus ensuring the presence of the position-dependent disturbance in the measured currents. Although this method guarantees a good position estimation, it requires low-level software modifications and introduces also some acoustic noise. By keeping the single-carrier PWM scheme, the position errors become non-negligible, but are consistent with the numerical results, and reflect the role of magnetic saturation as well as the excitation amplitude, which remains small at low speeds.

A natural extension of the study carried out here would be to test the estimation strategy in closed loop, i.e. using the estimated position in the control loop. Preliminary numerical results confirm the feasibility of such a method, but require experimental verification to complete the validation of this sensorless control scheme.

Bibliography

[AP87] S. Ardalan and J. Paulos. "An Analysis of Nonlinear Behavior in Delta-Sigma Modulators." In: *IEEE Transactions on Circuits and Systems* 34.6 (1987), pp. 593–603.

[ASS96] P. M. Aziz, H. V. Sorensen, and J. vn der Spiegel. "An Overview of Sigma-Delta Converters." In: *IEEE Signal Processing Magazine* 13.1 (1996), pp. 61–84.

[Åst83] K. J. Åström. "Analysis of Rohrs Counterexamples to Adaptive Control." In: *The 22nd IEEE Conference on Decision and Control* (1983), pp. 982–987.

[Åst84] K. J. Åström. "Interactions between Excitation and Unmodeled Dynamics in Adaptive Control." In: *The 23rd IEEE Conference on Decision and Control*. Dec. 1984, pp. 1276–1281.

[Aub05] J.-P. Aubin. *Applied Functional Analysis*. Second. Wiley, 2005.

[AW06] P.P. Acarnley and J.F. Watson. "Review of Position-Sensorless Operation of Brushless Permanent-Magnet Machines." In: *IEEE Transactions on Industrial Electronics* 53.2 (2006), pp. 352–362.

[BD11] F. Briz and M. W. Degner. "Rotor Position Estimation." In: *IEEE Industrial Electronics Magazine* 5.2 (June 2011), pp. 24–36.

[Bes69] J. G. Besjes. "On Asymptotic Methods for Non-linear Differential Equations." In: *Journal de Mécanique* 8.3 (1969), p. 357.

[Bia+08] N. Bianchi, S. Bolognani, J.-H. Jang, and S.-K. Sul. "Advantages of Inset PM Machines for Zero-speed Sensorless Position Detection." In: *IEEE Transactions on Industry Applications* 44.4 (2008), pp. 1190–1198.

[Bia+17] N. Bianchi, S. Bolognani, F. Tinazzi, and M. Zigliotto. "The Influence of Rotor Design on Active Flux-based Sensorless Synchronous Reluctance Motor Drives." In: *2017 IEEE International Symposium on Sensorless Control for Electrical Drives (SLED)*. 2017, pp. 7–12.

[BM61] N. K. Bogoliubov and Y. A. Mitropolski. *Asymptotic Methods in the Theory of Nonlinear Oscillations*. Gordon and Breach, 1961.

[BOZ99] S. Bolognani, R. Oboe, and M. Zigliotto. "Sensorless Full-digital PMSM Drive with EKF Estimation of Speed and Rotor Position." In: *IEEE Transactions on Industrial Electronics* 46.1 (1999), pp. 184–191.

[BP18] P. Bernard and L. Praly. "Convergence of gradient observer for rotor position and magnet flux estimation of permanent magnet synchronous motors." In: *Automatica* 94 (Aug. 2018), pp. 88–93.

[BP20] P. Bernard and L. Praly. "Estimation of position and resistance of a sensorless PMSM : a nonlinear Luenberger approach for a non-observable system." In: *IEEE Transactions on Automatic Control* (Mar. 2020).

[Bri+04] F. Briz, M. W. Degner, P. Garcia, and R. D. Lorenz. "Comparison of Saliency-based Sensorless Control Techniques for AC Machines." In: *IEEE Transactions on Industry Applications* 40.4 (July 2004), pp. 1107–1115.

[Bro] Broadcom. *ACPL-798j Optically Isolated Sigma-delta Modulator with LVDS Interface*.

[BT58] R. B. Blackman and J. W. Tukey. "The Measurement of Power Spectra from the Point of View of Communications Engineering - Part I." In: *Bell System Technical Journal* 37.1 (1958), pp. 185–282.

[BTZ03] S. Bolognani, L. Tubiana, and M. Zigliotto. "Extended Kalman Filter Tuning in Sensorless PMSM Drives." In: *IEEE Transactions on Industry Applications* 39.6 (2003), pp. 1741–1747.

[Che+00a] Z. Chen, M. Tomita, S. Doki, and S. Okuma. "New Adaptive Sliding Observers for Position and Velocity Sensorless Controls of Brushless DC Motors." In: *IEEE Transactions on Industrial Electronics* 47.3 (2000), pp. 582–591.

[Che+00b] Z. Chen, M. Tomita, S. Ichikawa, S. Doki, and S. Okuma. "Sensorless Control of Interior Permanent Magnet Synchronous Motor by Estimation of an Extended Electromotive Force." In: *Conference Record of the 2000 IEEE Industry Applications Conference. Thirty-Fifth IAS Annual Meeting and World Conference on Industrial Applications of Electrical Energy (Cat. No.00CH37129)*. Vol. 3. 2000, 1814–1819 vol.3.

[Che+03] Z. Chen, M. Tomita, S. Doki, and S. Okuma. "An Extended Electromotive Force Model for Sensorless Control of Interior Permanent-magnet Synchronous Motors." In: *IEEE Transactions on Industrial Electronics* 50.2 (2003), pp. 288–295.

[CL98] M. J. Corley and R. D. Lorenz. "Rotor Position and Velocity Estimation for a Salient-pole Permanent Magnet Synchronous Machine at Standstill and High Speeds." In: *IEEE Trans. Industry Applications* 34 (1998), pp. 784–789.

[Com15] P. Combes. "Signal injection and sensorless control of electrical motors." Theses. Ecole Nationale Supérieure des Mines de Paris, Dec. 2015.

[Com+16a] P. Combes, A. K. Jebai, F. Malrait, P. Martin, and P. Rouchon. "Adding Virtual Measurements by Signal Injection." In: *2016 American Control Conference (ACC)*. IEEE, July 2016.

[Com+16b] P. Combes, F. Malrait, P. Martin, and P. Rouchon. "An Analysis of the Benefits of Signal Injection for Low-speed Sensorless Control of Induction Motors." In: *2016 International Symposium on Power Electronics, Electrical Drives, Automation and Motion, SPEEDAM 2016*. 2016, pp. 721–727.

[Com+17] P. Combes, F. Malrait, P. Martin, and P. Rouchon. "Obtaining the Current-flux Relations of the Saturated PMSM by Signal Injection." In: *Proceedings IECON 2017 - 43rd Annual Conference of the IEEE Industrial Electronics Society*. Vol. 2017-January. 2017, pp. 2097–2103.

[Com+20] P. Combes, D. Surroop, P. Martin, and P. Rouchon. "Estimation of the amplitude of a periodic component in a measured signal through a Delta-Sigma modulator." Pat. EP3709500 (A1), US11264935 (B2), CN111697893 (A). 2020.

[Com+21a] P. Combes, D. Surroop, P. Martin, and P. Rouchon. "A Variable Speed Drive for the Sensorless PWM Control of an AC Motor by Exploiting PWM-Induced Artefacts." Pat. EP3799293 (A1), US11264935 (B2), CN112564583 (A). 2021.

[Com+21b] P. Combes, D. Surroop, P. Martin, and P. Rouchon. "A Variable Speed Drive for the Sensorless PWM Control of an AC Motor with Current Noise Rejection." Pat. EP4020793 (A1), US2022200507 (A1), CN114744947 (A). 2021.

[CT92] J. Candy and G. Temes. "Oversampling Delta-Sigma Data Converters : Theory, Design, and Simulation." In: 1992.

[DD03] I. Daubechies and R. DeVore. "Approximating a Bandlimited Function Using Very Coarsely Quantized Data: A Family of Stable Sigma-Delta Modulators of Arbitrary Order." In: *Annals of Mathematics* 158.2 (2003), pp. 679–710.

[DSM10] F. M. L. De Belie, P. Sergeant, and J. A. Melkebeek. "A Sensorless Drive by Applying Test Pulses without Affecting the Average-current Samples." In: *IEEE Transactions on Power Electronics* 25.4 (2010). cited By 66, pp. 875–888.

[ESD90] J. A. Ellison, A. W. Sáenz, and H. S. Dumas. "Improved Nth order averaging theory for periodic systems." In: *Journal of Differential Equations* 84.2 (Jan. 1990), pp. 383–403.

[Fag+11] A. Faggion, E. Fornasiero, N. Bianchi, and S. Bolognani. "Sensorless Capability of Fractional-slot Surface-mounted PM Motors." In: *2011 IEEE International Electric Machines Drives Conference (IEMDC)*. 2011, pp. 593–598.

[Fil88] A. F. Filippov. *Differential Equations with Discontinuous Righthand Sides. Control Systems*. Mathematics and its Applications. Kluwer, 1988.

[Fli+92] M. Fliess, J. Lévine, P. Martin, and P. Rouchon. "Sur les systèmes non linéaires différentiellement plats." In: *Comptes rendus de l'Académie des sciences. Série 1, Mathématiques* 315 (Jan. 1992), pp. 619–624.

[FSO92] T. Furuhashi, S. Sangwongwanich, and S. Okuma. "A Position-and-velocity Sensorless Control for Brushless DC Motors Using an Adaptive Sliding Mode Observer." In: *IEEE Transactions on Industrial Electronics* 39.2 (1992), pp. 89–95.

[Gao+07] Q. Gao, G. Asher, M. Sumner, and P. Makys. "Position Estimation of AC Machines Over a Wide Frequency Range Based on Space Vector PWM Excitation." In: *IEEE Transactions on Industry Applications* 43 (2007), pp. 1001–1011.

[GDLM05] A. Glumineau and J. De Leon-Morales. *Sensorless AC Motor Control: Robust Advanced Design Techniques and Applications*. Springer, May 2005.

[Gen+10] F. Genduso, R. Miceli, C. Rando, and G. R. Galluzzo. "Back EMF Sensorless-control Algorithm for High-dynamic Performance PMSM." In: *IEEE Transactions on Industrial Electronics* 57.6 (2010), pp. 2092–2100.

[GL93] L. Gurvits and Z. X. Li. "Smooth Time-periodic Feedback Solutions for Nonholonomic Motion Planning." In: *Nonholonomic Motion Planning*. Ed. by Zexiang Li and J. F. Canny. Boston, MA: Springer US, 1993, pp. 53–108.

[Gol05] A. Goldsmith. *Wireless Communications*. Cambridge University Press, 2005.

[GT04] C. S. Gunturk and N. T. Thao. "Refined Error Analysis in Second-order Sigma-Delta Modulation with Constant Inputs." In: *IEEE Trans. Inf. Theor.* 50.5 (May 2004), pp. 839–860.

[Gun03] C. S. Gunturk. "One-bit Sigma-delta Quantization with Exponential Accuracy." In: *Communications on Pure and Applied Mathematics* 56.11 (2003), pp. 1608–1630.

[GZ09] M. Ghanes and G. Zheng. "On Sensorless Induction Motor Drives: Sliding Mode Observer and Output Feedback Controller." In: *IEEE Transactions on Industrial Electronics* (2009), pp. 3404–3413.

[Ha+03] J-I. Ha, K. Ide, T. Sawa, and S-K. Sul. "Sensorless Rotor Position Estimation of an Interior Permanent-magnet Motor from Initial States." In: *IEEE Transactions on Industry Applications* 39.3 (2003), pp. 761–767.

[Har78] F. J. Harris. "On the Use of Windows for Harmonic Analysis with the Discrete Fourier Transform." In: *Proceedings of the IEEE* 66.1 (1978), pp. 51–83.

[Has+17] N.S. Hasan, N. Rosmin, D.A.A. Osman, and A.H.M Jamal. "Reviews on Multilevel Converter and Modulation Techniques." In: *Renewable and Sustainable Energy Reviews* 80 (2017), pp. 163–174.

[HD91] T. G. Habetler and D. M. Divan. "Acoustic Noise Reduction in Sinusoidal PWM Drives Using a Randomly Modulated Carrier." In: *IEEE Transactions on Power Electronics* 6.3 (1991), pp. 356–363.

[HLK92] J. Holtz, W. Lotzkat, and A. Khambadkone. "On continuous control of PWM inverters in the overmodulation range including the six-step mode." In: *Proceedings of the 1992 International Conference on Industrial Electronics, Control, Instrumentation, and Automation*. Vol. 1. 1992, pp. 307–312.

[HMP12] N. Henwood, J. Malaizé, and L. Praly. "A Robust Nonlinear Luenberger Observer for the Sensorless Control of SM-PMSM: Rotor Position and Magnets Flux Estimation." In: *IECON 2012 - 38th Annual Conference on IEEE Industrial Electronics Society*. 2012, pp. 1625–1630.

[Hog81] E. Hogenauer. "An economical class of digital filters for decimation and interpolation." In: *IEEE Transactions on Acoustics, Speech, and Signal Processing* 29.2 (1981), pp. 155–162.

[HZ93] S. Hein and A. Zakhor. "On the Stability of Sigma Delta Modulators." In: *IEEE Transactions on Signal Processing* 41.7 (1993), pp. 2322–2348.

[IY63] H. Inose and Y. Yasuda. "A Unity Bit Coding Method by Negative Feedback." In: *Proceedings of the IEEE* 51.11 (1963), pp. 1524–1535.

[IYM62] H. Inose, Y. Yasuda, and J. Murakami. "A Telemetering System by Code Modulation - ΔΣ Modulation." In: *IRE Transactions on Space Electronics and Telemetry* SET-8.3 (1962), pp. 204–209.

[Jeb+11] A. K. Jebai, F. Malrait, P. Martin, and P. Rouchon. "Estimation of Saturation of Permanent-magnet Synchronous Motors through an Energy-based Model." In: *2011 IEEE International Electric Machines Drives Conference (IEMDC)*. 2011, pp. 1316–1321.

[Jeb13] A. K. Jebai. "Sensorless Control of Synchronous Permanent Magnet motors by Signal Injection." PhD thesis. Ecole Nationale Supérieure des Mines de Paris, 2013.

[Jeb+14] A. K. Jebai, P. Combes, F. Malrait, P. Martin, and P. Rouchon. "Energy-based Modeling of Electric Motors." In: *53rd IEEE Conference on Decision and Control*. 2014, pp. 6009–6016.

[Jeb+16] A. K. Jebai, F. Malrait, P. Martin, and P. Rouchon. "Sensorless Position Estimation and Control of Permanent-magnet Synchronous Motors Using a Saturation Model." In: *International Journal of Control* 89.3 (2016), pp. 535–549.

[JL95] P. L. Jansen and R. D. Lorenz. "Transducerless Position and Velocity Estimation in Induction and Salient AC Machines." In: *IEEE Trans. Industry Applications* 31 (1995), pp. 240–247.

[JS11] H. Jiang and M. Sumner. "Sensorless Torque Control of a PM Motor Using Modified HF Injection Method for Audible Noise Reduction." In: *Proceedings of the 2011 14th European Conference on Power Electronics and Applications*. 2011, pp. 1–8.

[Jun+11] S.-H. Jung, S. Doki, S. Okuma, and M. Fujitsuna. "Sensorless Control Method with Relatively Low Frequency Signal Injection for Low Acoustic Noise." In: *Proceedings of the 2011 14th European Conference on Power Electronics and Applications*. 2011, pp. 1–7.

[Kah80] C. S. Kahane. "Generalizations of the Riemann-Lebesgue and Cantor-Lebesgue Lemmas." In: *Czechoslovak Mathematical Journal* 30.1 (1980), pp. 108–117.

[KB47] N. M. Krylov and N. K. Bogoliubov. *Introduction to Nonlinear Mechanics*. Princeton University Press, 1947.

[KG06] H.M. Kojabadi and M. Ghribi. "MRAS-based Adaptive Speed Estimator in PMSM Drives." In: *9th IEEE International Workshop on Advanced Motion Control, 2006*. 2006, pp. 569–572.

[KKK03] Y. S. Kim, S. K. Kim, and Y. A. Kwon. "MRAS-Based Sensorless Control of Permanent Magnet Synchronous Motor." In: *SICE 2003 Annual Conference (IEEE Cat. No.03TH8734)*. Vol. 2. 2003, 1632–1637 Vol.2.

[Kot16] M. Koteich. "Modélisation Et Observabilité Des Machines Électriques en Vue De La Commande Sans Capteur Mécanique." PhD thesis. Université Paris-Saclay, 2016.

[Kra+13] P. Krause, O. Wasynczuk, S. Sudhoff, and S. Pekarek. *Analysis of Electric Machinery and Drive Systems*. Third Edition. Wiley, 2013.

[KSL11] H. Kim, J. Son, and J. Lee. "A High-speed Sliding-mode Observer for the Sensorless Speed Control of a PMSM." In: *IEEE Transactions on Industrial Electronics* 58.9 (2011), pp. 4069–4077.

[Lan+13] P. Landsmann, D. Paulus, A. Dötlinger, and R. Kennel. "Silent Injection for Saliency Based Sensorless Control by Means of Current Oversampling." In: *2013 IEEE International Conference on Industrial Technology (ICIT)*. 2013, pp. 398–403.

[LB96] B. Lehman and R. M. Bass. "Extensions of Averaging Theory for Power Electronic Systems." In: *IEEE Transactions on Power Electronics* 11.4 (July 1996), pp. 542–553.

[LD10] B. P. Lathi and Z. Ding. *Modern Digital and Analog Communication Systems*. Fourth. Oxford University Press, 2010.

[Lee+10] J. Lee, J. Hong, K. Nam, R. Ortega, L. Praly, and A. Astolfi. "Sensorless Control of Surface-Mount Permanent-Magnet Synchronous Motors Based on a Nonlinear Observer." In: *IEEE Transactions on Power Electronics* 25.2 (Feb. 2010), pp. 290–297.

[LKH03] M. Linke, R. Kennel, and J. Holtz. "Sensorless Speed and Position Control of Synchronous Machines Using Alternating Carrier Injection." In: *IEEE International Electric Machines and Drives Conference, 2003. IEMDC'03*. Vol. 2. 2003, pp. 1211–1217.

[Luo+13] H. Luo, Y. Han, R. C. C. Cheung, X. Liu, and T. Cao. "A 0.8-V 230-μ W 98-dB Dr Inverter-based $\Sigma\Delta$ Modulator for Audio Applications." In: *IEEE Journal of Solid-State Circuits* 48.10 (2013), pp. 2430–2441.

[LZ14] J. M. Liu and Z. Q. Zhu. "Sensorless Control Strategy by Square-waveform High-frequency Pulsating Signal Injection into Stationary Reference Frame." In: *IEEE Journal of Emerging and Selected Topics in Power Electronics* 2.2 (2014), pp. 171–180.

[Mes+18] A. Messali, M. Aassad Hamida, M. Ghanes, and M. Koteich. "A Novel High Frequency Signal Injection Strategy for Self-sensing Control of Electric AC Machine Drives." In: *IECON 2018 - 44th Annual Conference of the IEEE Industrial Electronics Society*. 2018, pp. 343–348.

[OA98] S. Ogasawara and H. Akagi. "Implementation and Position Control Performance of a Position-sensorless IPM Motor Drive System Based on Magnetic Saliency." In: *IEEE Transactions on Industry Applications* 34.4 (1998), pp. 806–812.

[OG06] M. Ortmanns and F. Gerfers. *Continuous-time Sigma-Delta A/D Conversion, Fundamentals, Performance Limits and Robust Implementations*. Vol. 21. Springer, Jan. 2006.

[Par29] R. H. Park. "Two-reaction Theory of Synchronous Machines Generalized Method of Analysis-part I." In: *Transactions of the American Institute of Electrical Engineers* 48.3 (1929), pp. 716–727.

[Par33] R. H. Park. "Two-reaction Theory of Synchronous Machines — Part II." In: *Electrical Engineering* 52.1 (1933), pp. 44–45.

[Par61] E. Parzen. "Mathematical Considerations in the Estimation of Spectra." In: *Technometrics* 3.2 (1961), pp. 167–190.

[Pav+08] S. Pavan, N. Krishnapura, R. Pandarinathan, and P. Sankar. "A Power Optimized Continuous-time $\Delta\Sigma$ ADC for Audio Applications." In: *IEEE Journal of Solid-State Circuits* 43.2 (2008), pp. 351–360.

[PST17] S. Pavan, R. Schreier, and G. C. Temes. *Understanding Delta-Sigma Data Converters*. Wiley, 2017.

[PTS02] M. H. Perrott, M. D. Trott, and C. G. Sodini. "A Modeling Approach for Sigma-Delta Fractional-N Frequency Synthesizers Allowing Straightforward Noise Analysis." In: *IEEE Journal of Solid-State Circuits* 37.8 (2002), pp. 1028–1038.

[RCK93] T. A. D. Riley, M. A. Copeland, and T. A. Kwasniewski. "Delta-Sigma Modulation in Fractional-N Frequency Synthesis." In: *IEEE Journal of Solid-State Circuits* 28.5 (1993), pp. 553–559.

[RS04] E. Robeischl and M. Schroedl. "Optimized INFORM Measurement Sequence for Sensorless PM Synchronous Motor Drives with Respect to Minimum Current Distortion." In: *IEEE Transactions on Industry Applications* 40.2 (2004), pp. 591–598.

[Rui96] S. M. Ruiz. "An Algebraic Identity Leading to Wilson's Theorem." In: *The Mathematical Gazette* 80.489 (1996), pp. 579–582.

[RW97] S. Rabii and B. A. Wooley. "A 1.8-V Digital-audio Sigma-Delta Modulator in 0.8-mu/m CMOS." In: *IEEE Journal of Solid-State Circuits* 32.6 (1997), pp. 783–796.

[Sch17] R. Schreier. "The Delta-Sigma Toolbox." In: *Understanding Delta-Sigma Data Converters*. John Wiley & Sons, Ltd, 2017, pp. 499–537.

[Sch96] M. Schroedl. "Sensorless Control of AC Machines at Low Speed and Standstill Based on the INFORM Method." In: *IAS '96. Conference Record of the 1996 IEEE Industry Applications Conference Thirty-First IAS Annual Meeting*. Vol. 1. 1996, pp. 270–277.

[SCM21a] D. Surroop, P. Combes, and P. Martin. "Error Analysis of a Demodulation Procedure for Multicarrier Signals with Slowly-varying Carriers." In: *2021 29th European Signal Processing Conference (EUSIPCO)*. 2021, pp. 1636–1640.

[SCM21b] D. Surroop, P. Combes, and P. Martin. "Error Estimates in Second-order Continuous-time Sigma-Delta Modulators." In: *ICASSP 2021 - 2021 IEEE International Conference on Acoustics, Speech and Signal Processing (ICASSP)*. 2021, pp. 5445–5448.

[SCM21c] D. Surroop, P. Combes, and P. Martin. "Towards an Industrially Implementable PWM-injection Scheme." In: *2021 IEEE International Electric Machines Drives Conference (IEMDC)*. 2021, pp. 1–6.

[SHS06] M. Schrödl, M. Hofer, and W. Staffler. "Combining INFORM Method, Voltage Model and Mechanical Observer for Sensorless Control of PM Synchronous Motors in the Whole Speed Range Including Standstill." In: *e & i Elektrotechnik und Informationstechnik* 123.5 (2006), pp. 183–190.

[SL93] H. Sussmann and W. Liu. "Lie Bracket Extensions and Averaging: The Single-bracket Case." In: *Nonholonomic Motion Planning*. Ed. by Zexiang Li and J. F. Canny. Boston, MA: Springer US, 1993, pp. 109–147.

[SOO19a] J. Sorensen, D. O'Sullivan, and S. O'Meara. "Part 2: Optimized Sigma-Delta Modulated Current Measurement for Motor Control." In: 2019.

[SOO19b] J. Sorensen, D. O'Sullivan, and S. O'Meara. "Part 1: Optimized Sigma-Delta Modulated Current Measurement for Motor Control." In: *Analog Dialogue* 53 (2019).

[Sor15] J. Sorensen. "Sigma-Delta-conversion Used for Motor Control." In: *Proceedings of PCIM Europe 2015; International Exhibition and Conference for Power Electronics, Intelligent Motion, Renewable Energy and Energy Management*. 2015, pp. 1–8.

[SP08] M. Z. Straayer and M. H. Perrott. "A 12-bit, 10-MHz Bandwidth, Continuous-time Sigma-Delta ADC with a 5-bit, 950-ms/s VCO-based Quantizer." In: *IEEE Journal of Solid-State Circuits* 43.4 (2008), pp. 805–814.

[ST05] R. Schreier and G. C. Temes. *Understanding Delta-Sigma Data Converters*. New York, NY: Wiley, 2005.

[Sur+19a] D. Surroop, P. Combes, P. Martin, and P. Rouchon. "A New Demodulation Procedure for a Class of Multiplexed Signals." In: *Annual Conference of the IEEE Industrial Electronics Society (IECON)*. 2019, pp. 48–53.

[Sur+19b] D. Surroop, P. Combes, P. Martin, and P. Rouchon. "Third-order Virtual Measurements with Signal Injection." In: *2019 IEEE 58th Conference on Decision and Control (CDC)*. 2019, pp. 642–647.

[Sur+20a] D. Surroop, P. Combes, P. Martin, and P. Rouchon. "Adding Virtual Measurements by PWM-induced Signal Injection." In: *American Control Conference*. 2020, pp. 2692–2698.

[Sur+20b] D. Surroop, P. Combes, P. Martin, and P. Rouchon. "Sensorless Rotor Position Estimation by PWM-induced Signal Injection." In: *IECON 2020 The 46th Annual Conference of the IEEE Industrial Electronics Society*. 2020, pp. 367–372.

[SVM05] J. A. Sanders, F. Verhulst, and J. Murdock. *Averaging Methods in Nonlinear Dynamical Systems*. Second. Springer, 2005.

[SZ96] R. Schreier and B. Zhang. "Delta-Sigma Modulators Employing Continuous-time Circuitry." In: *IEEE Transactions on Circuits and Systems I: Fundamental Theory and Applications* 43.4 (1996), pp. 324–332.

[Tha01] N. T. Thao. "Overview on a New Approach to One-bit Nth Order Sigma-Delta Modulation." In: *ISCAS 2001. The 2001 IEEE International Symposium on Circuits and Systems (Cat. No.01CH37196)*. Vol. 1. 2001, pp. 623–626.

[Tha96] N. T. Thao. "Vector Quantization Analysis of Sigma-Delta Modulation." In: *IEEE Transactions on Signal Processing* 44.4 (1996), pp. 808–817.

[Tur60] G. Turin. "An Introduction to Matched Filters." In: *IRE Transactions on Information Theory* 6.3 (1960), pp. 311–329.

[TV94] N. T. Thao and M. Vetterli. "Deterministic Analysis of Oversampled A/D Conversion and Decoding Improvement Based on Consistent Estimates." In: *IEEE Transactions on Signal Processing* 42.3 (1994), pp. 519–531.

[Ver98] S. Verdú. *Multiuser Detection*. Cambridge University Press, 1998.

[VZ18] S. Vaez-Zadeh. *Control of Permanent Magnet Synchronous Motors*. Oxford, 2018.

[WM02] T. M. Wolbank and J. Machl. "A Modified PWM Scheme in Order to Obtain Spatial Information of AC Machines without Mechanical Sensor." In: *APEC. Seventeenth Annual IEEE Applied Power Electronics Conference and Exposition (Cat. No.02CH37335)*. Vol. 1. 2002, pp. 310–315.

[WX04] C. Wang and L. Xu. "A Novel Approach for Sensorless Control of PM Machines down to Zero Speed without Signal Injection or Special PWM Technique." In: *IEEE Transactions on Power Electronics* 19.6 (2004), pp. 1601–1607.

[WZX20] G. Wang, G. Zhang, and D. Xu. *Position Sensorless Control Techniques for Permanent Magnet Synchronous Machine Drives*. Springer, 2020.

[Yan09] L. L. Yang. *Multicarrier Communications*. Wiley, 2009.

[Yi+19] B. Yi, R. Ortega, H. Siguerdidjane, and W. Zhang. "An Adaptive Observer for Sensorless Control of the Levitated Ball Using Signal Injection." In: *IEEE Conference on Decision and Control*. 2019, pp. 6882–6887.

[Yoo+09] Y. Yoon, S. Sul, S. Morimoto, and K. Ide. "High Bandwidth Sensorless Algorithm for AC Machines Based on Square-wave Type Voltage Injection." In: *2009 IEEE Energy Conversion Congress and Exposition* (2009), pp. 2123–2130.

[YOZ18] B. Yi, R. Ortega, and W. Zhang. "Relaxing the Conditions for Parameter Estimation-based Observers of Nonlinear Systems Via Signal Injection." In: *Systems and Control Letters* 111 (2018), pp. 18–26.

[YSS04] L. Yao, M. S. J. Steyaert, and W. Sansen. "A 1-V 140-μ/w 88-dB Audio Sigma-Delta Modulator in 90-nm CMOS." In: *IEEE Journal of Solid-State Circuits* 39.11 (2004), pp. 1809–1818.

[YZ10] W. Yang and I. Zurbenko. "Kolmogorov-Zurbenko Filters." In: *WIREs Computational Statistics* 2.3 (2010), pp. 340–351.

[ZL16] Y. Zhang and J. Liu. "An Improved Q-PLL to Overcome the Speed Reversal Problems in Sensorless Pmsm Drive." In: *2016 IEEE 8th International Power Electronics and Motion Control Conference (IPEMC-ECCE Asia)*. 2016, pp. 1884–1888.

[Zur91] I. G. Zurbenko. "Spectral Analysis of Non-stationary Time Series." In: *International Statistical Review* 59.2 (1991), pp. 163–173.

RÉSUMÉ

La commande sans capteur des moteurs électriques à basse vitesse demeure une problématique industrielle à la fois complexe et fertile. La dégénérescence de l'observabilité à zéro de vitesse lorsque la position du rotor n'est pas mesurée représente en effet un enjeu industriel majeur pour la commande robuste des moteurs. Ce problème est classiquement résolu par la technique dite de l'injection de signal exogène. Elle consiste à exciter le système par une perturbation à haute fréquence afin d'engendrer une réponse HF qui porte l'information de position désirée. L'injection de signal traditionnelle présente néanmoins des inconvénients pratiques majeurs, tels que l'introduction de bruits acoustiques parasites ou encore la limitation de la fréquence d'injection par la modulation d'impulsion pour les systèmes électromécaniques contrôlés via un onduleur. Pour ces systèmes, les signaux d'entrée modulés créent de manière endogène des harmoniques qui induisent des effets similaires à l'injection de signal exogène, sans les limitations de cette dernière, laissant donc entrevoir la possibilité de réalisation d'un schéma de contrôle sans capteur ni perturbation forcée. Dans les deux cas — exogène et endogène — il reste nécessaire de séparer la composante HF de la sortie fondamentale pour pouvoir exploiter pleinement l'information de position induite, avec une procédure qui soit applicable au flux binaire en sortie d'un modulateur Sigma-Delta, que l'on retrouve désormais déployé sur certains variateurs de vitesse industriels.

On se propose d'étudier les propriétés de l'injection de signal exogène en utilisant la théorie de la moyennisation. L'application de cette théorie permet notamment d'obtenir une description précise des effets de l'injection sur le système et ses sorties. Pour l'injection de signal endogène, une étude analogue peut être reproduite en adaptant la théorie de la moyennisation aux systèmes hybrides contrôlés par une modulation des entrées. Est ainsi mise en évidence la possibilité de récupérer les mêmes informations que dans le cas exogène sans avoir recours à une perturbation externe. Afin d'extraire l'information contenue dans la perturbation induite, on développe une procédure de démodulation des signaux multiplexés, valide à la fois sur des mesures analogiques ou sur un bitstream Sigma-Delta. Des validations numériques et expérimentales sur des Moteurs Synchrones à Aimants Permanents viennent parachever cette étude, et soulignent les difficultés inhérentes au contrôle d'un MSAP.

MOTS CLÉS

Contrôle non-linéaire, Moteurs électriques, Modélisation, Traitement du signal, Contrôle sans capteur

ABSTRACT

Sensorless control of electric motors at low speed remains a complex and fertile industrial problem. The observability degeneracy at zero speed when the rotor position is not measured represents indeed a major industrial issue for the robust control of motors. This problem is classically solved by the well-known exogenous signal injection technique. It consists in superimposing a fast-varying signal to the control law in order to generate a high-frequency response that carries the desired position information. However, traditional signal injection has major practical drawbacks, such as the introduction of parasitic acoustic noise or the limitation of the injection frequency by the Pulse-Width Modulation for electromechanical systems controlled using an inverter. For these systems, the modulated input signals endogenously create harmonics that induce effects similar to exogenous signal injection, without the limitations of the latter, and thus allowing the possibility of realizing a sensorless control scheme without mechanical sensor nor external probing signal. In both cases —exogenous and endogenous— it is still necessary to separate the HF component from the fundamental output to be able to fully exploit the induced position information, with a procedure that is applicable to the output bistream of a Sigma-Delta modulator, which is now deployed in some industrial variable-frequency drives.

We propose to study the properties of the exogenous signal injection using the averaging theory. The application of this theory allows us to obtain a precise description of the injection effects on the controlled system and its outputs. For the endogenous case, a similar study can be conducted by adapting the averaging theory to hybrid systems controlled by a modulation of its inputs. The possibility of recovering the same information as in the exogenous case is thus highlighted without the need of an external perturbation. To extract the information contained in the induced perturbation, we develop a demodulation procedure for multiplexed signals, valid both on analog measurements and on a Sigma-Delta bitstream. Numerical and experimental validations on Permanent Magnet Synchronous Motors complete this study, and underline the inherent difficulties of PMSM control.

KEYWORDS

Nonlinear control, Electric motors, Modeling, Signal processing, Sensorless control